NASA CR-174691

NASA

VOLUME I
FINAL REPORT
MATERIALS FOR ADVANCED TURBINE ENGINES (MATE) — PROJECT 3
DESIGN, FABRICATION AND EVALUATION OF AN OXIDE DISPERSION STRENGTHENED SHEET ALLOY COMBUSTOR LINER

By
Robert J. Henricks
Keith D. Sheffler

February 1984

United Technologies Corporation
Pratt & Whitney Aircraft Group
Pratt & Whitney Engineering Division

Prepared for

National Aeronautics and Space Administration
Lewis Research Center
Contract NAS3-20072 Project 3

FOREWORD

This work was performed under sponsorship of the National Aeronautics and Space Administration Materials for Advanced Turbine Engines (MATE) contract NAS3-20072, Project 3 - Design, Fabrication, and Evaluation of an Oxide Dispersion Strengthened Sheet Alloy Combustor Liner. NASA MATE Program Managers were Charles P. Blankenship and Salvatore J. Grisaffe; the Project 3 Manager was Robert L. Dreshfield. Except as noted below, this work was performed in the Pratt & Whitney Engineering Division Materials Engineering and Research Laboratory under the direction of Allan Hauser. Pratt & Whitney MATE Program Managers were William Owczarski and Sid Blecherman; Project 3 Managers were Maury Gell, Bob Henricks and Keith Sheffler. Effort on Tasks I through V was supervised by Robert Henricks, with engineering and technical support provided by Walter Weigert and Joseph Cop. Design and analytical support were provided in Task I by Bruce Stauffer (Preliminary Engine Design Group) and John Polhemus (Combustor Analytical Group). Task II sheet manufacturing development was performed under subcontract at the High Technology Materials Division (formerly Stellite Division) of the Cabot Corp. under the direction of Michael Rothman and at the International Nickel Company, Sterling Forest Research & Development Laboratory under the direction of Mark Robinson. Task III rig test methods development and Task V rig testing were performed in the P&WED Structures Test Group by Paul Wawrzonek and Steve Tolman, with the assistance of Al Lucier. The Task VI engine test combustor component was designed by Bruce Kindseth (Preliminary Engine Design Group) and analyzed by James Dierberger and William Ackerman (Combustor Analytical Group). Component construction was supervised by Merritt Wight. Assistance in preparation of this final report was provided by Abamilik (Bill) Catao and Jeanine DeMasi.

This Page Intentionally Left Blank

TABLE OF CONTENTS

TABLE OF CONTENTS (Continued)

1.0 SUMMARY

This section provides an overview of significant program accomplishments. More detailed summaries of each of the program tasks are provided in advance of each task description in the body of the report.

The objective of this program was to evaluate the suitability of wrought Oxide Dispersion Strengthened (ODS) superalloy sheet for gas turbine engine combustor applications. The nominal compositions of the two alloys investigated are provided in Table 1-I. Both alloys are highly oxidation resistant yttria (Y_2O_3) dispersion strengthened MCrAl compositions, with MA956 being a ferritic (BCC) iron base and HDA8077 an FCC nickel base alloy. Both materials possess a coarse, highly anisotropic "pancake" grain structure upon which a substantial part of the elevated temperature strengthening is based.

TABLE 1-I

COMPOSITION OF COMBUSTOR CANDIDATE ODS ALLOYS

	Fe	Ni	Cr	Al	Ti	Y_2O_3
INCOLOY MA956	Bal	-	20.0	4.5	0.5	0.5
HDA 8077	-	Bal	16.0	4.0	-	0.8

Results of preliminary property tests, which included formability, tensile, creep, isothermal and thermal fatigue, cyclic oxidation, and alloy stability evaluations, indicated both alloys to be viable candidates for combustor applications, with neither material exhibiting a significant advantage in balance of properties. Comparison with a current combustor alloy (Hastelloy X) indicates that both alloys possess about 167°C (300°F) advantage of creep and oxidation resistance, but show no improvement of elevated temperature fatigue capability (Figure 1-1).

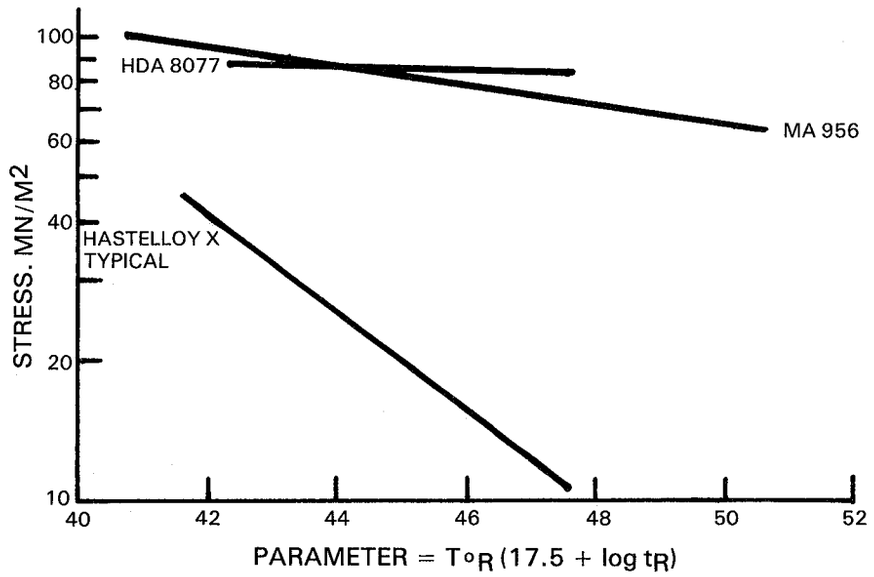

A) CREEP

$T_{°R}$ = TEMPERATURE, DEGREES RANKINE
t_R = RUPTURE LIFE, HOURS

HDA 8077
MA 956
HASTELLOY X

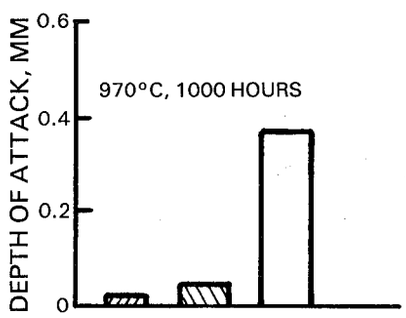

B) CYCLIC OXIDATION

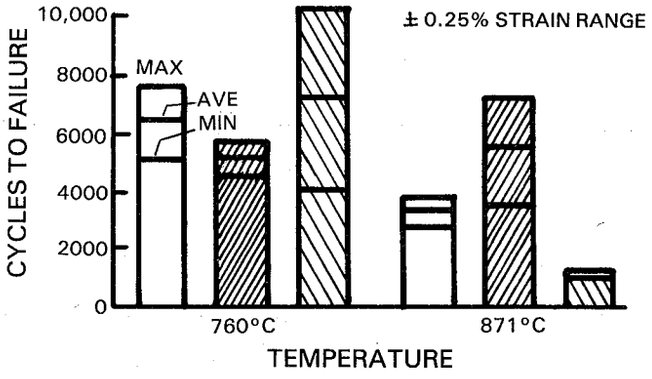

C) LOW CYCLE FATIGUE

Figure 1-1 Comparative Properties of ODS and Conventional Sheet Alloys

Process development efforts involving variations to the sheet rolling schedule, and consequent refinement of the grain structure, were not successful in improving the elevated temperature fatigue strength of either alloy. Efforts to demonstrate the manufacturing reproducibility of HDA8077 sheet also were not successful. The manufacturer of MA956 successfully produced a "scale-up" lot of material having properties comparable to earlier lots; MA956 thus was selected for the subsequently described rig and engine evaluations. Additional property data were generated on this material to support test hardware design and analysis requirements.

Preliminary joining evaluations indicated that brazing and mechanical fastening represented the most promising approaches to attachment of ODS combustor components. Braze procedures and materials were identified for joining of both ODS alloys to themselves and to Hastelloy X.

Combustor design studies were conducted to seek design approaches which would minimize thermal fatigue strains in ODS combustor components. Two segmented, mechanically attached, low strain design concepts were identified (Figure 1-2). As indicated in Table 1-II, both of these ODS designs offered a 4X improvement in life and a 0.21% decrease in direct operating cost as compared to conventional alloy combustor designs which were current at the beginning of this program.

Combustor rig test methods were developed and thermal cycle rig tests were performed on subscale MA956 and Hastelloy X combustor components similar to those illustrated in Figure 1-2. No cracking was observed in over 10,000 thermal cycles applied to each of the two designs and materials, thus confirming the high thermal fatigue tolerance of both segmented designs. These tests also confirmed the superior oxidation and thermal distortion resistance of the ODS alloy.

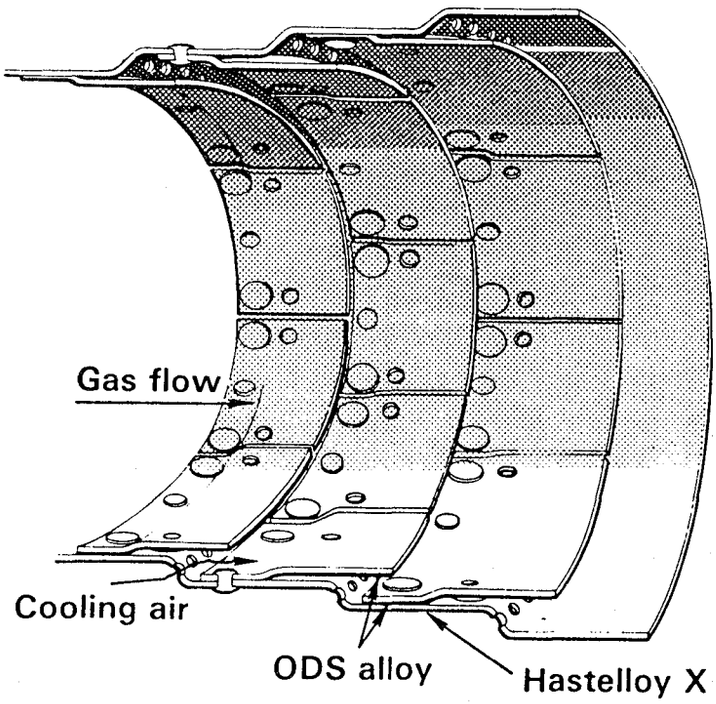

A) MECHANICALLY ATTACHED, FILM COOLED SEGMENTED LOUVER

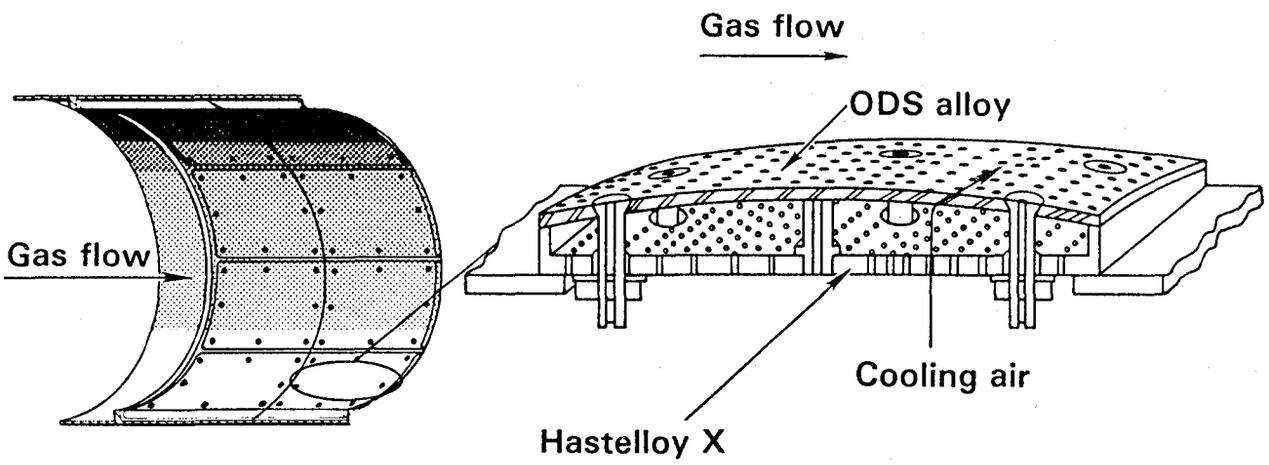

B) TRANSPIRATION COOLED, SEGMENTED TWIN-WALL DESIGN

Figure 1-2 Segmented Combustor Liner Concepts

TABLE 1-II

LIFE/COST COMPARISON OF DESIGNS (MA 956)

	Cooling[a] Air Percent W_{AB}	Total Strain, Range, Percent	Life[a] Cycles/hr	Cost[a]	Weight[a], lb	MC[a]	Change in DOC, Percent
JT9D base	1.00	~ 0.40	1.00	1.00	1.00	1.00	Base
Film cooled, segmented louver	1.00	0.145	4x	1.26x	1.06x	0.63x	-0.21
Segmented Twin wall	0.73	0.225	4x	1.48x	1.03x	0.65x	-0.21

[a]Relative value, i.e., (Value/Value for JT9D)
MC = Maintenance Cost
DOC = Direct Operating Cost

A hybrid PW2037 inner burner liner (IBL) containing MA956 and Hastelloy X components was designed and constructed. The louvered configuration was selected for this component because of the greater field experience with this type of construction and because of compatibility with the current PW2037 design. Photographs of an individual MA956 segment and of adjacent MA956 and Hastelloy X PW2037 IBL louvers are shown in Figure 1-3. This component will be endurance tested in a ground based PW2037 experimental engine pending availability of a suitable test opportunity.

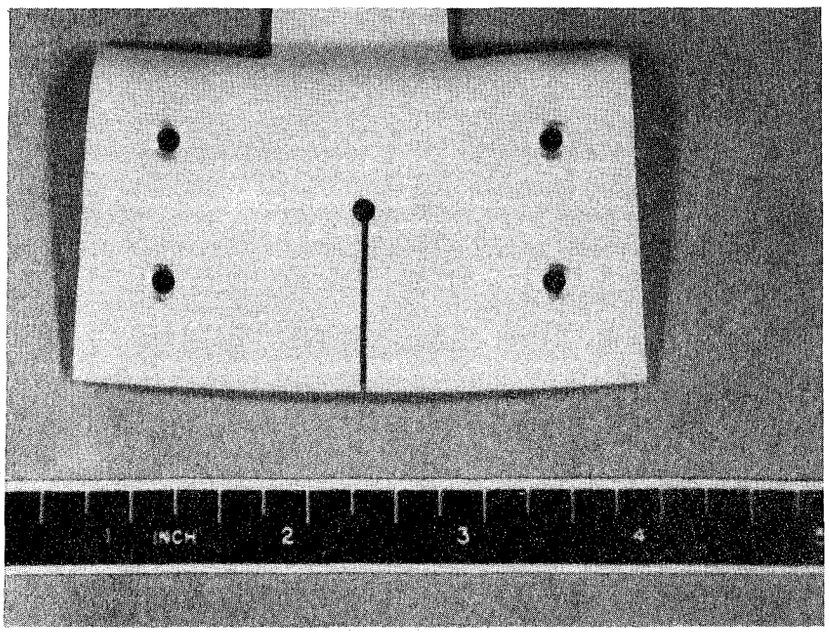

A) MA 956 SEGMENT

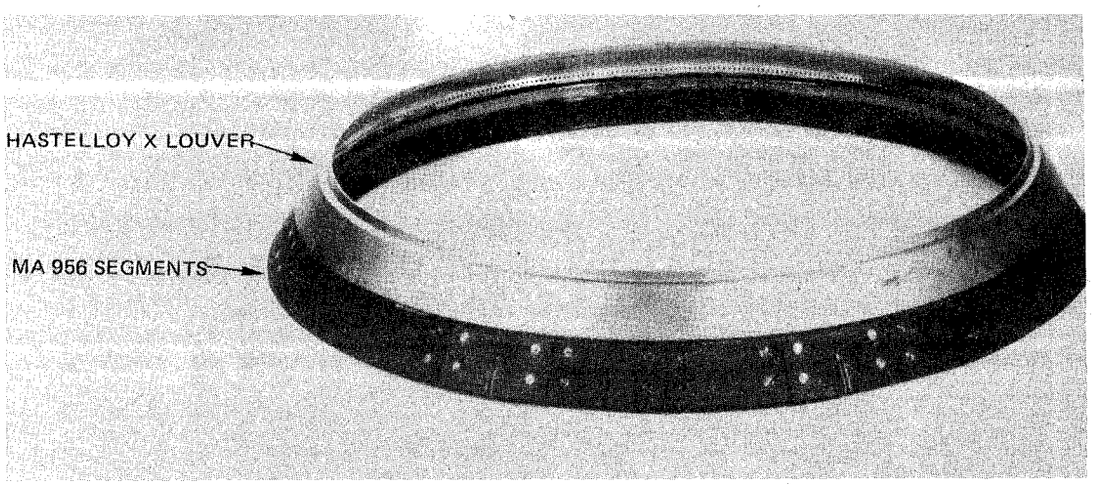

B) SECTION OF HYBRID INNER BURNER LINER

Figure 1-3 Section of Hybrid PW2037 Inner Burner Liner Containing Hastelloy X and Segmented MA 956 Louvers

2.0 INTRODUCTION

2.1 BACKGROUND

Advanced aircraft turbine engines expected to enter commercial service in the 1985 to 1990 time period will have performance, cost, and weight requirements that will necessitate the use of advanced materials technologies in their construction. A number of technologies which potentially meet these needs have been identified and are currently in various stages of development. To accelerate the development of selected material technologies to the point where they can be verified through engine testing, a cooperative Government/Industry effort, Materials In Advanced Turbine Engines (MATE), is being conducted under NASA sponsorship. This volume presents results of the first six tasks on MATE Project 3 - Design, Fabrication, and Evaluation of an Oxide Dispersion Strengthened Combustor Liner. FEDD Category 2 data, which will include Task VII engine evaluation and Task VIII post test analysis of oxide dispersion strengthened combustor components, will be reported in a future volume II of this Project 3 Final Report.

Combustor durability has become a serious problem in many current generation aircraft gas turbine engines. Advances in structural alloy metal temperature capability and in burner hardware cooling technology have not kept pace with demands for more efficient (higher gas temperature) engine performance. Hastelloy X burners designed for 870°C (1600°F) metal temperature operation are experiencing much hotter streak conditions with heavy penalties to operating life. Both improved burner materials and designs are required to provide the large durability increase essential to meet future aircraft turbine engine operation and maintenance cost goals.

A decrease in engine maintenance costs can result both from increased burner life and from reduced turbine section damage caused by burner distortion. The use of advanced Oxide Dispersion Strengthened (ODS) alloy sheet materials with improved creep strength and oxidation resistance compared to Hastelloy X has the potential to produce a significant increase in burner durability. The objective of this program was to evaluate the suitability of these alloys for gas turbine combustor applications.

Two advanced ODS sheet alloys were evaluated: Incoloy MA956 and Haynes Developmental Alloy (HDA) 8077. MA956 is a ferritic (BCC) FeCrAl alloy while HDA8077 is based on a NiCrAl composition with a FCC structure. Both alloys are strengthened by a sub-micron dispersion of yttria (Y_2O_3), and both depend on a relatively large, highly anisotropic grain structure for a substantial portion of their high temperature strength characteristics. Initial property comparisons with Hastelloy X indicate that these ODS alloys exhibit:

- o +167°C (300°F) advantage in creep strength
- o +167°C (300°F) advantage in cyclic oxidation resistance

However, these materials exhibit high temperature fatigue properties that show no improvement over Hastelloy X.

A substantial portion of the effort on this project was directed to evaluation of burner design modifications which would take advantage of the improved creep and oxidation resistance of ODS alloys while accommodating the reduced fatigue properties. Significant effort also was directed to improvement of ODS sheet fatigue strength by modification of processing and grain structure. Extensive material characterization also was included in the project plan, as described below.

2.2 PROGRAM SCOPE

Eight tasks were identified to meet the Project 3 objectives:

Task I - Preliminary Burner Design and Structural Analysis

This task involved preliminary design and analysis of five initial liner configurations, leading to selection and detailed analysis of two candidate ODS combustor designs.

Task II - Sheet Manufacture

The objectives of this task were to improve mechanical properties through modified sheet processing, and to demonstrate product reproducibility. These efforts were conducted under subcontracts by the International Nickel Company (MA956 alloy) and by the High Temperature Materials (formerly Stellite) Division of Cabot Corporation (HDA 8077 alloy).

Task III - Preliminary Evaluation

This task included: A) comparative evaluation of sheet material properties, B) evaluation of ODS joining methods, and C) development of combustor component rig test methods.

Task IV - Detailed Material Evaluation

Task IV was initiated by selecting one alloy for further evaluation based on the results of Tasks II and III. A more extensive property evaluation then was performed to investigate the mechanical, oxidation and metallurgical behavior of the selected alloy.

Task V - Subcomponent Thermal Cycle Tests

Using the test methods developed in Task IIIc, the two candidate combustor component designs were constructed from the selected alloy and were tested on thermal cycle rigs which closely simulated material performance in an engine environment.

Task VI - Engine Test Combustor Design and Construction

Based on results of the first five tasks, this task involved the selection of a single design concept and the design, analysis, and construction of a hybrid inner combustor liner incorporating ODS and Hastelloy X components for experimental evaluation in the PW2037 engine.

Task VII - Engine Test

Task VII will provide for engine test of the hybrid burner in a ground based PW2037 cyclic endurance engine with a target duration of at least 150 hours that is dependent on the structural integrity of the burner and the assurance of continued safe engine operation.

Task VIII - Post Test Evaluation

Task VIII will assess the performance of the ODS alloy hybrid burner in the engine test. This performance shall be evaluated in terms of the 1) capability to extend life of current alloy combustor liners, 2) decrease in maintenance costs achievable with ODS, 3) effect on direct operating costs and 4) overall benefits of incorporating ODS alloy liners in advanced turbine engines.

As indicated previously, this volume describes the results of Tasks I through VI; results of Task VII and VIII will be reported in a forthcoming Volume II.

3.0 TASK I - PRELIMINARY BURNER DESIGN AND STRUCTURAL ANALYSIS

3.1 INTRODUCTION AND SUMMARY

The objectives of this task were to identify five initial low strain design concepts for an oxide dispersion strengthened (ODS) combustor liner and, based on preliminary life prediction and cost analyses, to select two designs for more detailed analysis in this task and for experimental evaluation in subsequent tasks. This effort resulted in two candidate ODS combustor designs which provide significant decreases in direct operating cost and have predicted lives in excess of 10,000 cycles.

Initial design concepts identified in this task included three relatively conventional louvered designs with various combinations of film and impingement cooling and two more advanced transpiration cooled designs. One each of the louvered and transpiration cooled designs involved full annular hoop construction, with the remaining designs incorporating circumferential and axial segmentation of the louvers or panels to reduced thermally induced strains. Two separate preliminary analyses were conducted on each of these five designs using the respective properties for each of the two candidate ODS alloys (HDA 8077 and MA 956). Results of these analyses indicated that circumferential segmentation was necessary to achieve the 10,000 cycle life goal for an ODS combustor liner.

Results of the lifetime predictions were analyzed in combination with other factors including fabricability, repairability, weight, costs, and estimated risk to select two designs for further evaluation. This analysis led to the selection of a segmented film cooled louver and a segmented transpiration cooled panel design for detailed analysis. Both of these designs incorporated mechanical means for attachment of ODS louver or panel segments to a Hastelloy X outer shell.

Results of detailed structural analyses performed on each of these two designs confirmed the predicted life of >10,000 cycles for the film cooled louver design with one of the two candidate ODS alloys (MA 956), but indicated inadequate life coupled with cooling air leakage problems in the attachment area of the segmented transpiration cooled panel design. An alternative transpiration cooled design therefore was developed having a different attachment and sealing scheme. Detailed analysis of this design provided a predicted life in excess of 10,000 cycles for MA 956 alloy.

The following sections will described the analytical methods used for the structural and life prediction analyses, as well as the five initial designs, the selection methodology, and the revised transpiration cooled design and analysis.

3.2 DESIGN AND ANALYSIS METHODOLOGY

This section will describe the approach used to perform structural analyses and lifetime predictions for each of the candidate ODS combustor designs.

As shown in Figure 3-1, the method comprised three sequentially performed analyses, each of which incorporates specific material properties to ultimately yield a predicted operating life. An initial thermal analysis is performed using aerothermal boundary conditions couple with liner material thermal conductivity to establish a liner temperature distribution. Physical properties of the liner material (thermal expansion and modulus) then are used to establish thermal strain and stress distributions. Finally, the calculated strain and stress distribution are used together with known or estimated liner mechanical properties to calculate a predicted life. Details of each of these steps are discussed in the following paragraphs.

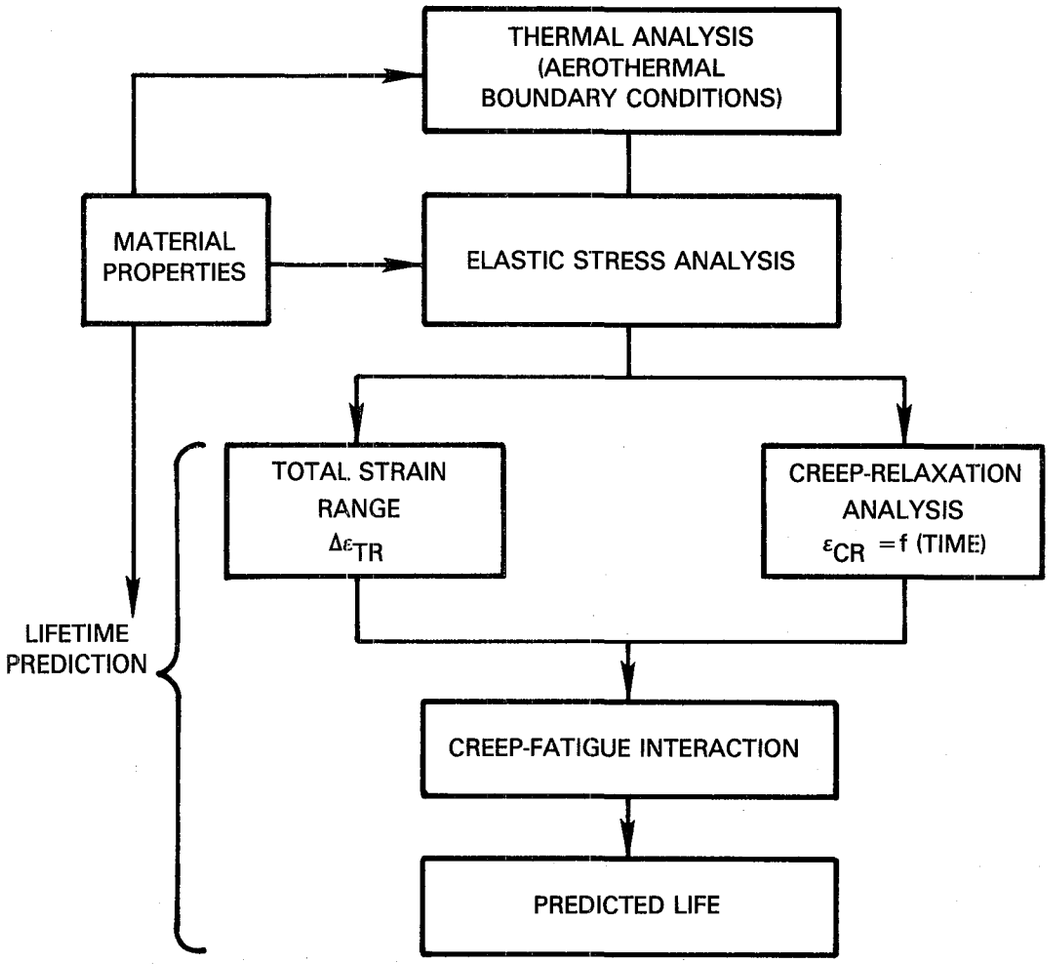

Figure 3-1 Burner Design and Life Prediction System

3.2.1 Thermal Analysis

A strong interdependence exists between aerodynamic and thermal analysis in a combustor environment. Changes in airflow distribution, i.e., cooling, combustion, and dilution flow alter the heat load characteristics of the combustion gases. An adequate solution to this complex problem is dependent upon the combined solution of aerodynamic, thermodynamic and heat transfer equations.

Current design methods include an aero-thermal analysis using a computerized combustor cooling liner design program. Given combustor geometry and inlet conditions of pressure distribution, temperature, and flow, the program first determines the airflow distribution within the combustor for isothermal flow.

Fuel then is included and internal gas temperatures are incrementally calculated at each station along the length of the burner as air is added. Mixing rates are simulated using an empirical correlation. Momentum pressure losses and internal static pressure distributions resulting from the combustion process are computed. The flow distribution and gas path temperature calculations are repeated until a negligible change in temperature distribution occurs in successive calculations. Upon completion of this iteration, convective and radiant heat loads are determined. Liner temperature distributions for the entire combustor are then computed using the appropriate thermal model for the cooling concept being investigated. At this point, the designer can isolate individual segments of the burner and, through direct iterations at a computer terminal, optimize the cooling flow in each segment to achieve the desired temperature. Through this procedure a detailed temperature and pressure distribution of the combustor is established for structural analysis.

Transient thermal analysis is normally not thought to be required. While experimental engine data indicate that the maximum temperature gradient in a louver can occur during the initial portion of a rapid engine acceleration, the predicted influence of this gradient overshoot on the louver fatigue life is considered negligible relative to the gradient that exists at the maximum power condition.

3.2.2 Elastic Stress Analysis

Structural analysis of combustor liner cooling geometries is conducted to determine the stress and strain distribution produced by the thermal and mechanical loads acting on the liner during an engine flight cycle. The predicted stress and strain values, together with the calculated metal temperatures, then are used to estimate the durability of the cooling scheme.

For continuous hoop structures, the analysis is performed using a finite element computer program where the liner is assumed to be composed of a linear elastic thin shell of revolution elements. For non-hoop configurations, other finite element options are available. By invoking compatibility between shell segments and using the appropriate boundary conditions, temperatures, and mechanical loads, the problem is reduced to the solution of a large set of

simultaneous, linear algebraic equations for the displacements at the nodal points adjoining the shell elements. Strains then are computed by differentiation of the displacement field; stresses can be retrieved through the use of Hooke's Law. A representative shell model of a series of conventional louvers is shown in Figure 3-2. Included are the local thickness increase associated with the seam weld joining louvers and a simulation of the cooling holes, in which the local element stiffnesses are reduced. A representative thermoelastic stress analysis for this kind of model is shown in Figure 3-3. Here, a more realistic model of an actual seam weld area has been used together with boundary conditions to simulate an infinite series of louvers with identical temperature distributions. For this particular analysis, a temperature difference of 278°C (500°F) exists between the weld-lip and knuckle regions. These temperatures would be typical of those predicted for a maximum power condition. The predicted thermoelastic stress distribution indicates significant portions of the louver to have exceeded the local yield strength of the material in both tension (knuckle) and compression (weld-lip). While these high stress levels are not possible in the actual component, they give some indication of the amount of plasticity and associated time dependent effects which occur due to the thermal loading.

The above example considered an axisymmetric temperature distribution. In reality, most combustors are subjected to circumferentially varying temperatures (streaks) resulting from an upstream disturbance of the cooling air or a partially blocked or misaligned fuel nozzle. This situation is handled in the linear elastic stress analysis by means of the principle of superposition of the elastic stress distributions. As shown in Figure 3-4, the "true" elastic solution is considered to be the sum of an axisymmetic temperature profile ($T_{average}$) and a circumferentially harmonic profile (ΔT). In general, most streak problems addressed in the stress analysis are associated with the number of fuel nozzles in the burner, making the assumption of the harmonic variation of temperature a good one.

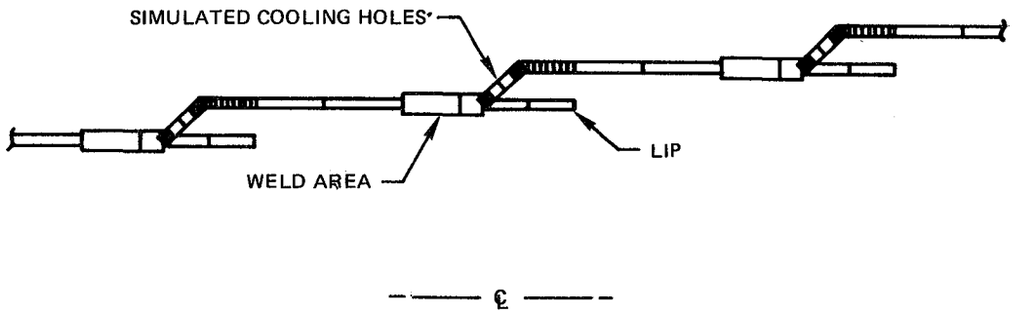

Figure 3-2 Section of Combustor Liner Shell Model

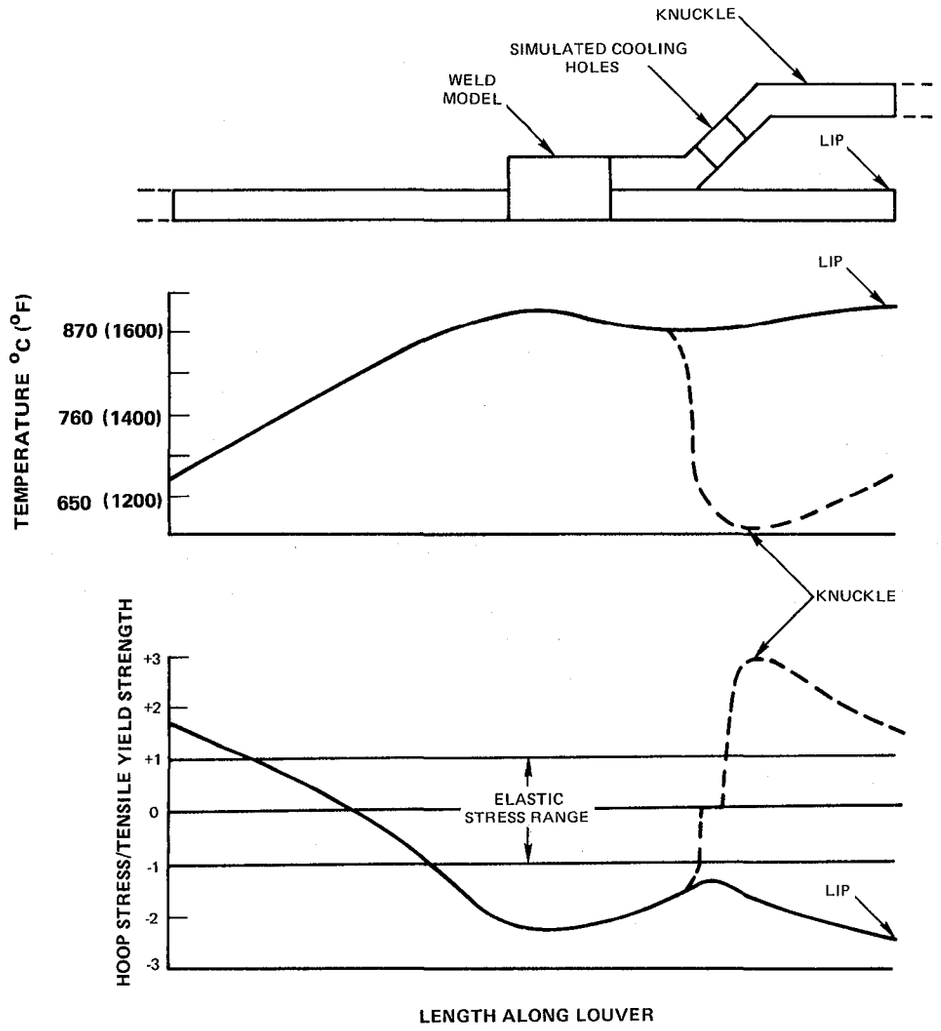

Figure 3-3 Temperature and Elastic Stress Distribution in a Conventional Louver Design

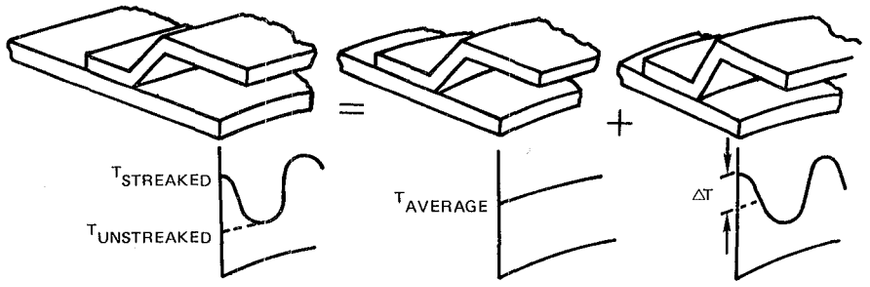

Figure 3-4 Streak Modeling Strategy Using Elastic Shell Stress Analysis

3.2.3 Life Prediction Analysis

The life prediction system used to calculate the life of the various candidate designs is outlined in Figure 3-5. This system incorporates the following steps as a basis for calculating burner lives:

1) strain harding characteristics are accurately defined in order to treat the critical properties of ODS alloys; e.g., high creep stress sensitivity and low creep ductility (Figure 3-6)

2) creep relaxation occurs as a monotonic stress decay (i.e., there is no plastic reversal)

3) creep relaxation strain is a function of temperature, time and geometry.

This approach combines the stress decay type of creep history with the calculated total strain range through the technique of "exhaustion of ductility" for the material as implied from low cycle fatigue data. This implied LCF ductility is one half of the extrapolated total strain for 1/4 cycle life, which in a fully reversed fatigue test approximates the tensile ductility. The interaction of creep and fatigue utilizing ductility exhaustion becomes the failure criterion for this design model. For ODS sheet alloys the ductility determined from tensile data and implied from LCF data is about five percent, whereas the prior creep ductility measured during testing can be as low as 0.1%. The conservative assumption of an 0.1% ductility for ODS alloys was utilized throughout Task I for life prediction calculations.

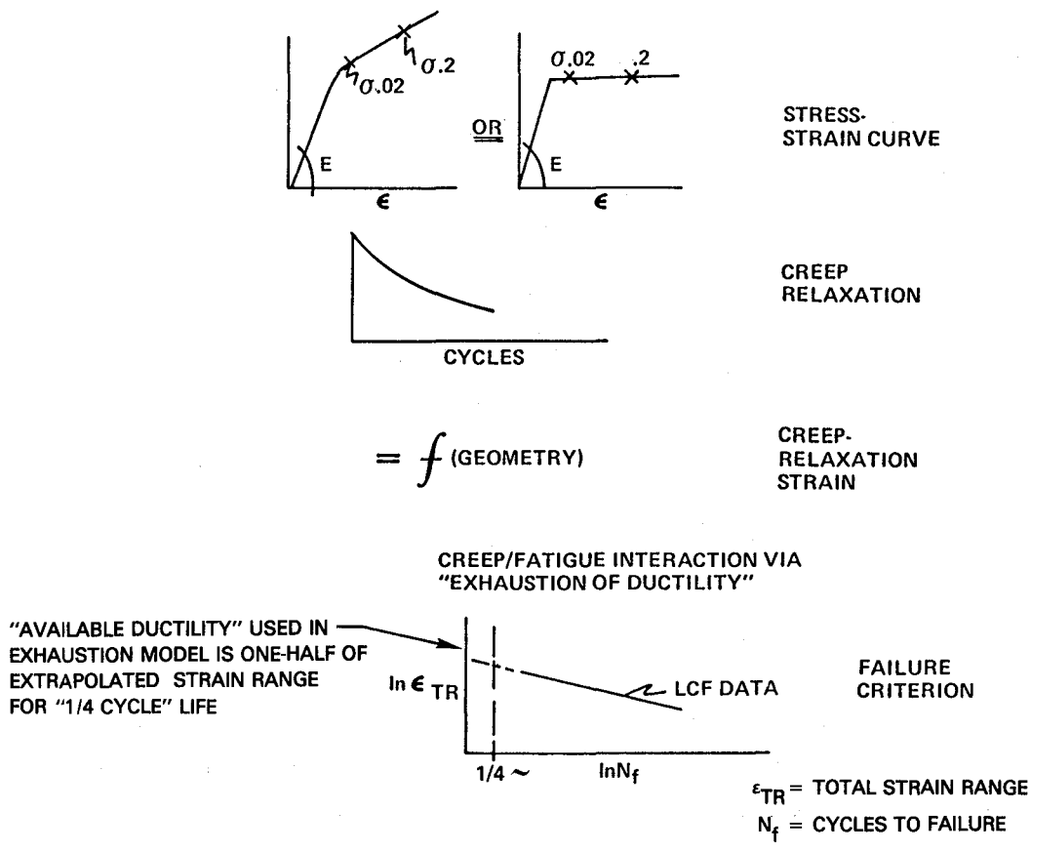

Figure 3-5 Schematic Outline of Combustor Life Prediction Design System

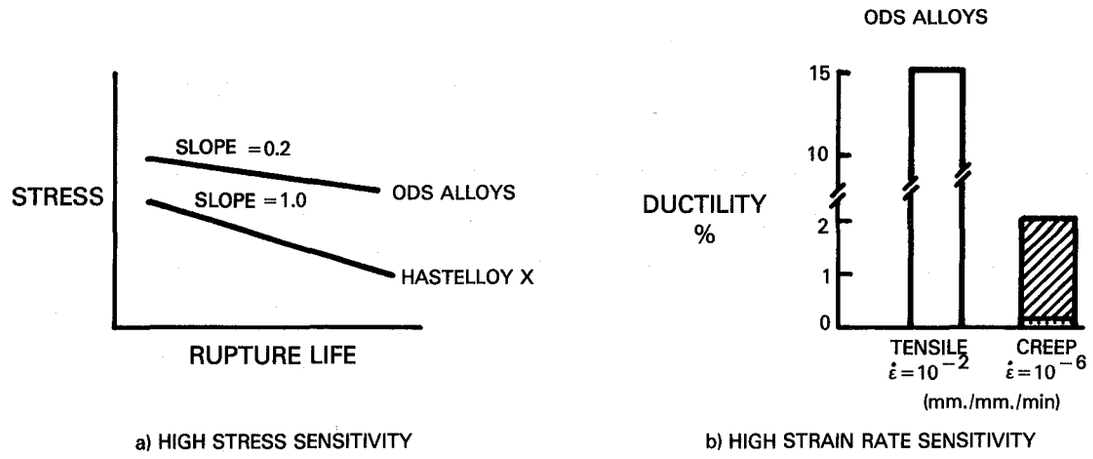

Figure 3-6 Critical Property Characteristics of ODS Alloys. Note the high creep stress sensitivity (small slope) of the ODS material as compared to a more conventional combustor alloy (Hastelloy X).

During the preliminary design and structural analysis of the five candidate schemes two different failure mechanisms were established, reflecting the critical aspects of the specific design. In each case, these limiting criteria are considered to be somewhat conservative. In the three louver-type candidate design configurations, the failure mechanism was defined as the time (cycles) to 0.1% creep strain. Because of the large differences between creep ductility and tensile or implied LCF ductility and the high strain rate sensitivity of ODS alloy ductility, the creep relaxation (stress vs. cycles) curve was utilized for lifetime predictions. For the two transpiration cooled configurations, a failure mechanism based on a fracture mechanics approach was assumed with "failure" occurring when cracks link up between adjacent cooling holes. In detail, this failure criterion is determined by using the available ODS alloy isothermal fatigue data to calculate the constant A in the crack growth equation $da/dN = A\Delta K^B$, where the exponent B is assumed to be the same as that currently used for Hastelloy X. From these values of A and B and using the predicted strain range and an initial flaw size of 0.025 mm (0.001"), the cycles to failure were obtained.

The structural analysis and life predictions were based on the projected engine and combustor design, thermal conditions, airflow requirements and engine operating conditions applicable to the Pratt & Whitney Energy Efficient Engine. Regardless of failure mechanism, predicted lifetimes were truncated at the program goal of 10,000 cycles, since projected lives greater than that become meaningless within the context of engine overhaul and repair considerations.

3.3 DESCRIPTION AND PRELIMINARY ANALYSIS OF FIVE INITIAL DESIGNS

A current film-cooled louver design (Figure 3-7) was analyzed initially to provide a baseline for evaluating the merits of the five candidate design schemes. With each louver forming a complete hoop in the current design, the axial temperature distribution (Figure 3-8) results in variations in relative thermal expansion which would cause each louver, if unconstrained, to seek a conical shape. If each louver were separate and experienced a linear axial temperature distribution, thermal stress levels would be minimal. However, the welding of the cold "knuckle" region to the hot louver lip region precludes any such stress-free expansion, and instead produces a "thermal constraint"

between the two regions (Figure 3-8). It is this joint that is calculated to be critical for the indicated temperature distribution. Figure 3-8 shows the strain range distribution for MA 956 and HDA 8077 alloys in a standard louver design. The predicted life of an ODS louver of conventional construction was not calculated.

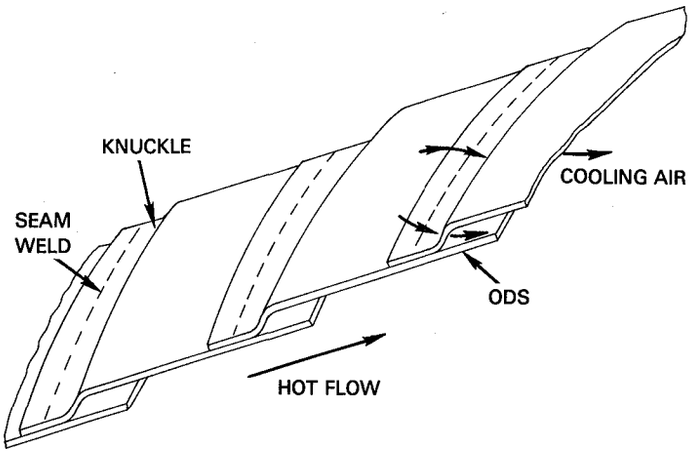

Figure 3-7 Conventional Film Cooled Louver

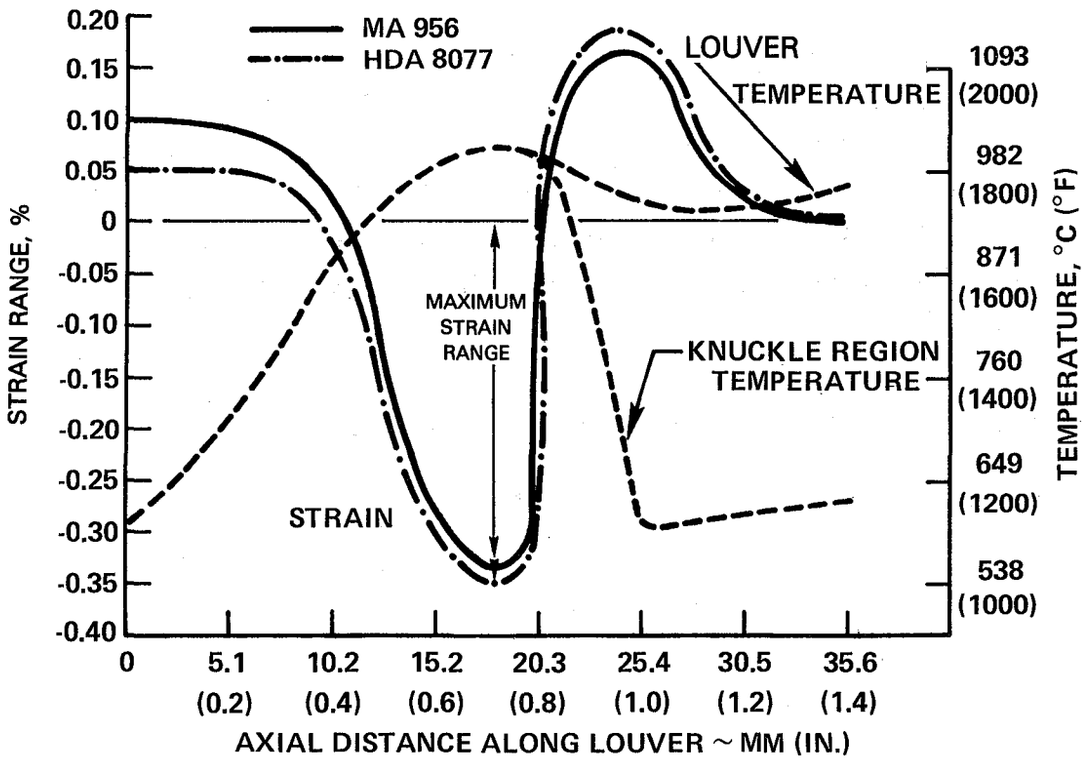

Figure 3-8 Strain Range Distribution of MA 956 and HDA 8077 Alloys in a Standard Louver Design

3.3.1 Design "A" - Extended Film Cooled Louver

This configuration (Figure 3-9), while maintaining full-hoop construction, addresses several of the features contributing to the high thermal strains in present designs. The louver has been extended to thermally shield the attachment area, thereby maintaining this area close to the cooling air temperature. The entire conventional alloy supporting shell structure is similarly maintained at these cooler temperatures. Thus, the supporting structure and the attachment portion of the ODS louver are at approximately the same temperature. Downstream the ODS louver temperatures increase as the louver becomes more exposed to the hot gases and as the cooling film becomes less effective.

As in the case of the standard louver design, the axial gradient has the effect of driving the cylindrical louver toward a conical configuration. The attachment location and louver extension permit some stress-relieving deformation resulting in a slightly improved strain range distribution (Figure 3-10) compared to the normal length louver. The calculated strain ranges shown in Figure 3-10 were based on construction of the supporting shell from Hastelloy X. The maximum strain ranges at the critical location 22.9 mm (0.9 inch) from the louver lip are on the order of 0.22 to 0.25 percent (compressive), and are due equally to the non-linearity of the axial temperature distribution and to the fixity at the shell-louver bond location. While the strain range could be reduced by achieving a more liner temperature gradient, further analysis indicated that such refinement of the temperature profile cannot be accomplished because the local thermal anomalies are intrinsic to this film cooled louver design and cannot be significantly altered by modification of the film cooling. Some reduction in thermal strain range may be achieved, however, by substituting a higher coefficient of expansion shell material, Tinidur, for Hastelloy X. This substitution of the Tinidur cold shell with its greater expansion allows the ODS louvers to seek a more stress free position (See Figure 3-11). The maximum strain range, the temperature at the critical location and the life predictions for this design are listed in Table 3-I. These calculated results indicate a slight reduction of maximum strain range to the order of 0.19 to 0.22 percent for the Tinidur shell.

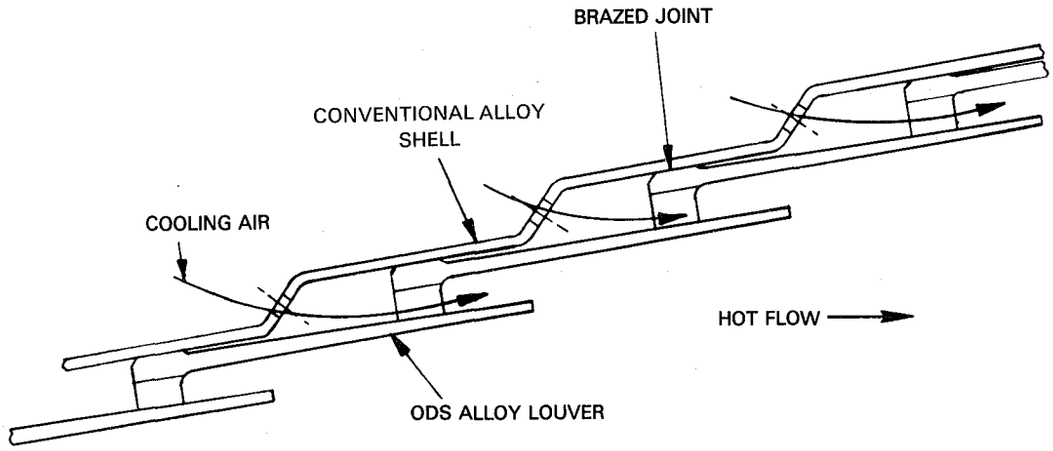

Figure 3-9 Design A - Extended Film Cooled Louver

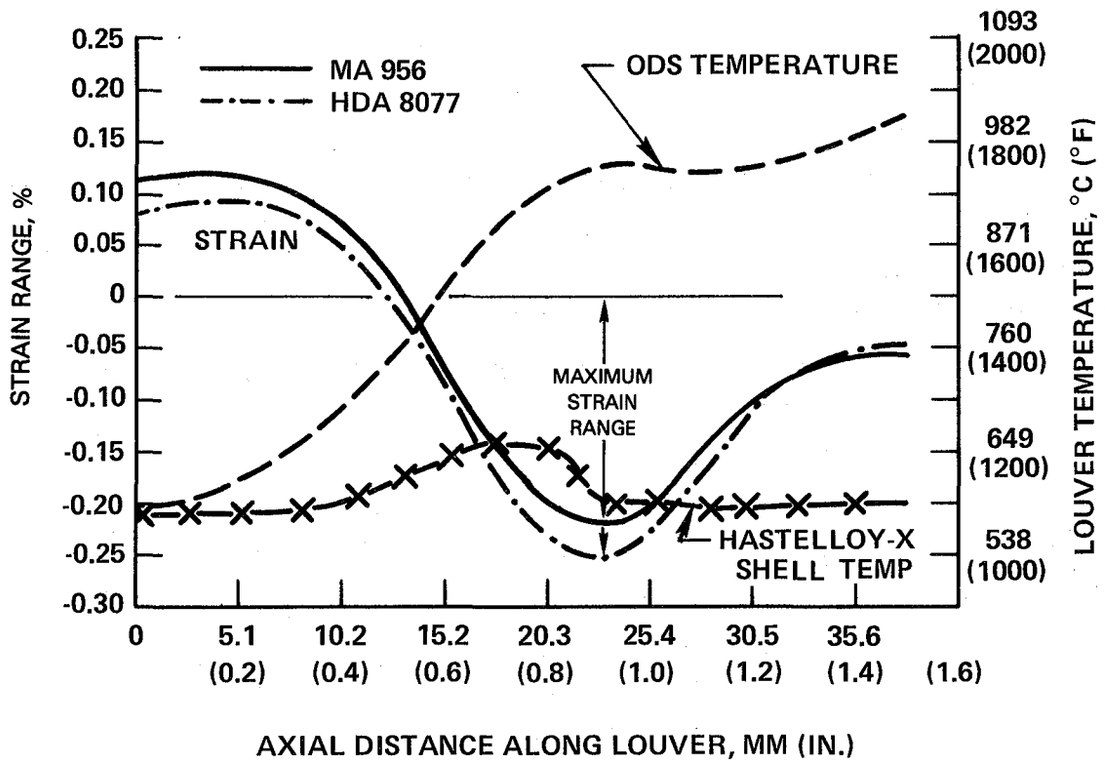

Figure 3-10 Extended Louver Design A. ODS louvers with Hastelloy X shell.

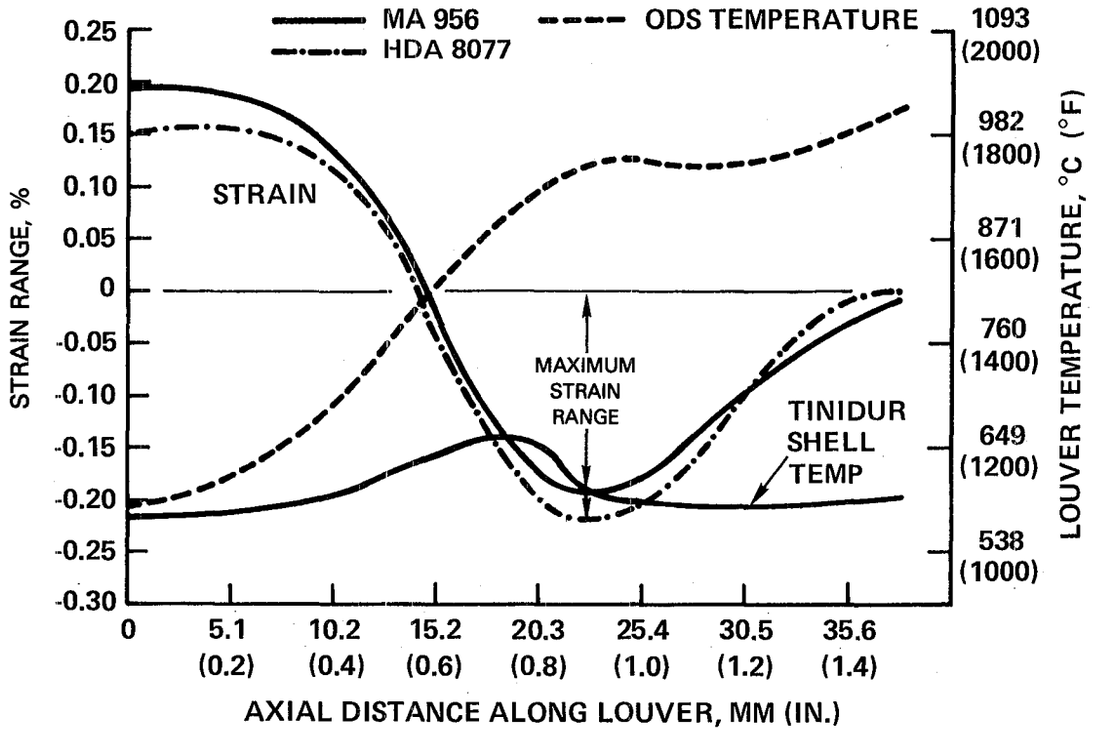

Figure 3-11 Extended Louver Design A. ODS louvers with Tinidur shell.

TABLE 3-I

STRAIN RANGE AND ENGINE LIFE FOR CANDIDATE ODS ALLOYS IN FIVE COMBUSTOR DESIGNS (ENERGY EFFICIENT ENGINE CONDITIONS)

	Design Scheme	Temp. at Critical Location °C (°F)	MA 956 Strain Range (%)	MA 956 Life (Cycles)	HDA 8077 Strain Range (%)	HDA 8077 Life (Cycles)
A.	Extended Film Cooled Louver					
	Hastelloy X/ODS	954 (1750)	0.22	1,500	0.25	<100
	Tinidur/ODS		0.19	10,000	0.22	<100
B.	Mechanically Attached, Film Cooled, Partially Segmented Louver	930 (1720)	0.11	10,000	0.11	10,000
C.	Mechanically Attached, Impingement/Film Cooled Partially Segmented Louver	1010 (1850)	0.09	10,000	0.19	<1,000
D.	Transpiration Cooled, Twin Wall (Tinidur Cold Wall)	938 (1720)	0.27	2,300	0.51	<100
E.	Mechanically Attached, Transpiration Cooled, Segmented Twin Wall	1010 (1850)	0.13	10,000	0.10	10,000

3.3.2 Design "B" - Mechanically Attached, Film Cooled, Partially Segmented Louver

The Design "A" configuration addressed many of the problems inherent in full hoop, film cooled louvered burner liner designs. The extended louver design, however, did retain the hoop construction and, therefore, the joining requirements of the baseline configuration. Since the life calculations for the extended louver did not reflect any strength/ductility debit due to bonding of the ODS sheet, a real concern exists in this regard. A very significant modification to the baseline and extended louver configurations is the elimination of the full hoop structure (hoop strains) through segmenting of the louver. As a result, a mechanically attached, segmented louver is considered attractive (Figure 3-12). By mechanically attaching each ODS segment to a Hastelloy X shell rigidly at only one location and providing room for differential thermal expansion at the other rivet and bushing locations, the only thermal strains present are those generated from the non-linear temperature variation within each segment (Figure 3-13). The critical location in this design is also the maximum strain location. The net effect is a significant reduction in strain range for both alloys with consequent improvement in life to the 10,000 cycle level (Table 3-I).

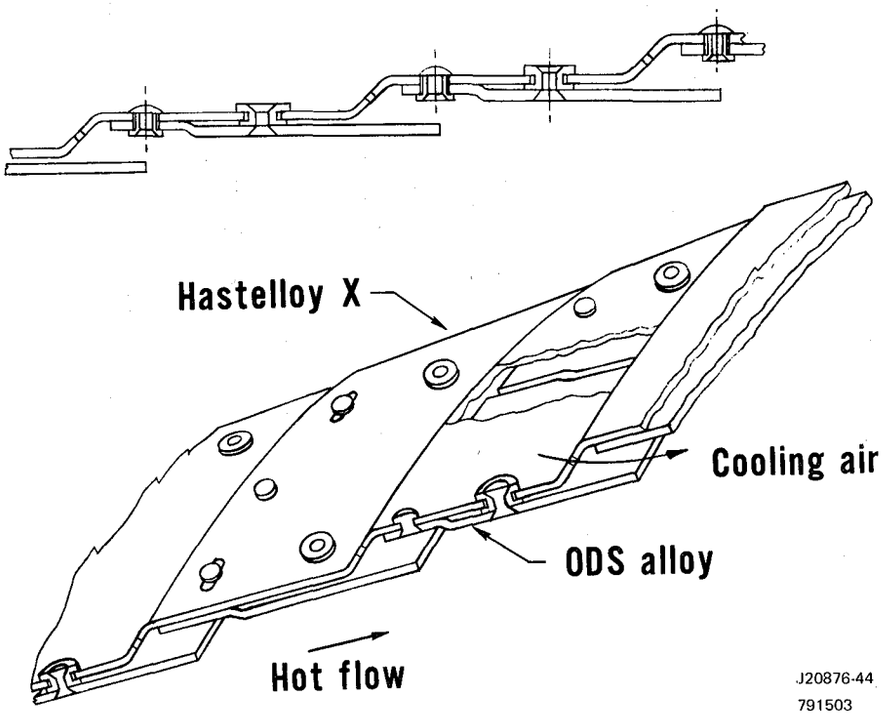

Figure 3-12 Design B - Mechanically Attached, Film Cooled Partially Segmented Louver

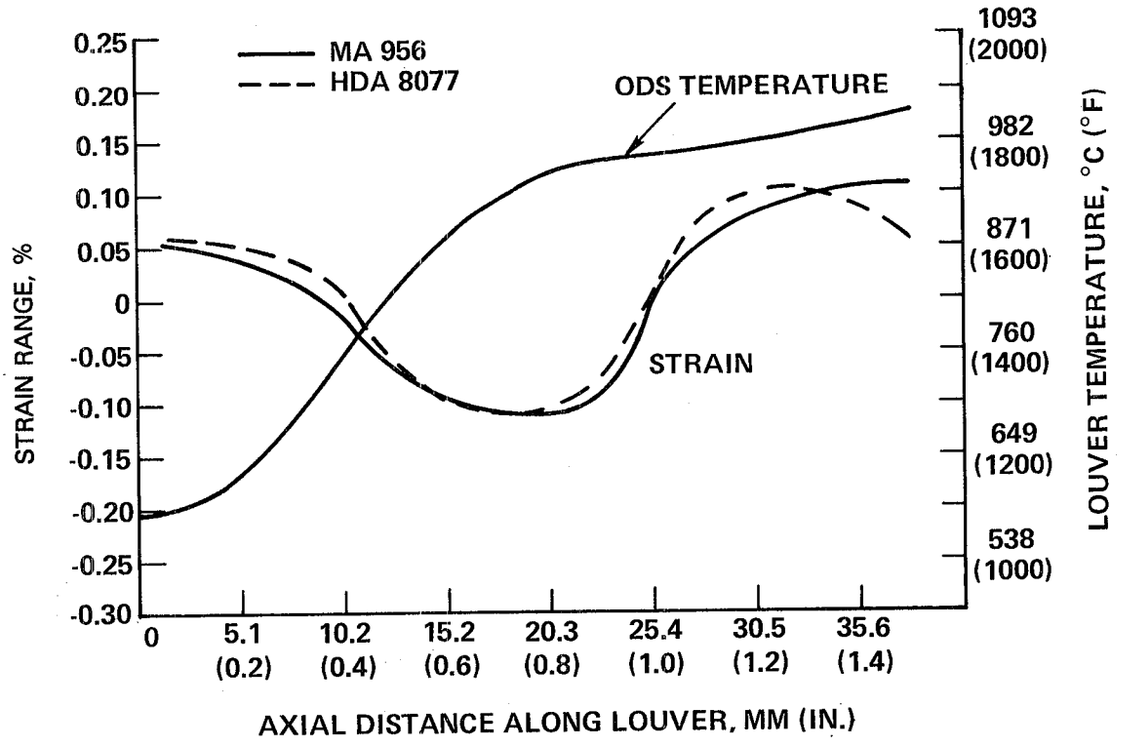

Figure 3-13 Design B - Mechanically Attached/Partially Segmented Film Cooled Louver

3.3.3 Design "C" - Mechanically Attached, Impingement/Film Cooled, Segmented Louver

This design constitutes a variation of the preceding segmented scheme. The film cooling has been augmented by impingement on the backside of the hot ODS sheet (Figure 3-14). The segments are no longer attached to the Hastelloy X backbone by mechanical fasteners, but rather by a series of brazes and tack welds of formed fasteners. In this design scheme ODS segments incorporate two flanges, one formed at the forward edge by bending of the ODS sheet and the other brazed on to the rear edge near the lip to form a louver type construction providing a cooling film. While this design incorporates a bond, it is subjected to a lower strain than the full hoop joints present in Design A. Assuming no debit in the bond location and a flange attachment scheme which permits the hotter ODS to grow relative to the Hastelloy X drum, the maximum strain levels at the louver lip shown in Figure 3-15 result in a MA 956 life similar to that for the previous configuration (Table 3-I). The HDA 8077 alloy exhibits twice the strain range of MA 956 in this scheme due to the higher coefficient of expansion for the nickel alloy; this higher strain range results in a calculated life of less than 1000 cycles for HDA 8077.

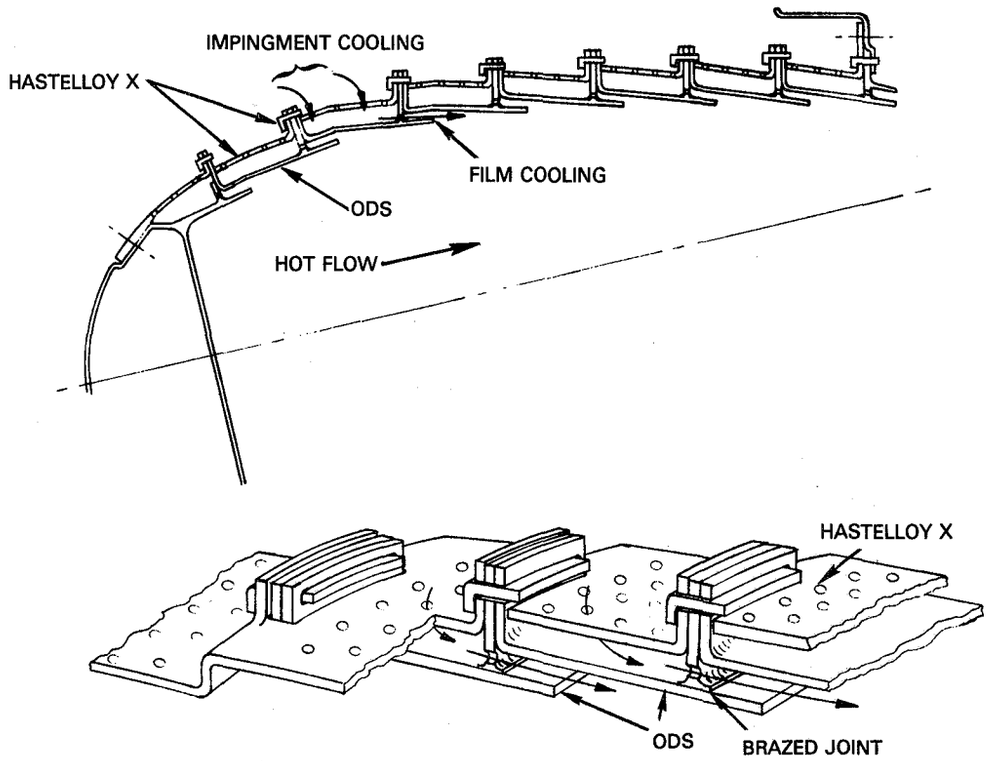

Figure 3-14 Design C - Mechanically Attached, Impingement/Film Cooled, Partially Segmented Louver

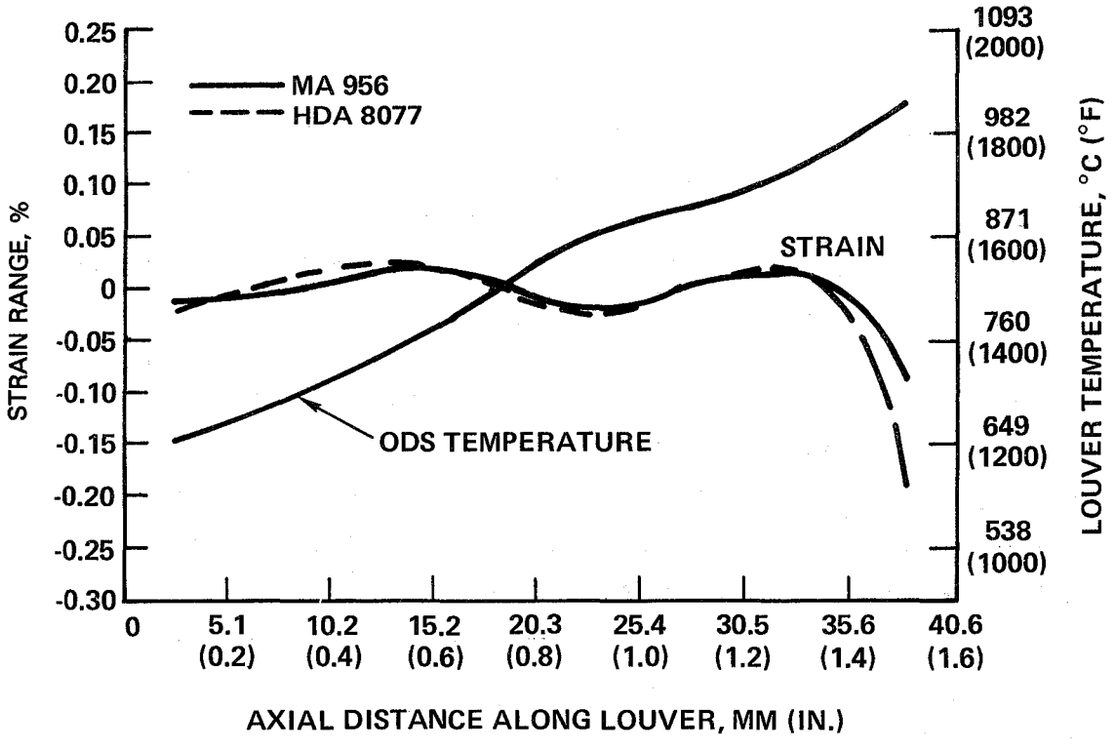

Figure 3-15 Design C - Mechanically Attached/Partially Segmented Louver Impingement/Film Cooled

3.3.4 Design "D" - Transpiration Cooled, Twin Wall

The two design concepts, "B" and "C", minimize the hot side/cold wall generated thermal strains by segmenting the hot side and providing only one connecting link per segment between the two walls, thus permitting stress free expansion. Such stress free expansion also may be achieved for a full hoop design as in scheme D (Figure 3-16). This is accomplished by supporting the hot ODS alloy drum within the cold drum with fingerlike springs attached to the cold side that can slide on the hot side allowing radial growth of the hotter ODS alloy drum. Hastelloy X initially was considered as the cold side material with the recognition that a cold side material with a higher coefficient of expansion might further minimize the strain levels. Execution of the stress analysis showed that the use of Hastelloy X as the cold side material resulted in extremely high strain levels in the ODS alloys at the contact points, with little ability to minimize this strain through softening of the supports without rendering them critical. The predicted ODS strain levels are far in excess of the materials capabilities and are not reported here. Substitution of the higher coefficient of expansion material, Tinidur, did succeed in reducing the ODS strain levels (Figure 3-17), but not to a level at which this configuration would be considered competitive (Table 3-I). The large difference in life between the two ODS alloys results primarily from the difference in the predicted strain levels due to differences of thermal expansion. The failure mechanism for this design is assumed to be crack link-up from adjacent transpiration holes.

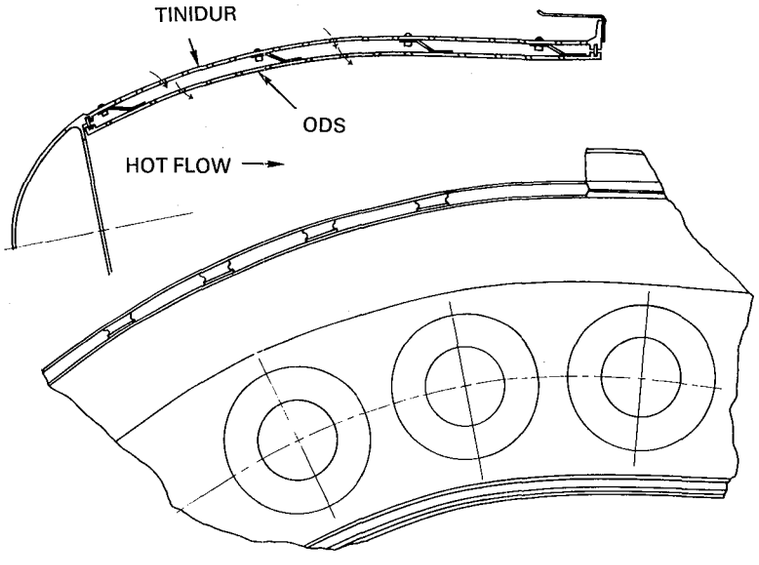

Figure 3-16 Design D - Transpiration Cooled Twin Wall

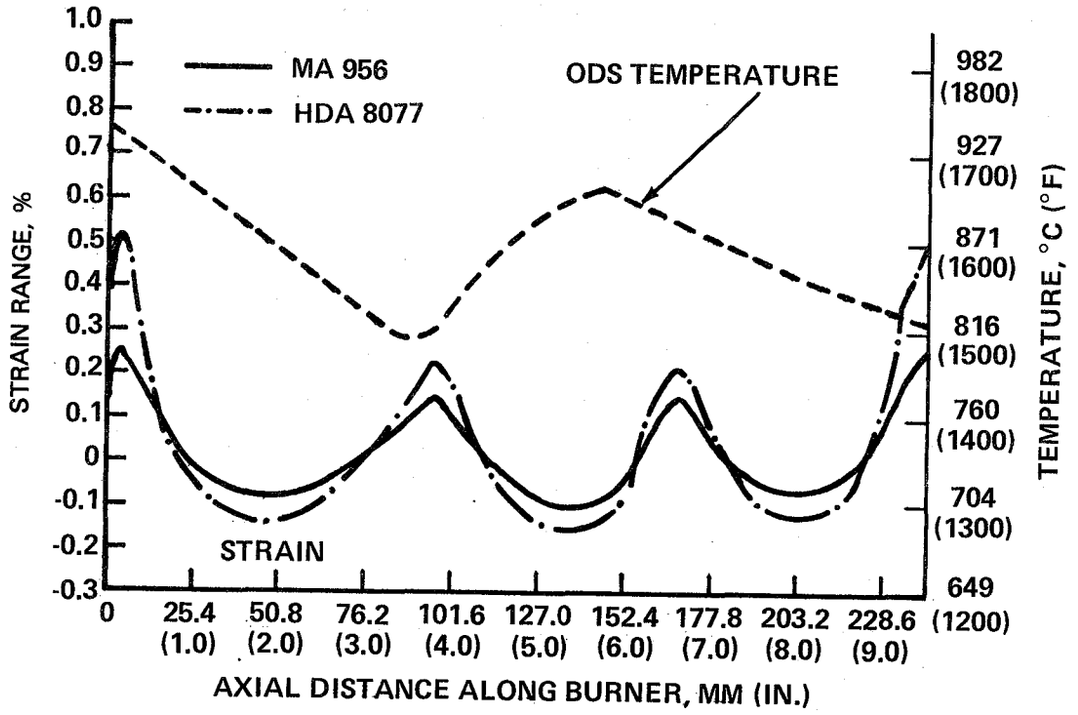

Figure 3-17 Design D - Transpiration Cooled Twin Wall Full Hoop with Tinidur Cold Wall

3.3.5 Design "E" - Mechanically Attached, Transpiration Cooled, Segmented Twin Wall

This scheme (Figure 3-18) constitutes a composite of those features identified as being significant in reducing thermal strain. This "twin wall" transpiration cooling scheme portrays an advanced cooling technique analyzed to be more effective than the film cooling and impingement/film schemes presented earlier and with the capability of reducing metal temperature and/or cooling flow. The particular advanced cooling design of the panels is not essential to the segmented configuration analyzed. In Design "D", in which the hot wall is a complete hoop, the low through thickness temperature gradient of the transpiration sheet is critical to achieving the design life goal. The use of both axial and circumferential segmentation, resulting in approximately 88.9 mm (3.5") panels, yields a configuration in which the pressure load is insignificant and, assuming proper sizing of the supporting rails, the hot and cold walls have been totally segregated from contributing to thermal strain. The only strain in the panel is produced by the gradients within the panel itself, particularly the gradients in the hook region (see Figure 3-18). In this design, the mechanical stresses due to pressure loads exceed the thermal stresses. As a result, the higher modulus of elasticity for HDA 8077 than for

MA 956 material generates a lower strain range for the HDA 8077 alloy (Figure 3-19 and Table 3-I). The failure mechanism, once again, is assumed to be linkup of cracks initiated at cooling holes. The prime concern with this configuration is the ability to minimize leakage without increasing strain levels.

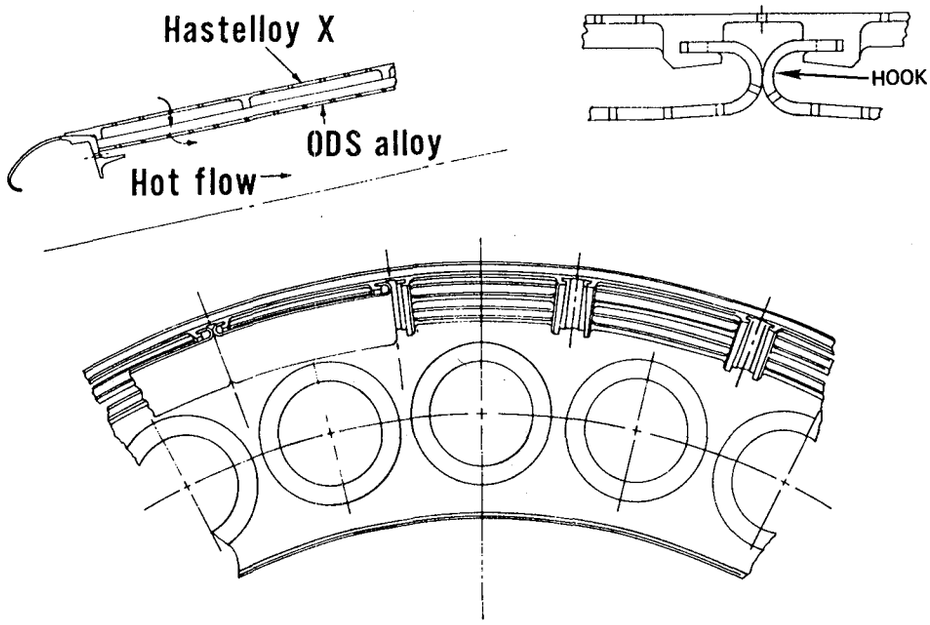

Figure 3-18 Design E - Mechanically Attached, Transpiration Cooled Segmented Twin Wall

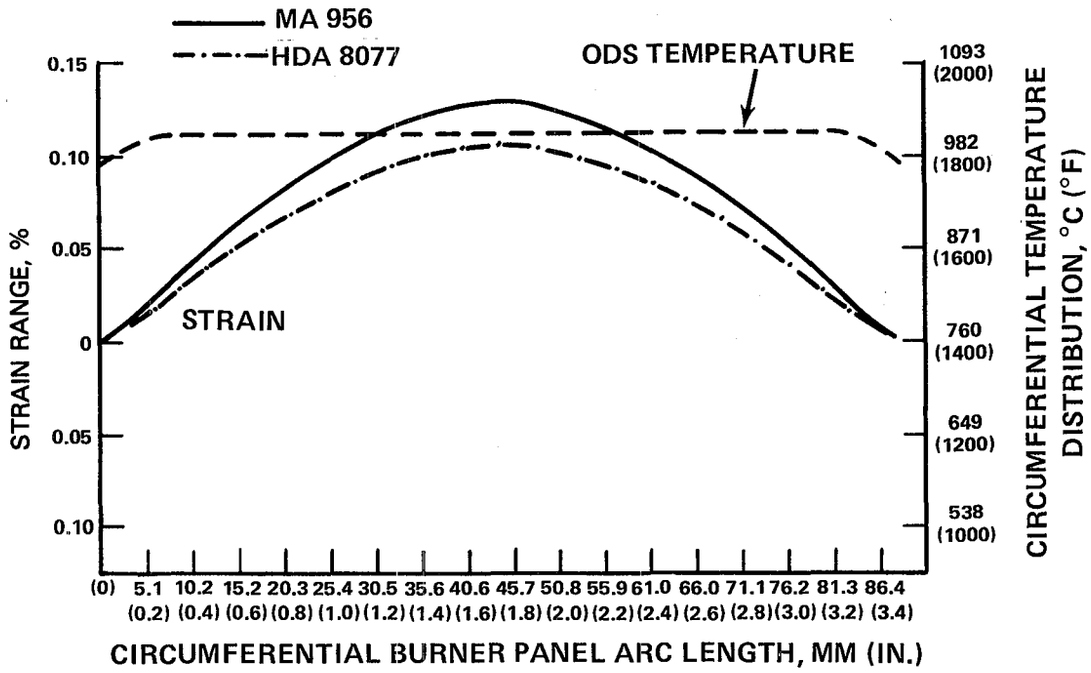

Figure 3-19 Design E - Mechanically Attached, Segmented, Transpiration Cooled Twin Wall

3.4 SELECTION OF TWO CANDIDATE DESIGNS

The selection of two preliminary burner design schemes for detailed analysis in this task and experimental evaluation in subsequent tasks was based on the following criteria:

- o Predicted Life
- o Fabricability
- o Maintenance Cost and Direct Operating Cost
- o Risk

Calculation of predicted life was discussed in the previous section (see Table 3-I). An assessment of fabricability considerations for each design is presented in Table 3-II. Certain construction difficulties were recognized as a part of the fabrication process, for example, the incorporation of welding full hoops of ODS in Designs A and D in a butt joint geometry. Although ODS materials exhibit relatively poor weldability it was assumed that hoops could be welded and that no debit in strain carrying capability would be applied to these welds. Similarly, it was assumed that in Design A and D, the Tinidur cold wall is easily weldable and that both the hot and cold walls can be weld repaired as required. Designs B, C and E can be fabricated with less difficulty; hot wall repair will be done by replacement of ODS segments.

An assessment of the impact of each design on maintenance and direct operating costs is presented in Table 3-III. The maintenance cost assessment combines material and labor cost and is based on the predicted lifetimes, on the initial construction cost of the burner and on the type of repair procedure employed. With the exception of Design D, all maintenance costs show a significant decrease compared to the baseline design. The impact on direct operating cost is derived by using the initial combustor fabrication cost, the overall weight of the combustor and the maintenance cost. The relative changes in direct operating cost represent decreases in overall engine operating cost and are not limited solely to combustor cost. These calculations show a decrease in direct operating cost for all five design schemes compared to the film cooled louver design (Table 3-III).

TABLE 3-II

FABRICABILITY AND REPAIR SUMMARY OF FIVE ODS COMBUSTOR DESIGNS

	Design Scheme	Construction Considerations	Repair Procedure
A.	Extended Film Cooled Louver	o Requires 80 mil ODS sheet to be machined to taper o Weldability of ODS o Fabricability of Tinidur	Standard Patch and Weld Repair
B.	Mechanically Attached, Film Cooled, Partially Segmented Louver	o Installation of rivets and bushings	Replace ODS Segments
C.	Mechanically Attached, Film and Impingement Cooled, Segmented	o Formability of ODS o Brazing of ODS	Replace ODS Segments
D.	Transpiration Cooled, Twin Wall (Tinidur Cold Wall)	o Weldability of ODS o Fabricability of Tinidur	Patch and Weld Repair
E.	Mechanically Attached, Transpiration Cooled, Twin Wall, Segmented	o Construction of Axial Leakage Seals	Replace ODS Segments

TABLE 3-III

RELATIVE COST FACTORS OF FIVE ODS COMBUSTOR DESIGNS
(ENERGY EFFICIENT ENGINE CONDITIONS, MA 956 ALLOY)

	Design	Cooling Air % W_{AB}	Life (Cycles)	Strain Range (%)	Maintenance Cost (MC)	Direct Operating Cost (DOC) (%)
A.	Cooled Louver Hastelloy X/ODS	45	1,500	0.22	1.0x	Base
	Extended Film Cooled Louver Tinidur/ODS	45	10,000	0.19	0.31x	-1.35
B.	Mechanically Attached, Film Cooled, Part-Seg.	45	10,000	0.11	0.22x	-1.57
C.	Mechanically Attached, Impingement/Film Cooled, Segmented	45	10,000	0.09	0.25X	-1.48
D.	Transpiration Cooled, Twin Wall (Tinidur)	33	2,300	0.27	0.71x	-0.40
E.	Mechanically Attached, Transpiration Cooled, Segment Twin Wall	33	10,000	0.13	0.23x	-1.52

TABLE 3-IV

RISK ASSESSMENT OF FIVE ODS COMBUSTOR DESIGNS

	Design Scheme	Fabricability Risk	Design/Structure Risk	Overall Risk
A.	Extended Film Cooled Louver	o Welds	o Full Hoops o No Debit for Weld Strength o Thick Sheet Properties	High
B.	Mechanically Attached, Film Cooled, Partially Segmented Louver	o No Experience with Riveted Construction	o Rivets/Bushings Carry No Load o Temperature Capability of Fasteners	Moderate
C.	Mechanically Attached, Film and Impingement Cooled, Segmented	o Forming and Brazing of ODS	o Braze Strength o Attachment Scheme	Moderate
D.	Transpiration Cooled, Twin Wall (Tinidur Cold Wall)	o Full Shell Required	o No Debit for Weld Strength o Durability of Finger Supports o Potential HFF Stresses	High
E.	Mechanically Attached, Transpiration Cooled, Twin Wall, Segmented	o Attachment Construction	o Leakage	Moderate

TABLE 3-V

RELATIVE COST FACTORS OF SELECTED ODS COMBUSTOR DESIGNS
(JT9D-59/70 Conditions, MA 956 Alloy)

		Cooling Air % W_{AB}	Strain Range (%)	Life (Cycles)	Cost	Weight	Maintenance Cost (MC)	Direct Operating Cost (DOC) (%)
	JT9D-59/70 (Base)	45	0.40	1.0	1.0	1.0	1.0	Base
B.	Mechanically Attached, Film Cooled, Partially Segmented Louver	45	0.11	4x	1.26x	1.06x	0.63x	-0.21
E.	Mechanically Attached, Transpiration Cooled, Segmented Twin Wall	33	0.13	4x	1.48x	1.03x	0.65x	-0.21

An assessment of the risk factors related to each of the candidate combustor designs is included in Table 3-IV. Because of the segmented structure and the elimination of any hoop strain carrying weld joints, Designs B, C and E represent schemes of moderate risk, although detailed analyses in the attachment areas are necessary. The full hoop construction in Designs A and D are considered high risk concepts from both construction and burner life viewpoints.

Based on the excellent predicted lives for both alloys, the beneficial maintenance and direct operating costs, and the estimate of moderate risk factors for fabrication and repairability, Designs B and E were selected for continued evaluation.

As noted previously, the above assessments and design selection were based on incorporation of each candidate design in the Pratt & Whitney Energy Efficient Engine. To confirm that these benefits are applicable to an engine which currently is in commercial service, these two designs were assessed relative to the JT9D-59/70 engine using the same design selection criteria. Comparison of these designs with the current JT9D louver Hastelloy X combustor in Table 3-V shows a four time improvement in life and reduction in maintenance cost and direct operating cost.

3.5 DETAILED STRUCTURAL ANALYSIS AND LIFE PREDICTION

As reported in the previous section, relatively simple stress analyses were performed on the five candidate combustor designs as a basis for selecting two design concepts for continued structural analysis and component evaluation. In this section, the two selected designs, Design B - the mechanically attached, film cooled, partially segmented louver and Design E - the mechanically attached, transpiration cooled, segmented twin wall, were analyzed in greater detail through the use of more refined finite element techniques.

As described below, this analysis confirmed the life benefits projected for Design B for one of the two candidate alloys (MA 956). Detailed analysis showed life in the attachment region of Design E to be inadequate. Problems also were anticipated with sealing of this design. Development of an alternative transpiration cooled design which met the 10,000 cycle design goal is described in a subsequent section.

3.5.1 Mechanically Attached, Film Cooled, Partially Segmented Louver

In the initial design effort the mechanically attached, riveted louver was analyzed considering only the circumferential stresses. For the more refined analysis, an elastic two-dimensional (2D) finite element approach incorporating the relatively small axial stress fields was utilized. This analysis defines the state of stress in the segmented hot wall and the relative motion between the segment and the Hastelloy X shell at the attachment locations to assure minimization of thermal constraint. Each segment was divided into a 110 element grid with ten elements used to define the segment circumferentially and eleven elements axially.

Results of this refined analysis yielded somewhat higher maximum strain ranges for both ODS alloys relative to those generated from the initial analysis (Table 3-VI); the temperature and strain profiles are shown in Figure 3-20. The critical strain range for MA 956 increased from 0.11 to 0.145 percent, while the strain range for HDA 8077 increased from 0.11 to 0.185 percent. Calculating the combustor liner life, as before, based on the number of cycles to reach 0.1 percent creep as the criterion, the life for MA 956 remains at 10,000 cycles, while the predicted life for HDA 8077 is reduced from 10,000 cycles to 2,000 cycles. It should be recalled that the initial predicted lifetimes for this riveted louver design in both ODS alloys were in excess of 10,000 cycles but were truncated at 10,000 cycles, since projected lives greater than this become meaningless within the context of engine overhaul and repair considerations. Based on the predicted 10,000 cycle life with at least one of the two candidate alloys, the mechanically attached, film cooled, partially segmented louver was deemed acceptable for experimental evaluation in subsequent tasks.

3.5.2 Mechanically Attached, Transpiration Cooled, Segmented Twin Wall

The transpiration cooled, segmented twin wall combustor was initially analyzed by treating the hooked panel configuration as a simple beam strip, permitting the effects of pressure loads and the partial effects of thermal gradients to be evaluated. In order to gain a better definition of the thermal strains, a

subsequent analysis was performed using the curved quadrilateral thick-shell element of a MARC* program. An elastic analysis was used for this configuration since the failure mechanism assumed is crack link up between adjacent cooling holes. The current method to predict the effect of hole arrays in a transpiration cooled geometry on the thermal-mechanical fatigue life employs the concept of linear elastic, isotropic fracture mechanics (Reference 3-1).

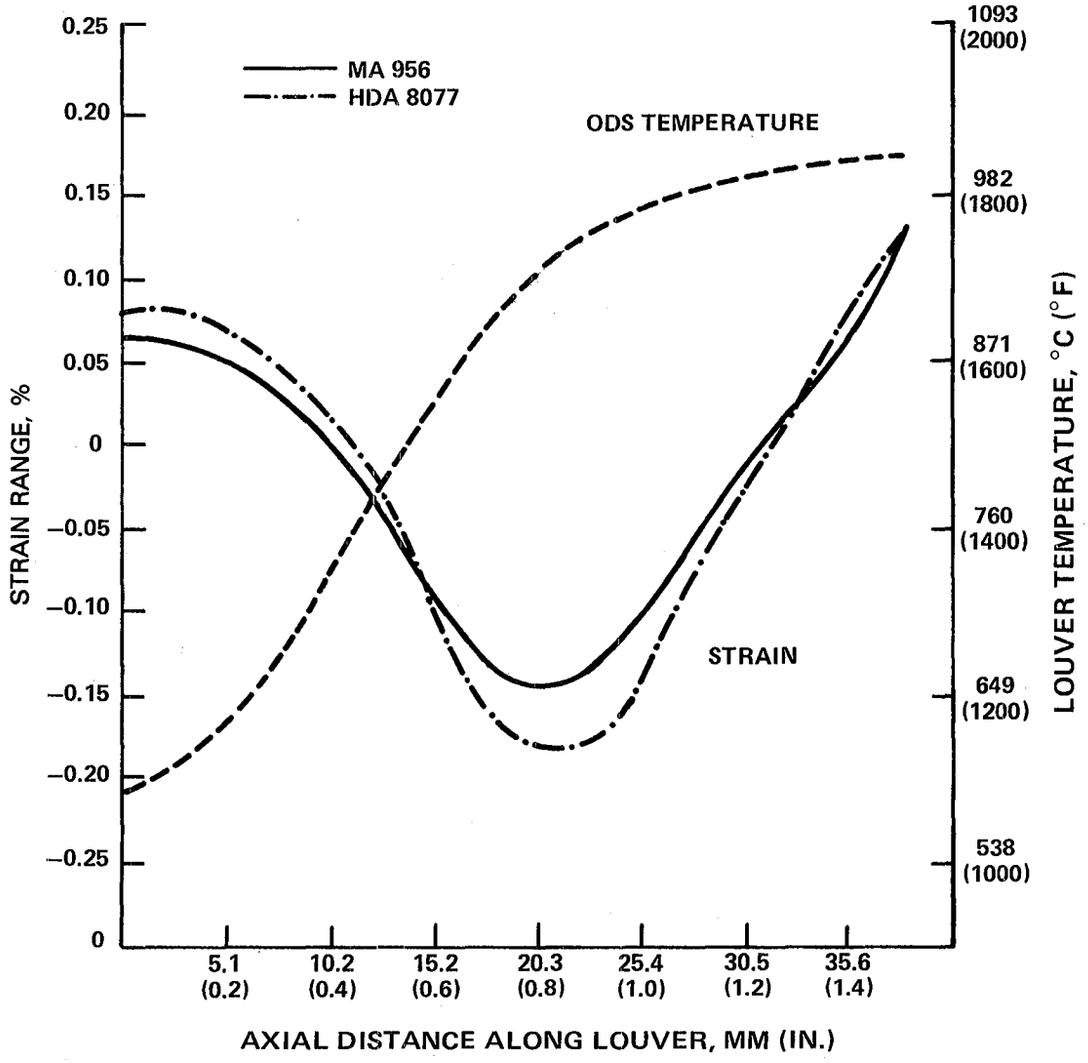

Figure 3-20 Strain and Temperature Profile for the Mechanically Attached Riveted Louver (Design B)

*MARC is a general purpose finite element program designed for the linear and non-linear analysis of structures in the static and dynamic regime.

TABLE 3-VI

STRAIN RANGE AND ENGINE LIFE FOR CANDIDATE ODS ALLOYS IN COMBUSTOR DESIGN B
(Mechanically Attached Segmented Film Cooled Louver)
(Energy Efficient Engine Conditions)

Analysis	Temperature at Critical Location °C (°F)	MA 956 Strain Range (%)	MA 956 Life Cycles	HDA 8077 Strain Range (%)	HDA 8077 Life Cycles
Preliminary 1D Analysis	930 (1720)	0.11	10,000	0.11	10,000
Detailed 2D Analysis	930 (1720)	0.145	10,000	0.185	2,000

The segmented twin wall design under consideration consists of twenty-four segments in the circumferential direction and two segments in the axial direction with the individual panels being 88.9 mm (3.5") and 127.0 mm (5.0") in size. For this thick-shell analysis, each panel was divided into a forty element grid; ten elements circumferentially and four elements axially. Using the symmetry of the segment and imposing appropriate boundary conditions resulted in a twenty element breakup with a coarse grid used in the hook region. No axial gradient was assumed. The thick-shell element allowed for definition of the gradient through the panel wall (thickness). Pressure and thermal loads were imposed and the panel was constrained radially at the axial midpoint of the hook extremity, as it is expected to act during engine operation. Stresses were then calculated at four "integration points" within each element.

The results of this stress analysis (Table 3-VII) show that for the flat portion of each panel the previously defined strain ranges (0.13% and 0.10% for MA 956 and HDA 8077, respectively) have remained at nearly the same levels. Similarly, projected panel life is unchanged from earlier predicted lives.

In the hook region, strains result from temperature differences between the hook and flat panel regions as well as from thermal gradients within the hook itself. Since configurational changes in both cooling hole pattern and cold wall attachment greatly affect strain ranges and predicted lives, the analysis becomes an iterative process through modifications in these areas. To generate a basis for comparison, the initial case that was analyzed assumed no cooling

TABLE 3-VII

STRAIN RANGE AND ENGINE LIFE FOR CANDIDATE ODS ALLOYS IN SEGMENTED TWIN WALL DESIGN (Energy Efficient Engine Conditions)

Analysis	Temperature at Critical Location °C (°F)	MA 956 Strain Range (%)	MA 956 Life Cycles	HDA 8077 Strain Range (%)	HDA 8077 Life Cycles
Flat Region					
Preliminary Beam Strip	1010 (1850)	0.130	10,000	0.100	10,000
Detailed MARC	1010 (1850)	0.139	10,000	0.153	10,000
Hook Region					
Detailed MARC (Optimum Cooling Design)	988 (1810)	0.294	4,000	0.320	1,400

air leakage at the sides of the hooks. This condition was achieved only by constraint of the edge of the hook along its entire length (axial direction). The MARC stress analysis for this case indicates a high effective strain level in the hook resulting in an unacceptable debit to predicted life.

Subsequent MARC analyses were performed to explore approaches for reduction of the high hook strains. Results of these analyses indicated that a 50 percent reduction in through-thickness thermal gradient would significantly lower the strain range and increase the design life to approximately 10,000 cycles. Cooling air passage geometry in both hot and cold walls was modified through an iterative process to select the optimum combination of strain range and maximum temperature at the critical location in the hot wall, while keeping within the limits of cooling air level and hot wall pressure drop. For the optimum cooling hole design, the reduction in thermal gradient was only ten percent, resulting in unacceptably low hook lives (Table 3-VII). To ameliorate this problem, a revised concept for transpiration cooled panel design was developed, as described in the next section.

3.6 REVISION OF MECHANICALLY ATTACHED, TRANSPIRATION COOLED, SEGMENTED TWIN WALL DESIGN "E"

To eliminate the attachment (hook) durability and seal problems anticipated with the previously described transpiration cooled design "E", a prestressed twin wall panel design concept was developed (Figure 3-21). The prestressed panel concept mechanically pre-loads (prestresses) a transpiration cooled panel at room temperature to a predetermined contour which duplicates the shape it will assume at the operating temperature of 1010°C (1850°F). An impingement plate which is used as a mandrel employs a contoured edge radius and a central positioning stud to form the desired deflected panel shape. To minimize cooling air leakage the prestressed transpiration cooled panel is attached to the impingement plate with a series of eight (8) studs. Since the edges of the panel are fastened to the frame of the impingement plate, leakage at the operating temperature of 1010°C (1850°F) is minimized. Analysis shows that leakage should be less than 10% of the panel cooling air. A 10.2 cm x 10.2 cm (4 in x 4 in) panel segment was selected for evaluation to facilitate subsequent manufacture of rig components for this program but the concept can be readily applied to other panel sizes and shapes.

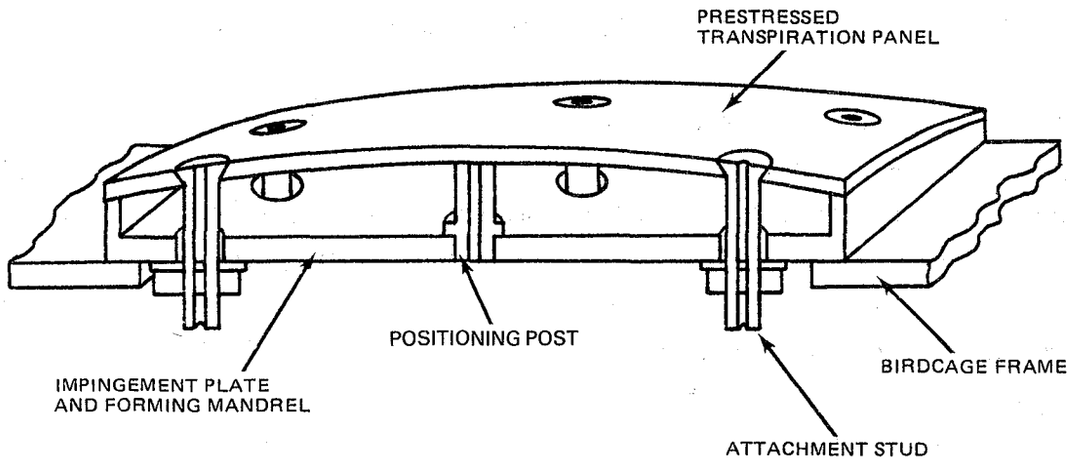

Figure 3-21 Cutaway Schematic of Prestressed Twin Wall Combustor Design (Cooling holes not shown)

At the point in the program where this redesign was being accomplished, a decision was made to select the ODS alloy MA 956 as the prime candidate for combustor demonstration. Analysis of the revised transpiration cooled design thus was conducted only for the MA 956 alloy.

This analysis indicated that during simulated engine operation the average temperature and the through thickness gradient increases, causing the mechanically induced prestresses to decrease to zero at operating temperature. The nature of this design is such that the largest stress occurs at 20°C (68°F) where the material strength is the highest. The location of the high stresses is in the corners of the panel at room temperature; however, during heatup stress redistribution occurs and the maximum stress is relocated to the center of each edge. Throughout the thermal loading, the maximum stress level remains below the proportional limit so that no plastic damage occurs.

Experience with multihole cooling schemes indicates that cracking will propagate from the holes in the region of highest tensile strain. For transpiration cooled designs, failure is defined as linkup of cracks emanating from adjacent cooling holes. In the prestressed panel design the hot side of the corner region of each panel is subjected to the largest tensile strain and is, therefore, the expected failure location. As a result of 1) prestress, 2) operating stress, 3) thermal cycle and 4) MA 956 material behavior, the calculated service life is in excess of 10,000 cycles. Table 3-VIII provides a comparison of strain levels and predicted lives for the initial hooked twin wall and the modified prestressed twin wall designs.

TABLE 3-VIII

STRAIN RANGE AND ENGINE LIFE
FOR MA 956 IN SEGMENTED TWIN WALL DESIGN
(Energy Efficient Engine Conditions)

	Temperature at Critical Locations	Strain Range, %	Life, Cycles
Initial Hook Twin Wall			
Flat Region	1010°C (1850°F)	0.139	10,000
Hook Region	988°C (1810°F)	0.294	4,000
Prestressed Twin Wall			
Corner	20°C (68°F)	0.225	10,000
Edge Center	As prestressed 1010°C (1850°F)	0.105	

The MA 956 attachment studs were analyzed separately. A thermal evaluation showed that the studs, with localized cooling through their centers, would maintain the same temperature as the panel. Structurally, the studs are prestressed at room temperature as a direct result of mechanically prestressing the transpiration cooled panel. At the operating temperatures of 1010°C (1850°F), the studs carry only a small pressure load, as there is no thermal interaction between the panel and studs due to the prestress deformation.

The success of the prestressed design concept hinges on the preformed panel shape duplicating the "shape" the panel seeks at operating temperature. Several studies were conducted to determine the criticality of the prestressed panel shape on the operating stress; these studies included the effects of contour variation and of local hot streaking. A realistic manufacturing tolerance on the contoured panel form is approximately 0.13 mm (0.005"). The studies indicate that within this tolerance range the operating stress of the transpiration panel is essentially unchanged. Since this change in contour of 0.25 mm (0.010") corresponds to approximately a 17°C (30°F) change in gradient through the panel, it can be concluded that the nominal contour is somewhat tolerant to minor changes in thermal gradient.

The initial baseline thermal analyses assumed that the entire panel was subjected to a uniform streak of 1010°C (1850°F). Since this may not be the case in an actual combustor operation, a tolerance study was conducted to determine the effects of local temperature streaking on the panel. Two cases were analyzed: the first, with a thin streak down the center of the panel and the second, with a streak covering half of the panel. The streak was assumed to be a 111°C (200°F) higher temperature increment and was incorporated as a step change in the analytical model. The results showed that a local streak in the center of the panel caused minimal additional damage and little change in predicted life. A streak over half of the panel was more severe and some local yielding was observed in the area of temperature discontinuity. Since this streak was applied as a step change, the results tend to be overly pessimistic, and it is believed that the actual operating stress will not exceed the yield stress. Based on this assumption, the revised mechanically attached, transpiration cooled, prestressed segmented twin wall design was judged acceptable for experimental evaluation in subsequent tests.

4.0 TASK II - SHEET MANUFACTURE

4.1 INTRODUCTION AND SUMMARY

The objectives of this task were to:

- Procure, for use in Task III, 1.86m^2 (20 ft^2) each of Incoloy MA956 and HDA8077 nominal 1.3mm (0.050in) thick sheet produced by the state-of-the-art process current at the beginning of the program.
- Conduct processing optimization studies with the goal of improving the elevated temperature fatigue properties of both alloys, while maintaining the good creep and formability of current state-of-the-art material.
- Demonstrate commercial reproducibility of sheet produced by the optimized processes.
- Develop process control specifications for control of commercial sheet manufacture.

In fulfillment of the first objective, 1.86m^2 (20 ft^2) each of nominal 1.3mm (0.050in) MA956 and HDA8077 sheet were produced respectively by the Henry Wiggin & Co., Ltd. (subsidiary of the International Nickel Co.) and by the High Technology Materials Division (formerly the Stellite Division) of the Cabot Corp. using processes which were state-of-the-art at the beginning of the program (late 1978). Properties measured on the initial lot of MA956 exhibited acceptable variability and were consistent with data obtained on this material prior to initiation of this program. Properties measured on the initial 20 ft^2 of HDA8077, which was comprised of three lots, were not consistent from lot-to-lot, nor with properties measured on this material prior to initiation of this program. The HDA8077 property showing the greatest lack of reproductibility was creep rupture life, which exhibited variations greater than four orders of magnitude at a given stress and temperature. The objective of the HDA8077 process optimization program thus was redirected from fatigue life improvement to improvement of property reproductibility, as described in a later paragraph.

The MA956 process optimization program was conducted under subcontract by the International Nickel Company Research and Development Center, Inc. The approach selected for elevated temperature fatigue improvement of MA956 involved variations of the processing which could decrease grain size, thereby increasing the number of "pancake" grains through the sheet thickness. This program was not successful in improving elevated temperature low cycle fatigue life. The process which was state-of-the-art at the beginning of the program thus was identified as the "optimum" process. Reproducibility of this process was demonstrated through production by Henry Wiggin and Company, Ltd. of a $4.65m^2$ ($50\ ft^2$) commercial lot which was delivered for use in the balance of this program. Properties of this lot were comparable to those measured on the initial $1.86M^2$ ($20\ ft^2$) lot. A process specification to be used for control of commercial sheet manufacture was provided by the vendor.

Process optimization of HDA8077 alloy was conducted under subcontract by the High Technology Materials Division of the Cabot Corporation. Based on the poor reproducibility of creep properties measured within the initial $1.86m^2$ ($20\ ft^2$) of this material, the primary objective of the process optimization program was redirected toward improving process reproducibility rather than fatigue strength. The approaches involved changes to the basic material chemistry (Y_2O_3 content) and variations to both the primary and secondary working procedures which would improve dispersion of the oxide strengthening phase and increase the number of grains through the sheet thickness. While substantial effort was expended and several experimental lots of material were produced with good creep properties, these properties were not reproduced in the $4.65m^2$ ($50\ ft^2$) lot of sheet fabricated at the conclusion of the Cabot program. Failure to reproduce experimental lot properties in the substantiation lot was attributed, at least in part, to a confusion of material identity during the experimental program. This confusion led to fabrication of the substantiation material with a lower than desirable Y_2O_3 content.

4.2 MA956 INITIAL PROCUREMENT

The initial 1.86m^2 (20 ft^2) lot of 1.2mm (0.048") thick sheet of MA956 lot ZDEW, was produced by the Henry Wiggin and Company, Ltd. using the commercial process current at the beginning of this contract (4th quarter of 1978). Vendor and PWA analyses of this material are listed in Table 4-I; 1100°C (2012°F) step loaded rupture properties reported by the vendor are presented in Table 4-II. These properties are consistent with those obtained on this alloy prior to initiation of this program. The moderate variability (about one order of magnitude on life) of these results is attributable to the extremely high stress sensitivity which is characteristic of ODS alloys as noted previously in figure 3-6. The lot consisted of 4 sheets, 61cm (24 in.) wide by 76.2cm (30") long delivered in the cold rolled and recrystallization annealed condition. Typical longitudinal and transverse microstructures of this material are shown in Figure 4-1. The material exhibits coarse, pancake-like grains which are elongated in both the longitudinal and long transverse directions. A uniform dispersion of 100-300 Angstrom Y_2O_3 particles is present throughout the structure. A microhardness transverse through the thickness of the sheet provided evidence of a work hardened surface layer up to 0.05 mm (0.002") deep (Table 4-III). This surface hardening is a result of grit blasting following recrystallization heat treatment to eliminate the surface oxidation that occurs during processing. As shown in Table 4-III, an 1177°C (2150°F)/30 minute/simulated Air Cool Thermal Treatment in hydrogen provides substantial recovery of this surface worked layer, with some reduction of hardness also noted in the center of the sheet.

TABLE 4-I
CHEMISTRY OF VARIOUS LOTS OF MA 956 ALLOY

Lot	Analyzed By	CR	AL	Y_2O_3	Ti	Si	Mn	B	Ni	Fe	O	N	C	AR(1)
Nominal	-	20.0	4.5	0.50	0.50	-	-	-	-	Bal	-	-	-	-
ZDEW	Wiggin	18.9	5.1	0.50	0.34	NA	NA	NA	NA	Bal	0.20	0.034	NA	NA
ZDEW	PWA	17.9	4.6	0.38	0.31	0.15	0.074	0.002	0.15	Bal	0.13	0.037	0.190	0.7
ZDCE	Wiggin	18.4	4.4	0.45	0.32	NA	NA	NA	NA	Bal	0.19	0.038	NA	NA
XBB-004	Wiggin	19.5	4.3	0.50	0.32	NA	NA	NA	NA	Bal	0.21	0.029	NA	NA
XBB-004	PWA	20.6	4.3	0.52	0.35	0.22	0.10	<0.002	0.40	Bal	0.11	0.030	0.023	NA

NA - Not Analyzed

(1) PPM

TABLE 4-II

STRESS RUPTURE STRENGTH OF MA 956 SHEET LOT ZDEW AT 1100°C (2012°F)(1)

Max. Stress, Mn/M^2	Life at Max. Stress, hr
68.9 (10.0)	14.0
58.6 (8.5)	4.0
58.6 (8.5)	5.0
68.9 (10.0)	1.0

(1) Tests conducted at INCO Research & Development Center, Sterling Forest, N.Y. Specimen loaded at 48.2 Mn/M^2 (7.0 ksi) and step-loaded 10.3 Mn/M^2 (1.5 ksi) every 24 hours until failure.

TABLE 4-III

MICRO-HARDNESS OF MA956 SHEET LOT ZDEW (CONVERTED TO ROCKWELL "C" SCALE)

As Received		Annealed 1177°C (2150°F)/30 Min/Hydrogen/Simulated Air Cool	
Center	Surface	Center	Surface
23-26	30-34	18-24	24-26

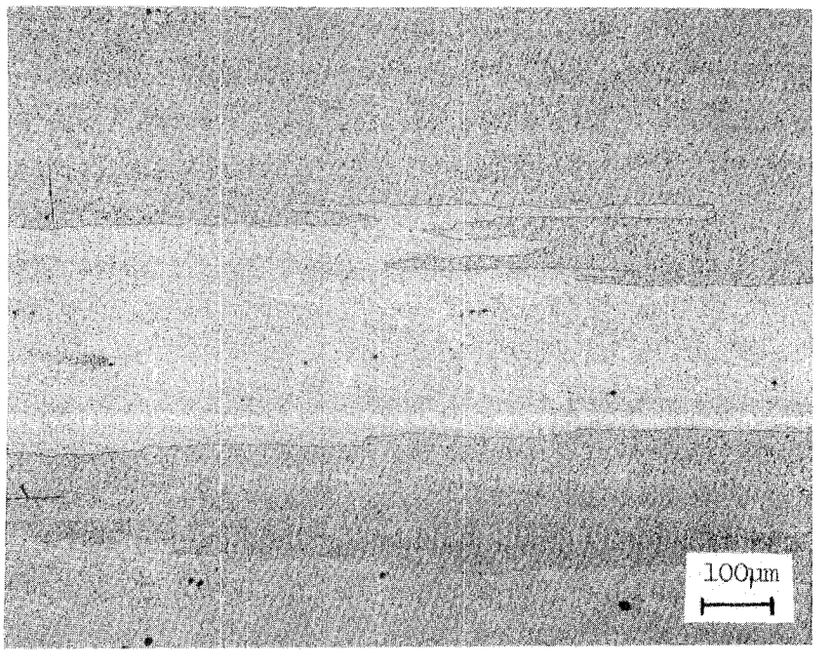

A) LONGITUDINAL

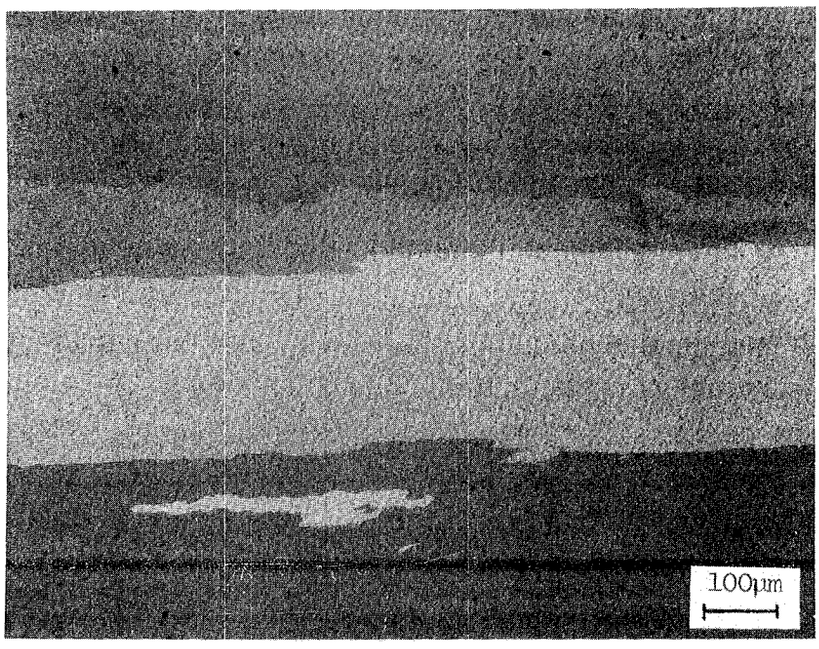

B) TRANSVERSE

Figure 4-1 As Received Microstructure of MA 956 Lot ZDEV

4.3. MA956 PROCESS OPTIMIZATION

The goal of this effort was to improve the elevated temperature fatigue capability of MA956 alloy, while maintaining the excellent formability and creep properties characteristic of commercially produced sheet. This effort was conducted under subcontract at the Inco Research and Development Center, Inc., Sterling Forest, New York. The following description of this effort is based in part on a project report submitted to PWA by Inco (Reference 4-1).

The approach to improving the elevated temperature fatigue properties of MA956 involved an attempt to refine the grain size, with a target structure of about 10 pancake grains of high aspect ratio through the ≈1.3mm (0.050") sheet thickness, as opposed to the 2 to 4 grains typically observed in commercial sheet. This structural alteration was to be accomplished by modifications to the thermomechanical processing route employed to convert the mechanically alloyed powder to sheet. As insufficient time was available for modification and scale-up of changes in MA956 powder production or consolidation, processing changes were limited to those concerning rolling and in-process annealing schedules. The overall amount of working needed to convert billet to sheet was fixed by starting and finishing product sizes.

The process optimization program plan involved initial production of sheet produced from six experimental process routings, one of which was designed to similate the commercial process. Initial characterization of these six sheet lots, including microstructural evaluation, room temperature tensile and formability (bend) testing, and 982°C (1800°F) step loaded stress rupture testing, was performed by Inco R&D. Based on evaluation of these results, the three most promising processes were selected for further evaluation, including additional formability (Erichson and deep draw cup) tests performed at Inco R&D and elevated temperature creep and low cycle fatigue testing performed at PWA. Selected results on the previously delivered commercial heat ZDEW also were included for comparison with the experimental process results.

These data were analyzed to select an optimum process. Based on this analysis, the commercial process used to produce the initially procured heat ZDEW was judged to provide the optimum balance of creep, elevated temperature low cycle fatigue, and formability in MA956 sheet. Details of these process trials and results are provided in the following paragraphs.

4.3.1 Initial Screening Test

Starting material for all process trials was a single 79.5Kg (175 lb) billet produced from powder lot ZDCE by Henry Wiggin and Company, Ltd. using standard commercial methods. Chemical analysis of this billet is reported in Table 4-I. This billet was sectioned into six pieces and each piece was converted to nominal 1.3mm (0.050") sheet by one of six different process routes selected on the basis of previous experience. Process modifications involved changes to the commercial hot rolling temperature and various process annealing sequences. The commonalities and differences among the six routes are shown in Table 4-IV. The baseline route simulated the commercial reduction practice. Following hot rolling, material from each of the six process routes was cold rolled to 1.3mm (0.050"), recrystallized 30 minutes at 1316°C (2400°F), and given a light "scotch brite" surface treatment to remove annealing scale. About $0.4m^2$ ($4\ ft^2$) of material was produced by each process, typically in the form of six pieces having nominal dimensions of 15.2 X 40.6cm (6 X 16 inch).

TABLE 4-IV

PROCESS VARIATIONS STUDIED IN MA956 PROCESS OPTIMIZATION PROGRAM

Process Route Designation	Hot Rolling Temperature	In-Process Anneal Practice
A	T1	A1
Baseline	T1	A2
B	T1	A3
C	T2	A1
D	T2	A2
E	T2	A3

Metallographic evaluation in both orthogonal in-plane directions (longitudinal and long transverse) indicated significant variations of recrystallized grain morphology produced by the various process routings. As shown in the longitudinal sections presented in Figure 4-2, the structure produced by the baseline process and modified processes A, C, and D exhibit a grain size and shape typical of commercial MA956 sheet (Figure 4-1), with perhaps a slight grain refinement and regions of finer grains near the surface. An example of this refined surface structure is shown more clearly in Figure 4-3. Processes B and E, which share the common annealing practice A3 (Table 4-IV) exhibit fine surface grains oriented near 45° to the plane of the sheet. In general, none of the processes produced the target microstructure of approximately ten uniform size grains of high aspect ratio distributed through the sheet thickness.

To provide additional information on which to base selection of the three best process routes for further evaluation, room temperature tensile and formability and 982°C (1800°F) stress rupture tests were performed on the six experimental lots at Inco R&D. All machined test specimens were given a (2150°F)/30 minute stress relief to eliminate any potential residual working resulting from specimen fabrication. Room temperature formability tests were conducted by bending sheet samples around a mandrel having a radius of twice the sheet thickness. After bending to 145°, which was the maximum bend angle permitted by the test tooling, specimens which passed this test without cracking were subsequently bent in a vice to a flat 180°. Stress ruputure tests were performed at 1800°F using a step-load procedure involving initial loading at 27.6 MN/m^2 (4Ksi) followed by successive 10.3 MN/m^2 (1.5Ksi) uploads at 24 hour intervals until failure.

The life at maximum stress then was used to calculate a stress for 20 hour life by assuming a linear relationship with a slope of -0.03 between the logarithim of the rupture stress and the logarithim of the rupture life; i.e.,

$$\ln \sigma_{20} = \ln \sigma_i - 0.03 (\ln {}_{20} - \ln t_i)$$

where σ_{20} = stress for 20 hour life

σ_i = maximum stress

t_i = life at maximum stress

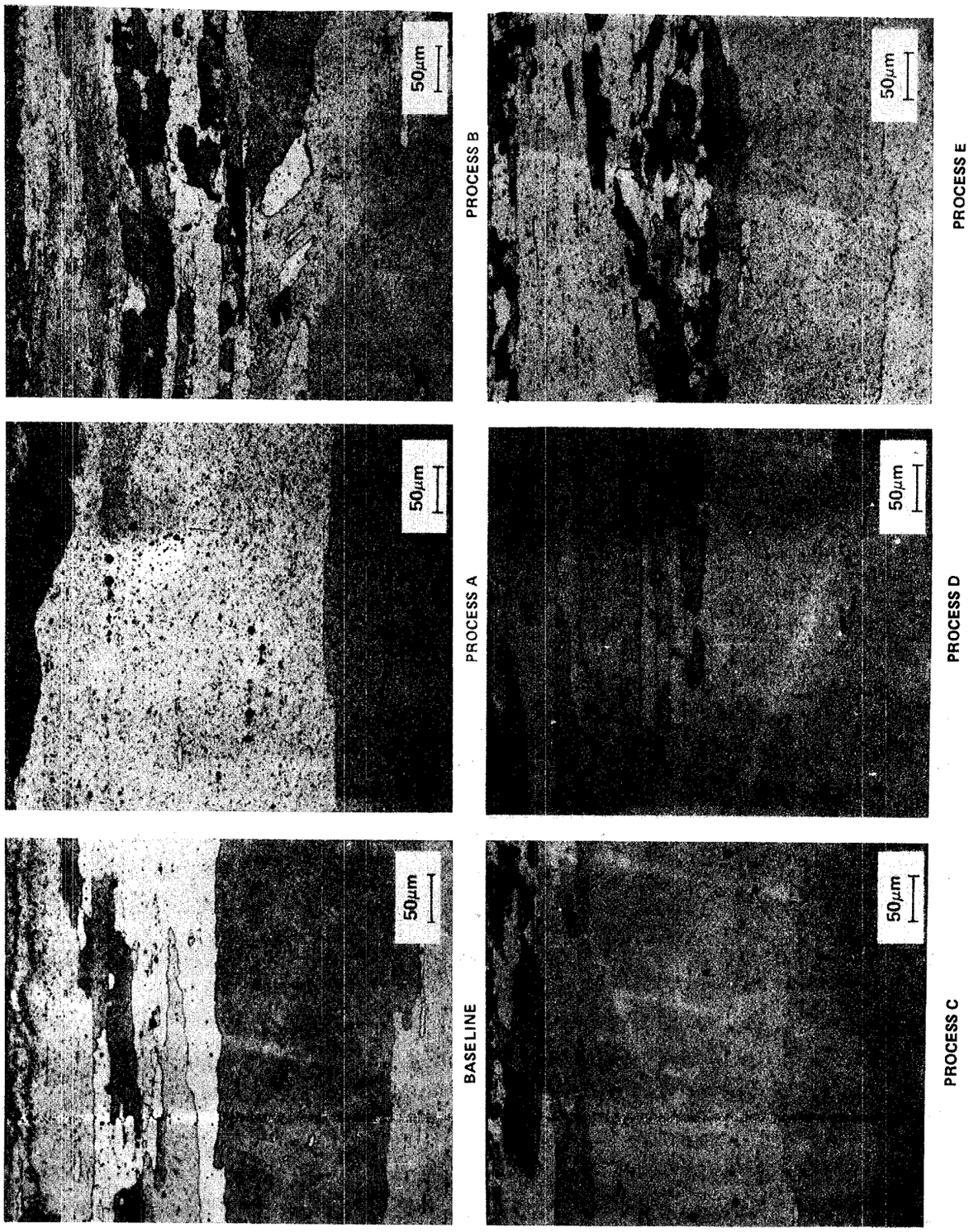

Figure 4-2 Longitudinal Microstructures Observed in MA 956 Processed by Various Methods

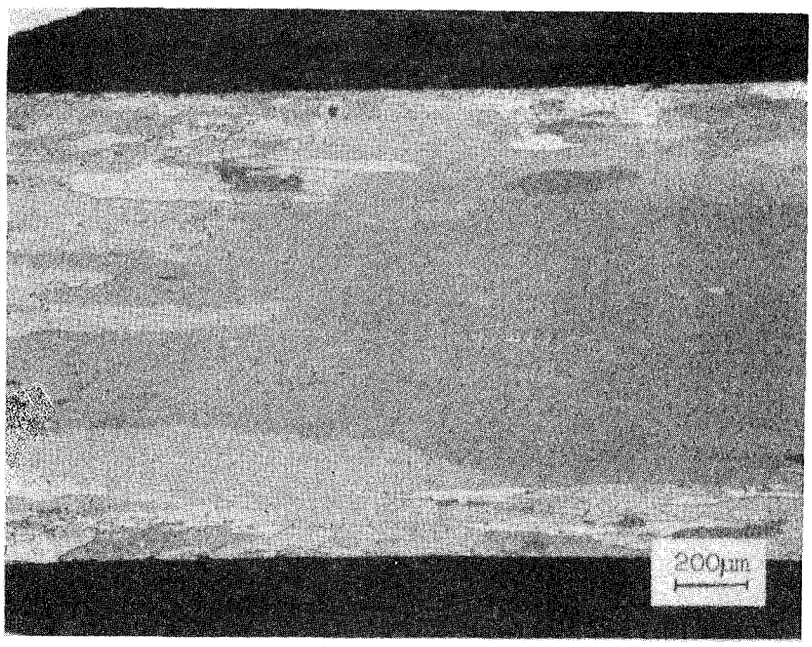

Figure 4-3 Microstructure of Experimental Baseline Process of MA 956 Showing Discontinuous Fine, Aligned Structure at Surface

Results of room temperature tensile, bend, and 982°C (1800°F) stress rupture tests conducted by Inco R&D are presented in Tables 4-V and 4-VI; tensile and stress rupture results are summarized and compared in Figures 4-4 and 4-5. All specimens but one, a transverse specimen from sheet made by process B, successfully passed both the 145/2T and the 180° bend tests. All processes provided room temperature tensile strength and ductility properties typical of commercial MA956 sheet except for processes B and D, which exhibited somewhat lower ductilities in the transverse and longitudinal directions, respectively. Except for these two moderate ductility reductions, a high level of planar isotropy of tensile properties was exhibited. Stress rupture of sheet produced by processes B and E were poor; this result is attributed to the presence of many small, high angle grains noted previously in the microstructures (Figure 4-2). While the baseline process and processes A, C, and D exhibit strengths more typical of commercial MA956 sheet, processes C and D exhibit poor isotropy of rupture strength (low transverse strength) which is attributed to the hot rolling practice common to these processes (Table 4-IV).

TABLE 4-V

ROOM TEMPERATURE FORMABILITY AND TENSILE PROPERTIES OF MA956 PROCESSED BY SIX DIFFERENT ROUTES

Tests Conducted at INCO Research Development Center, Sterling Forest, N.Y.

Process	Test Orientation	145°/2T Bend Test(1)	Tensile Properties 0.2% YS(2) MN/M²	(ksi)	UTS MN/M²	(ksi)	Elong. %
Baseline	L	No Cracks	535.7	(77.7)	639.9	(92.8)	12.0
	L	No Cracks	526.8	(76.4)	615.7	(89.3)	10.0
	T	No Cracks	528.2	(76.6)	643.3	(93.3)	12.0
	T	No Cracks	521.3	(75.6)	630.9	(91.5)	12.0
A	L	No Cracks	528.8	(76.7)	625.4	(90.7)	14.0
	L	No Cracks	539.2	(78.2)	637.1	(92.4)	13.0
	T	No Cracks	522.6	(75.8)	630.9	(91.5)	15.0
	T	No Cracks	526.1	(76.3)	645.4	(93.6)	13.0
B	L	No Cracks	560.6	(81.3)	696.4	(101.0)	12.0
	L	No Cracks	587.4	(85.2)	698.5	(101.3)	11.0
	T	No Cracks	568.8	(85.2)	679.2	(98.5)	9.0
	T	Fine Cracks	578.5	(83.9)	699.8	(101.5)	10.0
C	L	No Cracks	521.3	(75.6)	617.1	(89.5)	12.0
	L	No Cracks	515.7	(74.8)	612.3	(88.8)	13.0
	T	No Cracks	513.0	(74.4)	633.0	(91.8)	15.0
	T	No Cracks	518.5	(75.2)	650.9	(94.4)	11.0
D	L	No Cracks	519.9	(75.4)	615.0	(89.2)	12.0
	L	No Cracks	501.3	(72.7)	573.7	(83.2)	7.0
	T	No Cracks	519.3	(75.4)	635.7	(92.2)	15.0
	T	No Cracks	531.6	(77.1)	660.5	(95.8)	13.0
E	L	No Cracks	510.2	(74.0)	638.5	(92.6)	10.0
	L	No Cracks	542.6	(78.7)	668.8	(97.0)	12.0
	T	No Cracks	528.8	(76.7)	664.0	(96.3)	15.0
	T	No Cracks	530.9	(77.0)	664.7	(96.4)	14.0

(1) Note that all specimens which passed the 145° bend test subsequently were bent to 180° in a vice with no cracks observed.

(2) Crosshead Rate = 0.30 mm/mm/min

TABLE 4-VI

982°C (1800°F) STRESS-RUPTURE PROPERTIES OF MA956 PROCESSED BY SIX DIFFERENT ROUTES

Tests Conducted at INCO Research Development Center, Sterling Forest, N.Y.

Process	Test Orientation	Maximum Stress(1) MN/m²	(ksi)	Rupture Life(2) hr.	Elong %	Calculated Stress for Rupture in 20 Hours MN/m²	(ksi)
Baseline	L	69.0	(10.0)	3.8	7.1	65.5	(9.5)
	L	58.6	(8.5)	15.4	4.4	57.9	(8.4)
	T	58.6	(8.5)	0.1	2.7	50.3	(7.3)
	T	48.3	(7.0)	16.0	4.4	48.3	(7.0)
A	L	69.0	(10.0)	5.1	4.4	66.2	(9.6)
	L	69.0	(10.0)	19.9	4.4	69.0	(10.0)
	T	58.6	(8.5)	3.5	2.7	55.8	(8.1)
	T	58.6	(8.5)	3.2	4.4	55.2	(8.0)
B	L	37.9	(5.5)	0.2	3.6	33.1	(4.8)
	L	37.9	(5.5)	12.4	3.6	37.2	(5.4)
	T	27.6	(4.0)	18.0	1.8	27.6	(4.0)
	T	27.6	(4.0)	13.8	1.8	27.6	(4.0)
C	L	69.0	(10.0)	13.1	5.3	68.3	(9.9)
	L	69.0	(10.0)	11.6	4.4	67.6	(9.8)
	T	48.3	(7.0)	10.2	(3)	47.6	(6.9)
	T	48.3	(7.0)	5.7	4.4	46.2	(6.7)
D	L	58.6	(8.5)	23.9	3.6	58.6	(8.5)
	L	69.0	(10.0)	5.8	5.3(4)	66.2	(9.6)
	T	48.3	(7.0)	0.1	3.6	41.4	(6.0)
	T	48.3	(7.0)	7.3	2.7	46.9	(6.8)
E	L	37.9	(5.5)	2.6	3.6	35.8	(5.2)
	L	37.9	(5.5)	2.1	5.3	35.2	(5.1)
	T	27.6	(4.0)	9.7	(3)	26.9	(3.9)
	T	27.6	(4.0)	10.2	1.8	26.9	(3.9)

(1) Step loaded as follows:

27.6 Mn/M² (4 ksi)/24hr + 37.9 Mn/M² (5.5 ksi)/24 + 48.2 Mn/M² (7 ksi)/24 hr + 58.6 Mn/M² (8.5 ksi)/24 hr + 68.9 Mn/M² (10 ksi)/24 hr (see text)

(2) Life = Time at Failure (maximum) Stress

(3) Not Measured (Double fracture in gage length)

(4) Broke on gage mark

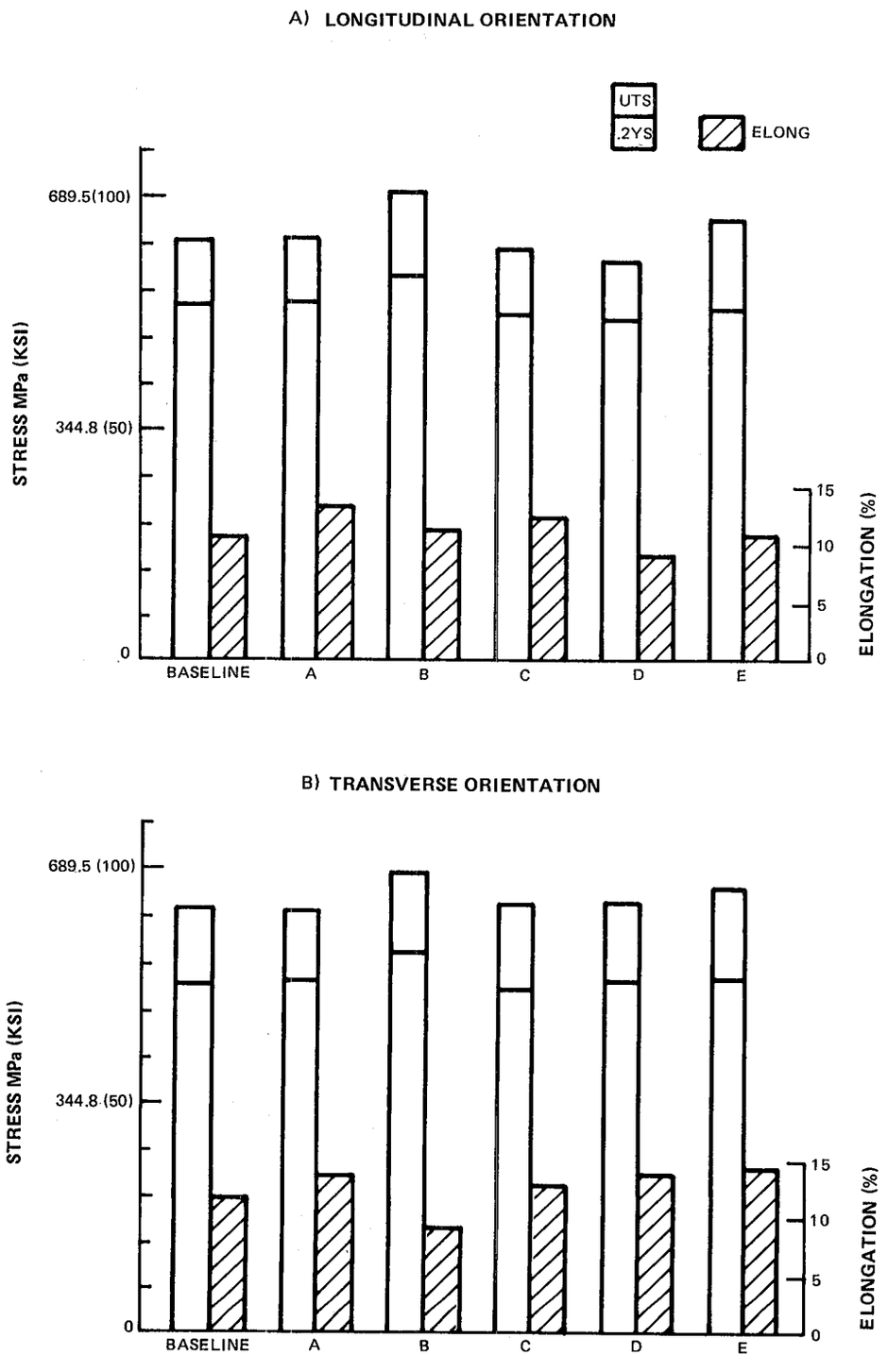

Figure 4-4 Room Temperature Tensile Properties of MA 956 Produced by Six Processing Routes

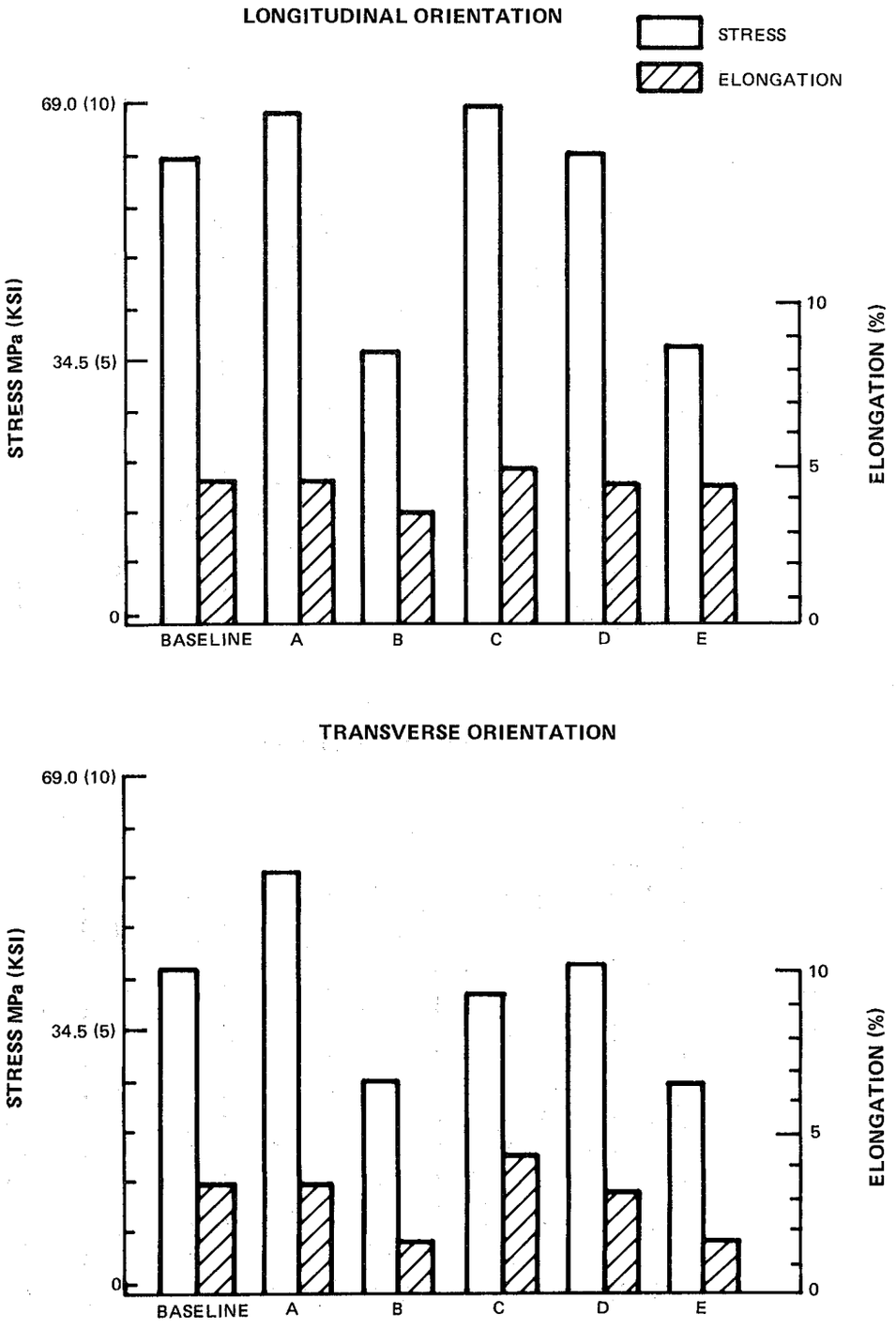

Figure 4-5 Stress-Rupture Properties of MA 956 Produced by Six Processing Routes (Stress to produce rupture in 20 Hrs. at 982°C(1800°F)).

Based on the results described above, the baseline process and processes A and C were selected for further evaluation. Processes B and E were eliminated on the basis of poor stress rupture properties, while process D was eliminated on the basis of poor transverse rupture strength and somewhat reduced longitudinal tensile ductility.

4.3.2 Screening of Selected Processes

Further evaluations of the three selected processes (baseline process, process A, and process C) included additional formability (Erichson Cup and deep draw cup) tests performed at Inco R&D center together with through thickness microhardness measurements, Olsen Cup formability, 871 and 932°C (1600 and 1800°F) low cycle fatigue, and 982°C (1800°F)/62.1 MN/m^2 (9Ksi) creep tests conducted at PWA. All Task IIIA commercial lot ZDEW formability, LCF, and creep rupture results which were available at the time this task was performed were used for comparison with results on the experimental lots. In the Erichson Cup test, cup height at failure rates the stretchability of the sheet, with greater height indicating improved stretchability. Deep drawing behavior was rated by the critical blank diameter (diameter of the largest blank that can be successfully drawn) as determined in the deep draw test. Details concerning the low cycle fatigue and creep tests can be found in Section 5.1.

Microhardness measurements on the three selected experimental lots, which received a light "scotch brite" treatment following the 1316°C (2400°F) recrystallization anneal, indicated no work hardened surface such as was observed on the commercially produced grit blasted lot ZDEW.

Results of room temperature formability tests (Table 4-VII) indicate no significant differences among the three experimentally produced sheet lots or between the experimentally and commercially produced sheet, despite the surface worked layer on the commercial material. This observation is consistent with results obtained on annealed specimens in Task IIIa, (Section 5.1), which indicate that this surface worked layer does not significantly affect MA956 formability.

TABLE 4-VII

ROOM TEMPERATURE FORMABILITY OF MA956 FROM SELECTED PROCESSING ROUTES

Process	(1) Olsen Cup Depth mm. (in.)	(2) Erichsen Cup Depth mm. (in.)	(3) Deep Draw Blank Diameter mm. (in.)	No. Tested	No. Passed
Experimental:					
Baseline	8.0 (0.315) 8.5 (0.334)	8.9 (0.35) 8.6 (0.34) 8.9 (0.35)	55.9 (2.2) 54.0 (2.1)	3 3	0 3
A	8.3 (0.328) 8.4 (0.330)	8.9 (0.35) 8.6 (0.34) 8.9 (0.35)	55.9 (2.2) 54.0 (2.1)	3 3	1 3
C	8.0 (0.315) 8.4 (0.330)	8.9 (0.35) 8.6 (0.34) 8.4 (0.33)	55.9 (2.2)	3	2
Commercial:					
lot ZDEW	8.3 (0.325) 8.5 (0.335)	>7.1 (>0.28)	54.0 (2.1)	3	2

1 Tests conducted at PWA using no lubricant

2 Tests conducted at INCO Research & Development Center using the following conditions:

Punch	22 mm (7/8 inch) dia bolt
Die	25 mm (1 inch) dia.
Clamping force	908 Kg (2000 lb)
punch speed	25 mm (1 inch)/minute
lubrication	Oil and polyethylene sheet

3 Tests conducted at INCO Research and Development Center using the following conditions:

Punch	32 mm (1.26 inch) dia. flat bottom
Die	34.44 mm (1.36 inch) dia.
Clamping force	454kg (1000 lb)
Punch Speed	25 mm (1 inch)/minute
Lubrication	Oil & Polyethylene sheet

Low cycle fatigue results are presented in Table 4-VIII and compared in Figure 4-6. At 871°C (1600°F), material from Processes A and C display comparable LCF lives to the commercially processed material (lot ZDEW), while the experimentally processed Baseline, processed to the nominal commercial route, shows lower LCF life. However, at 982°C (1800°F) the commercially processed material displays superior LCF lives compared to all three experimentally processed sheets which are similar in life.

TABLE 4-VIII

LOW CYCLE FATIGUE PROPERTIES OF MA956 PRODUCED BY SELECTED PROCESSING ROUTES

(Fully Reversed Bending, ±0.25% Strain, 0.67Hz)

Temperature °C (°F)	Process:	Life (cycles to failure)			
		Commercial		Experimental	
		ZDEW	Baseline	A	C
871 (1600)		3540	5337	3900	4780
871 (1600)		4840	3144	7410	7099
871 (1600)		7150	3366	4508	5054
Average		5177	3939	5273	5644
982 (1800)		3320	2323	2898	3117
982 (1800)		4650	2809	2857	1466
982 (1800)		2700	-	2603	3023
Average		3557	2566	2786	2535

Creep test results (Table 4-IX and Figure 4-7) indicate the experimentally processed baseline material to be superior in rupture life to material produced by processes A and C; however, the commercially processed heat ZDEW exhibits better creep-rupture life and ductility than any of the experimentally processed materials. This result may be attributable to the somewhat finer surface grain structure of the experimentally processed material (Figure 4-3). Longitudinal ductilities of the commercial heat are significantly in excess of the 0.1% limit used in the Task I component life prediction system, indicating that MA956 life predictions made in Task I should be conservative.

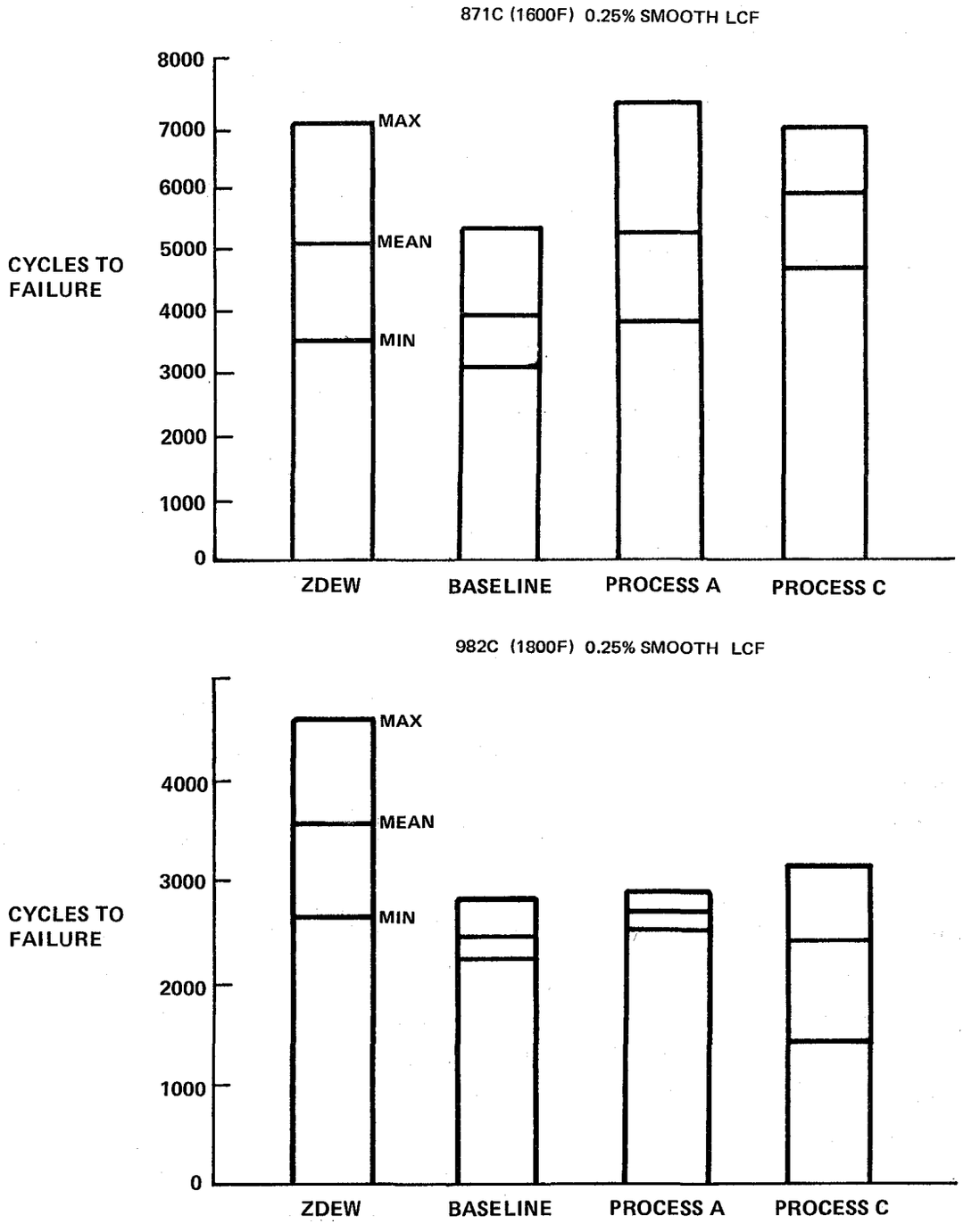

Figure 4-6 Low Cycle Fatigue Lives of MA 956 Produced by Selected Processing Routes

TABLE 4-IX

982°C (1800°F) CREEP-RUPTURE PROPERTIES OF MA956 FROM SELECTED PROCESSING ROUTES

Process	Orientation	Stress MN/m^2	Stress (ksi)	Time to 0.1% Creep (hr)	Rupture Life (hr)	Prior[3] Creep %
ZDEW	L	62	(9)	1.5	4555.7[1]	0.81[1]
(Commercial)	L	62	(9)	8.0	4555.6[1]	0.52[1]
	L	69	(10)	34.4	4175.6	---(2)
ZDEW	T	62	(9)	42.2	109.2	0.15
(Commercial)	T	62	(9)	35.3	304.7	0.13
Baseline	L	62	(9)	42.9	398.0	0.23
	L	62	(9)	42.1	1346.2[1]	0.23[1]
Baseline	T	62	(9)	16.5	223.2	0.24
	T	62	(9)	18.5	70.0	0.15
A	L	62	(9)	3.7	4.6	0.21
	L	62	(9)	1.1	1.5	0.12
A	T	62	(9)	0.4	1.5	0.21
	T	62	(9)	1.0	2.3	0.17
C	L	62	(9)	27.6	54.5	0.15
	L	62	(9)	33.4	129.1	0.24
C	T	62	(9)	0.4	1.3	0.20
	T	62	(9)	0.3	0.9	0.21

(1) Test Discontinued, No Failure

(2) Suspect Data-Not Reported

(3) Creep Strain immediately prior to (within two hours of) failure

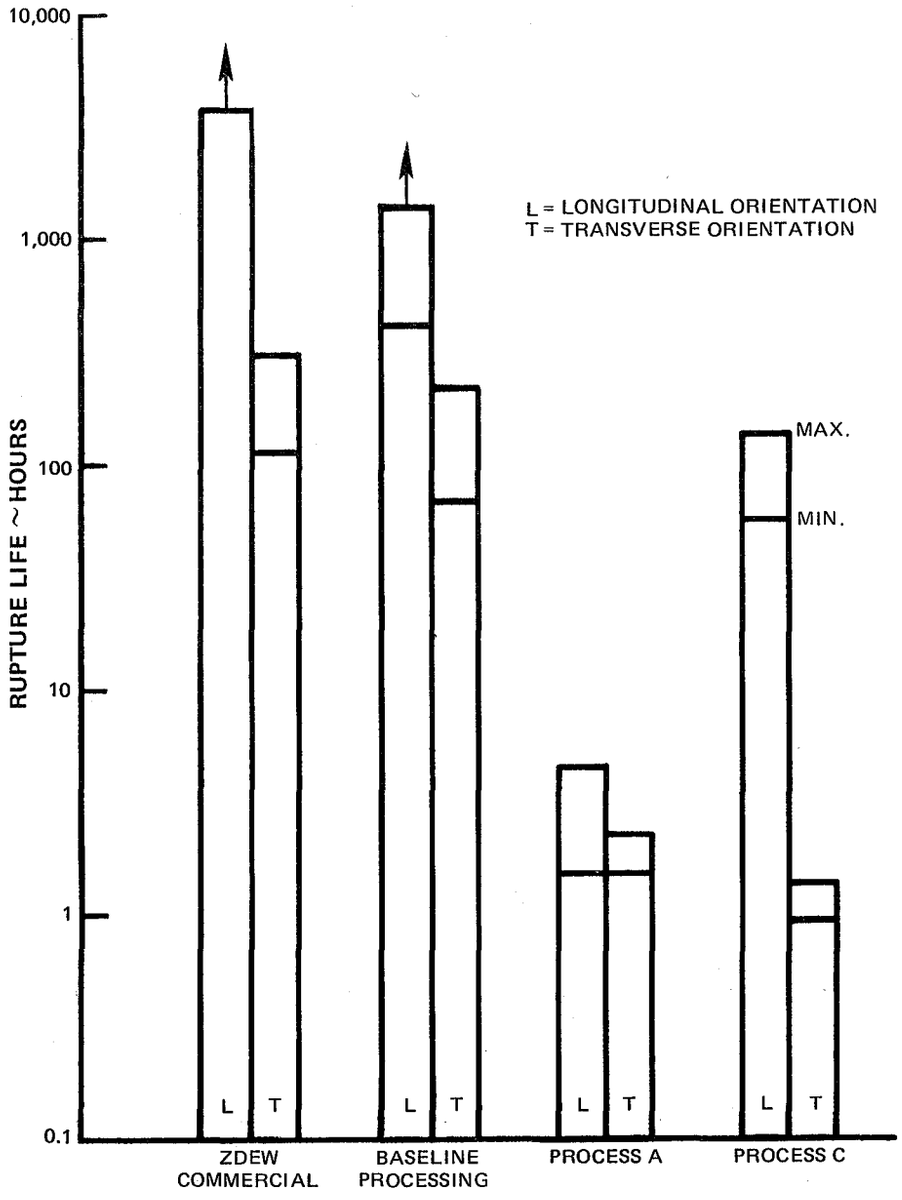

Figure 4-7 Creep-Rupture Properties of MA 956 at 982°C(1800°F)/62 MN/m^2 (9 ksi)

Based on the results discussed above, an optimum process routing was selected. All data generated on the three laboratory sheet lots and the commercial sheet lot were analyzed and individually ranked from 1 to 3, with 1 indicating the best performance. A decision analysis chart then was constructed, see Table 4-X. Based on this analysis, the sheet lot with the best (lowest) score was ZDEW, the commercial sheet lot. The commercial process current at the beginning of this program thus was selected as the optimum process for production of MA956 sheet.

TABLE 4-X

DECISION ANALYSIS CHART - MA956 PROPERTY RANKINGS

	Creep Rupture				LCF			
Process	Transverse Life	Longitudinal Life	Transverse Prior Creep	Longitudinal Prior Creep	1600°F Life	1800°F Life	Formability	Score
A	3	3	2	2	2	2	2	16
Baseline	2	1-2	2	2	2^+	2	2	13^+-14^+
C	3	2	2	2	2	2	2	15
Commercial (ZDEW)	2	1	2	1	2	2^-	2	12^-

Code: 1 = Excellent
2 = Good-Average
3 = Poor

- = Slightly Better
+ = Slightly Worse

4.4 MA956 PROCESS CONTROL AND REPRODUCIBILITY DEMONSTRATION

To demonstrate reproducibility of the selected process, and to provide material for use in the balance of the program, a 5.1m^2 (55ft^2) lot of MA956 sheet (lot XBB-004) was produced by Henry Wiggin & Company Ltd. Chemical analysis and results of 1100°C (2012°F) rupture tests performed at Wiggin are presented respectively in Tables 4-I and 4-XI; typical microstructures are shown in Figure 4-8. Microhardness of this sheet was in the range of Rc 21 to 24 throughout the sheet thickness, with no apparent work hardened surface layer such as that found in the grit blasted sheet from lot ZDEW. Approximtely 0.5m^2 (5 ft^2) of this material was delivered to Inco Research & Development Center for formability, tensile, and stress rupture evaluation prior to delivery of the remaining 4.6m^2 (50 ft^2) to P&WA. As was done with previous tests, all mechanical property specimens were stress relieved for 30 minutes at 1177°C (2150°F) prior to testing. Results of these tests

(Table 4-XII) indicate that the properties of lot XBB-004 are comparable to or better than those of the initial lot ZDEW, thus demonstrating the required commercial reproducibility of MA956 sheet manufacture. To assure continued reproducibility in future lots of MA956 sheet, a process control specification for control of commercial sheet manufacture was developed for the optimum commercial process. This specification is reproduced in Table 4-XIII.

TABLE 4-XI

STRESS RUPTURE STRENGTH AT 1100°C (2012°F) (1)

MA956 Lot XBB-004

Test Orientation	Max Stress MN/M^2	(ksi)	Life at Max. Stress (hr)
L	79.2	(11.5)	10
	79.2	(11.5)	10
T	68.9	(10.0)	23
	58.6	(8.5)	5

(1) Tests conducted at Henry Wiggin & Company, Ltd.; Specimen loaded at 48.2 Mn/M^2 (7.0 ksi) and step-loaded 10.3 Mn/M^2 (1.5 ksi) every 24 hours until failure

LONGITUDINAL TRANSVERSE

Figure 4-8 Microstructure of MA 956 Lot XBB-004

TABLE 4-XII

ACCEPTANCE EVALUATION OF MA956 LOT XBB-004

(Tests Conducted At INCO Except As Noted)

Formability

145°/180° From Temperature Bend Tests[1]

Orientation	Results
L	No Cracks
L	No Cracks
T	No Cracks
T	No Cracks

P&W Bend Tests: 2T Pass

Erichsen Cup Depth[2]

mm	(in)	
9.6	(0.38)	
9.4	(0.37)	Conducted by INCO
8.1	(0.32)	
8.0	(0.32)	
8.5	(0.38)	Conducted by P&W
8.7	(0.34)	

Deep Draw Cup Depth[2]

Blank Diameter mm (in)	Number Tested/ Passed
54 (2.13)	3/3
56 (2.20)	3/3

Mechanical Properties

RT Tensile

Orientation	0.2% YS MN/M^2(ksi)	UTS MN/M^2(ksi)	Elongation %
L	559.9 (81.2)	641.9 (93.1)	14
L	553.0 (80.2)	653.6 (94.8)	12
T	574.4 (83.3)	689.5 (100.0)	5*
T	575.7 (83.5)	708.1 (102.7)	12

* Specimen broke at gage mark

o 982°C (1800°F) Stress-Rupture[3]

Orientation	Maximum Stress Mn/M^2 (ksi)	Life at Maximum Stress Hours	Elongation %	Calculated Stress for 20 Hour Life, Mn/M^2(ksi)
L	58.7 (8.5)	14.1	3.1	57.9 (8.4)
L	69.0 (10.0)	4.6	3.1	66.2 (9.6)
T	69.0 (10.0)	5.9	3.6	66.2 (9.6)
T	69.0 (10.0)	9.7 (4)	-	>67.6 (>9.8)

(1) See text for procedures

(2) See Table 4-VII for test conditions

(3) Loading Sequence: 37.9 Mn/M^2 (5.5 ksi) 24 hour + 48.3 Mn/M^2 (7 ksi) 24 hours + 58.6 Mn/M^2 (8.5 ksi) 24 hour + 69.0 Mn/M^2 (10 ksi) 24 hour until failure

(4) Grip Failure

TABLE 4-XIII

PROCESS CONTROL SPECIFICATION FOR COLD ROLLED AND FULLY HEATED TREATED MA956 SHEET

1) Mechanically Alloy powder.
2) Blend powder.
3) Fill mild steel can.
4) Extruded to sheet bar using preheat temperature in range 1000 - 1150°C (1832 - 2102°F).
5) Prepare for hot rolling. Decan and surface grind.
6) Hot roll to the required hot rolled gauge using preheat temperature range of 1000 - 1150°C (1832 - 2102°F).
7) Shear to remove edge cracks.
8) Pickle.
9) Cold roll to required gauge.
10) Anneal.
11) Straighten.
12) Shear to required size.
13) Vac blast both sides of sheet.
14) Test to specification requirements.
15) INSPECT.

4.5 HDA 8077 INITIAL PROCUREMENT

The initial 1.86m^2 (20 ft^2) of HDA8077 alloy was supplied by the High Technology Materials Division of the Cabot Corporation in the form of three lots, designated MS151, MS153, and MS154, processed by nominally identical routes from a common powder blend. Chemical analysis of this material is reported in Table 4-XIV; microstructures of each lot are shown in Figure 4-9. The material consists of coarse, pancake-like grains which are elongated in both the longitudinal and long-transverse directions. As indicted by comparison of Figures 4-9 a and b, the microstructure of HDA8077 is isotropic in the plane of the sheet as a result of cross rolling during processing. Comparison of Figures 4-9 b, c, and d indicates that the microstructure is not consistent, with islands of fine, unrecrystalized grains being present in amounts which vary from lot-to-lot. Microhardness traverses through the thickness of sheets from each lot indicated a work hardened surface layer up to 0.05mm (0.002 inches) deep in lot MS154 (Table 4-XV). This surface hardening is presumed to result from grit blasting to remove surface oxidation after recrystallization heat treatment. HDA8077 normally is pickled after grit blasting; for the MS151 and MS153 sheets, the work hardened surface apparently was removed during chemical pickling. As indicated in Table 4-XV, an 1177°C (2150°F)/30 minute/Hydrogen/Simulated air cool stress relief provided some recovery of the work hardened surface layer of MS154 without producing any surface recrystallization, but caused some through-thickness hardening as a result of γ' precipitation. To prevent through thickness hardening, subsequent property evaluations were performed using a rapid cool from the stress relief temperature.

TABLE 4-XIV
CHEMICAL ANALYSIS OF HDA-8077 SHEET

Lot	Analyzed By	CR	AL	Y_2O_3	Ti	Si	Mn	B	Ni	Fe	O	N	C	He(2)
Nominal	-	16.0	4.0	0.80	-	-	-	-	Bal.	-	-	-	-	-
MS151	Vendor	15.9	4.1	0.98	NA	NA	NA	NA	Bal.	0.25	NA	NA	NA	NA
MS153 (1)														
MS154	PWA	15.8	3.8	1.13	0.01	0.04	0.002	0.004	Bal.	0.23	0.42	0.039	0.035	1.2
Lot C	PWA	16.2	3.9	0.80	0.03	0.02	0.06	0.002	Bal.	-	0.07	0.025	0.021	NA

NA = Not Analyzed

(1) Representing Common Chemistry of Three indicated lots produced from common starting stock

(2) PPM

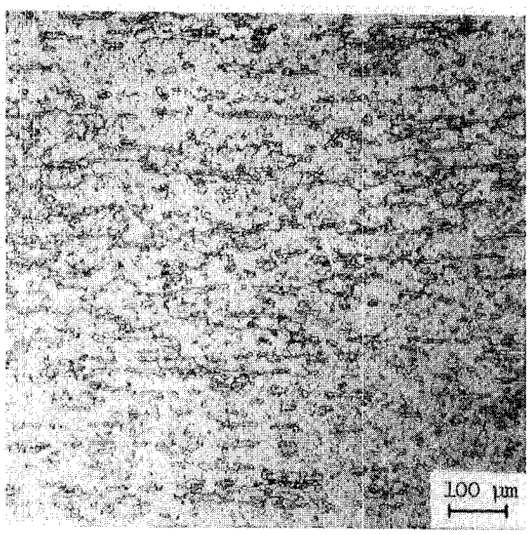

A) LOT MS - 151 TRANSVERSE

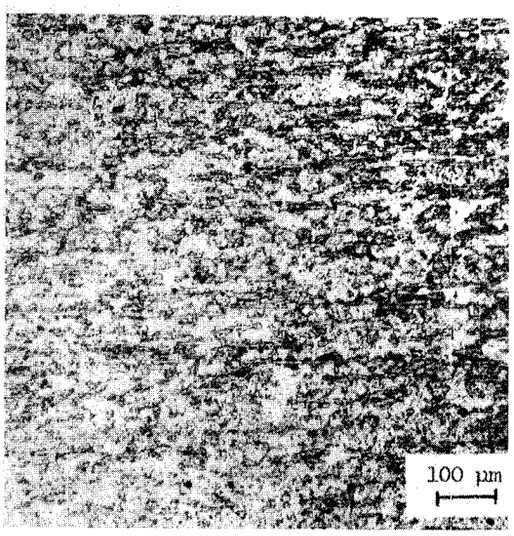

B) LOT MS 151 LONGITUDINAL

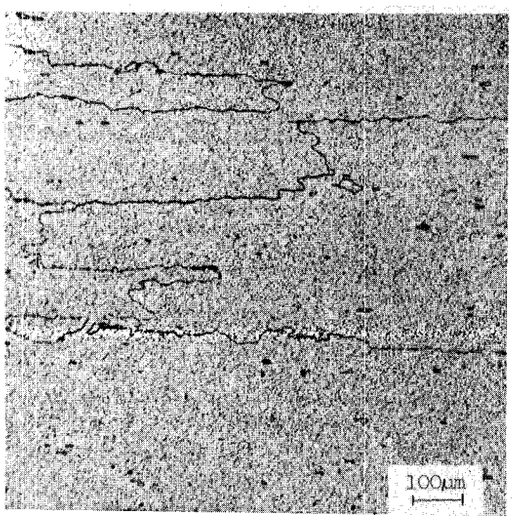

C) LOT MS - 153 LONGITUDINAL

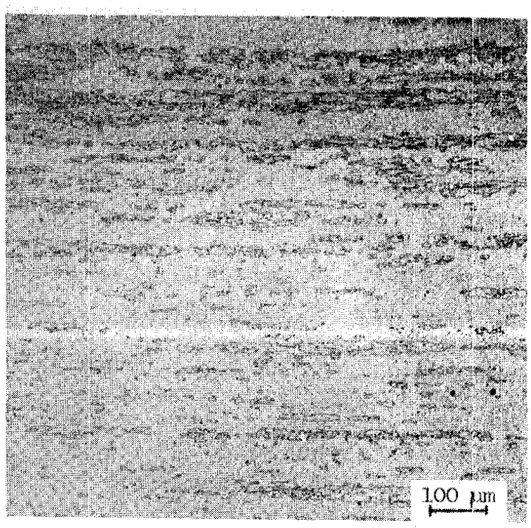

D) LOT MS - 154 LONGITUDINAL

Figure 4-9 Microstructures of Three Initial Lots of HDA 8077

TABLE 4-XV

MICROHARDNESS OF HDA8077 SHEET
(Converted to Rc)

	As Received		Annealed 1177°C (2150°F)/30 min./Hydrogen/ Simulated Air Cool	
	Center	Surface	Center	Surface
Lot MS151	22-26	22-26	30-33	30-33
Lot MS153	24-29	24-29	---	---
Lot MS154	25-29	30-35	31-34	31-34

4.6 HDA8077 PROCESS OPTIMIZATION

Early results of property tests conducted on Task IIIa (Section 5.1), which were obtained prior to initiation of this process optimization effort, indicated substantial property variability among the three initial lots of HDA8077. The property which varied most was creep-rupture life, which exhibited over four orders-of-magnitude spread among the three lots. Because of this variability, the objective of the process optimization program was redirected from fatigue life improvement to improvement of process reproducibility. This effort was conducted under subcontract by the High Technology Materials Division (formerly Stellite Division) of the Cabot Corporation. Some of the results of this effort are summarized in Reference 4-2. The reader is cautioned that the Y_2O_3 oxide contents reported in Table 3 of Reference 4-2 are incorrect, as discussed in the following paragraphs.

The initial plan called for six experimental process routings to be investigated, with the best three of these to be further screened for selection of an optimum process which then would be substantiated through production of 4.65m^2 (50 ft^2) of material for use in subsequent tasks. In the modified plan, seven billets were produced using two different primary consolidation procedures, as shown in Table 4-XVI. Variation of nominal aluminum and dispersoid (Y_2O_3) contents were evaluated with one of the two primary consolidation routes. Secondary breakdown variables investigated included rolling temperature and direction, reduction per pass, and heat treatment parameters (temperature and cooling rate).

TABLE 4-XVI

Primary consolidation method and nominal Al and Y_2O_3 composition of 22.7kg (50 lb) billets used for the initial Cabot High Technology Material Division Process Optimization program.

Billet No.	Consolidation Method	Nominal composition (wt. %) Al	Y_2O_3
1, 2, 3	Forge	4.2	1.25
4	Hip	4.2	1.25
5	Hip	4.6	1.00
6	Hip	4.6	1.25
7	Hip	4.6	1.50

Evaluation of hot rolled sheet processed from these seven billets indicated that consistent microstructures were not produced. A review of these and earlier results suggested that much of this variation might be attributable to initial powder producing techniques and to the mechanical alloying parameters.

As a result of this review, a second process optimization program was initiated to provide sheet with consistent properties. Thirteen 2.27Kg (5lb) billets were formulated using different powder lots than were used for the previous large billets. Specific powder blends used to produce each of these thirteen billets are shown in Table 4-XVII. All billets were separately processed using nominally identical parameters to yield sheets approximately 305 mm x 305 mm (12 in X 12 in). A 50.8 mm (2 inch strip) was cut from the end of each sheet and was annealed at 1343°C (2450°F) for recrystallization. After pickling with an HCl-H_2O_2 solution to remove any surface work hardening and oxidation, each sheet was evaluated using room temperature cup and bend tests and at 982°C (1800°F)/82.7 mN/m^2 (12 ksi) creep-rupture tests.

TABLE-XVII

Powder lots used to produce 2.27 kg (5 lb) billets for the Cabot High Technology Materials Division Process Optimization Program.

Billet No.	Powder Lot
MS 208, 211, 212	At 426
MS 213, 214	AT 427
MS 215 - 222	AT 430(1)

(1) Blend of AT 428 & AT 429

As shown by the typical microstructure presented in Figure 4-10, the microstructures of these sheets were consistent and exhibited little of the fine, unrecrystallized grain structure such as that seen in some of the initial sheet lots (Figure 4-9). Formability and creep test results obtained on the thirteen experimental lots are reported in Table 4-XVIII. While the ability of some of these sheets to pass a 180° bend test was marginal, variation of cup formability from lot-to-lot and within sheet lots was somewhat less than seen previously. Significant inter and intra-lot variability of rupture life continued to be exhibited, however, indicating that a consistent and reproducible process had yet to be achieved.

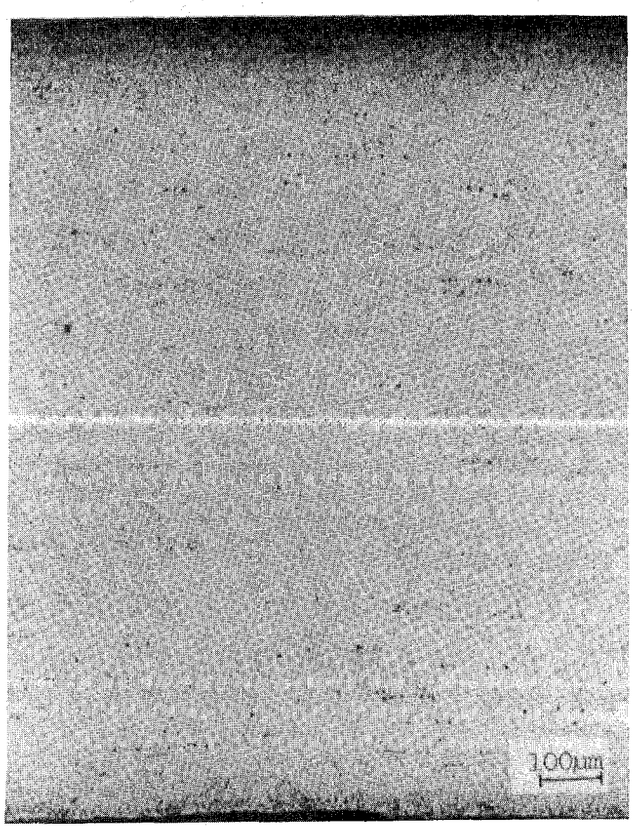

Figure 4-10 Microstructure of HDA 8077 Sheet MS 222

TABLE 4-XVIII

PROPERTIES OF SHEETS PRODUCED IN CABOT HDA 8077 SMALL BILLET PROGRAM

Lot Number	Cup Depth mm (inch)	180° Bend (Pass/No. of Tests)	Creep at 982°C (1800°F) and 92.7 MN/m^2 (12 ksi) Rupture Life (hrs)	Time to 0.1% (hrs)	Time to 0.5% (hrs)	Prior[1] Creep (%)	RT Elong. (%)
MS 208	6.10 (0.260)	0/4; 3/4	9.8	0.1	--	0.38	6.8
	7.49 (0.295)		0.2	--	--	--	14.3
	8.64 (0.340)		0.2	--	--	0.58	6.9
			50.1	2.5	45.5	0.57	1.2
			98.1	6.0	86.5	0.53	1.2
			330.4	4.0	232.0	0.79	3.6
			179.2	3.0	--	0.45	1.0
			6.8	1.5	--	0.40	3.6
MS 211	7.49 (0.295)	6/6	10.0	0.5	8.9	0.58	3.5
	7.37 (0.290)						
	7.87 (0.310)						
MS 212	6.60 (0.260)	4/6	39.7	1.0	33.3	0.71	9.2
	7.11 (0.280)						
	7.62 (0.300)						
MS 213	7.62 (0.300)	6/6	8.6	0.4	5.7	1.17	3.1
	8.26 (0.325)						
	8.51 (0.335)						
MS 214	7.37 (0.290)	6/6	26.4	2.2	--	0.46	5.1
	7.62 (0.300)						
	8.89 (0.350)						
MS 215	10.41 (0.410)	1/6; 3/4	20.3	1.0	13.6	0.89	4.4
	8.64 (0.340)						
	8.26 (0.350)						
MS 216	8.51 (0.335)	6/6	61.0	--	--	--	6.2
	9.40 (0.370)						
	10.16 (0.400)						
MS 217	7.37 (0.290)	4/6	3.6	0.6	--	0.31	3.6
	8.51 (0.335)						
	9.65 (0.380)						

TABLE 4-XVIII (Continued)

Lot Number	Cup Depth mm (inch)	180° Bend (Pass/No. of Tests)	Creep at 982°C (1800°F) and 92.7 MN/m² (12 ksi) Rupture Life (hrs)	Time to 0.1% (hrs)	Time to 0.5% (hrs)	Prior[1] Creep (%)	RT Elong. (%)
MS 218	7.75 (0.305)	6/6	8.7	0.1	3.8	1.64	8.6
	8.26 (0.325)						
	8.26 (0.325)						
MS 219	7.49 (0.295)	6/6	0.3	--	--	--	4.4
	7.49 (0.295)		13.2	0.6	9.4	0.64	2.5
	8.84 (0.350)		15.8	3.8	15.3	0.51	6.8
			2.3	0.3	1.9	0.57	3.2
			9.2	0.5	5.1	1.04	3.1
			2.7	0.3	--	0.15	1.9
MS 220	7.75 (0.305)	6/6	1.7	0.1	1.0	1.05	14.2
	9.02 (0.355)		19.8	7.7	19.0	0.57	6.0
			35.1	0.3	14.4	1.09	3.7
			72.5	0.9	54.0	0.66	3.6
			103.2	2.5	79.2	0.57	2.7
MS 221	7.62 (0.300)	6/6	23.6	0.5	20.8	0.63	1.3
	7.75 (0.305)						
	8.89 (0.350)						
MS222	7.62 (0.300)	2/6	12.3	2.0	--	0.39	4.4
	7.75 (0.305)		23.2	0.1	11.9	1.01	4.4
	8.26 (0.325)		16.9	0.6	10.6	1.30	10.0
			2.7	0.5	--	0.20	0.9
			209.8	0.5	45.0	1.68	--

(1) Creep strain immediately prior to (within two hours of) failure.

In an effort to identify the cause of rupture life variation in these thirteen HDA8077 sheet lots, a number of process and mechanical test variables were evaluated as to their effect on rupture life. No correlation was found between rupture life and creep test machine. While the large scatter of properties within any one sheet prevented a rigorous correlation of properties with small process differences among the nominally identical sheets, no life correlation appeared to exist between sheets processed at different times.

Because of the difficulty in working with this γ' strengthened alloy, small variations of sheet thickness and flatness occur during hot rolling. To determine if such variations might influence results of creep-rupture tests, a

number of tests were conducted on specimens which were measured at numerous locations along the gage length prior to testing. Results indicated that, while thickness variations as large as 0.051 mm (0.002 in) were present, fracture locations did not show any preference for areas of minimum thickness.

Optical metallography of failed creep specimens with a wide range of lives revealed 1-4 grains through the thickness of the sheet with no dependency of rupture life on grain size. With only a few grains through the thickness, the time to failure apparently is very sensitive to grain orientation and grain boundary angle of these grains. It was thought that an increase in the number of grains might reduce this sensitivity, resulting in less scatter in rupture life.

Based on the above information, Cabot embarked on a third processing program with the objective of increasing the number of through-thickness "pancake" grains to decrease the scatter in creep-rupture life. Process variables included billet consolidation procedures, hot rolling temperatures and reduction schedules, as well as Y_2O_3 content and the use of finish cold rolling as an alternate to the previously used procedure of hot rolling to size. Characteristics evaluated included microstructure, formability and creep rupture properties of the sheet product.

Evaluation of cold worked sheet annealed in the 871-1343°C (1600-2450°F) range indicated that this approach was unsuccessful in producing a "pancake" grain morphology. Undesireable fine equiaxed grains were produced at all temperatures following 20-40% finish cold reductions.

The most promising hot rolling processing routes were duplicated using partial billets and the "best" four again were duplicated using full size billets. Test results of these most promising routes and their duplicate sheets are shown in Table 4-XIX.

TABLE 4-XIX

CABOT HDA8077 PROCESS IMPROVEMENT PROGRAM - PROCESSING ROUTES AND PROPERTIES

Billet Ident	Process Ident	Billet Size	Y_2O_3 Content %	Minimum Number of Through Thickness Grains	Microstructure	Average Olsen Cup mm (in)	982°C (1800°F) Creep/Rupture 82.7 mn/m² (12 ksi) Hr.	89.6 mn/m² (13 ksi) Hr.	96.5 mn/m² (14 ksi) Hr.	Prior Creep %
A1-1	A	1/3 billet	0.8	10	Pancake Grains Oxide Banding		190.1 101.5 139.7 119.1			0.35 0.39 0.49 0.36
A2-2	A	1/3 billet	0.8	15	Pancake Grains, Many Fine Grains, Oxide Banding	3.48 (0.137)	-			-
A3-2	B	1/3 billet	0.8	3	Pancake Grains, Many Fine Grains, Oxide Banding	7.16 (0.282)	50.1 63.5 55.5			0.42 0.57 0.68
A6-2	B	1/3 billet	0.8	10	Pancake Grains, Many Fine Grains, Oxide Banding	4.57 (0.180)	4.8 3.2 3.8			0.54 0.39 0.58
A7	B	Full Billet	0.8	5	Pancake Grains, Some Fine Grains, Oxide Banding	6.76 (0.266)	27.5 25.2 45.4 92.3 67.7			0.14 0.78 0.61 0.28 0.24
A4-2	C	1/3 billet	0.8	6	Pancake Grains, Many Fine Grains, Oxide Banding	3.86 (0.152)	50.6 40.0 58.8			0.46 0.45 0.60
A5-2	C	1/3 billet	0.8	12	Pancake Grains, Many Fine Grains, Oxide Banding	3.89 (0.153)	109.9 63.7			0.45 0.36
A8-2	D	1/3 billet	0.8	6	Pancake Grains, Oxide Banding	8.26 (0.325)	153.1 73.4 59.9			0.38 0.46 0.49
A9-2	D	1/3 billet	0.8	7	Pancake Grains, Fine Grains Within Pancake Grains	7.85 (0.309)	12.1 20.0 7.3 42.0			0.41 0.37 0.56 0.62
A10	D	Full billet	0.8	7	Pancake Grains	7.85 (0.309)	133.0 208.9			0.77 0.42
A11-2	E	1/3 billet	0.8	6	Pancake Grains, Many Fine Grains, Oxide Banding	6.73 (0.265)	3.3 13.6 9.0			1.02 1.63 0.97
A12-2	E	1/3 billet	0.8	-		7.37 (0.290)	10.4 16.5 6.4 251.8* 250.0*	 245.5 159.0		0.49 0.54 0.69 0.34 0.23
B3-2	B	1/3 billet	1.3	6	Pancake Grains	7.34 (0.289)	251.8* 251.8*	12.4 427.9		1.68 0.38
B6-2	B	1/3 billet	1.3	2	Pancake Grains	6.81 (0.268)		106.3 7.4 50.9		0.53 0.16 0.29
B4-2	C	1/3 billet	1.3	4	Pancake Grains	5.46 (0.215)	306.9* 306.1* 235.0* 234.9*	24*	59.4 62.7 76.1 104.5	0.36 0.33 0.32 0.25
B5-2	C	1/3 billet	1.3	8	Pancake Grains, Many Fine Grains	4.78 (0.188)			44.4 17.4 13.6 6.4	0.73 0.83 0.33 0.19
B7	C	Full billet	1.3	6	Pancake Grains	5.23 (0.206)			35.0 164.1 260.4	0.38 0.21 0.32
B8-2(1)	D	1/3 billet	1.3	6	Pancake Grains, Many Fine Grains	-	258.4* 234.0* 239.8*	100.9 92.9 120.9		0.45 0.44 0.84
B9-2(1)	D	1/3 billet	1.3	7	Pancake Grains, Some Fine Grains	6.73 (0.265)		214.9 220.2 162.0		0.64 0.60 0.70
B10(1)	D	Full billet	1.3	8	Pancake Grains	7.95 (0.313)		154.8 347.8 > 400.0+		0.19 0.51 > 0.30+
B11-2	E	1/3 billet	1.3	10	Pancake Grains	6.78 (0.267)	285.5* 209.2* 257.5* 210.9*	87.2 136.3 134.2 116.3 272.2		0.35 0.32 0.35 0.29 0.35
B12-2	E	1/3 billet	1.3	-	---	6.60 (0.260)		28.9 64.0 55.3 52.1		0.22 0.37 0.23 0.41

* Uploaded

\+ Discontinued

(1) Selected sheet process

Because of confusion of material identity by Cabot, the oxide contents of the billets described in Table 4-XIX were incorrectly stated in all previously published reports on this program, and in Reference 4-2. The values noted in Table 4-XIX ARE CORRECT. As discussed below, this confusion led to misinterpretations which were considered to be responsible, at least in part, for the unsuccessful conclusion of the HDA8077 process improvement program.

Evaluation of the correct results reported in Table 4-XIX leads to three conclusions:

1) Sheet macro- and microstructure as well as cup formability are controlled by the finish rolling schedule.

2) Increasing the number of through-thickness "pancake" grains from 2 or 3 to as many as ten is beneficial in producing consistent creep rupture properties.

3) Superior creep rupture properties are achieved with high (1.37%) Y_2O_3 content.

Based on the results and conclusions discussed above, Process D, which was used to produce sheets B8-2, B9-2, and B-10, was selected as the optimized processing schedule. These sheets, which contained as many as ten grains through the thickness (Figure 4-11), exhibited the best combination of sheet formability, 982°C (1800°F) creep rupture strength, and creep ductility. Because of the material misidentification at Cabot, the preferred Y_2O_3 content was incorrectly identified as 0.8 percent for the optimized sheet.

4.7 HDA 8077 PROCESS REPRODUCIBILITY

To demonstrate reproducibility of the excellent properties demonstrated by sheets B8-2, B9-2 and B10, an additional 4.6m^2 (50 ft^2) of HDA8077 sheet, designated lot "C", was manufactured by Cabot using the optimized process "D". For reasons discussed in the last section, the aim chemistry of this lot was 0.8% rather than the preferred level of 1.3% Y_2O_3. The analyzed composition of this material is reported in Table 4-XIV. Typical longitudinal and transverse microstructures (Figure 4-12) show a uniform grain structure

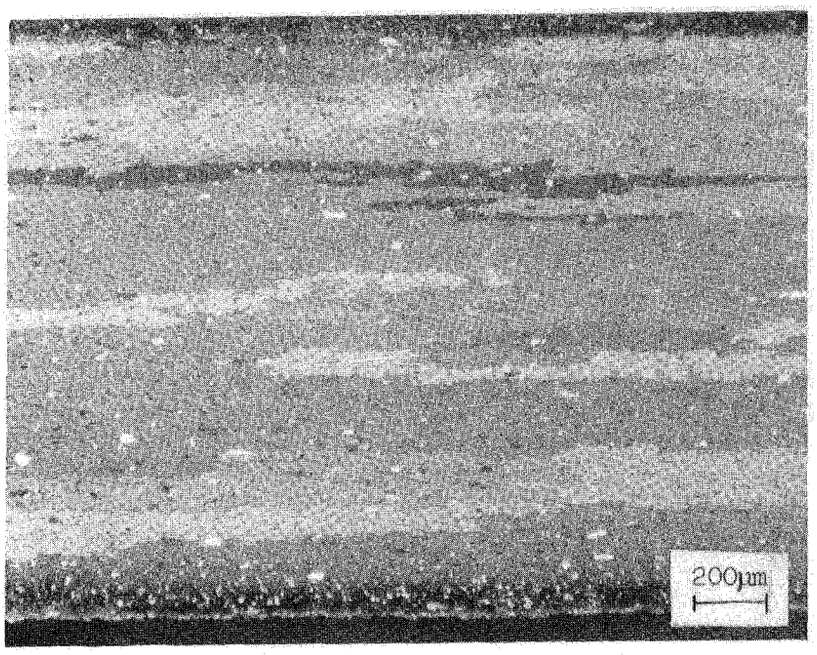

Figure 4-11 Typical Microstructure of Selected HDA 8077 Processing Route

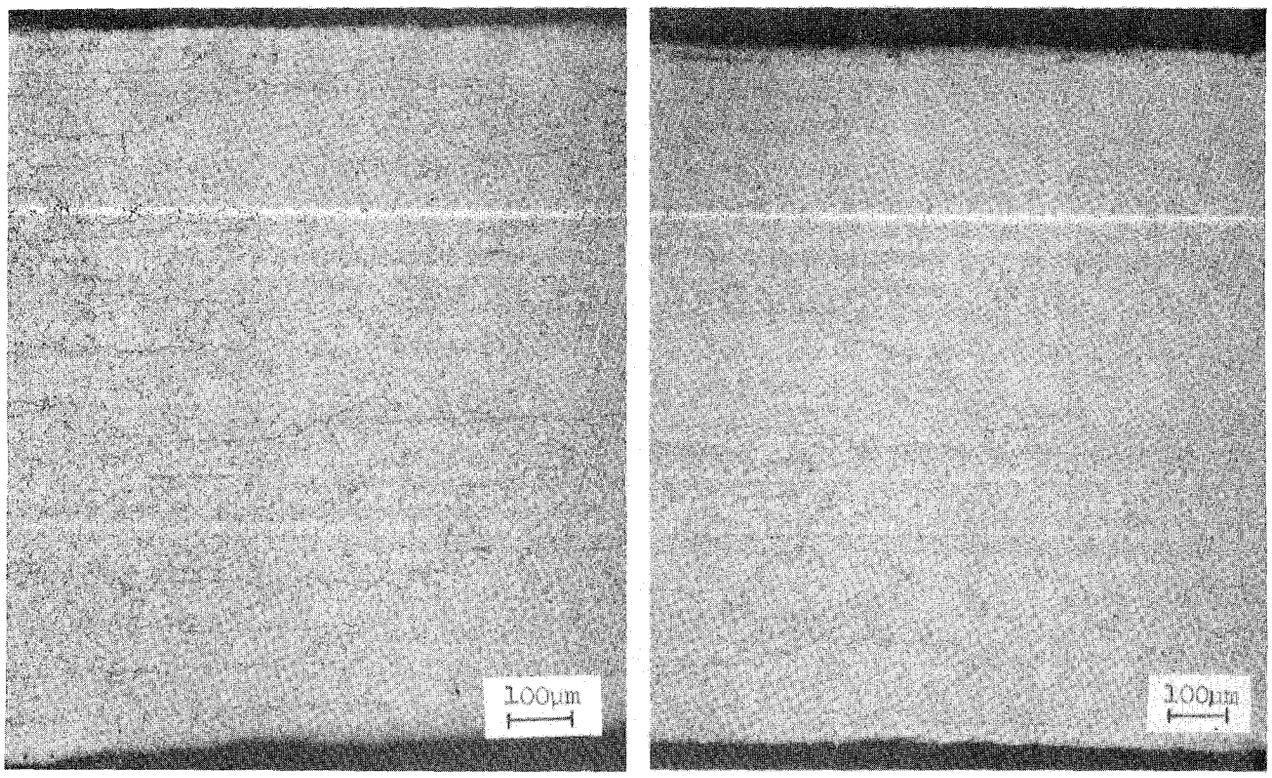

LONGITUDINAL HDA 8077 TRANSVERSE

Figure 4-12 As Received Microstructure of HDA 8077 Lot C

with more grains through the sheet thickness than were found in the initial material. Results of hardness, Erichson cup, and bend tests (Table 4-XX) indicate the hardness and formability of this material are comparable to that of the initial material delivered at the beginning of the program. However, this lot exhibits lower 982°C (1800°F) creep rupture life (Table 4-XXI) than that shown by the optimized experimental sheets B8-2, B9-2 and B-10 (designated "Lot B" in Table 4-XXI). The poor creep performance of this material is attributed to the low Y_2O_3 content. Because the compositional misinterpretation was not recognized by Cabot at this point in the program, further attempts were made to improve the creep properties of the 0.8% Y_2O_3 material. These attempts involve variation of initial powder sizes directed toward improvement of the Y_2O_3 distribution. These attempts were not successful in improving the creep strength of the 0.8% Y_2O_3 composition, and the evaluation of HDA8077 on this program thus was terminated.

TABLE 4-XX

FORMABILITY OF HDA-8077 LOT C SHEET PROCESSED BY THE OPTIMIZED ROUTING

	Sheet C-4	Sheet C-20	Sheet C-45
Micro-Hardness (Converted to Rc Scale)	24-28	24-28	24-28
Erichsen Cup	8.0mm (0.317")	5.3mm (0.210")	5.3mm (0.208")
	8.6mm (0.340")	5.6mm (0.220")	6.2mm (0.245")
Bend Test (Around Dia. T=Sheet Thickness	2T Fail 3T Pass	3T Fail 4T Pass	3T Fail 4T Pass

TABLE 4-XXI

CREEP-RUPTURE PROPERTIES OF HDA 8077
LOTS B AND C AT 982°C (1800°F)

Lot	Stress Mn/M²	Stress (ksi)	Time to 0.1% Creep hrs.	Rupture Life hrs.	Prior Creep %	RT Elong. %
B Lot (Cabot Tests)	89.6	(13)	1 to 44	93 to 633	0.19 to 0.84	--
C Lot (Cabot Tests)	89.6	(13)	--	0.4	--	5.80
			--	0.7	--	2.40
	82.7	(12)	--	1.2	0.30	5.00
	75.8	(11)	--	6.6	0.23	2.50
			0.3	35.0	0.78	3.40
			14.0	63.4	0.50	4.00
	68.9	(10)	37.5	90.6	0.37	1.40
	68.9	(10)	14.0	214.0	1.10	1.90
			23.0	295.1	0.31	2.50
C Lot (P&WA Tests)	75.8	(11)	10.0	56.0	0.45	1.27
	75.8	(11)	73.6	172.3	0.55	1.40

5.0 TASK III - PRELIMINARY EVALUATIONS

The objectives of this task were to:

A) Conduct preliminary, comparative property evaluations of the two candidate ODS alloys, MA 956 and HDA 8077

B) Evaluate methods for joining of ODS alloys

C) Develop experimental methods for rig evaluation of ODS combustor components

Details of each of these three efforts are discussed in the following sections.

5.1 TASK III - A PRELIMINARY MATERIAL EVALUATION

5.1.1 Introduction and Summary

The objective of this subtask was to perform preliminary comparative property tests on the two candidate oxide dispersion strengthened alloys, MA 956 and HDA 8077. Material used for these tests was obtained from MA 956 Lot ZDEW and HDA-8077 Lots MS 151, MS 153, and MS 154. The compositions and microstructures of these materials are described in Section 4. Properties evaluated include fabricability, tensile, creep, isothermal and thermal fatigue, oxidation, and alloy stability. Details of test methods and results are described in the following sections. Briefly, neither alloy showed a significant advantage in balance of properties. MA 956 exhibits slightly better formability, isothermal low cycle fatigue, and oxidation resistance, while HDA 8077 is somewhat superior in creep strength and rupture ductility, isothermal high cycle fatigue, and thermal fatigue cracking resistance. While MA 956 was shown to be susceptible to room temperature embrittlement as a result of elevated temperature exposure, it was concluded that this phenomena was not a significant limitation on the suitability of this alloy for segmented combustor application. It was thus concluded that both alloys are highly promising candidates for combustor sheet applications.

Where available, properties measured on the oxide dispersion strengthened alloys were compared to Hastelloy X, a currently used combustor sheet alloy. This information was obtained from various sources; formability, tensile, and creep data were taken from manufacturers information sheets. Thermal fatigue and oxidation tests were conducted concurrently with ODS tests in this program. Information on isothermal fatigue and alloy stability were not available in a form suitable for comparison. Based on evaluation of these data, both of the ODS alloys show approximately a 167°C (300°F) advantage in creep and oxidation over Hastalloy X.

5.1.2 Formability

Formability of candidate alloys was evaluated using Erichson cup and bend tests. In the Erichson cup test, a sample sheet is pressed into a cup form by the use of a hemispherical punch. The maximum cup depth to which the material may be pressed without cracking is taken as an indication of sheet formability. The bend test measures the minimum radius, stated in multiples of sheet thickness, over which sheet material can be bent without cracking.

Formability test results are listed in Table 5-I cup depths are plotted in Figure 5-1 together with typical Hastelloy X properties. These results indicate that as-received ODS alloy formability ranges between one-half and two-thirds that of the current combustor alloy, with MA 956 being slightly better than HDA 8077. Significant variability is seen among the three lots of 8077 alloy.

As noted in Section 4, MA 956 Lot ZDEW and HDA 8077 Lot MS 154 were observed to have a surface worked layers in the as-received condition (Tables 4-III and 4-XV). To investigate the influence of this surface hardened layer on formability, tests were conducted on material annealed 1/2 hour at 1177°C (2150°F) in hydrogen. A rapid cool was applied to the 8077 alloy to avoid through thickness hardening, attributed to γ' precipitation, which was observed in Task II. MA 956 material was given the equivalent of a "still air cool".

TABLE 5-I

FORMABILITY OF OXIDE DISPERSION STRENGTHENED ALLOYS

Alloy	Lot	Condition	Erichson Cup, mm (in.)	Bend Test[3]
MA 956	ZDEW	As Received	8.3 (0.325) 8.5 (0.335)	2T PASS
MA 956	ZDEW	Annealed[1]	8.3 (0.325) 7.8 (0.307)	2T PASS
HDA 8077	MS 151	As Received	7.6 (0.298) 7.1 (0.278)	3T PASS
HDA 8077	MS 151	Annealed[2]	6.7 (0.265) 6.2 (0.245)	3T PASS
HDA 8077	MS 153	As Received	6.5 (0.254) 6.2 (0.244)	3T PASS
HDA 8077	MS 154	As Received	4.8 (0.190) 4.1 (0.160)	3T PASS
HDA 8077	MS 154	Annealed[2]	3.8 (0.150) 4.6 (0.183)	4T PASS

1) Hydrogen annealed 1177°C (2150°F), 1/2 hour, simulated air cool.

2) Hydrogen annealed 1177°C (2150°F), 1/2 hour, simulated rapid air cool.

3) Minimum radius, in multiples of sheet thickness, over which sheet may be bent without cracking; minimum of 2 longitudinal and 2 transverse tests.

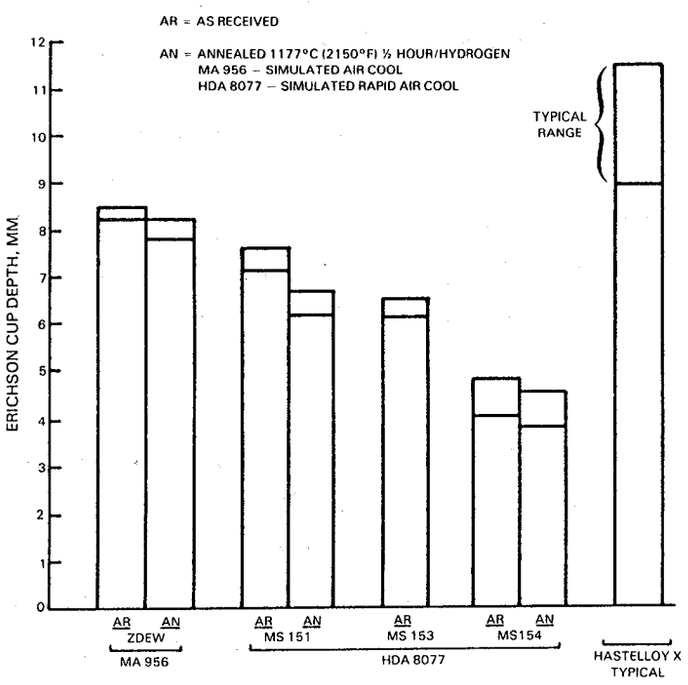

Figure 5-1 Formability Range of Various Sheet Alloys

As shown in Figure 5-1, annealing did not significantly change the formability of either alloy. In the case of MA 956, this observation is consistent with the Task II observation that the formability of as-received ZDEW, with the surface worked layer, is comparable to that of an experimental lot of MA 956 which did not have a surface worked layer (Table 4-VII). These observations taken together strongly indicate that the presence of a surface worked layer does not significantly influence MA 956 sheet formability. These results also indicate that the relatively poorer formability of HDA 8077 Lot MS 154, as compared to Lots MS 151 and MS 153, is intrinsic to this lot of material and is not the result of the surface worked layer observed on MS 154.

5.1.3 Tensile and Creep

Room temperature and 982°C (1800°F) tensile and 982°C (1800°F) creep properties of the two candidate ODS alloys were evaluated per ASTM E-8, E-21, and E-139, respectively, using the test specimen shown in Figure 5-2. Limited creep testing of MA 956 also was conducted at 1093°C (2000°F). Finish machined specimens were annealed 1/2 hour at 1177°C (2150°F) in hydrogen to eliminate the effect of residual machining stresses on property measurements. All tensile tests were conducted with a cross head speed of 0.127 mm (0.005 in.)/minute. (Results of a parallel, company sponsored study of strain rate effects are reported in Reference 5-1.) Elevated temperature tensile and creep tests on MA 956 were conducted with the loading axis both parallel and perpendicular to the rolling direction. HDA 8077, which is cross rolled and thus nominally isotropic, was tested only parallel to the final rolling direction.

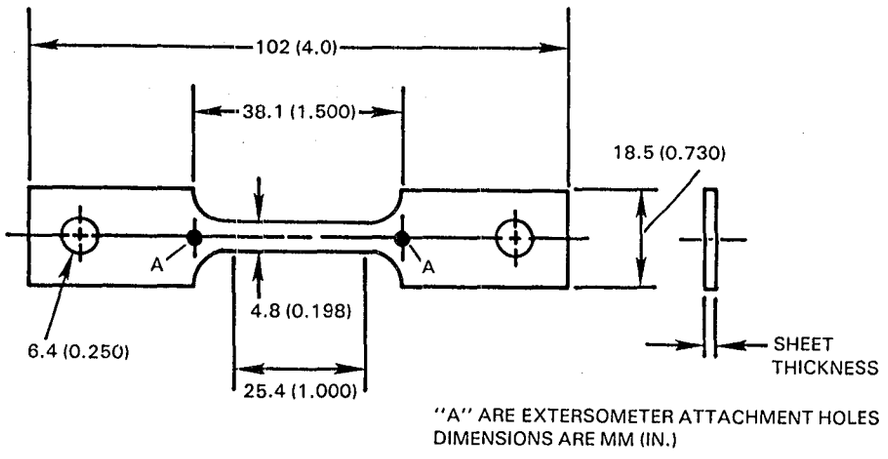

Figure 5-2 Specimen Used for Evaluation of Sheet Alloy Tensile and Creep Properties

5.1.3.1 Tensile Results

MA 956 and HDA 8077 tensile test results are listed in Tables 5-II and 5-III, respectively. Results of room and elevated temperature longitudinal tests are plotted respectively in Figures 5-3 and 5-4, together with typical Hastelloy X properties. Because of lot-to-lot variability found in the HDA-8077 results, comparisons between this alloy and the other two must be made with caution. At room temperature, both the yield and ultimate strengths of MA 956 appear to be slightly below average HDA 8077 properties. The elongation of MA 956 is comparable to that of HDA 8077 Lots MS 151 and 154, and substantially below that of MS 153, which also exhibits the lowest strength of the three HDA 8077 lots tested. Both ODS alloys clearly have higher yield strengths and substantially lower ductilities than Hastelloy X. The ultimate strength of MA 956 is less than Hastelloy X; the average ultimate of HDA 8077 appears to be slightly higher.

The 902°C (1800°F) longitudinal yield and ultimate strength of the two ODS alloys are very close, indicating very little work hardening at this temperature (Figure 5-4). Both alloys exhibit roughly comparable yield strengths and significantly lower ultimate strengths and ductilities as compared to Hastelloy X. Variability of 982°C (1800°F) HDA 8077 strength is somewhat less than seen at room temperature; however, substantial variability of elongation still is seen. Variability not withstanding, the elevated temperature ductility of MA 956 is significantly less than that of HDA 8077.

Examination of the data in Table 5-II shows relatively little anisotrophy 982°C (1800°F) MA 956 tensile properties. Both the ultimate and yield strengths are virtually identical, while transverse ductility is somewhat less than longitudinal.

Typical longitudinal fractures found in the two ODS alloys are shown in Figure 5-5. These photomicrographs show evidence of extensive localized plastic deformation (necking) in MA 956 at both test temperatures. HDA 8077 exhibits significant less localized deformation despite the higher measured elongation.

TABLE 5-II

TENSILE PROPERTIES OF MA 956 LOT ZDEW

Orientation[1]	Temperature °C (°F)	0.2% Yield Strength Mn/m^2 (KSI)	Ultimate Tensile Strength Mn/m^2 (KSI)	Percent Elongation in 25.4mm (1 in.)
Longitudinal	25 (77)	545.0 (79.1)	630.4 (91.5)	11.9
Longitudinal	25 (77)	558.8 (81.1)	647.7 (94.0)	13.3
Longitudinal	982 (1800)	106.8 (15.5)	108.9 (15.8)	5.8
Longitudinal	982 (1800)	106.8 (15.5)	110.9 (16.1)	6.0
Transverse	982 (1800)	107.5 (15.6)	110.2 (16.0)	3.7
Transverse	982 (1800)	104.0 (15.1)	105.4 (15.3)	3.8

Crosshead Rate = 0.127 mm (0.005 in.)/minute

1) Longitudinal = Parallel to rolling direction
Transverse = Transverse to rolling direction

TABLE 5-III

LONGITUDINAL TENSILE PROPERTIES OF HDA 8077

Lot	Temperature °C (°F)	0.2% Yield Strength Mn/m^2 (KSI)	Ultimate Tensile Strength Mn/m^2 (KSI)	Percent Elongation in 25.4mm (1 in.)
MS 151-4	25 (77)	737.7 (107.0)	1000.2 (145.1)	15.7
MS 153-2	25 (77)	501.9 (72.8)	671.8 (97.4)	28.9
MS 153-4	25 (77)	515.5 (74.8)	705.2 (102.3)	23.4
MS 154-2	25 (77)	717.3 (104.0)	828.6 (120.2)	14.8
MS 151-4	982 (1800)	86.0 (12.5)	102.5 (14.9)	11.1
MS 153-2	982 (1800)	106.5 (15.5)	107.3 (15.6)	14.0
MS 153-4	982 (1800)	109.2 (15.8)	109.2 (15.8)	12.7
MS 154-2	982 (1800)	115.0 (16.7)	115.0 (16.7)	23.2

Crosshead Rate = 0.127 mm (0.005 in.)/minute

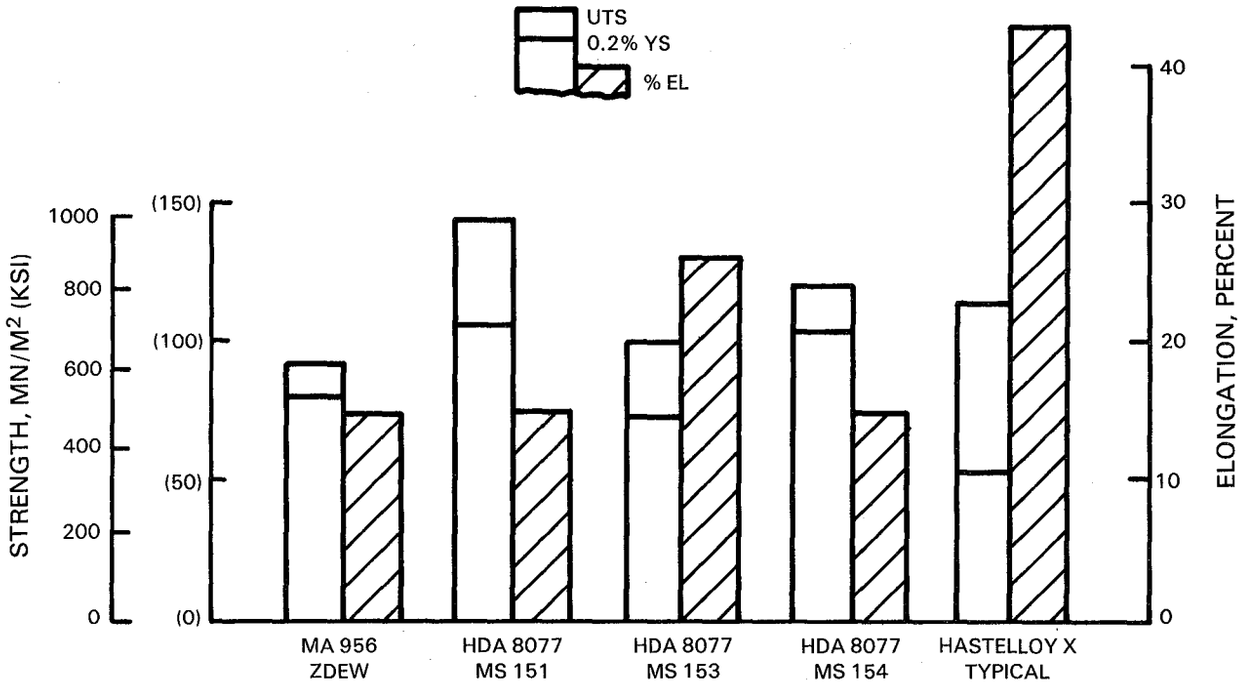

Figure 5-3 Room Temperature Tensile Properties of Various Sheet Alloys (Oxide dispersion strengthened alloys tested parallel to rolling direction).

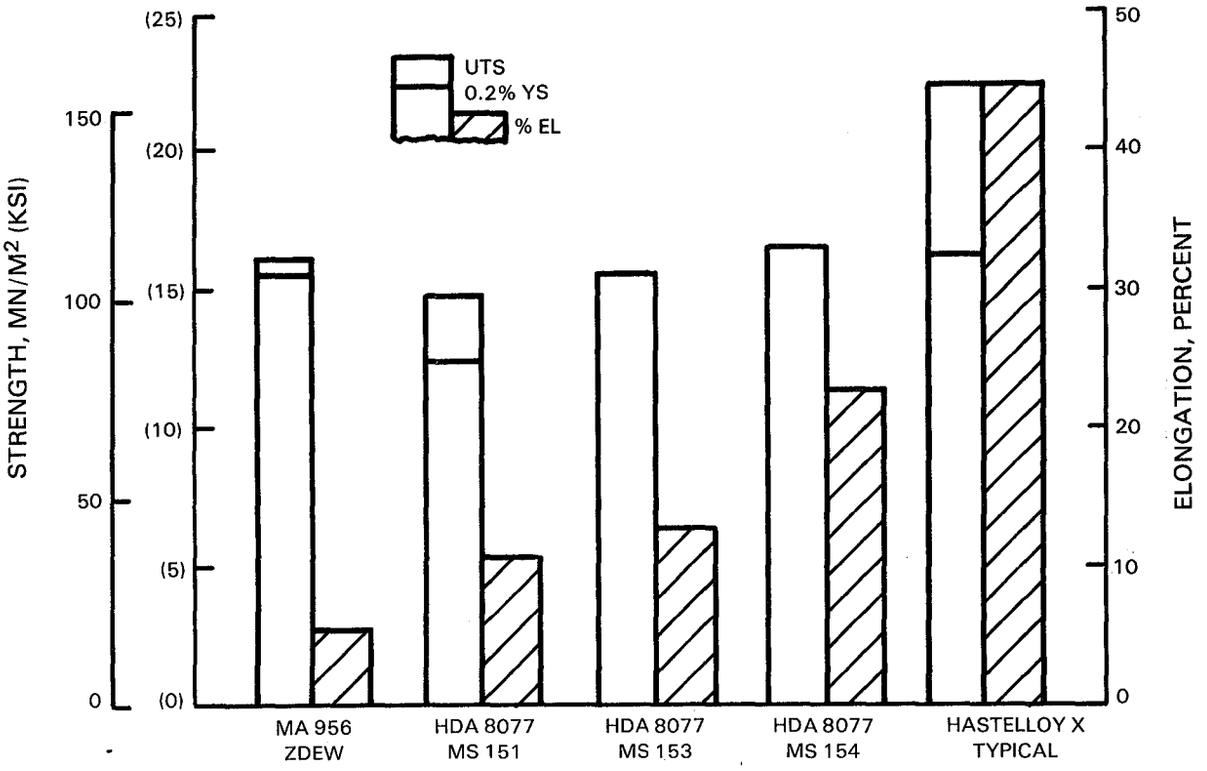

Figure 5-4 982C (1800F) Tensile Properties of Various Sheet Alloys (Oxide dispersion strengthened alloys tested parallel to rolling direction).

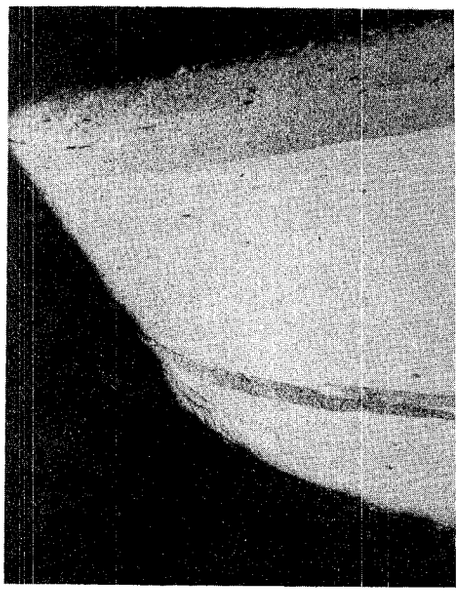

a) MA 956 Z DEW R.T. 200 μm

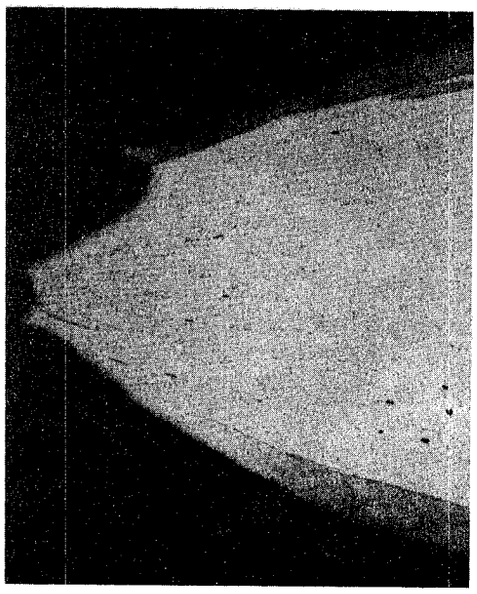

b) MA 956 Z DEW, 982°C (1800°F) 200 μm

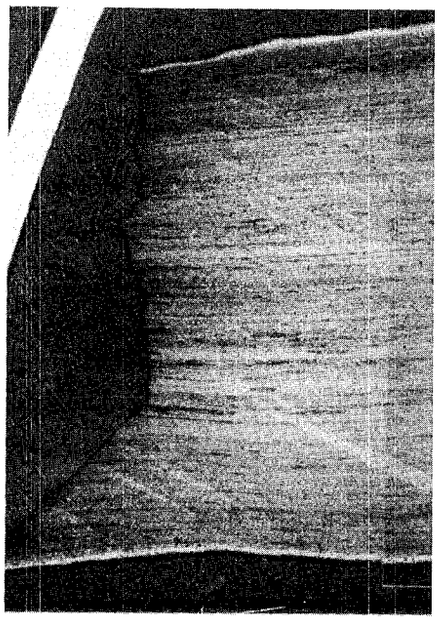

c) HA 8077 MS-154, R.T. 200μm

d) HA 8077 MS-151, 982°C (1800°F) 200μm

Figure 5-5 Longitudinal Tensile Fractures of ODS Alloys

The 982°C (1800°F) HDA 8077 specimen shows evidence of extensive secondary cracking having an intergranular appearance. The transverse fracture appearance of MA 956 tested at 982°C (1800°F) (Figure 5-6) is similar to the longitudinal fracture morphology, with significant necking being observed.

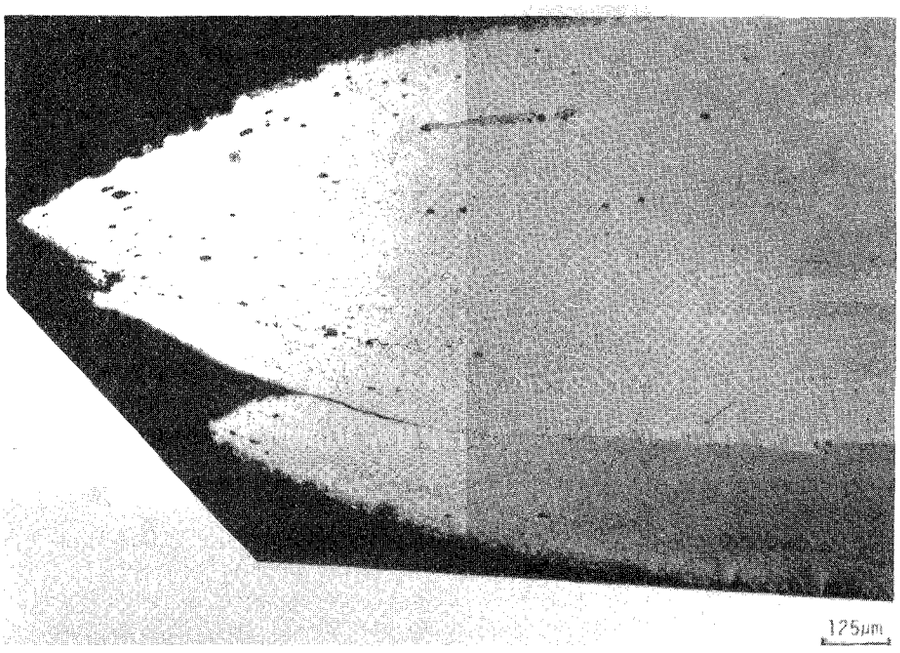

Figure 5-6 982C (1800F) Transverse Tensile Fracture of MA 956 Lot ZDEW

5.1.3.2 Creep Results

Results of 982°C (1800°F) creep tests on both candidate alloys are presented in Table 5-IV A; results of duplicate 1093°C (2000°F) tests on MA 956 are reported in Table 5-IV B. Rupture life data for the ODS alloys is compared to typical Hastelloy X properties in Figure 5-7. Creep capability of the MA 956 alloy clearly is vastly superior to that of the current combustor alloy. Assuming a Larson-Miller constant of 20, the difference shown in Figure 5-7 translates to more than 167°C (300°F) creep advantage for MA 956 compared to Hastelloy X at 68.9 mN/m^2 (10 KSI). While the HDA 8077 alloy shows the potential to have equivalent or even better creep properties than MA 956, the 8077 lot-to-lot variability is extreme, with rupture lives at 82.7 mN/m^2 (12 KSI) ranging from 0.3 to over 3,000 hours. This variability is addressed in more detail in Section 4. The rupture ductility of HDA 8077 is significantly better than that of MA 956, particularly when measured in terms of creep extension measured immediately prior to failure (Table 5-IV, prior creep). Both alloys exhibit significantly less rupture ductility than Hastelloy X, which typically is in the range of 15 to 45% at 982°C (1800°F).

TABLE 5-IV A

CREEP-RUPTURE PROPERTIES OF ODS ALLOYS AT 982°C (1800°F)

Alloy	Lot	Orientation[3]	Stress Mn/m^2 (KSI)	Time to 0.1% Creep (hrs)	Time to 0.5% Creep (hrs)	Time to Rupture (hrs)	Prior[2] Creep (%)	RT Elongation (%)
MA 956	ZDEW	L	62.1(9)	1.5	1862.0	>4455.7*	>0.81*	nm[1]
MA 956	ZDEW	L	62.1(9)	8.0	4050.0	>4455.6*	>0.52*	nm[1]
MA 956	ZDEW	L	69.0(10)	34.4	1580.9	4175.6	nm[1]	3.4
MA 956	ZDEW	L	82.7(12)	70.0	-	611.9	0.18	2.0
MA 956	ZDEW	T	62.1(9)	42.2	-	109.2	0.15	2.8
MA 956	ZDEW	T	62.1(9)	35.3	-	304.7	0.13	2.9
HDA 8077	MS 151-4	L	82.7(12)	-	0.03	0.3	1.39	nm[1]
HDA 8077	MS 151-4	L	89.6(13)	-	-	0.1	1.54	6.5
HDA 8077	MS 153-2	L	86.2(12.5)	0.10	5.8	16.2	1.00	4.0
HDA 8077	MS 153-2	L	86.2(12.5)	0.26	14.6	25.5	1.24	5.5
HDA 8077	MS 153-4	L	86.2(12.5)	0.18	20.0	95.1	1.27	4.5
HDA 8077	MS 153-4	L	86.2(12.5)	0.12	26.9	50.0	0.71	4.5
HDA 8077	MS 154-2	L	82.7(12)	5.17	653.3	>3613.2*	>1.38*	>1.05
HDA 8077	MS 154-2	L	89.6(13)	0.08	3.86	14.7	1.84	7.4

*Test Discontinued, No Failure

1) nm = Not measured
2) Percent creep measured within 2 hours of failure
3) L = Parallel to Rolling Direction
   T = Transverse to Rolling Direction

TABLE 5-IV B

LONGITUDINAL CREEP-RUPTURE PROPERTIES OF
MA 956 LOT ZDEW AT 1093°C (2000°F), 68.9 MN/m^2 (10 KSI)

Time to 0.1 Percent Creep Hours	Time to Rupture Hours	Prior Creep Percent	R. T. Elongation Percent
3.5	582.3	0.66	2.4
7.0	137.7	0.39	4.0

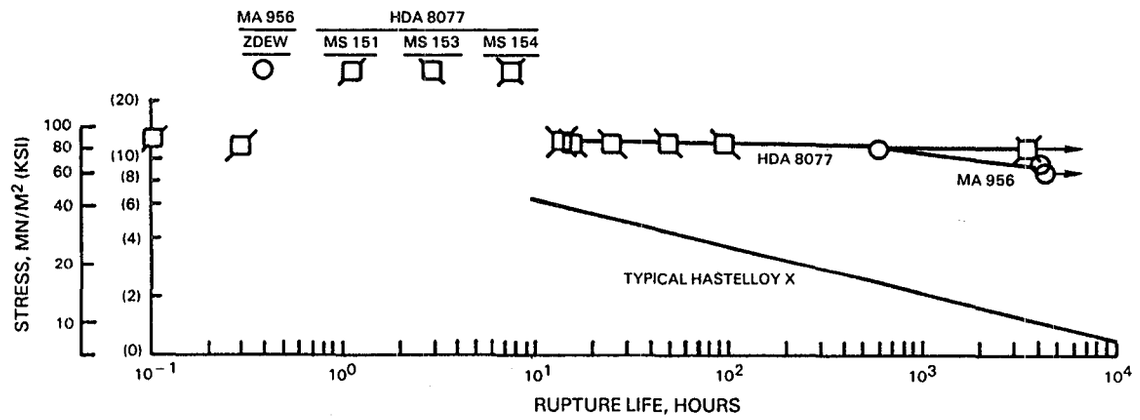

Figure 5-7 982C (1800F) Rupture Life of Various Sheet Alloys (Oxide dispersion strengthened alloys tested parallel to rolling direction).

A typical MA 956 creep fracture (Figure 5-8) shows evidence of localized plastic deformation as seen in the elevated temperature tensile failures. This observation must be interpreted with caution, however, as the necking is seen only in one side of the sheet and may represent deformation which occurred during overload failure. This possibility is supported by the significant difference seen between the very small elongation reported immediately prior to failure (0.18%) and the substantially larger elongation (2%) measured after failure. It also is consistent with observation made by Whittenberger MA 956 bar material (Reference 5-2). Whittenburger proposes that creep "deformation" occurs by the nucleation and slow growth of transgranular cracks, producing a flat fracture surface in the area of "creep fracture," with extensive plastic deformation in the overload area. Evidence of significant void formation is seen in the creep exposed microstructure; however, similar voids are seen in stress-free thermal exposures, as discussed in Section 5.1.7.1. What is not seen in stress free exposures is the preferential association of what appear to be voids with what appear to be incipient transgranular secondary creep cracks oriented perpendicular to the stress axis (arrows in Figure 5-8). It is not clear from this evidence whether: a) localized stress induced void coalescence is responsible for creep crack initiation, or b) local strain concentration is responsible for preferential void nucleation in the vicinity of incipient cracks, or c) this is simply a form of "microdimpled" fracture with dimples nucleated either at second phase inclusions (such as carbides or nitrides) or even perhaps at Y_2O_3 dispersoids. Additional work is required to clarify this question.

A typical MA 956 transverse creep fracture is shown in Figure 5-9. This fracture shows less evidence of localized deformation, which may simply mean that the particular section examined did not contain any of the overload area. As in the longitudinal fracture, void formation is seen distributed more or less uniformly throughout the central position of the sheet and also located preferentially at incipient transgranular secondary creep cracks. Interpretation of this latter observation is subject to the same question raised previously in discussion of the longitudinal fracture morphology.

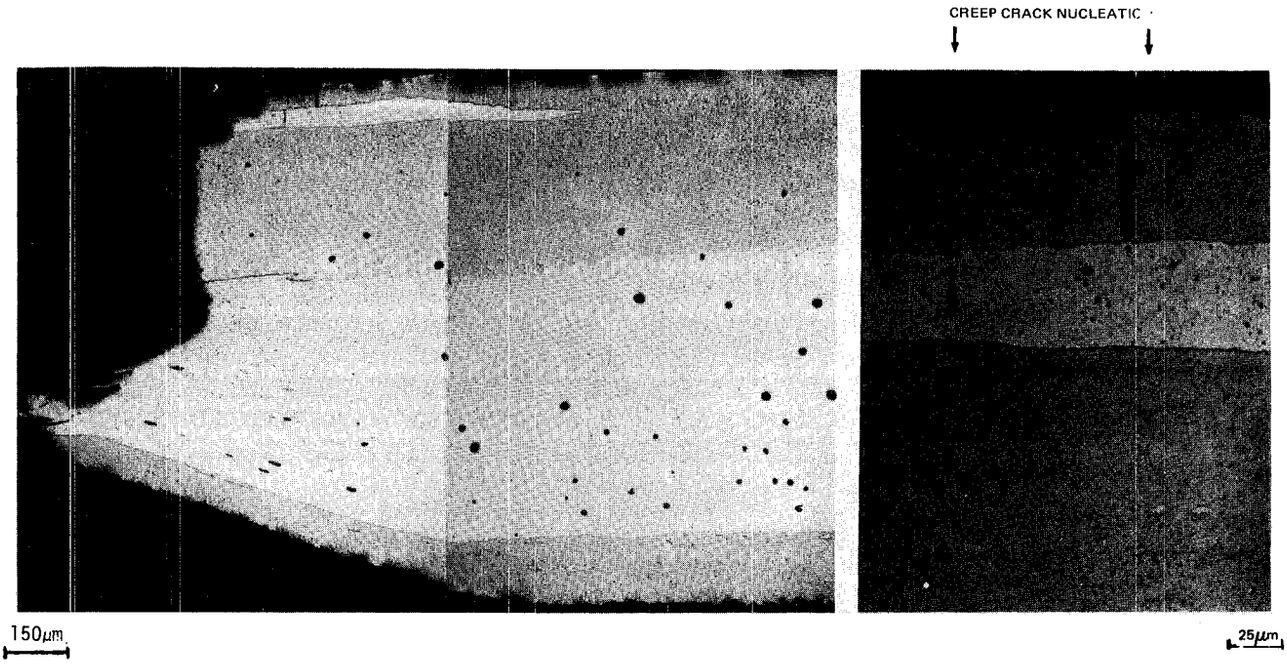

Figure 5-8 Fracture Appearance of MA 956 Lot ZDEW Longitudinal Creep Specimen Tested to Rupture in 612 Hours at 982C (1800F) and 82.7 MN/m^2 (12 ksi). Creep extension immediately prior to failure 0.18%; Rupture elongation 2.0%. Note voids located preferentially towards the center of the sheet. Also note incipient creep cracks transverse to the stress axis (arrows).

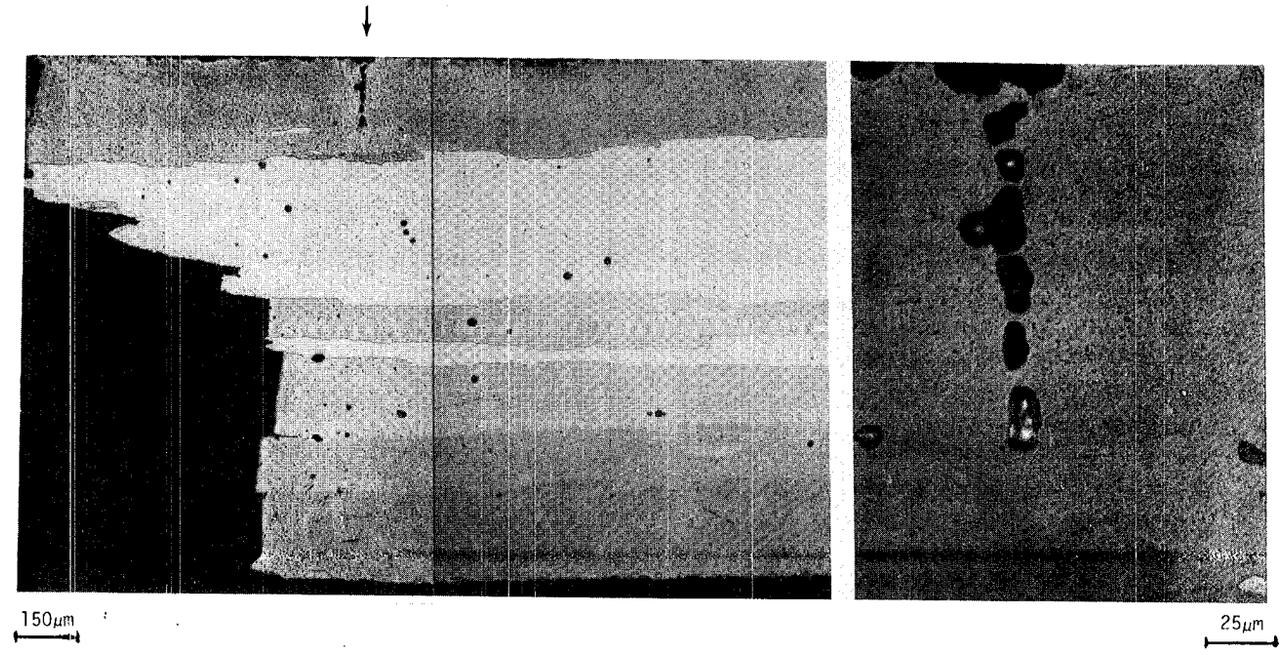

Figure 5-9 Fracture Appearance of MA 956 Lot ZDEW Transverse Creep Specimen Tested to Failure in 305 hrs. at 982C (1800F), 62.1 MN/m^2(9 ksi). Creep extension immediately prior to failure 0.13%; Rupture elongation 2.9%. Higher magnification photomicrograph shows detail of incipient creep crack seen in top grain of lower magnification photomicrograph (arrow).

Photomicrographs of creep fractures observed in two different lots of HDA 8077 are shown in Figures 5-10 and 5-11. The structure seen in the very short time (0.1 hr.) creep fracture of Lot MS 151 is virtually identical to the previously discussed 982°C (1800°F) tensile failure morphology, with evidence of extensive secondary cracking having what appears to be an intergranular morphology. In striking contrast is the longer time failure seen in Figure 5-11, which shows much less evidence of the intergranular-appearing secondary cracks. This evidence suggests that the difference of creep strength between these two lots is related to the difference of as-received grain size and morphology which can be seen in Figure 4-9.

5.1.4 Isothermal Fatigue

MA 956 and HDA 8077 annealed sheet specimens were fatigue tested in displacement controlled, fully reversed bending at temperatures of 760°C (1400°F), 871°C (1600°F), and 982°C (1800°F). Tests at a calculated strain range of 0.005 mm/mm, which caused failures in the "low cycle fatigue" range of 10^2 to 10^4 cycles, were conducted on the specimen shown in Figure 5-12 at a frequency of 0.67 hz. Test machine fixturing and linkages are designed to cyclically bend this specimen in a circular arc, with outer fiber strain being calculated from measured specimen thickness and radius of curvature. "High cycle fatigue" tests at lower strain ranges were conducted at 30 hz using the specimen shown in Figure 5-13. This specimen is tested in cantilevered bending with uniform strain being provided through the gage section by the precisely machined taper. Outer fiber strain is calculated from measured specimen dimensions and displacements. Both types of specimens are heated in resistance wound furnaces for elevated temperature testing. In both tests, failure is defined as separation of the specimen into two pieces.

Isothermal fatigue test results obtained on the "low cycle" and high cycle" fatigue specimens are presented in Tables 5-V and 5-VI, respectively. Results of 760°C (1400°F) and 982°C (1800°F) tests are compared graphically in Figure 5-14. As was the case with the tensile and creep results, comparison between the two alloys must be with some caution because of lot-to-lot scatter of the HDA 8077 data. Variability notwithstanding, the HDA 8077 alloy clearly is

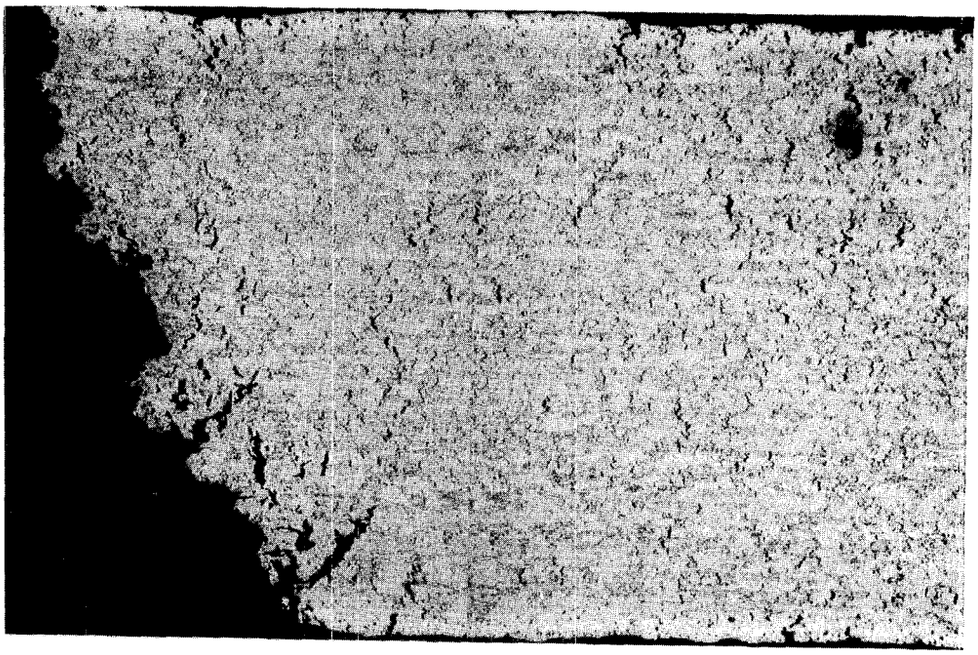

Figure 5-10 Fracture Appearance of HDA 8077 Lot MS 151 Creep Specimen Tested to Rupture in 0.1 hrs. at 982C (1800F), 89.6 MN/m^2 (13 ksi). Creep extension immediately prior to failure 1.54%; rupture elongation 6.5%. Not extensive secondary cracking having an intergrannular appearance.

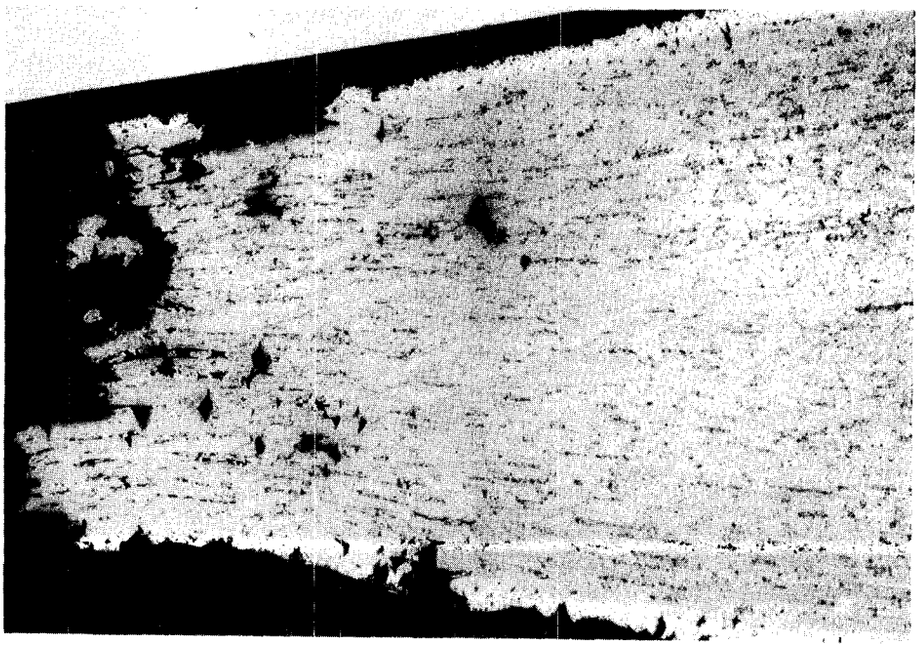

Figure 5-11 Fracture Appearance of HDA 8077 Lot MS 154 Creep Specimen Tested to Rupture in 14.7 hrs. at 982C (1800F), 89.6 MN/m^2 (13 ksi). Creep extension immediately prior to failure 1.84%; Rupture elongation 7.4%.

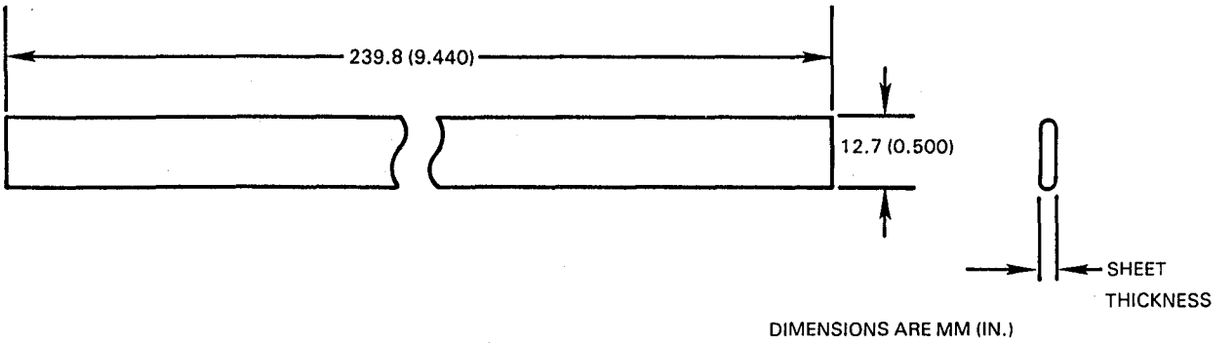

Figure 5-12 Low Cycle Fatigue Bend Specimen

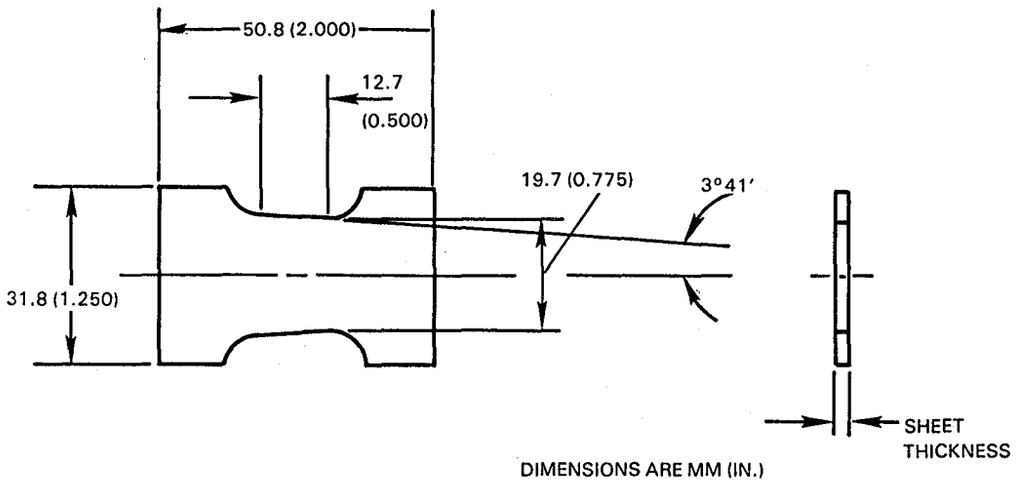

Figure 5-13 High Cycle Fatigue Bend Specimen

TABLE 5-V

FATIGUE RESULTS OBTAINED ON ODS ALLOYS TESTED IN
FULLY REVERSED BENDING AT 0.67 Hz, 0.005 mm/mm TOTAL STRAIN RANGE

Alloy	Lot	Temperature °C (°F)	Failure Life (Cycles)
MA 956	ZDEW	760 (1400)	4480
MA 956	ZDEW	760 (1400)	6350
MA 956	ZDEW	871 (1600)	3540
MA 956	ZDEW	871 (1600)	4840
MA 956	ZDEW	871 (1600)	7150
HDA 8077	MS 151	871 (1600)	4490
HDA 8077	MS 154-2	871 (1600)	2100
MA 956	ZDEW	982 (1800)	3320
MA 956	ZDEW	982 (1800)	4650
MA 956	ZDEW	982 (1800)	2700
HDA 8077	MS 151-4	982 (1800)	2940
HDA 8077	MS 153-2	982 (1800)	1622
HDA 8077	MS 153-2	982 (1800)	1499
HDA 8077	MS 153-2	982 (1800)	1343
HDA 8077	MS 153-4	982 (1800)	1335
HDA 8077	MS 153-4	982 (1800)	1401
HDA 8077	MS 153-4	982 (1800)	1367
HDA 8077	MS 154-2	982 (1800)	710
HDA 8077	MS 154	982 (1800)	1470
HDA 8077	MS 154	982 (1800)	1900

TABLE 5-VI

FATIGUE RESULTS OBTAINED ON ODS ALLOYS
TESTED IN FULLY REVERSED BENDING AT 30 Hz

Alloy	Lot	Temperature °C (°F)	Total Strain Amplitude mm/mm	Applied Cycles	Remarks
MA 956	ZDEW	760 (1400)	0.00120	10^7	Discontinued, Uploaded
			0.00183	8.5×10^6	Discontinued, Uploaded
			0.00236	9.60×10^4	Failed
MA 956	ZDEW	760 (1400)	0.00183	10^7	Discontinued, Uploaded
			0.00214	2.7×10^5	Failed
MA 956	ZDEW	760 (1400)	0.00196	5.65×10^6	Failed
HDA 8077	MS 151	760 (1400)	0.00340	3.44×10^6	Failed
HDA 8077	MS 151	760 (1400)	0.00345	2.39×10^6	Failed
HDA 8077	MS 154	760 (1400)	0.00280	10^7	Discontinued, Uploaded
			0.00310	10^7	Discontinued, Uploaded
			0.00340	10^7	Discontinued, Uploaded
			0.00366	6.86×10^6	Failed
HDA 8077	MS 154	760 (1400)	0.00380	1.8×10^6	Failed
MA 956	ZDEW	982 (1800)	0.00077	10^7	Discontinued, Uploaded
			0.00094	10^7	Discontinued, Uploaded
			0.00110	6.2×10^6	Failed
MA 956	ZDEW	982 (1800)	0.00120	1.96×10^6	Failed
MA 956	ZDEW	982 (1800)	0.00200	6.78×10^4	Failed
HDA 8077	MS 151	982 (1800)	0.00160	10^7	Discontinued, Uploaded
			0.00190	10^7	Discontinued, Uploaded
			0.00210	8.50×10^6	Failed
HDA 8077	MS 151	982 (1800)	0.00220	2.20×10^5	Failed
HDA 8077	MS 154	982 (1800)	0.00200	1.26×10^7	Discontinued, Uploaded
			0.00230	2.97×10^6	Failed
HDA 8077	MS 154	982 (1800)	0.00230	7.74×10^6	Failed

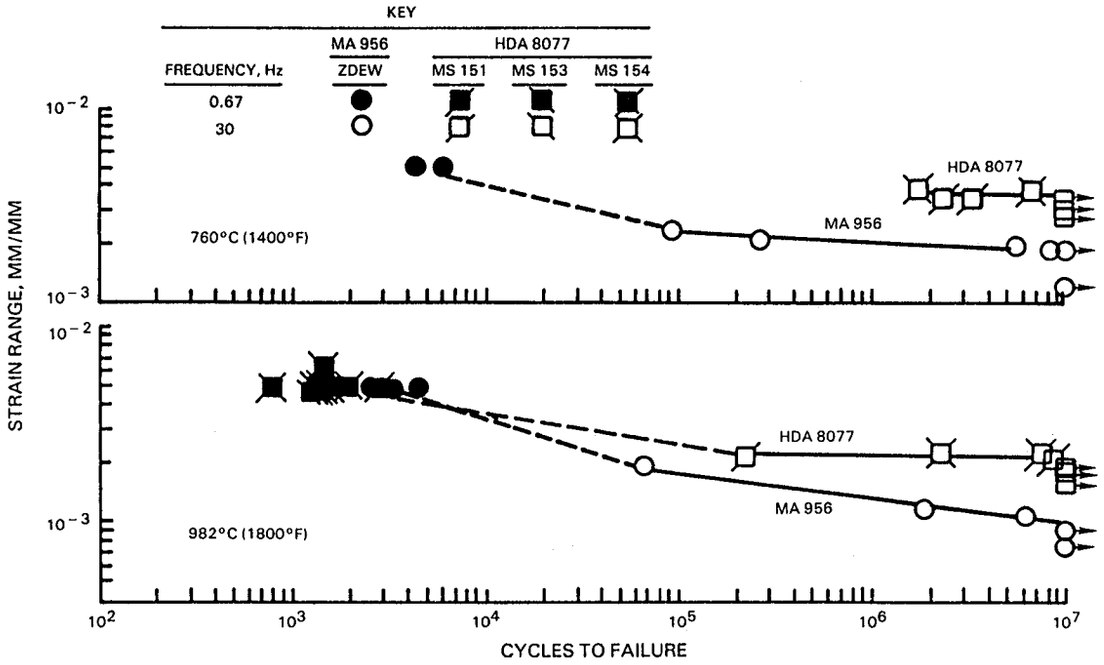

Figure 5-14 Comparison of Reversed Bending Fatigue Results Obtained on MA 956 and HDA 8077 Alloys

superior in the high cycle range, with 10^7 cycle strain range capability roughly double that of MA 956 at both 760°C (1400°F) and 982°C (1800°F). Based on only one result, the 982°C (1800°F) low cycle fatigue life of the best of the three lots of HDA 8077 (MS 151) appears to be somewhat below average results for MA 956. This result is consistent with data obtained at 871°C (1600°F), where respective average lives for MA 956 and HDA 8077 are 5177 and 3295 cycles at 0.005 mm/mm strain range (Table 5-VI). Thus, it appears that MA 956 has somewhat superior low cycle fatigue and much inferior high cycle fatigue capability as compared to HDA 8077.

Metallographic examination of fractured MA 956 982°C (1800°F) fatigue specimens revealed similar low cycle fatigue and high cycle fatigue fracture characteristics (Figure 5-15). Surface initiated, transgranular cracks propagated through the specimen and produced intergranular cracks (delamination) parallel to the principal stress axis. Similar fracture characteristics were observed at lower temperatures.

Metallographic examination of HDA 8077 high cycle fatigue fractures revealed transgranular crack propagation perpendicular to the principal stress axis at both test temperatures. Typical fractures at 982°C (1800°F) are shown in Figure 5-15. The 982°C (1800°F) low cycle fatigue fracture characteristics are similar to the high cycle fatigue characteristics with the exception of evidence of intergranular cracking along stringers of fine grains parallel to the principal stress axis in the low cycle fatigue fractures.

5.1.5 Thermal Fatigue

Comparative "Hot Spot Blister" thermal fatigue tests were conducted on MA 956, HDA 8077, and Hastelloy X using the disk-shaped test specimen shown in Figure 5-16. This test, shown in Figure 5-17, is designed to produce localized distortion and thermal fatigue cracking similar to that produced by flame impingement on a combustor louver. Finite element analysis of this test has indicated that, with a measured through thickness gradient on the order of 22°C (40°F), the temperature-strain phase relationship experienced on the surface of the disk opposite the point of heat application ("cold side") closely simulates that experienced in a combustor application, with tensile strain occurring during the low temperature and compressive strain during the high temperature portion of the cycle. The strain-temperature phase relationship on the opposite ("Hot") side tends to be the opposite of this (tension hot, compression cold), with a substantially lower calculated strain range.

The test procedure involves alternate localized oxy-acetylene torch heating and forced air cooling at the center of the disk. The outer periphery of the disk is maintained at a "background" temperature of 538°C (1000°F) by the propane burner shown in Figure 5-17, while the center of the disk is cycled between the 538°C (1000°F) background temperature and a predetermined maximum temperature. For this series of tests, hot spot temperature was measured by a thermocouple spot welded to the back side of the disk. Five series of tests were conducted at respective maximum cold side temperatures (T_{max}) of 871°C (1600°F), 927°C (1700°F), 982°C (1800°F), 1038°C (1900°F), and 1093°C (2000°F). Heating and cooling rates were the same regardless of T_{max}; therefore the heating cycle varied from six to ten seconds and the cooling

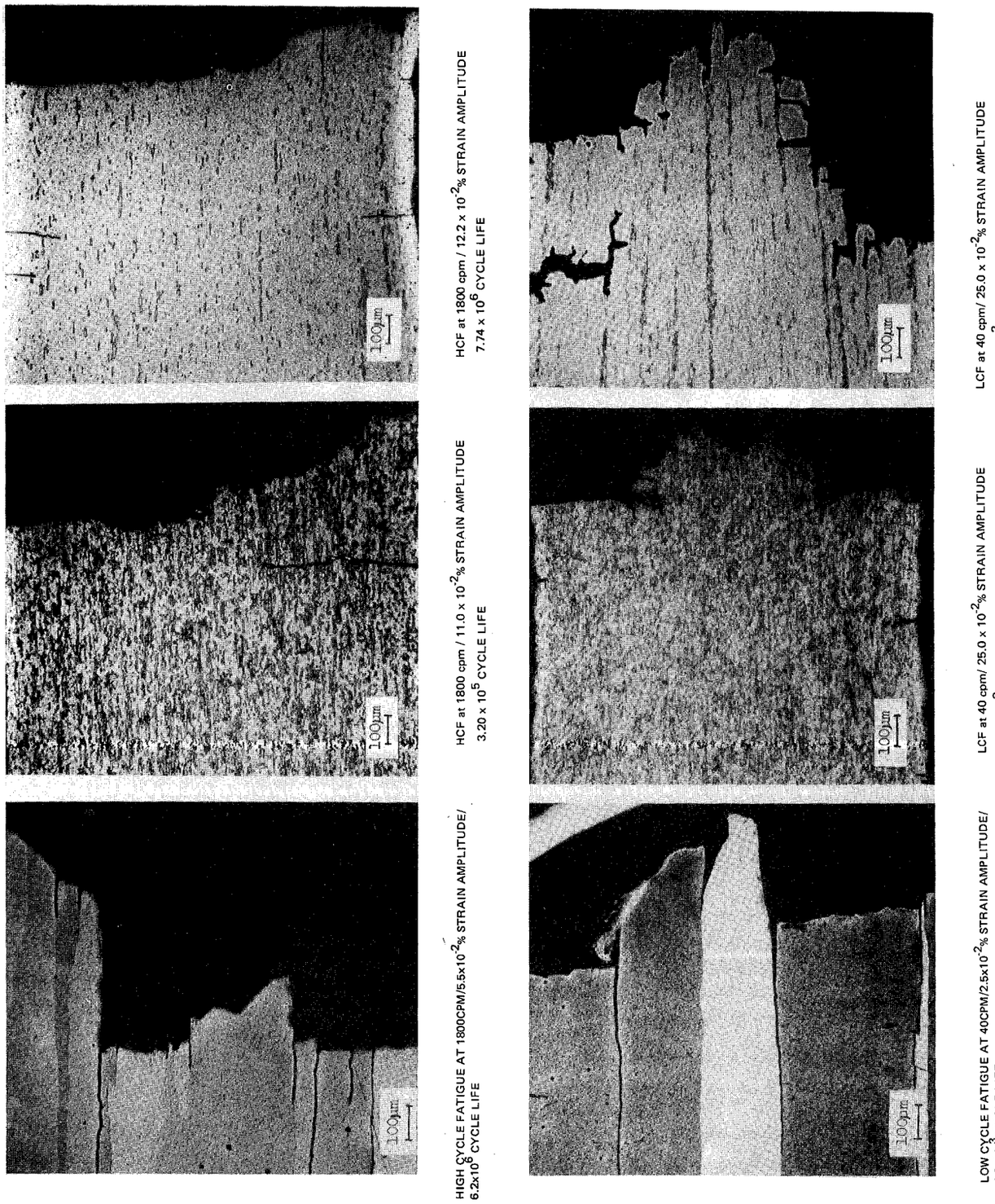

Figure 5-15 Fatigue Fracture Microstructures of MA 956 and HDA 8077 Tested at 982C (1800F) in Fully Reversed Bending (indicated strain amplitudes are one-half the total strain range).

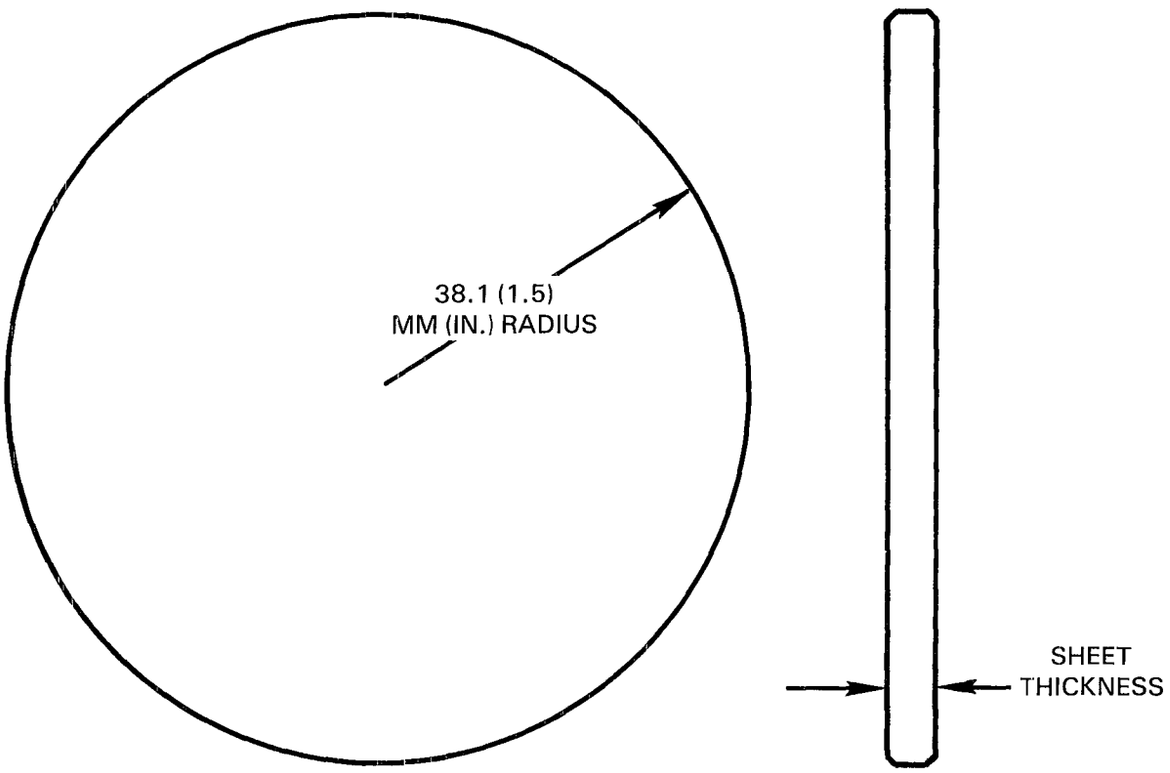

Figure 5-16 Hot Spot Blister Thermal Fatigue Test Specimen

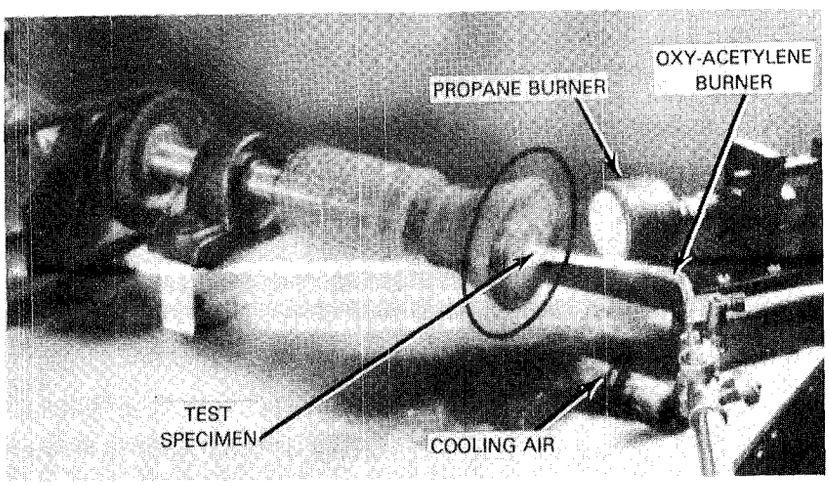

Figure 5-17 Hot Spot Blister Thermal Fatigue Rig

rate from three to five seconds depending on the T_{max} being evaluated. This variation resulted in a variation of cycle rate from approximately seven cycles per minute for specimens cycled between 538°C (1000°F) and 871°C (1600°F) to approximately four cycles per minute for specimens cycled from 538°C (1000°F) to 1093°C (2000°F).

To evaluate progressive thermal distortion, hot spot deflection height was measured every 100 cycles using a profilometer. A typical example of a thermally distorted specimen is shown in Figure 5-18. Degree of surface cracking also was noted visually during these inspections. An example of visually observable cold and hot side surface cracking is shown in Figure 5-19. At least one and in most cases two or three specimens were tested to 500 cycles. In addition, based on observed surface crack initiation lives, selected specimens were tested to shorter numbers of cycles and examined metallographically to assess depth of crack penetration and degree of surface oxidation as a function of applied cycles.

Results of progressive thermal distortion measurements on all three alloys are summarized in Figure 5-20. These results clearly demonstrate the superior distortion resistance of both ODS alloys as compared to Hastelloy X, with relatively little difference being seen between the two oxide dispersion strengthened materials. As shown in Figure 5-20c, selective 982°C (1800°F) tests were interrupted after five cycles to measure deflection. Results of these measurements indicate that the majority of the distortion in the ODS alloys occurs very early in testing. Hastelloy X, on the other hand, continues to distort progressively up to the maximum exposure investigated. As seen by comparison of Figures 5-20a through e, this trend becomes more pronounced as the maximum hot spot temperature increases.

As indicated earlier, the strain range calculated on the cold side of the specimen, where the strain-temperature phase relationship best simulates that of a combustor louver, is larger than the strain range on the hot side. As expected on the basis of this calculation, cracking is visually observed to initiate at a smaller number of cycles on the cold side than on the hot side. Results of metallographic cold wall crack penetration measurements on specimens tested with a T_{max} of 982°C (1800°F) are presented in Figure 5-21. As expected, the thermal fatigue cracking resistance of both ODS alloys is poor compared to Hastelloy X, with HDA 8077 exhibiting better performance than MA 956.

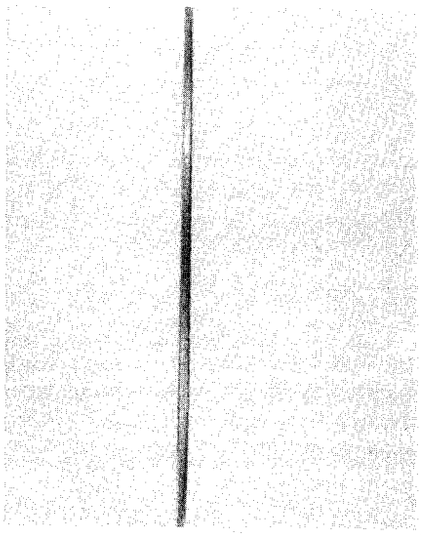

a) EDGE VIEW BEFORE TEST

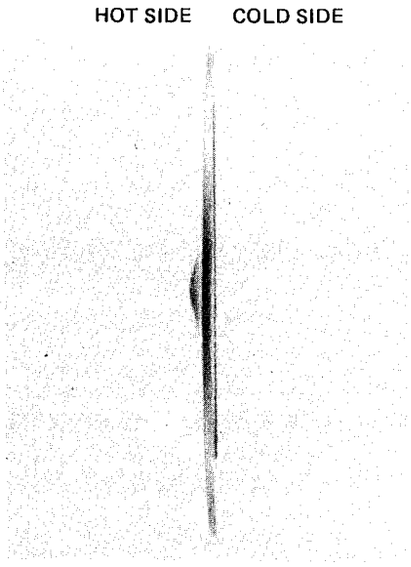

b) EDGE VIEW AFTER TEST

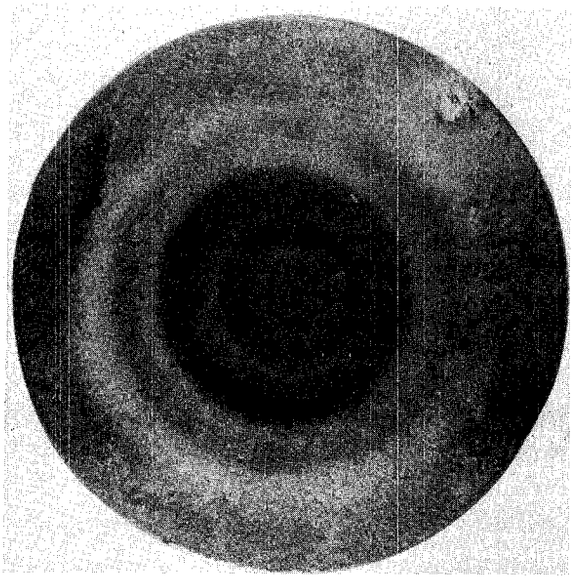

c) HOT SIDE VIEW AFTER TEST

Figure 5-18 Photographs of Hot Spot Blister Thermal Fatigue Test Specimens

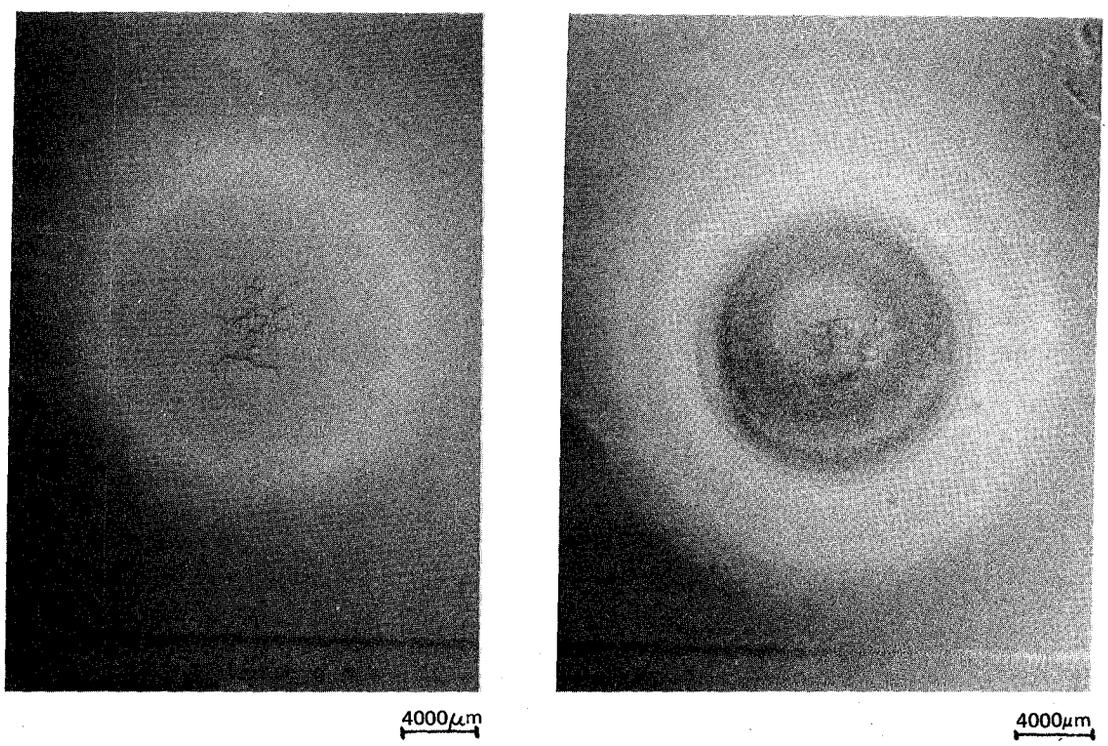

Figure 5-19 Surface Cracking Observed on MA 956 Hot Spot Blister Thermal Fatigue Specimens Exposed 500 Cycles to a Tmax of 1038C (1900F)

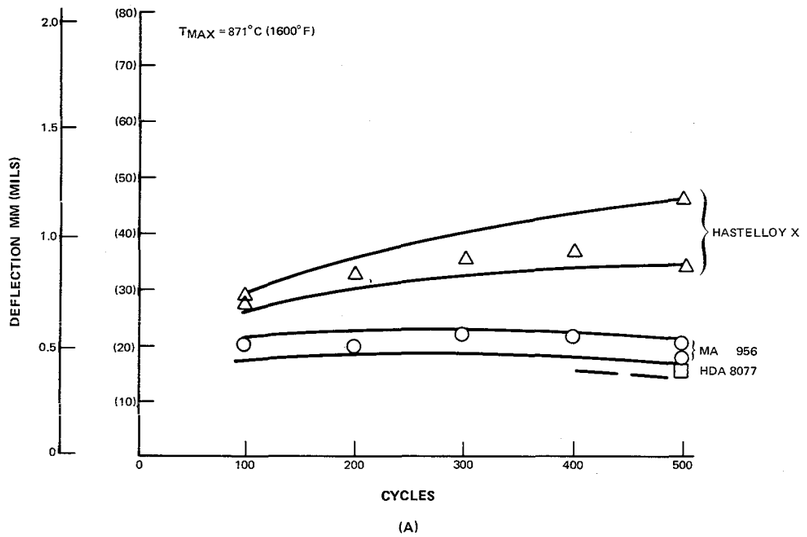

(A)

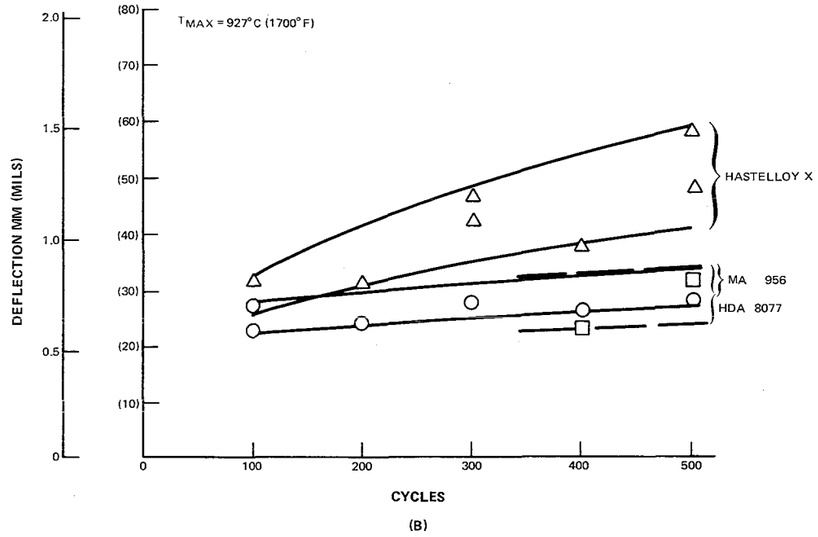

(B)

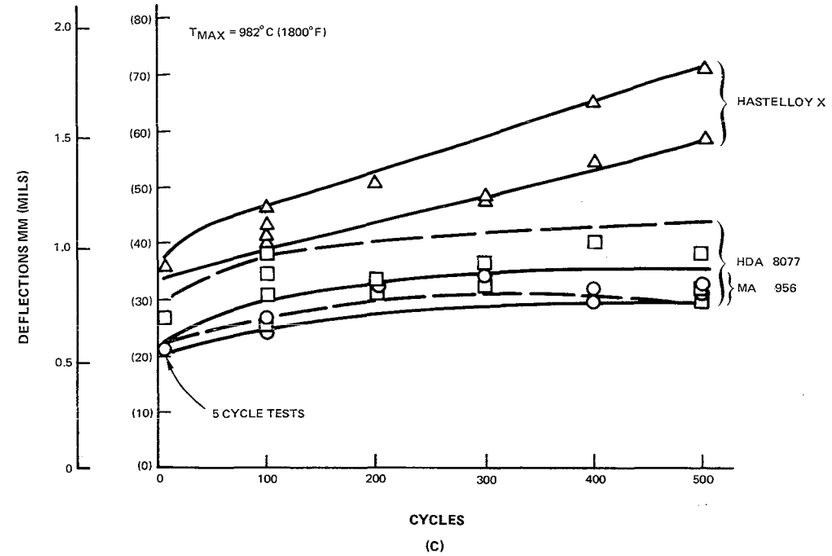

(C)

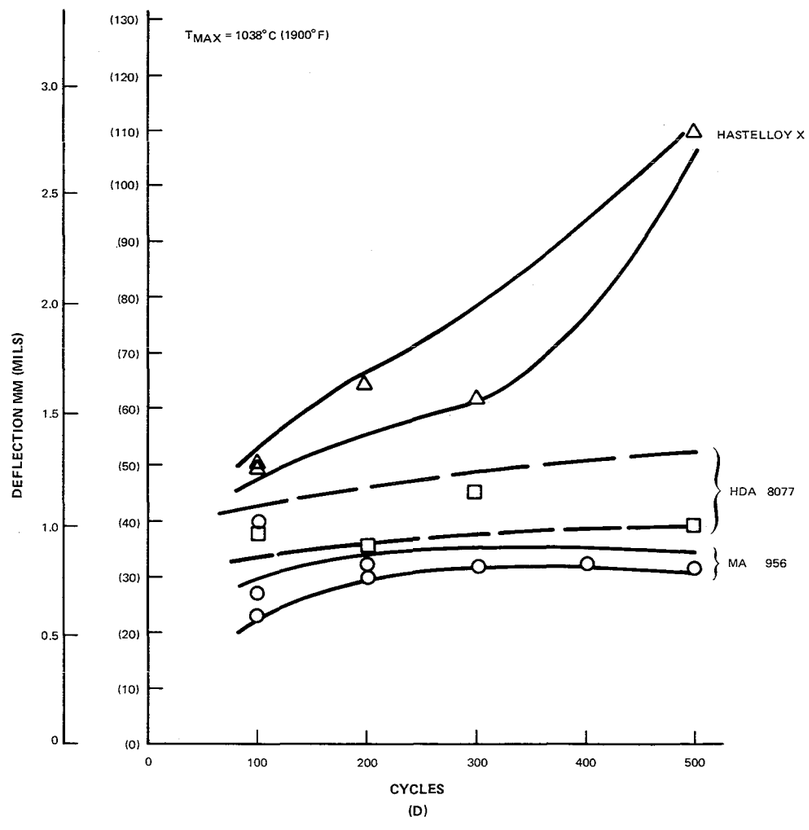

(D)

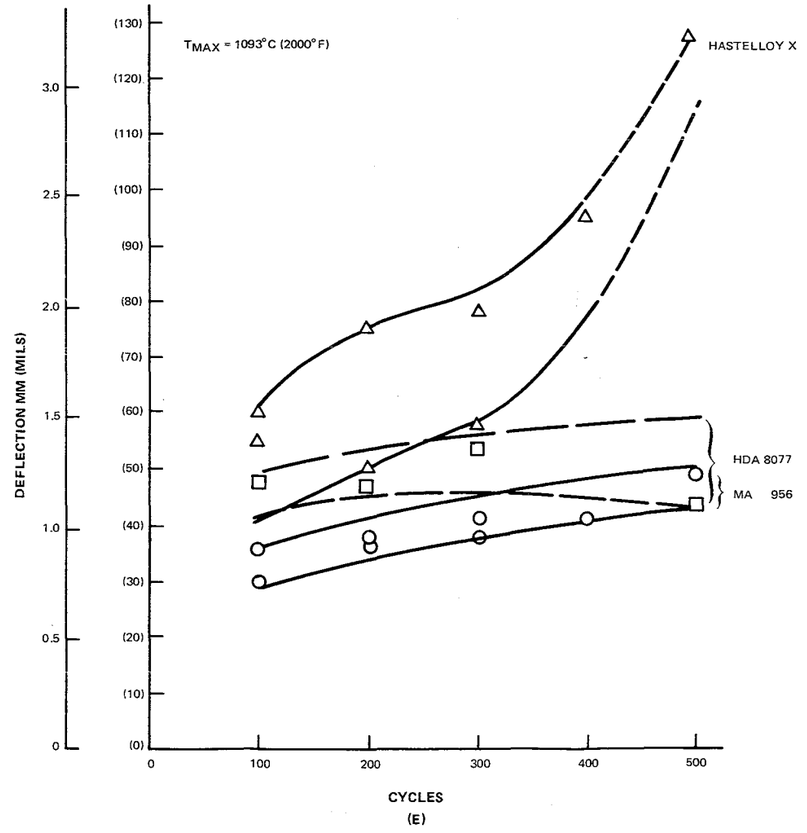

(E)

Figure 5-20 Thermal Fatigue Deflection Comparison (T_{min} = 538C (1000F)

This Page Intentionally Left Blank

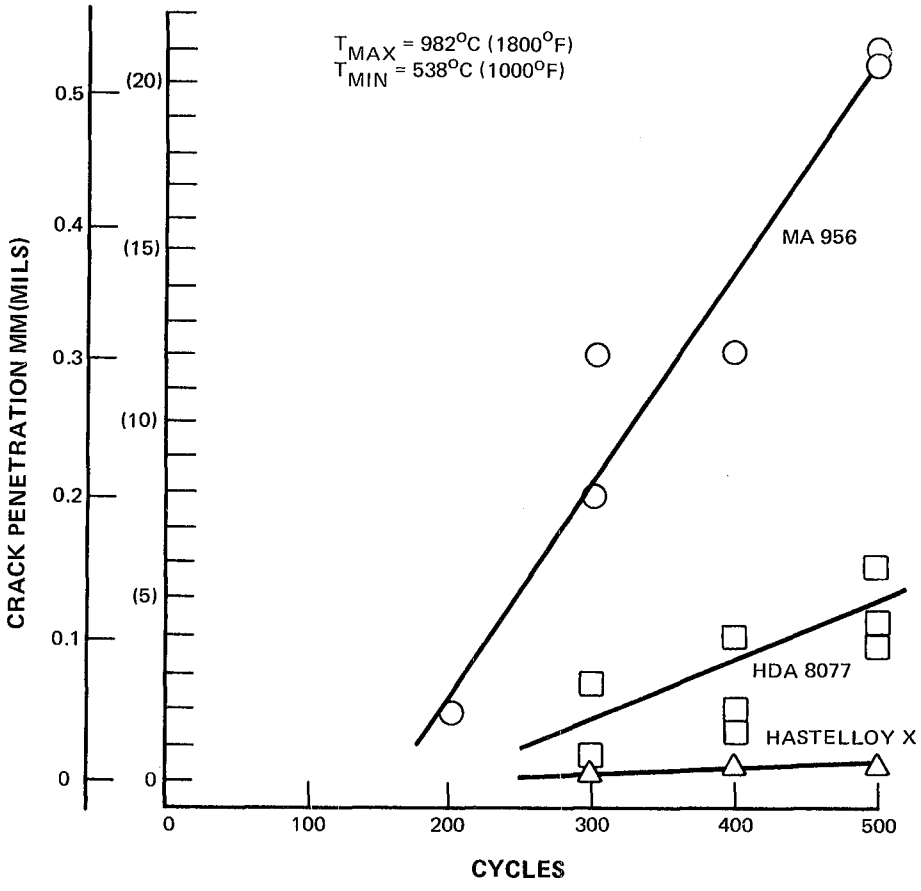

Figure 5-21 Hot Spot Blister Thermal Fatigue Test Cold Wall Cracking Comparison

Metallographic observations of crack morphology and oxidation damage observed on specimens tested with a T_{max} of 982°C (1800°F) are summarized in Figure 5-22. Minimal intergranular cracking but extensive surface oxidation was evident on the hot and cold sides of the Hastelloy X specimens (Figure 5-22a). The MA 956 specimens exhibited only minimal oxidation associated with numerous transgranular initiated, intergranular cracks in both the hot and cold sides of the specimens (Figure 5-22b). The transgranular cracks in the cold side of the specimens initiated along slip bands in areas of fine recrystallized grains, apparently the result of the high calculated strain range (0.8%) at T_{max} = 982°C (1800°F). Once the transgranular cracks intersect a longitudinal grain boundary, cracking or delamination occurs along that boundary. At some point, a transgranular crack will reinitiate from this grain boundary and proceed to the next boundary, repeating the crack propagation process. Transgranular cracking and grain boundary delamination were also

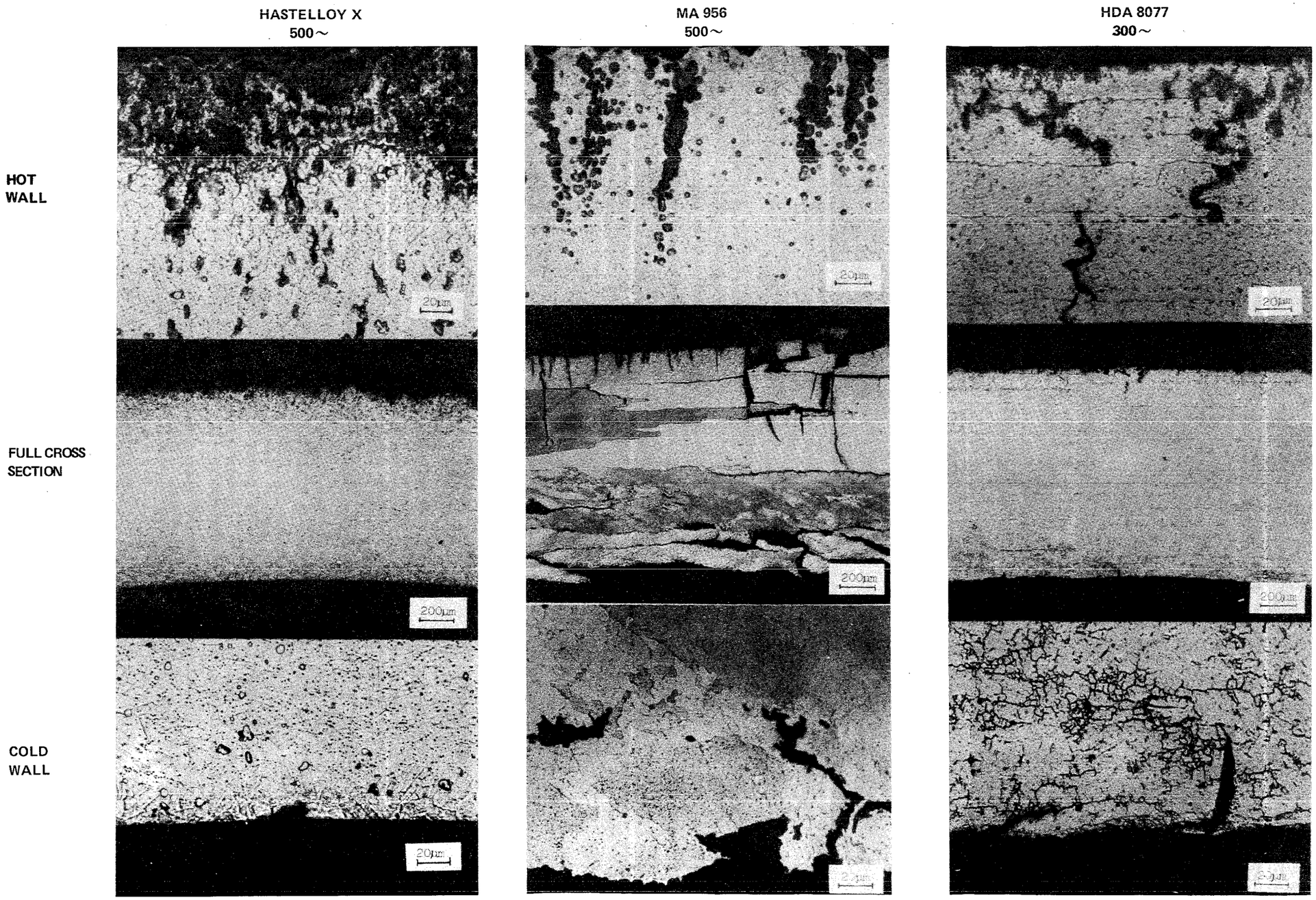

Figure 5-22 Typical Microstructures Observed in Hot Spot Blister Specimens Cycled Between 538C (1000F) and 982C (1800F)

This Page Intentionally Left Blank

evident in the hot side of the MA 956 specimens. These hot wall cracks appear to initiate as voids which coalesce to form cracks. HDA 8077 specimens exhibited transgranular cold side cracking and intergranular hot side cracking (Figure 5-22c); slight oxidation was present on both sides of the specimens. Extensive twinning and recrystallization were observed at the cold wall of the HDA 8077 specimens after 300 cycles at 982°C (1800°F), but no preferential cracking was associated with these fine grain areas.

5.1.6 Cyclic Oxidation

Cyclic burner rig oxidation tests were conducted at 982°C (1800°F) on Hastelloy X and both candidate ODS alloys. This test involves cyclic flame heating and forced air cooling of the sheet metal specimen illustrated in Figure 5-23. To perform this test, twelve specimens are installed in a carousel which is rotated in the exhaust gases of a Jet A fueled burner, as shown in Figure 5-24. Specimen temperature is measured and controlled using an optical pyrometer and automatic feedback fuel controller. To provide thermal cycling, the burner periodically is moved away and compressed air is directed onto the specimens. Total cycle duration is six minutes, with four minutes of heating and two minutes of forced air cooling. Based on measured transients, the specimens are at the indicated test temperature for approximately 3 minutes per cycle.

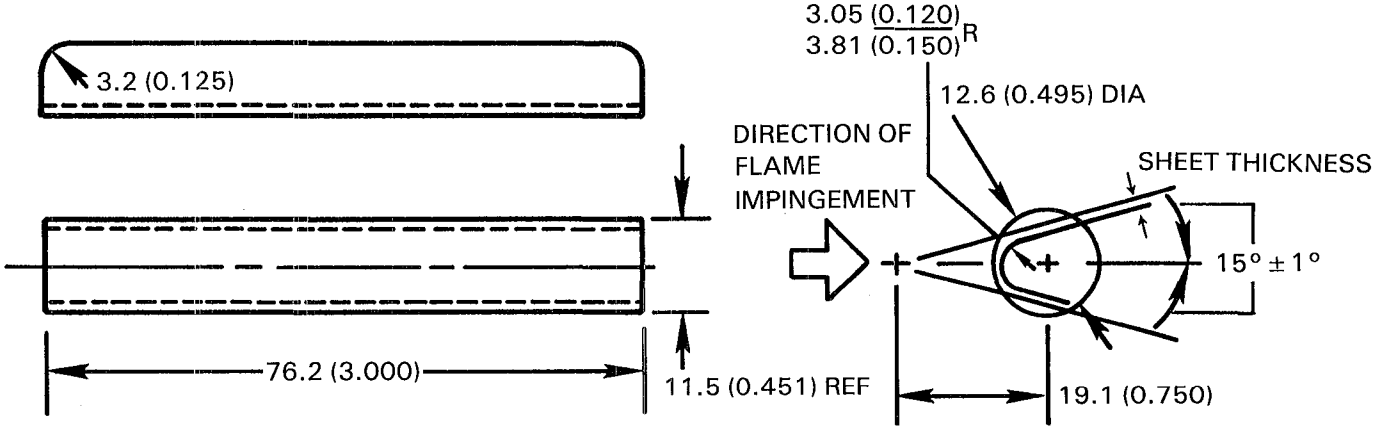

Figure 5-23 Sheet Metal Oxidation Burner Rig Test Specimen

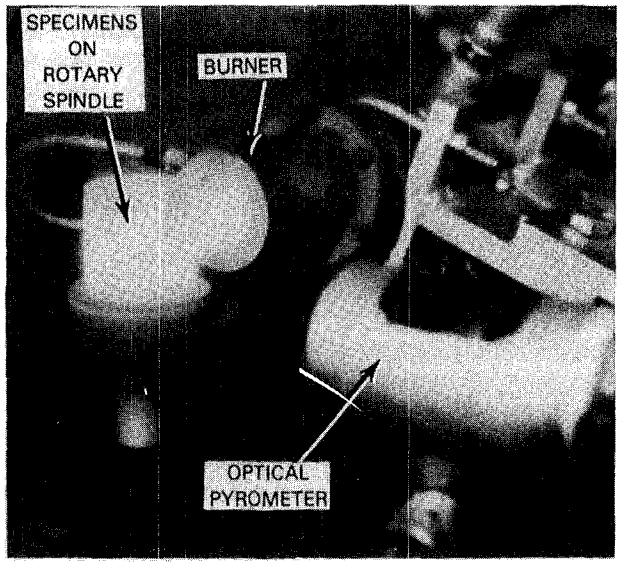

Figure 5-24 Burner Rig in Operation During the Hot Portion of the Cycle

To evaluate the depth of oxidation attack, replicate specimens of each alloy exposed for respective periods of 100, 250, 500, 750, and 1000 hours were sectioned and examined metallographically. Photographs comparing the surface appearance of specimens cycled for 1000 hours are shown in Figure 5-25; depth of attack data are presented in Figure 5-26. These results clearly show the large oxidation benefit of both ODS alloys as compared to the current combustor material, with MA 956 being slightly better than HDA 8077. The oxidation resistance exhibited by the ODS alloys at 982°C (1800°F) is approximately equal to that provided by Hastelloy X at 816°C (1500°F). The increased distortion resistance resulting from the higher creep strength of the ODS materials also is apparent in Figure 5-25, which shows severe distortion of the Hastelloy X specimen. Surface recrystallization associated with the previously mentioned surface worked layer on as-received MA 956 Lot ZDEW is apparent in Figure 5-25d. Structural changes resulting from thermal exposure are discussed more fully in the following section.

5.1.7 Alloy Stability

Retention of material properties in service is an important aspect of material suitability for elevated temperature applications. Because of this importance, several investigations were conducted to evaluate the stability of the two candidate ODS alloys. To assess microstructural stability, metallographic

a) MA 956 LEADING EDGE

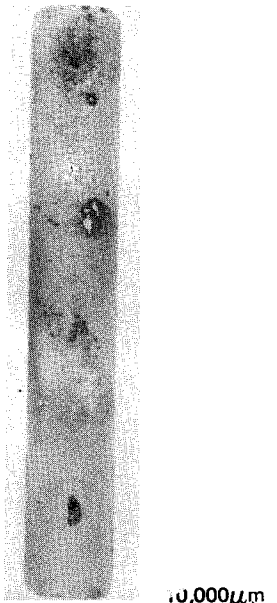

b) HDA 8077 LEADING EDGE

c) HASTELLOY X LEADING EDGE AND SIDE VIEWS

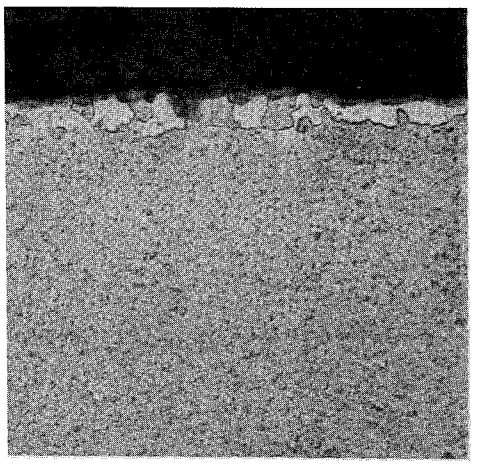

d) MA 956

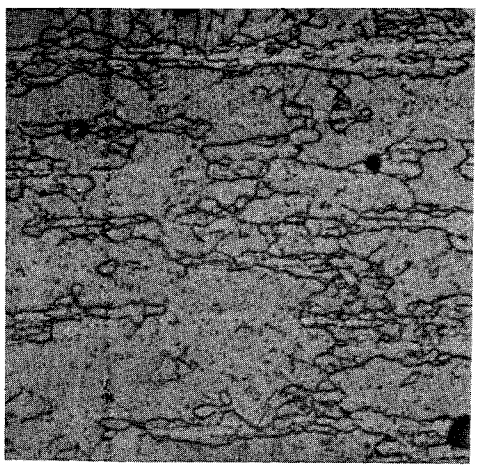

e) HDA 8077

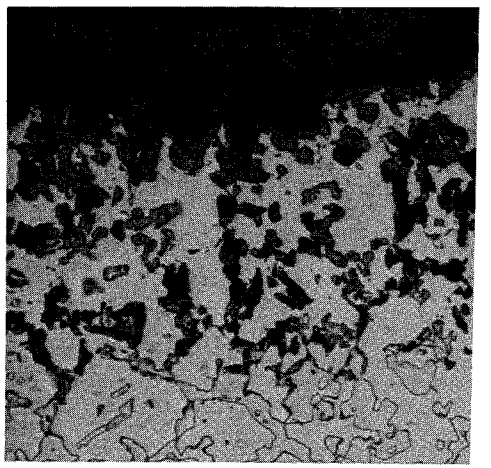

f) HASTELLOY X

Figure 5-25 Surface Appearance of Cyclic Oxidation Test Specimens Tested 1000 hrs at 982C (1800F)

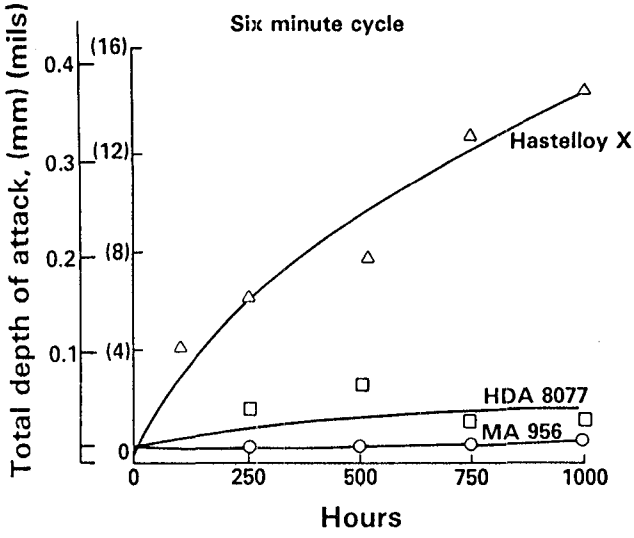

Figure 5-26 982C (1800F) Cyclic Oxidation Test Results

examinations and hardness tests were conducted on furnace exposed samples of as-received alloy and of material which was cold worked 20% to simulate forming strain introduced during component fabrication. Selected post-exposure property tests also were conducted to measured property retention. the direction of this latter effort was influenced by earlier observations of severe room temperature embrittlement resulting from creep exposure of other oxide dispersion strengthened alloys (Reference 5-3), and from furnace exposure of MA 956 alloy (Reference 5-4). This latter phenomenon was reported by the alloy manufacturer during the course of this program. As reported in the following sections, post-creep embrittlement was not observed in either candidate alloy, and the post-exposure embrittlement of MA 956 was judged not to be a significant limitation on the suitability of the alloy for combustor applications.

5.1.7.1 Effect of Thermal Exposure on Hardness and Microstructure

5.1.7.1.1 Exposure of As-Received Material

Stability of the two candidate oxide dispersion strengthened alloys was evaluated by measuring changes of hardness caused by furnace exposure for various periods. Variations in hardness with temperature and time to 5000 hours are shown in Figure 5-27 for MA 956 Lot ZDEW and HDA 8077 Lot MS 151.

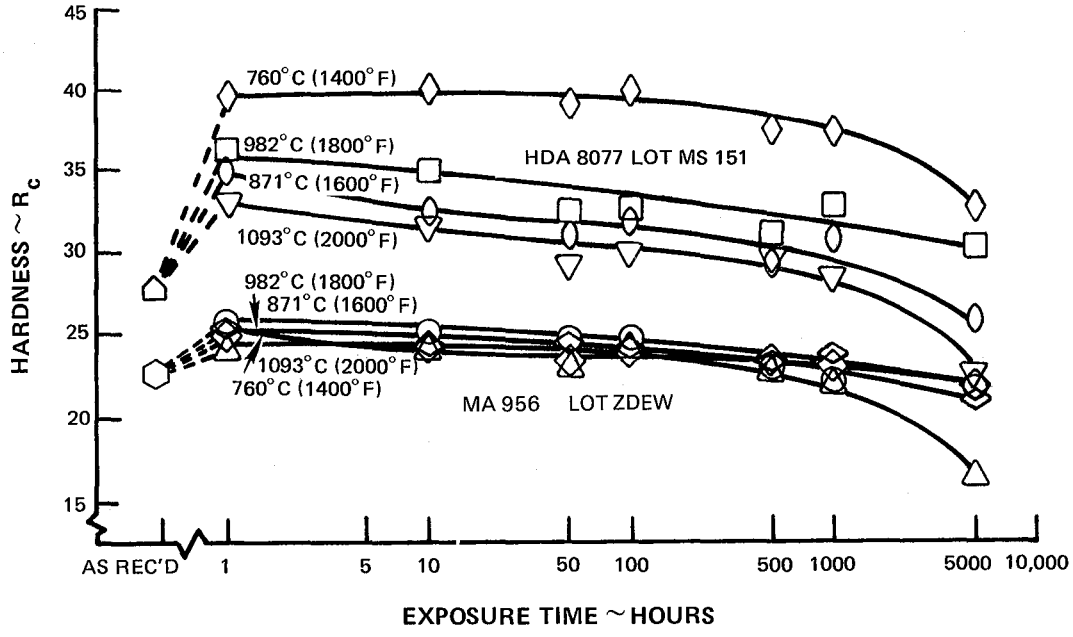

Figure 5-27 Variation of MA 956 and HDA 8077 Hardness with Exposure Time at Various Temperatures

MA 956 exhibits a small initial increase in hardness at all temperatures, followed by a small gradual decrease in hardness out to 5000 hours at temperatures up to 982°C (1800°F). Exposure at 1093°C (2000°F) results in a significant decrease in hardness between 1000 and 5000 hours. These variations of MA 956 hardness were attributed to the precipitation, growth and subsequent coarsening of a second phase with increased temperature and exposure time. Typical photomicrographs of this phase are shown in Figure 5-28. This phase initially was thought to be a carbide; however, a recent report from the alloy manufacturer refers to nitrides (Ref. 5-4).

MA 956 sheet exposed for 5000 hours at all temperatures investigated displayed a narrow (10 μm (3.9 x 10^{-4} in.)) band of recrystallized grains on the sheet surfaces (Figure 5-29). This surface recrystallization was attributed to surface working caused by the grit blasting operation employed during sheet manufacture (see Section 4). Surface recrystallization was observed as early as 1000 hours at 760°C (1400°F) and 871°C (1600°F) and 500 hours at 983°C (1800°F) and 1093°C (2000°F).

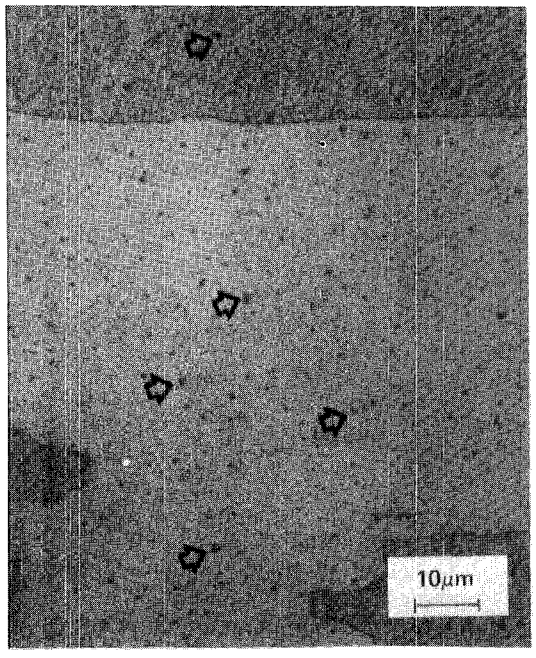

A) AS RECEIVED

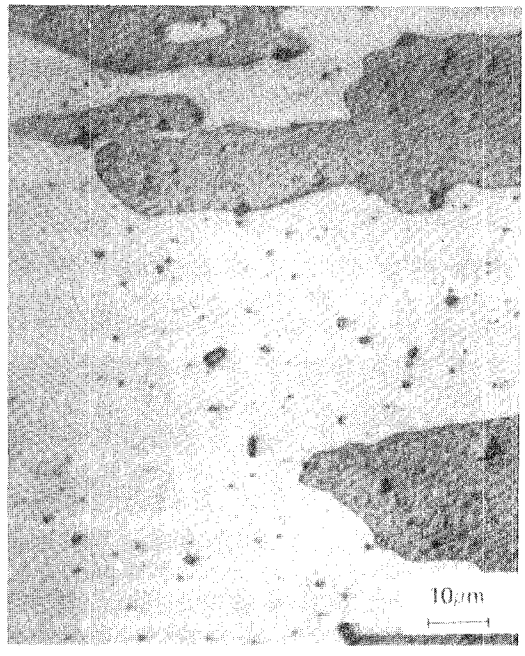

B) EXPOSED 1000 HOURS

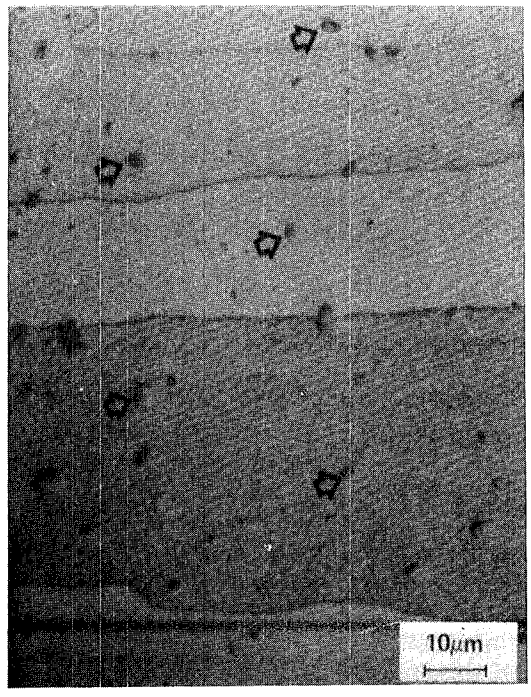

C) EXPOSED 5000 HOURS

Figure 5-28 Carbide or Nitride Phase Observed in MA 956 Lot ZDEW Exposed for Various Times at 1093C (2000F)

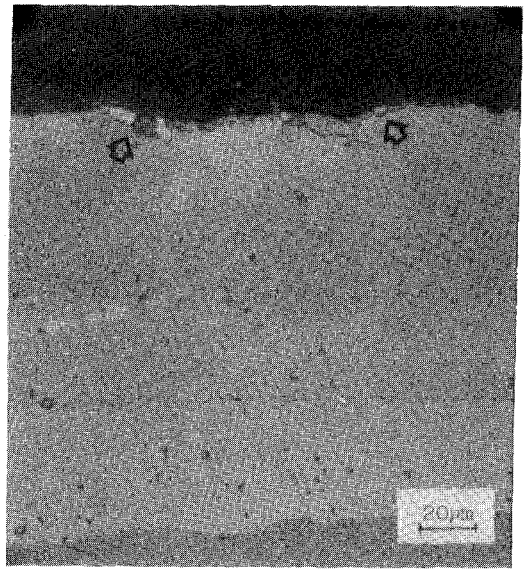

1093°C(2000°F) – 5000 HOURS

Figure 5-29 MA 956 Lot ZDEW Typical Surface Recrystallized Layer

As noted in Section 4, the surface hardening found in MA 956 Lot ZDEW is eliminated by annealing at 1177°C (2150°F) for 1/2 hour. Exposure of annealed samples of Lot ZDEW at 760°C (1400°F) and 1093°C (2000°F) for 10, 50, 100, and 500 hours indicated that residual effects of surface working still were present after annealing. Detailed examination of the 1177°C (2150°F)/1/2 hour as-annealed material revealed isolated pockets of surface recrystallization to a depth of 5μm (2.0×10^{-4} in.). During subsequent stability exposures at 760°C and 1093°C (1400°F and 2000°F) for 10 hours, this layer achieves a uniform depth of 10μm (3.9×10^{-4} in.) and shows no additional growth with longer time. Additional studies of MA 956 Lot XBB-004 (see Section 4) indicate that surface recrystallization of MA 956 is eliminated with improved processing. Sheet processed with a light scotch bright treatment rather than grit blasting shows no evidence of surface recrystallization after these same heat treatments.

HDA 8077 Lot MS-151 exhibited an initial increase in hardness at all temperatures (Figure 5-27), attributed to gamma prime precipitation, which was suppressed with a rapid cool from the recrystallization temperature during processing. Material exposed at 760°C (1400°F) exhibited the highest hardness of the four exposure temperatures investigated and had significant grain growth after 5000 hours (Figure 5-30). Exposures at 871°C and 982°C (1600°F and 1800°F) for 5000 hours resulted in the precipitation of coarse gamma prime

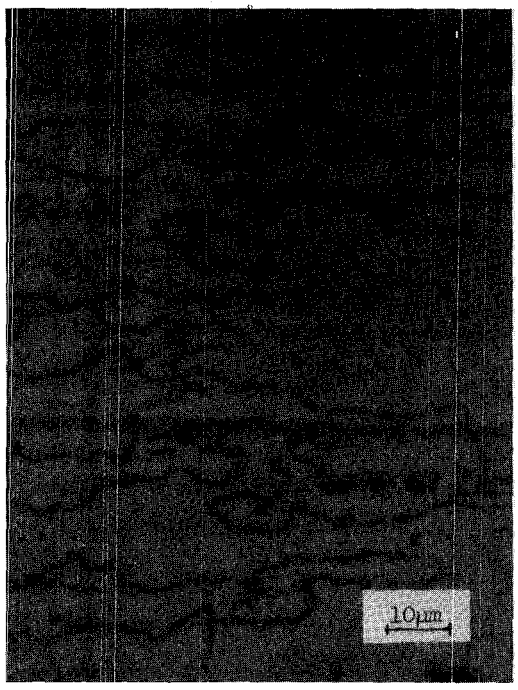

a) 760°C (1400°F)

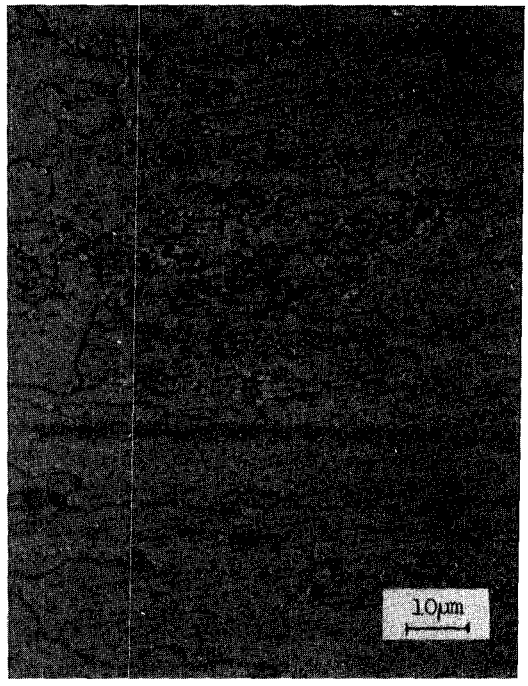

b) 871°C (1600°F)

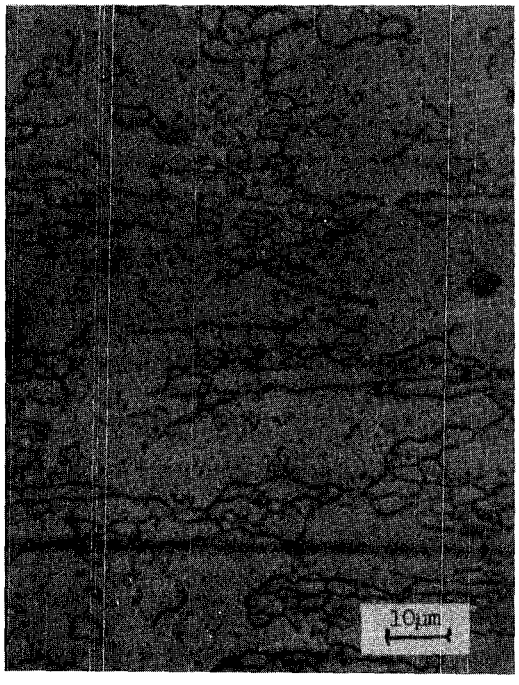

c) 982°C (1800°F)

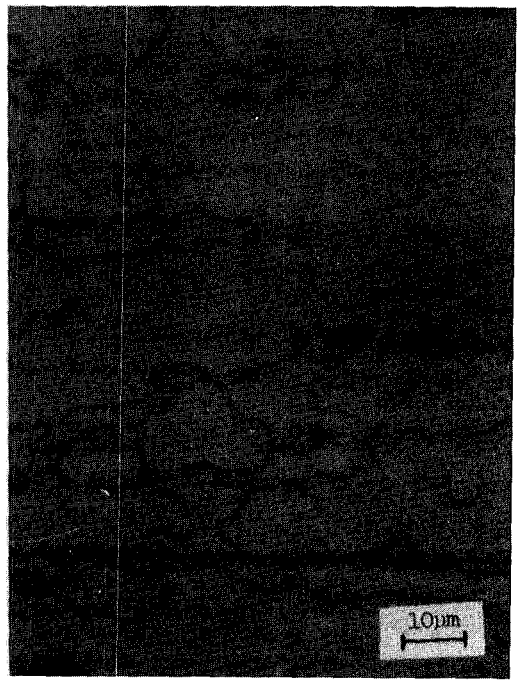

d) 1093°C (2000°F)

Figure 5-30 Microstructures of HDA 8077 Lot MS 151 After 5000 Hours Exposure

and a carbide phase which impeded grain growth (Figure 5-30). The presence of overaged coarse gamma prime resulted in a lower hardness than the 760°C (1400°F) exposure. All exposures at 1093°C (2000°F) resulted in lower hardness values due to re-solutionizing of gamma prime. At 1093°C (2000°F) grain growth was not observed until after 500 hours of exposure when the carbide phase was no longer in the microstructure and grain growth could proceed. Exposure of HDA 8077 lot MS 153 for times up to 1000 hours at 871°C (1600°F) and 1093°C (2000°F) indicated changes of hardness and microstructure similar to those observed in lot MS 151, including the formation of internal voids discussed in the following paragraph. The microstructure of material exposed at 871°C (1600°F) contained overaged γ' in the matrix and grain boundaries and showed traces of microtwinning (Figure 5-31a). In addition, a γ' denuded zone was evident on the sheet surfaces. Material exposed at 1093°C (2000°F) was observed to microtwin extensively during exposure (arrows, Figure 5-31b).

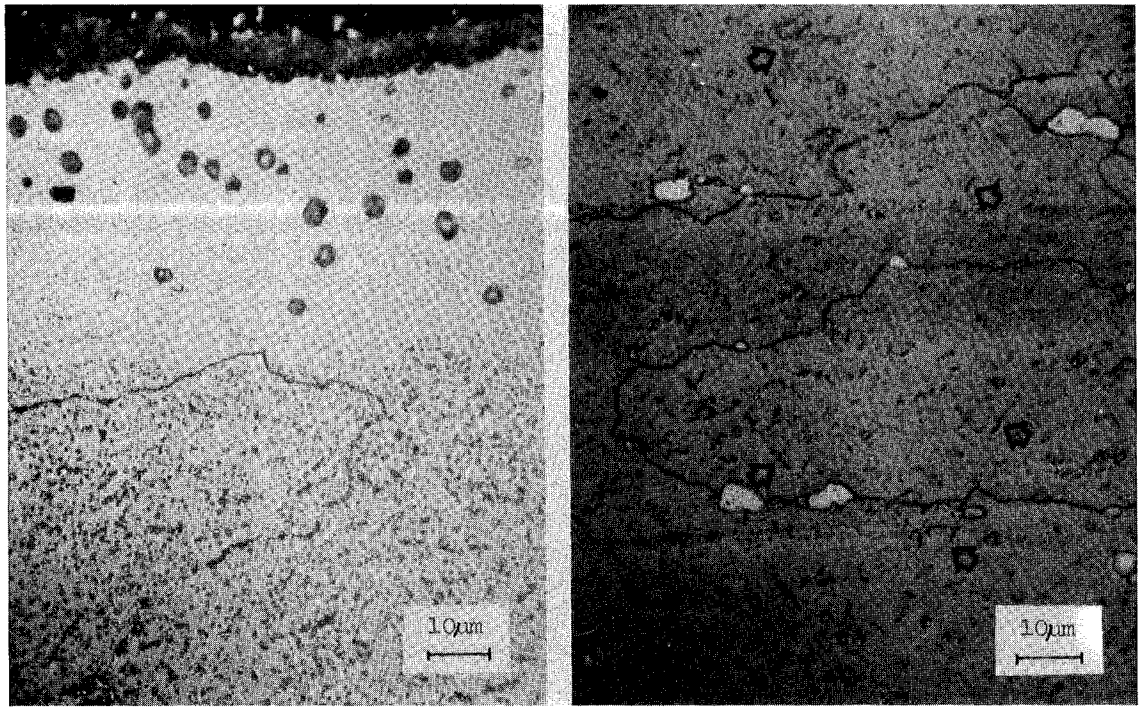

(A) 871°C (1600°F)

(B) 1093°C (2000°F) ARROWS SHOW MICRO TWINS

Figure 5-31 Microstructure of HDA 8077 Lot MS 153 After 1000 Hours of Exposure

Formation and growth of internal voids was observed in both alloys after long time exposures above 760°C (1400°F). Voids first appeared near the sheet surfaces. However, as time progressed, the voids became larger and concentrated in the center regions of the sheet as shown in Figures 5-32 and 5-33.

To characterize and better understand the void formation phenomenon, coupons of recrystallized and unrecrystallized material from the same respective lots of MA 956 and HDA 8077 were exposed in air at 1093°C (2000°F) for 1, 10, 50, 100, 500 and 1000 hours. As-rolled and recrystallization annealed samples of the MA 956 baseline experimental lot (see Section 4) and of HDA 8077 lot MS 149 were obtained from the respective sheet manufacturers for this experiment. In the unrecrystallized material no void formation occurred until the onset of recrystallization which was after 10 hours in MA 956 and after 50 hours in HDA 8077. At that time, void formation was observed to occur in the same manner as it did in recrystallization annealed material. Voids formed at the surface and after longer times became concentrated in the center of the sheet. Figures 5-34 and 5-35 show the progression of void formation in unetched samples of MA 956 and HDA 8077.

To investigate the influence of furnace atmosphere on void formation in MA 956, identical coupons were exposed in air and in argon for 10 hours at 1093°C (2000°F). As shown by comparison of Figures 5-36 a and b, furnace atmosphere appears to have little influence on the formation of voids in this alloy.

5.1.7.1.2 Exposure of 20% Cold Worked Material

To investigate the effect of cold work experienced during combustor fabrication on the stability of ODS alloys, samples of MA 956 lot ZDEW and HDA 8077 lots MS 151 and MS 154 were cold rolled 20% and exposed for various times up to 1000 hours at 1093°C (2000°F). Both alloys show hardness increases after rolling above that of the as-received material (Figure 5-37); however, one hour of exposure at 1093°C (2000°F) relaxes much of the cold working as indicated by the decrease in hardness levels. Hardness levels remain relatively constant out to 100 hours of exposure; however, reductions in hardness were observed after 500 and 1000 hour exposures in both materials.

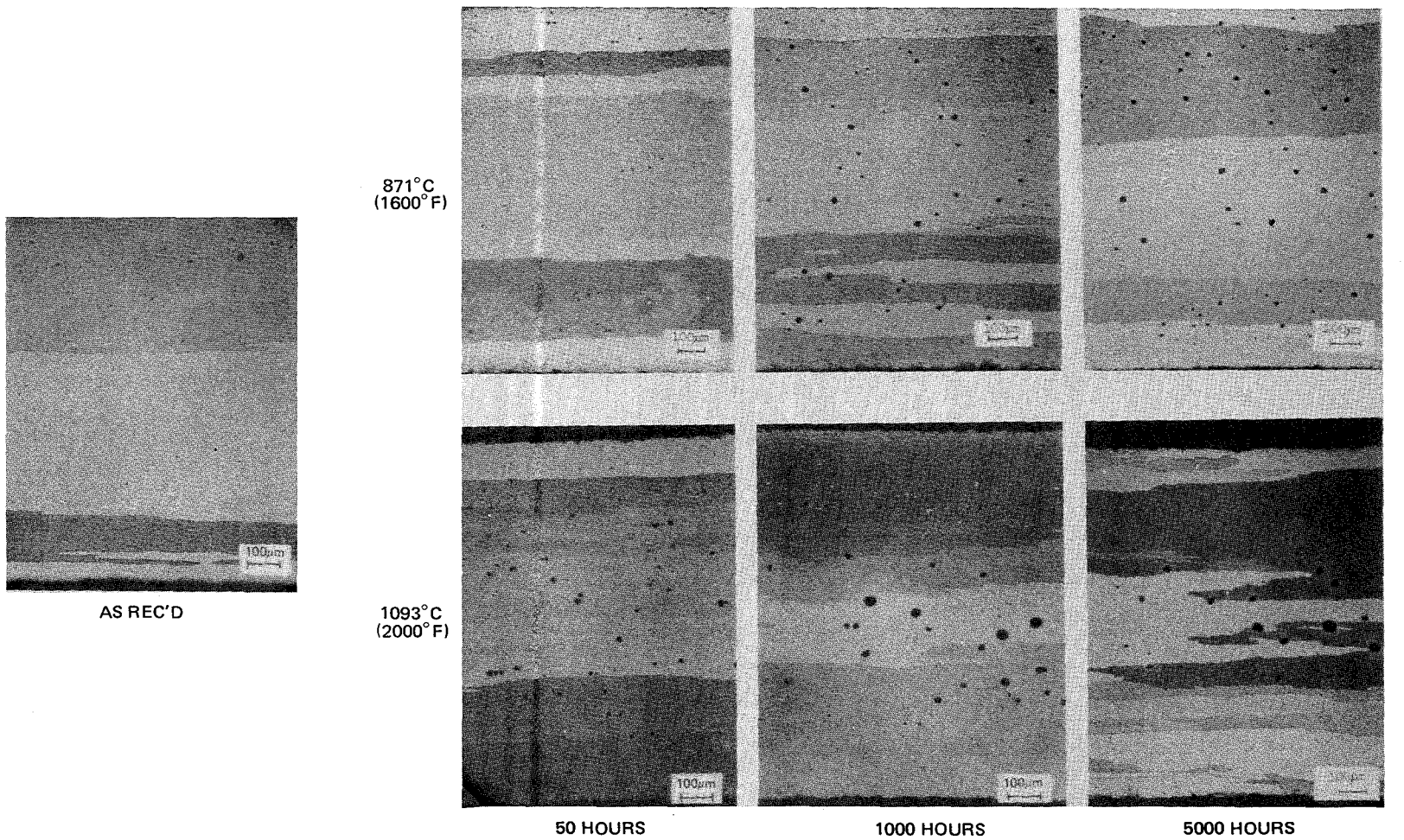

Figure 5-32 Void Formation Observed in Thermally Exposed MA 956 Lot ZDEW

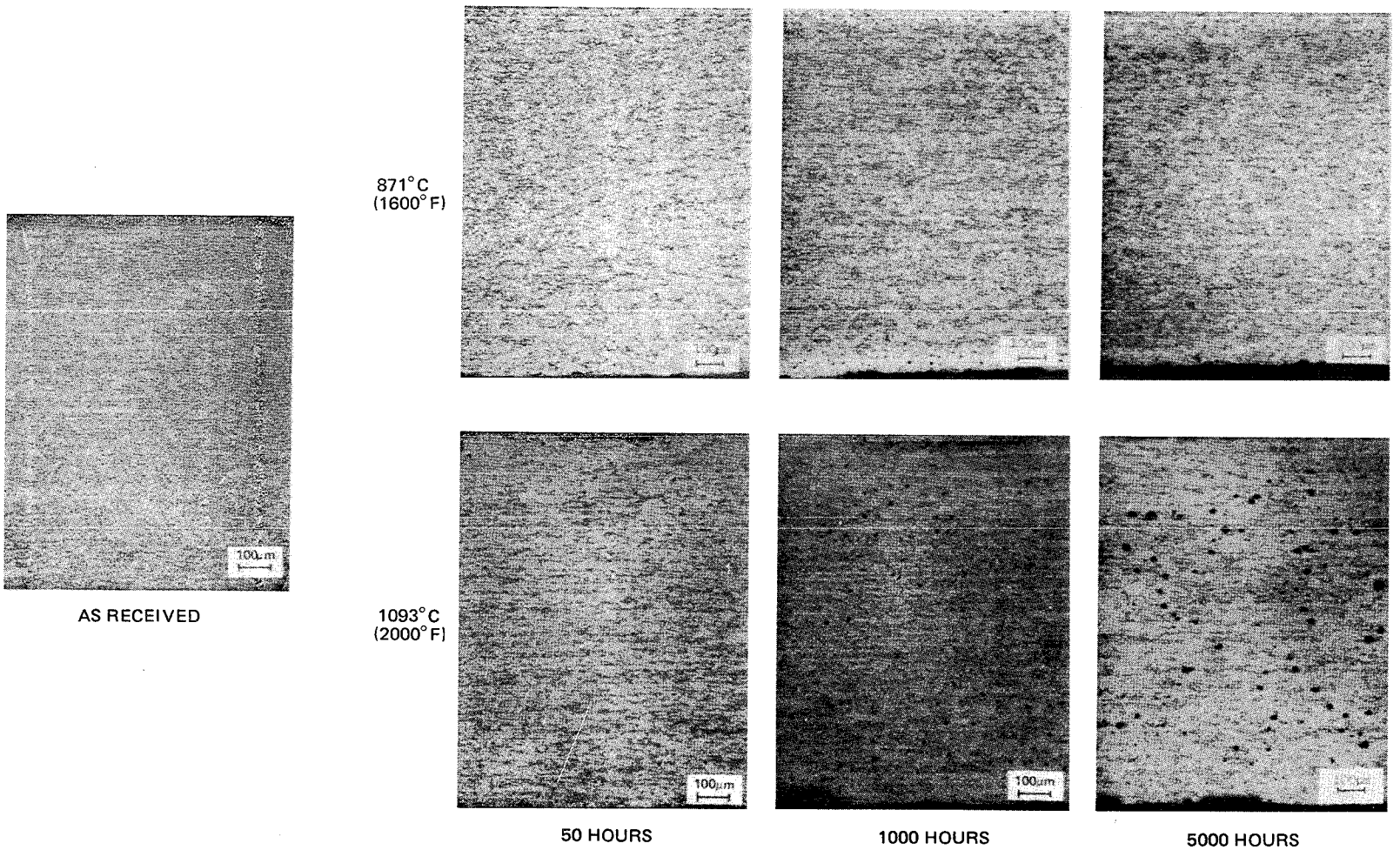

Figure 5-33 Void Formation Observed in Thermally Exposed HDA 8077 Lot MS 151

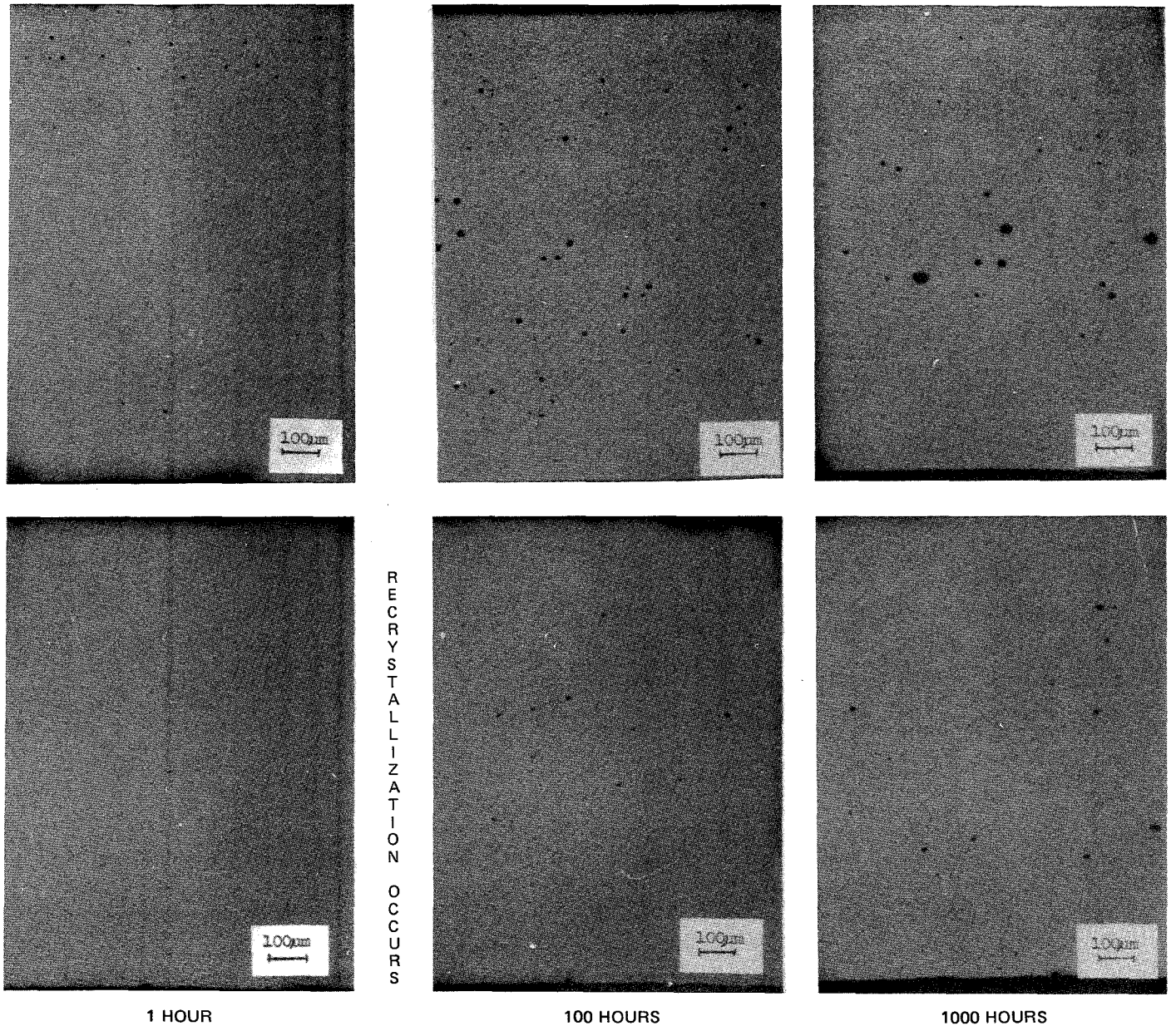

Figure 5-34 Void Formation at 1093C (2000F) in Recrystallized and Unrecrystallized MA 956 Experimental Baseline Sheet

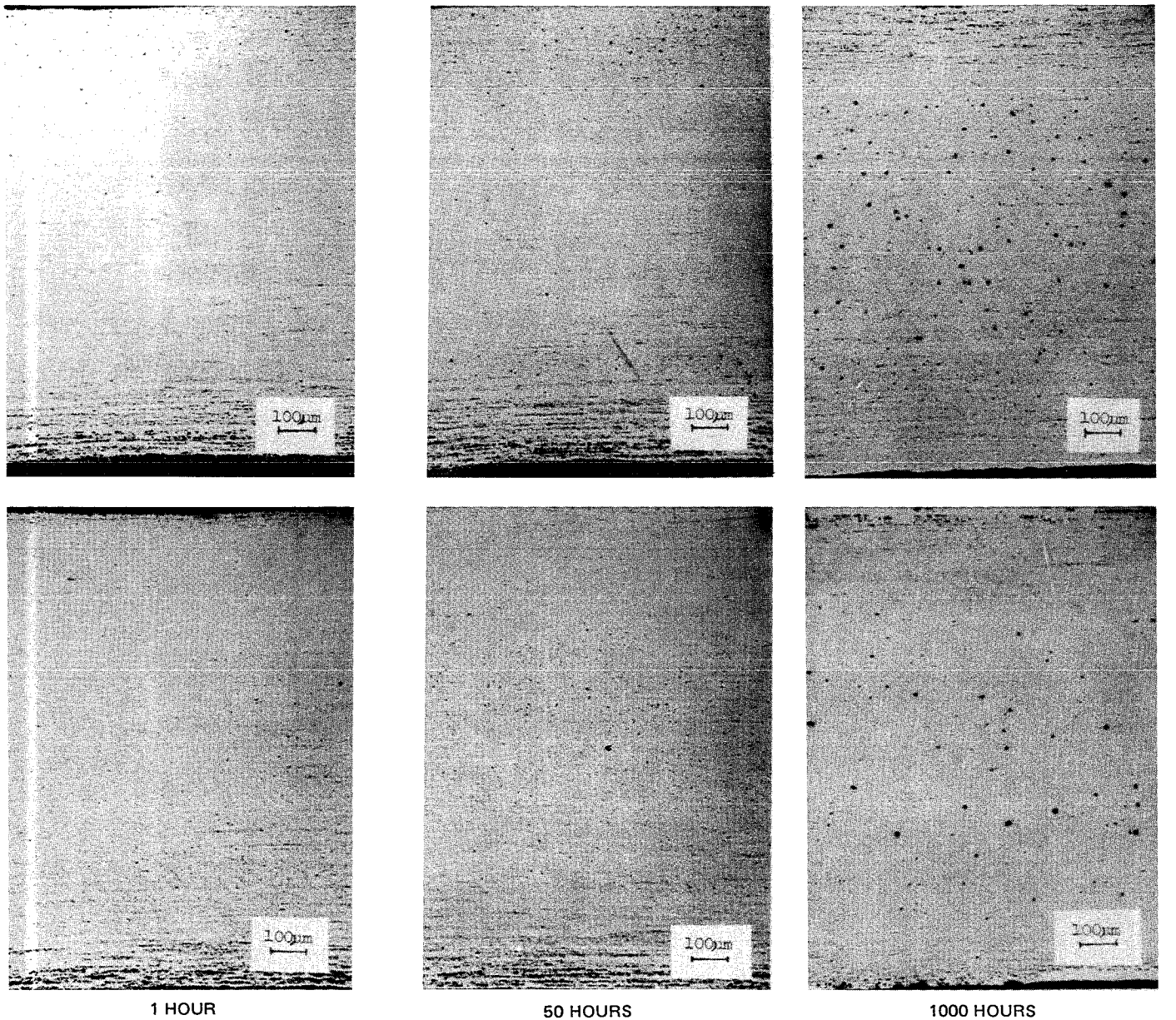

Figure 5-35 Void Formation at 1093C (2000F) in Recrystallized and Unrecrystallized HDA 8077 Lot MS 149 Sheet

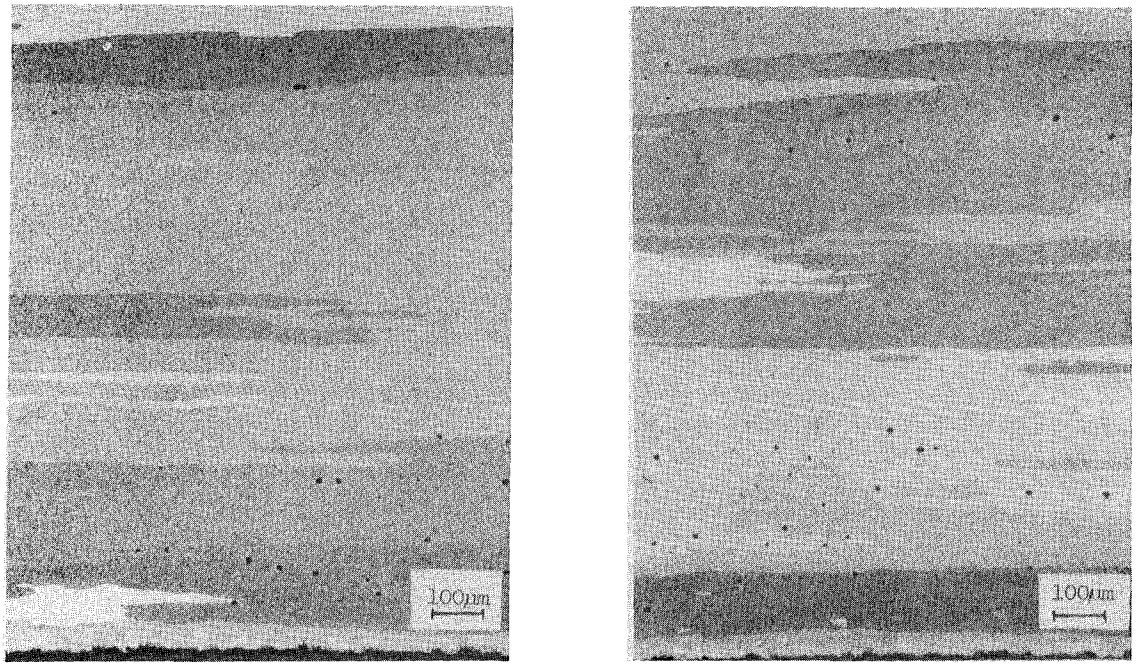

A) AIR EXPOSED

B) ARGON EXPOSED

Figure 5-36 Influence of Furnace Atmosphere on the Formation of Voids in MA 956 Lot ZDEW Exposed for 10 Hours at 1093C (2000F)

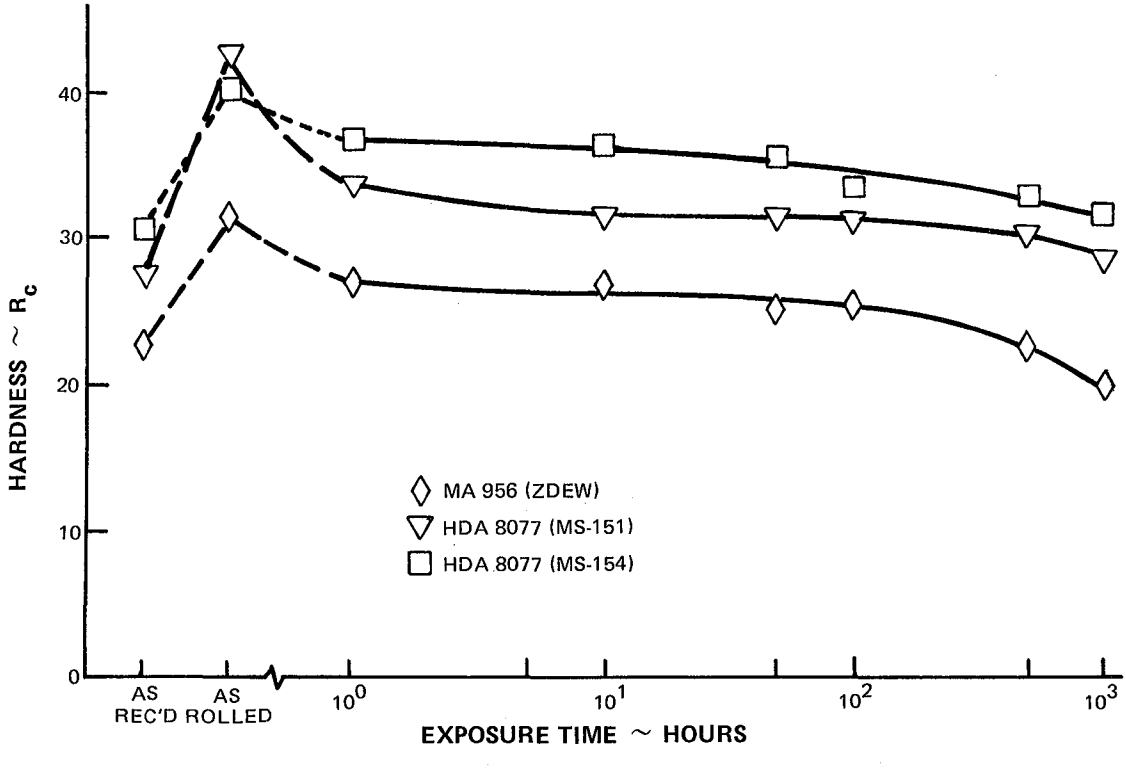

Figure 5-37 Variation of Hardness With Exposure Time at 1093C (2000F) for 20% Cold Worked Material

After 10 hours of exposure, no additional surface recrystallization or grain growth occurred in MA 956 beyond that observed in as-received sheet (compare Figure 5.1-38a with Figure 5-29). After 10 hours of exposure, no additional grain growth occurred in HDA 8077 (Figure 5-38b). The cold work imparted by rolling HDA 8077 is relieved by recrystallization occurring progressively from the surface to the center of the sheet; however, stringers of unrecrystallized grains in the starting material fail to recrystallize after 1000 hours of exposure at 1093°C (2000°F) (Figure 5-39). Also seen in Figure 5-39 is void formation similar to that observed in the as-received stability evaluation of both alloys.

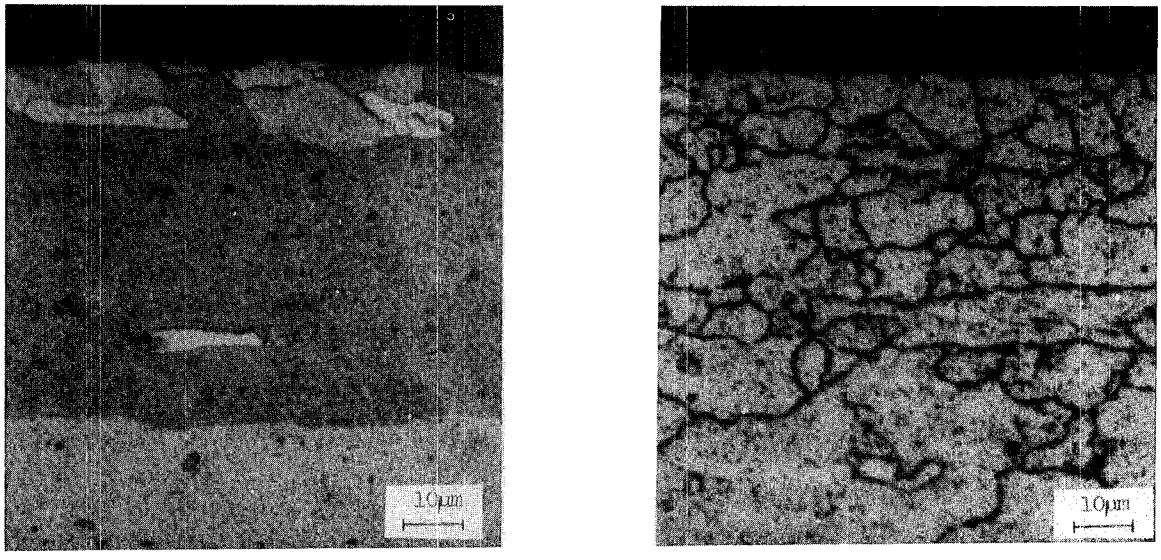

A) MA 956 B) HDA 8077

Figure 5-38 Surface Recrystallization of 20% Cold Worked ODS Sheet After 1093C (2000F)/10 Hours

5.1.7.2 Effect of Thermal Exposure on Elevated Temperature Properties

To assess the effect of thermal exposure on ODS alloy properties, 982°C (1800°F) tensile, creep, and low cycle fatigue tests were conducted on MA 956 lot ZDEW and HDA 8077 lot MS 154 exposed at 1043°C (2000°F) for 50 and 500 hours, respectively. Exposed specimens had the previously discussed voids present in the microstructures, in addition to surface oxidation which was not removed prior to testing. The 982°C (1800°F) tensile, creep, and low cycle fatigue properties measured on exposed specimens are compared to as-received

MA 956
ZDEW

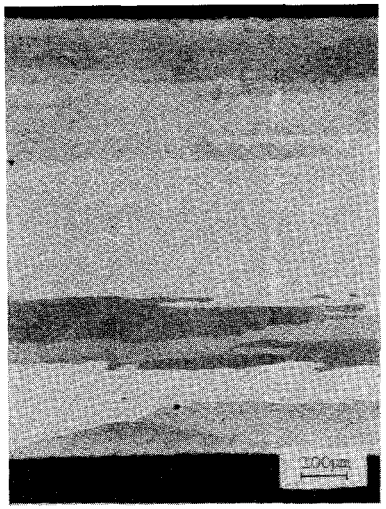

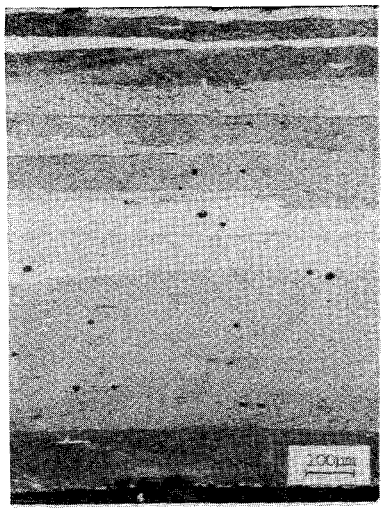

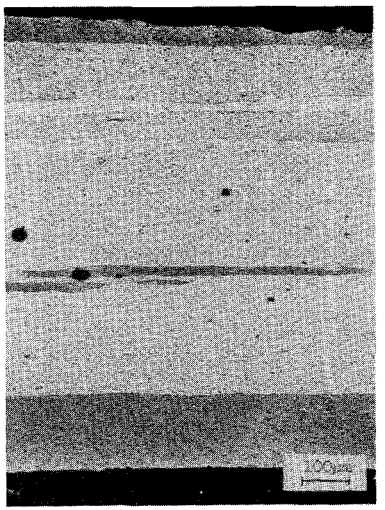

HDA 8077
MS - 154

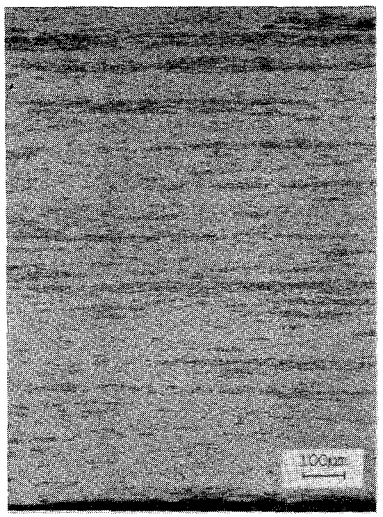

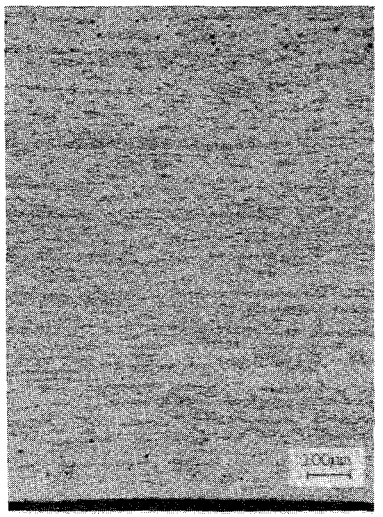

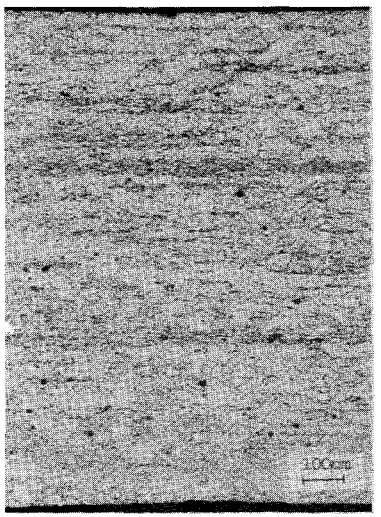

As Cold Rolled

50 Hour Exposure

1000 Hour Exposure

Figure 5-39 Recrystallization of 20% Cold Worked ODS Sheet

material properties in Table 5-VII. These results indicate relatively little influence of exposure on 982°C (1800°F) tensile properties. However, creep (both life and ductility) and low cycle fatigue capability are significantly degraded by the prior exposure. While the reduction of creep life seems quite large, this result must be interpreted with some caution. As noted previously, the slope of the Larson-Miller curve for both alloys is very small, so that the substantial life debits noted in Table 5-VII correspond to a relatively small creep strength reduction on the order of 20%. In addition, rupture ductilities on exposed specimens remain above the 0.1% design limit used in design of the ODS combustor panels (Section 3). Similar effects have been observed in other high temperature combustor alloys. A reduction in the creep life of Hastelloy X has been demonstrated by Mitsubishi (Reference 5-5) showing that a thermal exposure at 950°C (1742°F) for 1000 hours decreases creep strength by 10%. Post-exposure reductions of Hastelloy X tensile ductility and impact resistance also have been reported (References 5-6 and 5-7). Mechanical testing of material with prior thermal exposure will overstate any property debits that are temperature and time dependent and that normally occur throughout the life of a turbine engine component.

TABLE 5-VII

COMPARISON BETWEEN AS-RECEIVED AND EXPOSED 982°C (1800°F) MECHANICAL PROPERTIES OF ODS ALLOYS

	MA 956 Lot ZDEW		HDA 8077 Lot MS 154	
Test and Condition	As Received	Exposed 1093°C (2000°F) 50 Hr	As-Received	Exposed 1093°C (2000°F) 500 Hr
Tensile: Strain Rate = 0.005 $(min)^{-1}$				
0.2% YS MN/m^2 (ksi)	106.8 (15.5)	104.0 (15.1)	115.0 (16.7)	104.7 (15.2)
UTS MN/m^2 (ksi)	110.2 (16.0)	106.8 (15.5)	115.0 (16.7)	106.1 (15.4)
Elongation %	5.9	5.0	23.2	19.2
Creep: MN/m^2 (ksi)	69.0 (10)	69.0 (10)	82.7 (12)	82.7 (12)
Rupture Life Hours	4175.6	10.8, 12.1	>3613.4(2)	21.7, 68.5
Prior Creep, %	0.5(1)	0.02, 0.11	>1.38(2)	0.34, 0.86
LCF: Strain Range = +0.25%				
Life, Cycles	3557	1842	1360	504

(1) Estimated value

(2) Test discontinued, no failure

To investigate the cause(s) of the observed property reductions, metallographic evaluation of tested specimens was performed. Typical fracture microstructures of MA 956 tested before and after the 1093°C (2000°F)/50 hours exposure are shown in Figure 5-40. Both tensile fractures show a high degree of specimen necking with evidence of elongated voids in the exposed sample. No evidence of preferential cracking at voids was observed.

Fractures of creep specimens exhibited primarily transgranular crack propagation perpendicular to the applied stress axis. The exposed material showed cavitation in the transverse grain boundaries (arrows, Figure 5-40) not observed in unexposed samples. As discussed in Section 5.1.3.2, transgranular creep cavitation was observed in non-exposed specimens (see Figure 5-8). The transverse intergranular cavitation in exposed samples leads to intergranular cracking, evident at several locations on the fracture surface, which increases the applied stress on the remaining material resulting in premature creep failure. The larger voids present in the microstructure of the unexposed material creep-rupture tested for 4175.6 hours are attributed to thermal exposure and not the applied stress. No evidence of preferential cracking at these voids was observed. Void formation on transverse boundaries (cavitation) of exposed material was observed only after creep testing; these transverse intergranular voids are not present in as-exposed material (see Figure 5-32). Based on these observations, it is hypothesized that the voids formed during static exposure are not themselves important in the fracture of this alloy, but rather that the high temperature exposure may cause chemistry, second phase or surface changes that weaken the transverse boundaries in creep, resulting in early transverse boundary creep cavitation and premature failure.

Metallographic examination of MA 956 low cycle fatigue fractures included in Figure 5-40 shows transgranular cracking and delamination along longitudinal grain boundaries and failure through crack link-up. No evidence of preferential crack propagation from or through voids formed during static exposure was observed; however, extensive surface cracking observed in the exposed sample suggests that surface effects may be responsible for the low cycle fatigue life reductions. As described in a subsequent section, this observation was confirmed by removal of the surface oxidized layer from exposed samples. Removal of this layer fully restores the low cycle fatigue properties of exposed MA 956.

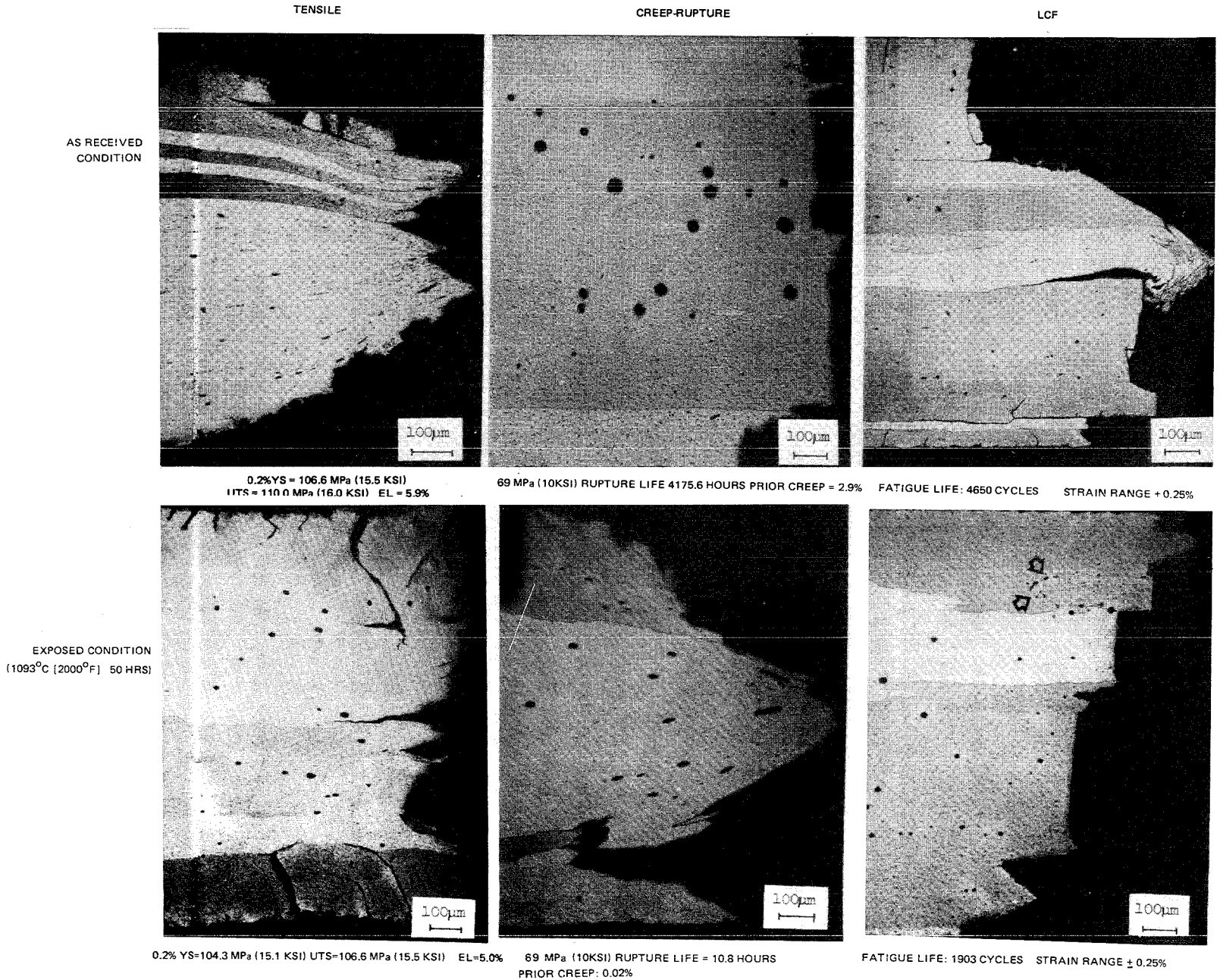

Figure 5-40 Fracture Microstructures of MA 956 Lot ZDEW After 982C (1800F) Testing

Post-test fracture microstructures of HDA 8077 Lot MS 154 with and without prior exposure at 1093°C (2000°F) for 500 hours are shown in Figure 5-41. Tensile fracture microstructures showed heavy slip bands and transverse cracking at transverse grain boundaries and at fine grain stringers in both conditions. No evidence of preferential cracking at voids was observed.

Creep fracture microstructures shown in Figure 5-41 exhibit intergranular initiated transgranular failure in both the exposed and unexposed conditions. No preferential cracking was observed at or passing through voids formed during static exposure. After 5000 hours of exposure, the sheet specimen displayed an oxidized surface, a zone denuded of gamma prime below the surface and overaged gamma prime in the remainder of the material. These observations suggest that the substantial reduction in creep life and prior creep ductility after exposure may be related to both surface and internal chemistry and phase changes rather than to void formation.

The low cycle fatigue fracture microstructures of unexposed HDA 8077 show much more crack propagation along longitudinal grain boundaries and stringers of fine grains than the exposed test specimen (Figure 5-41). Both low cycle fatigue fractures show transgranular crack propagation perpendicular to the stress axis. The 500 hour exposure resulted in considerable surface oxidation and a large gamma prime denuded zone. These effects result in earlier surface crack initiation during low cycle fatigue bend testing, resulting in the debit in life.

5.1.7.3 Effect of Post-Exposure Surface Treatment on Low Cycle Fatigue Properties

As indicated previously, room temperature embrittlement of exposed MA 956, which is discussed in more detail in the next section, was attributed by the alloy manufacturer to the formation of an extremely adherent oxide sale during exposure of this alloy (Reference 5-4). To determine if this effect was responsible for exposure induced low cycle fatigue life reduction, the effect of post-exposure surface treatments on low cycle fatigue life was investigated. Samples of HDA 8077 alloy also were studied in this investigation.

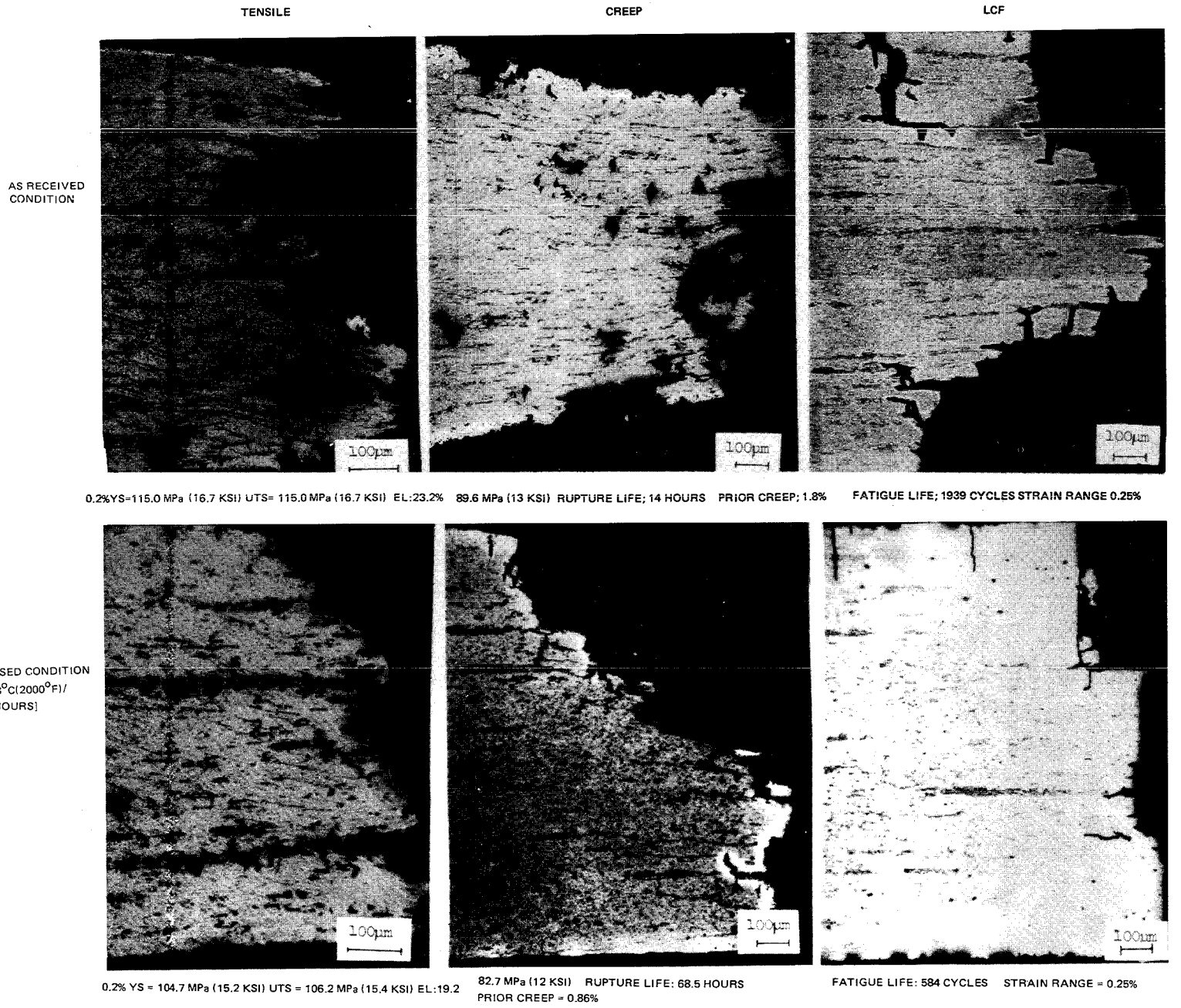

Figure 5-41 Fracture Microstructures of HDA 8077 MS 154 After 982C (1800F) Testing

MA 956 and HDA 8077 low cycle fatigue specimens were exposed in air at 1093°C (2000°F) for 50 and 500 hours, respectively, and were then vapor blasted to remove surface oxidation. Additional specimens of MA 956 were grit blasted to remove surface oxidation, thereby simulating the Wiggin surface cleaning technique used after recrystallization heat treatment and duplicating the surface finish of as-received MA 956 Lot ZDEW. Grit blasted sheet material also received a standard 1177°C (2150°F), 1/2-hour anneal. Low cycle fatigue test results are summarized in Table 5-VIII and in Figure 5-42. The low cycle fatigue life of exposed and vapor blasted sheet was increased over the life of as-exposed material (no surface cleaning) and was similar to the minimum values for the baseline (as-received and annealed) material. Exposed, grit blasted and annealed MA 956 sheet showed large increases in low cycle fatigue life over as-exposed sheet and exposed and vapor blasted sheet. In fact, the low cycle fatigue life of exposed, grit blasted, and annealed sheet was equivalent to the baseline material. These results indicate that the observed debit in low cycle fatigue life is due to surface oxidation/chemistry changes that occur during high temperature exposure rather than to internal void formation. Metallographic examination of failed specimens showed that no preferential crack propagation had occurred through the voids which had been produced during the 1093°C (2000°F) static exposure. Both alloys exhibited a light oxide layer after exposure, which was removed by vapor blasting. The MA 956 specimens exhibited a layer of fine recrystallized grains up to a depth of 10μ m after the 1093°C (2000°F) exposure, which was not removed by vapor blasting. Examination of the exposed, grit blasted and annealed samples revealed little surface recrystallization.

TABLE 5-VIII

982°C (1800°F) LOW CYCLE FATIGUE PROPERTIES OF ODS ALLOYS;
FULLY REVERSED BENDING AT ±0.25% AND 0.67 Hz

Material Condition	Life in Cycles	
	MA 956, Lot ZDEW	HDA 8077, Lot MS 154
o As-received and annealed at 1177°C (2150°F) for 1/2 hour in hydrogen	2700 3320 4650	710 1470 1900
o Exposed at 1093°C (2000°F)*	1690 1903 1932	412 517 584
o Exposed at 1093°C (2000°F)* and vapor blasted	2470 2560	640 860
o Exposed at 1093°C (2000°F)*, grit blasted and annealed at 1177°C (2150°F) for 1/2 hour	3700 4600	- -

*MA 956 exposed for 50 hours; HDA 8077 exposed for 500 hours, both in air.

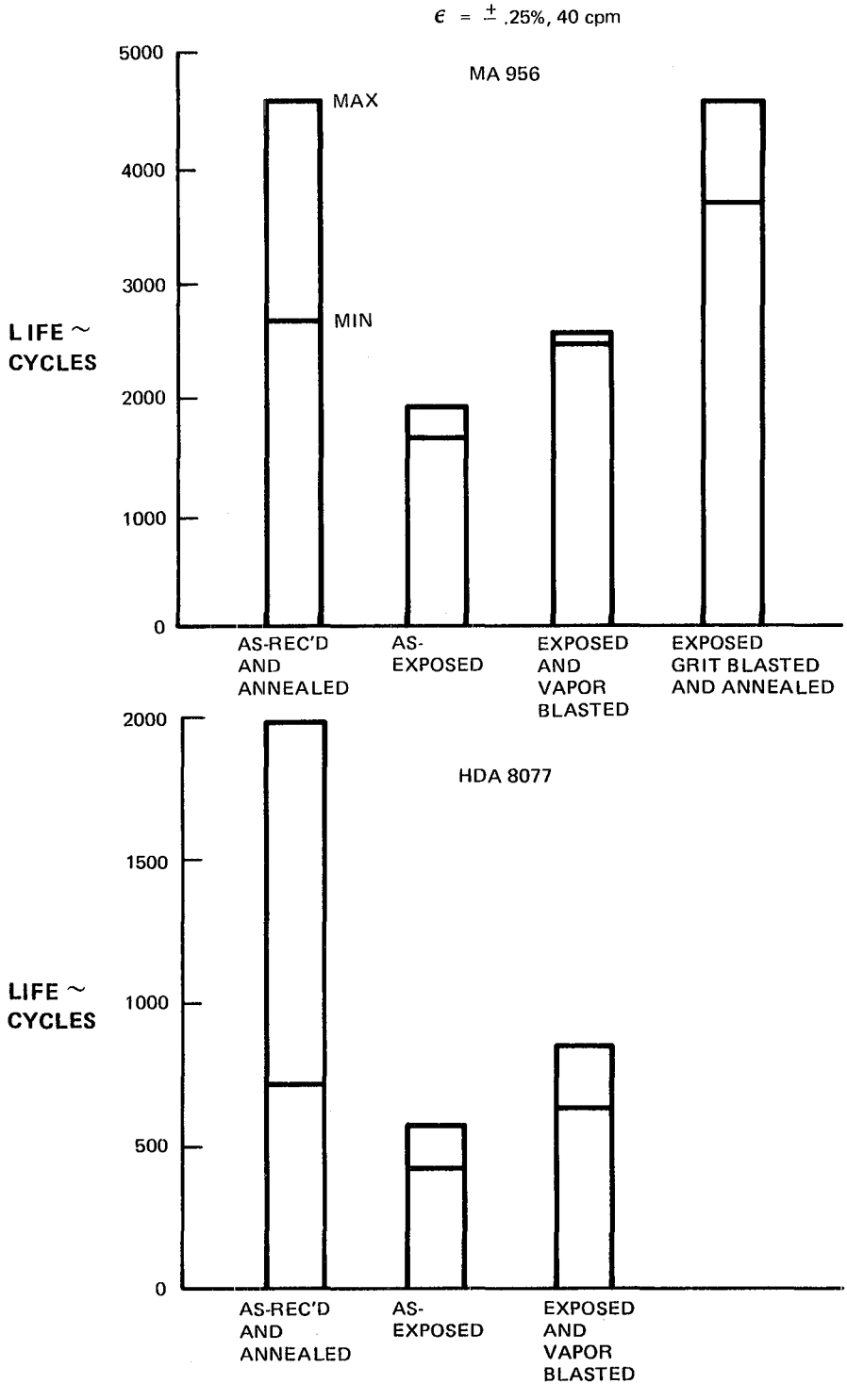

Figure 5-42 LCF Comparison of ODS Alloys at 982C (1800F)/ ± 0.25% Strain, 0.67 Hz

5.1.7.4 Effect of Thermal Exposure on Room Temperature Ductility

As indicated previously, results reported by the MA 956 manufacturer during the course of this program indicated that a severe reduction of room temperature ductility could result from long time exposure at or above 982°C (1800°F) (Reference 5-4).

To briefly summarize the manufacturers observations, room temperature tensile elongations can be lowered from typical values of 12-15 percent to 1-2 percent after exposures of several hundred hours at or above 982°C (1800°F). The tensile fracture mode changes from a ductile mode exhibiting substantial necking of the sheet prior to failure in unexposed material, to a cleavage mode with no significant neck development after exposure. Several phenomenological observations suggest that this embrittlement results somehow from interaction between the base metal and the extremely adherent oxide scale which forms on MA 956:

- Embrittlement does not appear in specimens from which oxide scale is removed after exposure.
- Vacuum exposed specimens are not embrittled.
- Vacuum pre-exposed specimens which subsequently are exposed in air form a non-adherent, porous, undulated oxide scale and are not embrittled.
- On embrittled specimens with variable scales, where local spallation of non-adherent scale has occurred, fracture initiates at adherent scale patches.

Other relevant observations on the embrittlement phenomenon were:

- Cyclic exposure causes embrittlement similar to static exposure.
- Susceptibility to embrittlement varies significantly from lot-to-lot.
- There is no effect of specimen orientation.
- Exposed specimens tested at 149°C (300°F) are not embrittled.

The bulk of the initial INCO embrittlement data was generated on material which did not represent lots of material used on this program. Two series of tests therefore were conducted on this task to determine if lot ZDEW was susceptible to this phenomenon. Post-exposure tensile tests were conducted at INCO R&D Center. At Pratt & Whitney, the Erichson test (described in Section 5.1.2) was used as a measure of post-exposure ductility. Post-exposure cup tests were performed on both candidate alloys to determine if HDA 8077 showed any susceptibility to embrittlement.

Post-exposure tensile tests at INCO were conducted on material with and without the hydrogen anneal that routinely was used to relieve surface working on all specimens tested in this task. Results of these tests (Table 5-IX) showed that lot ZDEW may be susceptible to embrittlement. These results also indicate that material in the hydrogen annealed condition may be slightly more susceptible to embrittlement than as-received material.

TABLE 5-IX

ROOM TEMPERATURE TENSILE ELONGATION OF MA 956 (PERCENT)[1]

Lot	Pre-Exposure[2] Condition	Exposure Temperature °C (°F)	Exposure Time, Hours[3] 500	1000	2000
ZDEW	AR	982 (1800)	12,12	10,14	14,14
ZDEW	AR+HA	982 (1800)	12,12	15,14	12,1
ZDEW	AR	1093 (2000)	11,11	14,3	N.T.

1) Tests conducted at INCO R&D Center; A, B represent results of duplicate tests.

2) AR - As Received
HA - Hydrogen Annealed 1/2 Hour at 1177°C (2150°F)

3) N.T. - Not Tested

Results of Erichson cup tests conducted on MA 956 lot ZDEW and HDA 8077 lot C are plotted respectively in Figures 5-43 and 5-44. Samples of lot C (see Section 4) were obtained from the manufacturer for post-exposure cup evaluation because material from the three lots of 8077 evaluated earlier in this task were not available. Examination of the data presented in these two plots leads to several conclusions. First, cup fabricability is as or more sensitive an indication of embrittlement than uniaxial tensile elongation. Second, for the exposure condition evaluated, HDA 8077 does not appear susceptible to the embrittlement phenomenon. Third, MA 956 lot ZDEW is susceptible to embrittlement. The engineering implications of this susceptability are discussed below.

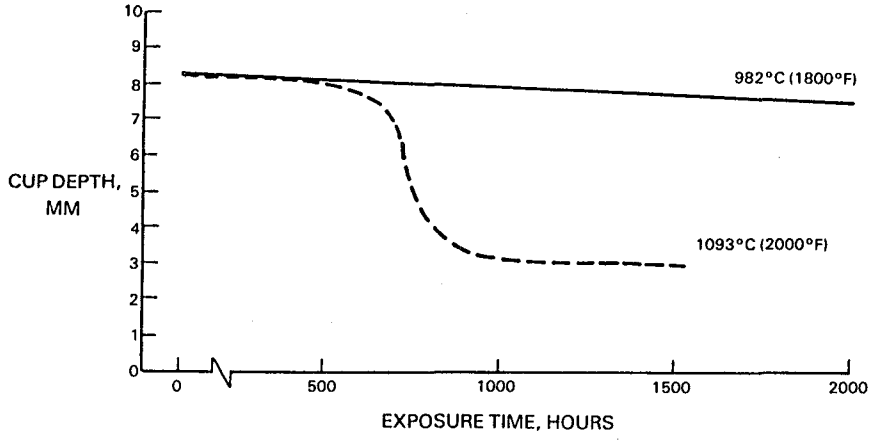

Figure 5-43 Erichsen Cup Depth of MA 956 Lot ZDEW After 982C and 1093C (1800F and 2000F) Exposures

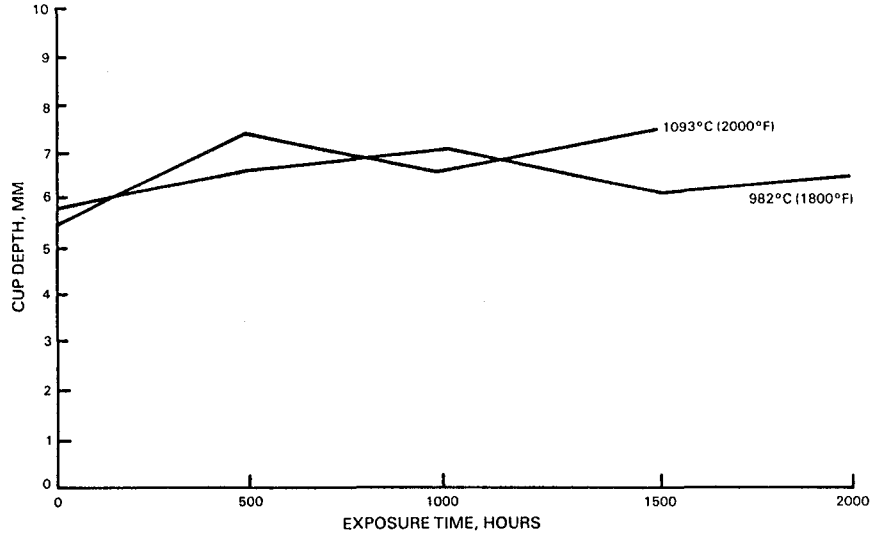

Figure 5-44 Erichsen Cup Depth of HDA 8077 Lot C After 982C and 1093C (1800F and 2000F) Exposures

Careful consideration of the engineering property requirements for ODS combustor alloys, discussed previously in Section 3, leads to the conclusion that room temperature tensile embrittlement does not represent a life limiting property change. The ductility of the material is reduced only at test temperatures below 149°C (300°F), and not at typical combustor material operating temperatures, which are well above 149°C (300°F). Failure modes which are of primary concern in the combustor segment are creep-rupture, thermal fatigue, and oxidation. To accommodate the known limits on rupture ductility of ODS alloys, combustor segments were designed with a creep limit of 0.1 percent, which is well below the 1 to 2 percent room temperature tensile ductility of embrittled material. Results of isothermal low cycle fatigue tests (Figure 5-42), which are taken as an indication of thermal fatigue capability, indicate that, while both alloys suffer some loss of fatigue capability as a result of exposure, the loss is not nearly as severe as is the loss of room temperature ductility. As pointed out previously, post exposure property measurements must be interpreted with some caution, as they tend to overstate the effect of material degradation which proceeds concurrently with elevated temperature tests of "as-received" material. The only potentially detrimental effect of combustor alloy embrittlement might be on reduced repairability of engine serviced components. Since the repair process envisioned for the ODS combustor involves segment removal and replacement, the possible impact of embrittlement on repairability is not of concern. To summarize, based on the considerations discussed above, the room temperature embrittlement resulting from elevated temperature exposure of MA 956 alloy is not considered to be a serious limitation on the potential for its application as a gas turbine combustor material for civil or commercial applications.

5.1.7.5 Effect of Creep Exposure on Room Temperature Ductility

As noted previously, virtually complete loss of room temperature ductility has been reported to result from the accumulation of relatively small creep strains in other oxide dispersion strengthened materials (Reference 5-3). To evaluate the potential for this type of embrittlement in the two candidate ODS combustor alloys, the three creep specimens which were not creep tested to

failure in the previously described creep evaluation program (see Table 5-IV) were tensile tested to failure at room temperature. Results of these tests, Table 5-X, show no evidence of post-creep embrittlement in either of the two candidate alloys.

TABLE 5-X

INFLUENCE OF PRIOR CREEP EXPOSURE ON
THE ROOM TEMPERATURE TENSILE PROPERTIES OF CANDIDATE ODS ALLOYS

		Prior Creep Exposure at 982°C (1800°F)			Tension Test Results		
Alloy	Lot	Stress mN/m^2 (ksi)	Time (Hr)	Accumulated Creep Strain (Percent)	0.2% Yield Strength mN/m^2 (ksi)	Ultimate Tensile Strength mN/m^2 (ksi)	Percent Elongation in 2.5 cm (1 inch)
MA 956	ZDEW	NONE	(As Received, Table 5-II)		551.9 (80.1)	639.4 (92.8)	12.6
MA 956	ZDEW	62.1 (9)	4455.7	0.81	576.0 (83.6)	637.3 (92.5)	14.8
MA 956	ZDEW	62.1 (9)	4455.6	0.52	578.1 (83.2)	656.6 (95.3)	13.0
HDA 8077	MS 154	NONE	(As Received, Table 5-III)		717.3 (104.0)	828.6 (120.2)	14.8
HDA 8077	MS 154	82.7 (12)	3613.2	1.38	653.2 (94.8)	760.7 (110.4)	16.2

5.1.8 Alloy Comparison

The objective of this comparison was to determine if either of the two candidate oxide dispersion strengthened sheet alloys has a substantial advantage for segmented combustor applications. The three main criteria for this evaluation are creep, oxidation, and three separate measures of expected thermal fatigue resistance (creep ductility, isothermal low cycle fatigue, and hot spot blister cracking resistance). Because of the variability among the three lots of HDA 8077 evaluated on this program, P&W test results obtained on other lots of this alloy prior to the beginning of the program were included in the comparison in an effort to represent the potential of this alloy if produced with close manufacturing control. While only one lot of MA 956 was tested in this program, results on this lot are consistent with P&W data obtained on several other lots prior to the beginning of the program, and thus are considered representative. Some of these results also are included in the comparison to provide the broadest possible data base.

Creep strength capability of the two alloys is summarized and compared in Figure 5-45a. HDA 8077 alloy clearly has a creep strength advantage, and has the added benefit of being isotropic. As noted in a previous section, both alloys have at least a 167°C (300°F) creep advantage over a current generation combustor alloy (Hastelloy X).

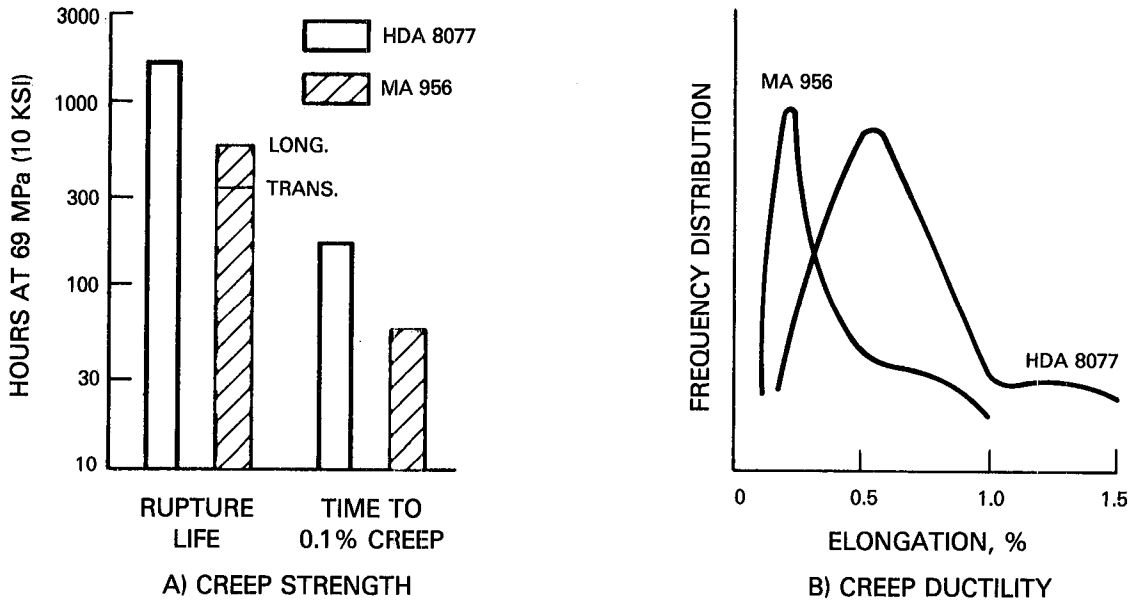

Figure 5-45 982C (1800F) ODS Alloy Creep Comparison

Oxidation resistance was compared previously in Figure 5-26. This comparison showed some advantage for MA 956 as compared to HDA 8077, with both alloys again showing at least 167°C (300°F) benefit compared with Hastelloy X.

The three measures of expected thermal fatigue resistance (creep ductility, isothermal low cycle fatigue, and hot spot blister cracking) are summarized respectively in Figures 5-45b, 5-46, and 5-21. While HDA 8077 alloy exhibits a significant advantage in creep ductility and hot spot blister cracking, MA 956 clearly has better resistance to low cycle fatigue failure. As expected, both alloys are significantly more susceptible to thermal fatigue cracking than the current combustor alloy (Figure 5-21).

Results of the above comparison are summarized in Table 5-XI. In the two areas where the ODS alloys have a large benefit compared to the current material, HDA 8077 holds the advantage in creep while MA 956 has better oxidation resistance. In thermal fatigue, which is expected to be the life limiting property of ODS alloys, neither candidate alloy has a clear cut advantage. Based on this property comparison, it is concluded that both alloys are equally promising as candidates to replace current generation gas turbine combustor materials.

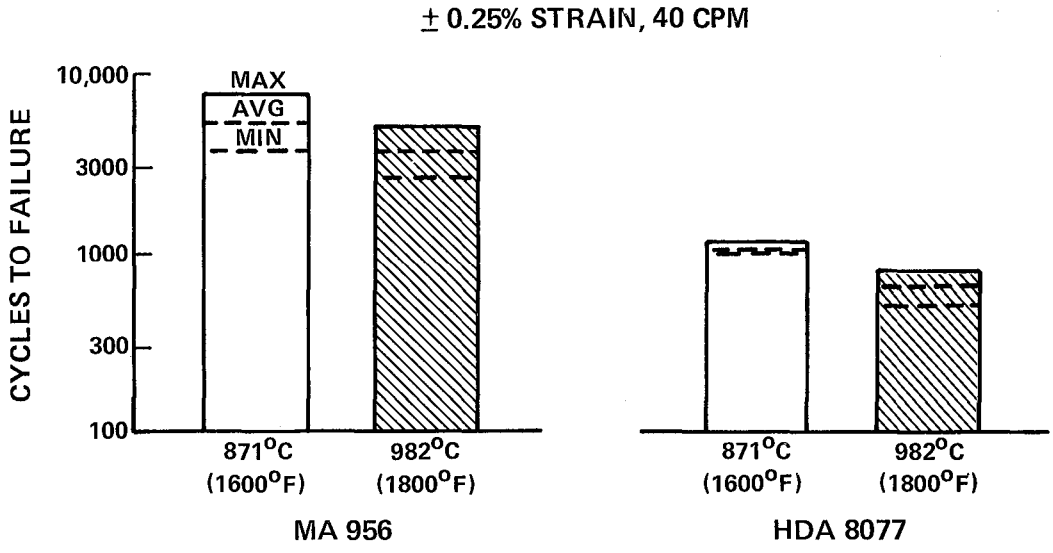

Figure 5-46 ODS Alloy Isothermal Low Cycle Fatigue Comparison

TABLE 5-XI

ODS ALLOY PROPERTY SUMMARY

Property	MA 956	HDA 8077
Creep strength		X
Oxidation resistance	X	
Thermal fatigue resistance		
Creep ductility		X
Isothermal LCF	X	
Hot spot blister test		X

X = Property Advantage

5.2 TASK IIIB - JOINING STUDIES

5.2.1 Introduction and Summary

The objective of this sub-task was to investigate methods for joining of oxide dispersion strengthened alloys, both to themselves and to a conventional combustor material (Hastelloy X). This investigation was carried out in two phases. In the first phase, preliminary evaluations were made of four joining approaches including flash butt, electron beam, and resistance seam welding and brazing. Evaluation of these joints was limited primarily to non-destructive inspection (visual and fluorescent penetrant) and metallographic examination. Based in part on these results, and in part on results of the concurrent Task I design studies which focused on mechanical attachment as the primary means of segment assembly, with brazing as a possible alternate or supplementary joining method, the second phase was directed toward investigation of brazing and riveting, including measurement of joint properties. Results provided an optimized set of brazing alloy/parameters for each ODS alloy, together with braze and rivet property data for use in the Task VI design phase.

5.2.2 Preliminary Joining Methods Evaluation

The purpose of this study was to obtain a preliminary evaluation of four methods for joining of the two candidate oxide dispersion strengthened sheet alloys. These four methods involved two types of butt joints (flash butt and electron beam welding) and two types of lap joints (resistance seam welding and brazing). Flash and electron beam butt welding were evaluated only for joining like-ODS alloys (i.e., MA956/MA 956 and HDA 8077/HDA 8077 Joints). Joints made by these two methods were evaluated nondestructively (visual and fluorescent penetrant inspection) and by metallographic examination. Resistance seam welding and brazing were evaluated both for like-ODS joints and for joints between each of the two candidate ODS alloys and Hastelloy X. In addition to Non-Destructive Examination (NDI) and metallography, lap peel tests were conducted on these joints. Joining parameters used for these initial trails are summarized in Table 5-XII.

TABLE 5-XII

PARAMETERS USED FOR INITIAL JOINING TRAILS

Flash Butt Welding Parameters

- Hastelloy X machine setup
- 7.6 mm (0.30") interference
- Amperage varied ±15% around Hastelloy X amperage to assess microstructure variations
- Two joint configurations:
  - Flat ends, both (longitudinal cracking)
  - Tapered end/flat end (improved flow)

Electron Beam Butt Welding Parameters

- All welds done at 120 KV
- Three variables:
  - Amperage: 3.5-4.0 mA.
  - Circle generator diameter: 0.8 - 1.3 mm (0.030" - 0.050")
  - Table speed: 4.9 - 7.2 cm $sec.^{-1}$ (115 - 170 in $min.^{-1}$)
- Desirable Settings:

  120 KV/4mA/0.8 mm (0.030") Circle Diameter/7.2 cm $sec.^{-1}$ (170 in $min.^{-1}$) table speed.

Resistance Seam Welding Parameters

Machine: Sciaky 125 KVA
Machine Setting (All held constant):

- Initial squeeze	15%	- Pressure (Constant Height):	
Preheat cycle	6	- pounds down	4100
Weld:		- pounds up	1450
- heat cycle	18	- Drive-Intermittent	45
- cool cycle	1	(7 cycles/cm (18 cycles/inch))	
- current delay cycle	15	- Index cycle	18
- quench cycle	2	- Delay index cycle	19
		- Hold index cycle	19
- Phase shift:		- Forge initiation:	
- weld	44.2	- cycles	90
- post heat	52.8	- impulses	Temper cool

Brazing Parameters

- Two braze alloys/brazing temperatures
  - METGLAS® BNi2/1052°C (1925°F) (Poor Joints)
  - METGLAS® BNiIA/1149°C (2100°F) (Improved Joints)
  - All brazing done in vacuum - $5x10^{-4}$ torr
  - Joint pressures applied and maintained by thermal expansion tooling
  - 0.0381 mm (0.0015 in) thick amorphous nickel-base brazing foils employed
  - Joints preheated to just below braze alloy solidus to stabilize the temperature prior to brazing
  - No post braze diffusion treatment employed for trials

® Registered Trademarks of the Allied Chemical Corp.

Results of NDI and metallographic evaluation of each of these four types of joints are summarized in Tables 5-XIII and 5-XIV. Peel test results on the lap joints also are included in Table 5-XIV. Each of these sets of results are discussed in the following paragraphs.

TABLE 5-XIII

BUTT WELD TRIAL RESULTS

Joining Process	Material Combination	Nondestructive Results No. of Welds Cracked/ No. of Welds	Metallographic Observations
Flash/Butt	o MA 956 - MA 956 - Square Geometry	2/12	- Longitudinal grain boundary cracking
	- Tapered Geometry	0/3	- No microstructural cracking - Improved metal flow
	o HDA 8077-HDA 8077 - Square Geometry	2/12	- Longitudinal grain boundary cracking
	- Tapered Geometry	0/3	- No microstructural cracking - Improved metal flow
Electron Beam	o MA 956 - MA 956	2/12 cracks & inclusions	- Fine grained fusion zone - Some phase agglomeration and porosity in fusion zone
	o HDA 8077 - HDA 8077	0/12	- Dendritic fusion zone - Phase agglomeration in fusion zone

TABLE 5-XIV

LAP JOINT TRIAL RESULTS

Joining Process	Material Combination	Nondestructive Results No. of Welds Cracked/ No. of Welds	Metallographic Observations	Peel Testing Failure Location
Resistance Seam Weld	o MA 956 - MA 956	1/12	- Heavy oxide in fusion zone - Cracking	- HAZ (Heat Affected Zone)
	o MA 956 - Hastelloy X	0/12		- HAZ (MA 956 only)
	o HDA 8077 - HDA 8077	1/12	- Cracking	- HAZ
	o HDA 8077 - Hastelloy X	1/12 cracks & porosity	- Porosity and inclusions in the fusion zone - Cracking	- HAZ (HDA 8077 or Hastelloy X)
Braze				
o METGLAS® BNi2	o MA 956 - MA 956	5/5 porosity	- Entrapped oxides - Incipient melting - Porosity - Inadequate coverage	- BAZ (Braze Affected Zone)
o METGLAS® BNi1A	o MA 956 - MA 956	0/10	- Entrapped oxides	- BAZ
	o MA 956 - Hastelloy X	0/10	- Limited entrapped oxides	- Brazed material and BAZ (MA 956)
	o HDA 8077 - HDA 8077	0/10	- Traces of entrapped oxides	- Braze material
	o HDA 8077 - Hastelloy X	0/10	- Traces of entrapped oxides	- Base metal (HDA 8077 or Hastelloy X)

® Registered Trademarks of the Allied Chemical Corp.

Flash butt welding trials were conducted with parameters normally used for joining Hastelloy X, with slight changes in amperage levels. Two pre-weld joint configurations were investigated. Initial trials using squared (flat end) work pieces showed a tendency towards longitudinal grain boundary cracking in both ODS alloys. In addition, large oxide inclusions were present along the weld interface in HDA 8077. To eliminate these problems and improve material flow, one of the work pieces was machined to a taper while the other end piece was machined flat. Flash butt welding of this geometry resulted in sound welds showing good flow characteristics in both ODS alloys, as shown in Figure 5-47. For identical geometry work pieces, weld microstructures showed little variation with changes of amperage level, indicating that these ODS materials are relatively insensitive to small variations of this parameter. Both alloys showed bands of recrystallized grains at the weld interface area and phase agglomeration in the heat affected zones (HAZ); this phase agglomeration is assumed to be carbide or nitride growth in MA 956 and gamma prime coarsening in HDA 8077.

All electron beam (EB) welding was done at 120 KV. Amperage, circle generator diameter and table speed were varied as indicated in Table 5-XII. NDI and metallographic examination indicated that a desirable narrow fusion zone and narrow HAZ can be produced by minimizing the welding time in both ODS alloys (Table 5-XIII). Figure 5-48 shows an EB weld in MA 956 containing a fine grained central zone, occasional void formation and some phase agglomeration. Figure 5-49 shows an EB weld in HDA 8077 with a dendritic pattern in the fusion zone and some phase agglomeration.

Resistance seam welding trials were conducted on a Sciaky 125KVA welding machine; machine settings were held constant for all material combinations and are summarized in Table 5-XII. NDI examination of all resistance welds revealed various amounts of weld metal expulsion dependent upon initial sheet flatness and hardness. HDA 8077 showed some porosity and inclusions in the fusion zone while MA 956 welds contained large amounts of oxide. Both alloys exhibited occasional cracks (Table 5-XIV). Typical microstructures are shown in Figure 5-50. Peel testing showed both ODS to ODS alloy joints to fail in the HAZ (Table 5-XIV). The MA 956 to Hastelloy X joints failed in the MA 956 HAZ, while HDA 8077 to Hastelloy X joints failed in either HAZ. These results suggest the fusion zones to be stronger than HAZ areas.

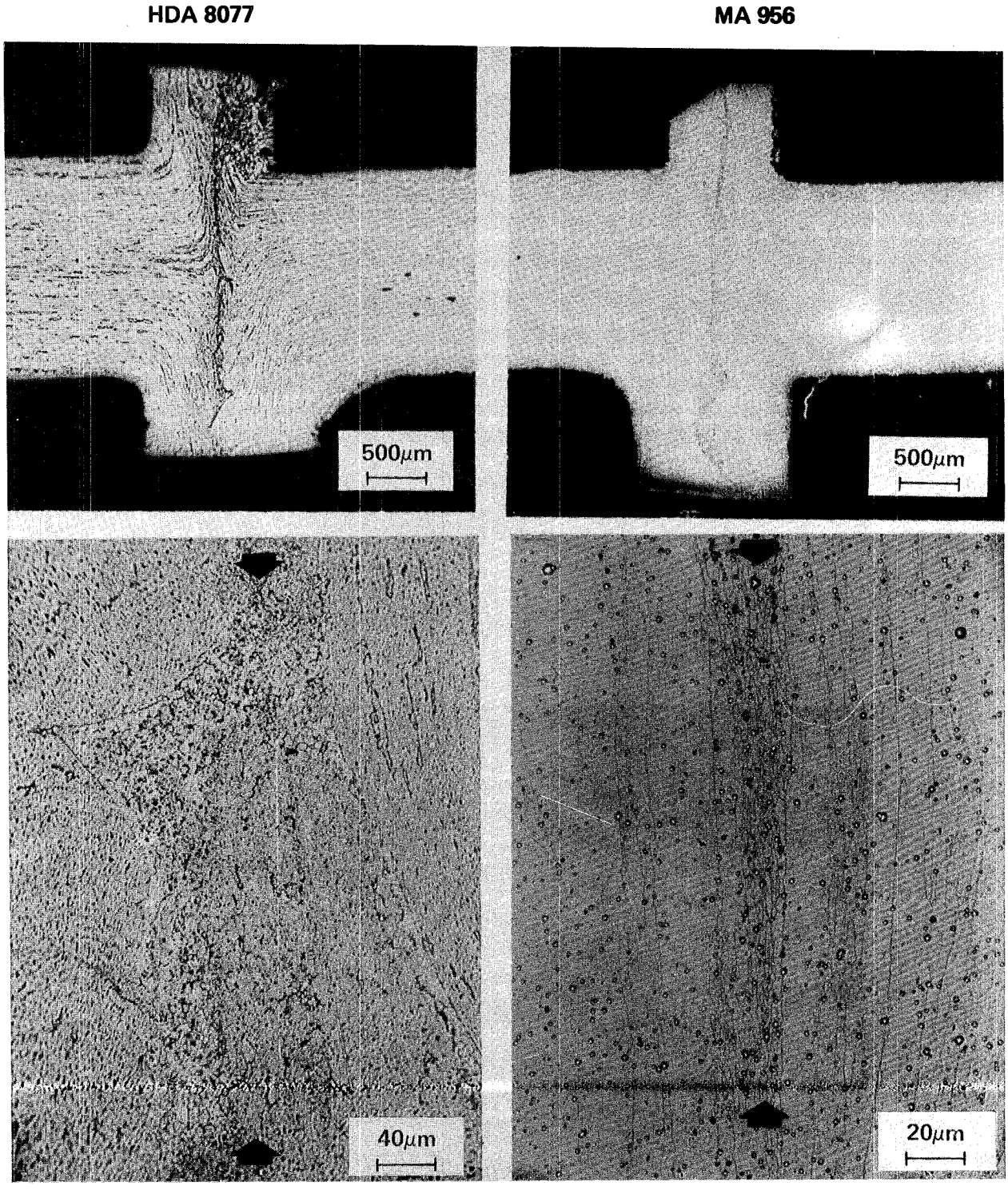

Figure 5-47 Flash Butt Welds (arrows show weld interface)

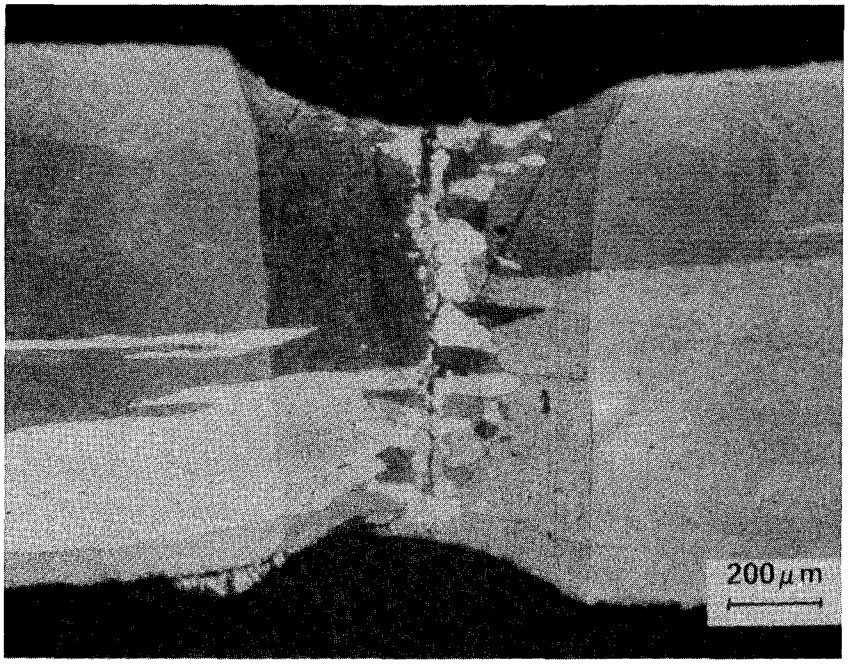

Figure 5-48 Electron Beam Weld in MA 956

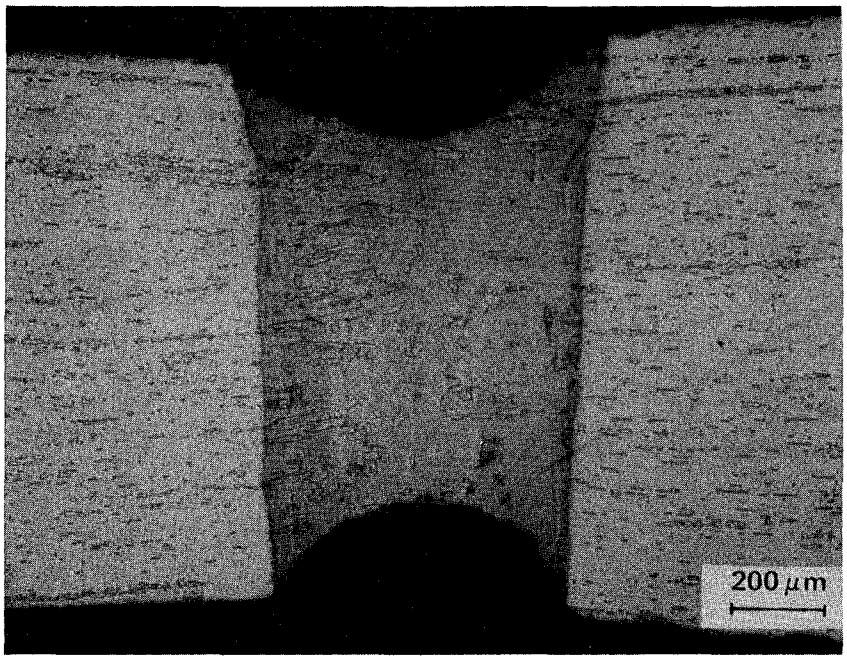

Figure 5-49 Electron Beam Weld in HDA 8077

RESISTANCE SEAM WELD IN MA956

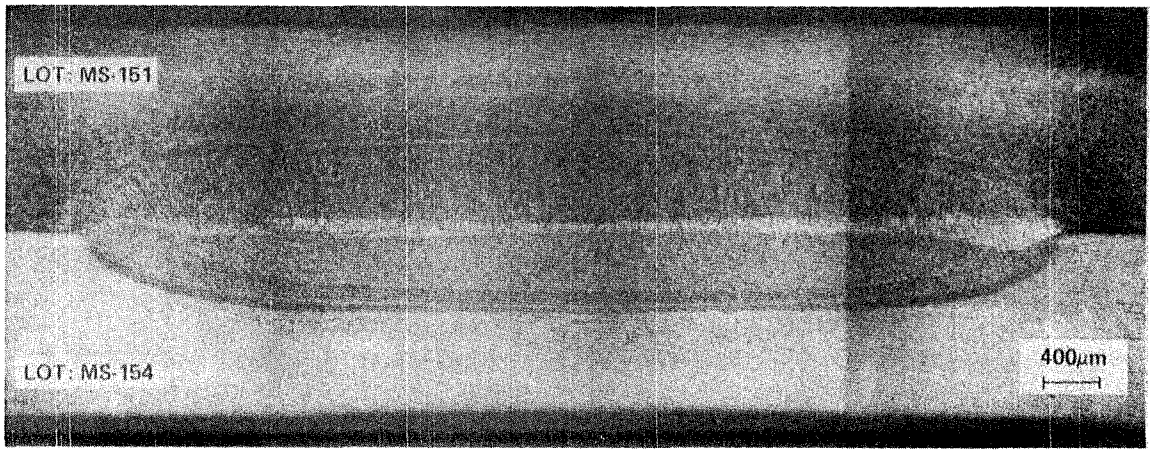

RESISTANCE SEAM WELD IN HDA 8077

Figure 5-50 Typical Resistance Seam Welds

Vacuum braze trails were conducted in the 1052-1149°C (1925-2100°F) range at $5x10^{-4}$ torr pressure using thermal expansion tooling to apply and maintain joint pressure. Brazing parameters and braze alloy chemistries are listed in Table 5-XII. Specimens were preheated to approximately 28°C (50°F) below the solidus temperature of the braze alloy to stabilize thermal gradients prior to brazing. No post-braze diffusion heat treatment was employed in these trials. As noted in Table 5-XIV, initial trials with METGLAS[R] BNi2 foil resulted in incomplete coverage and high levels of porosity in MA 956 - MA 956 braze joints. Subsequent trials therefore were conducted with METGLAS[R] BNi1A foil, which produced joints with minimal porosity (Figure 5-51) and provided good joint coverage in both alloys except for some lack of coverage in fillet areas which might be improved by supplemental paste application. Entrapped oxide evident in MA 956 joints was attributed to insufficient surface cleaning prior to brazing. HDA 8077 braze joints were free of any oxide contamination.

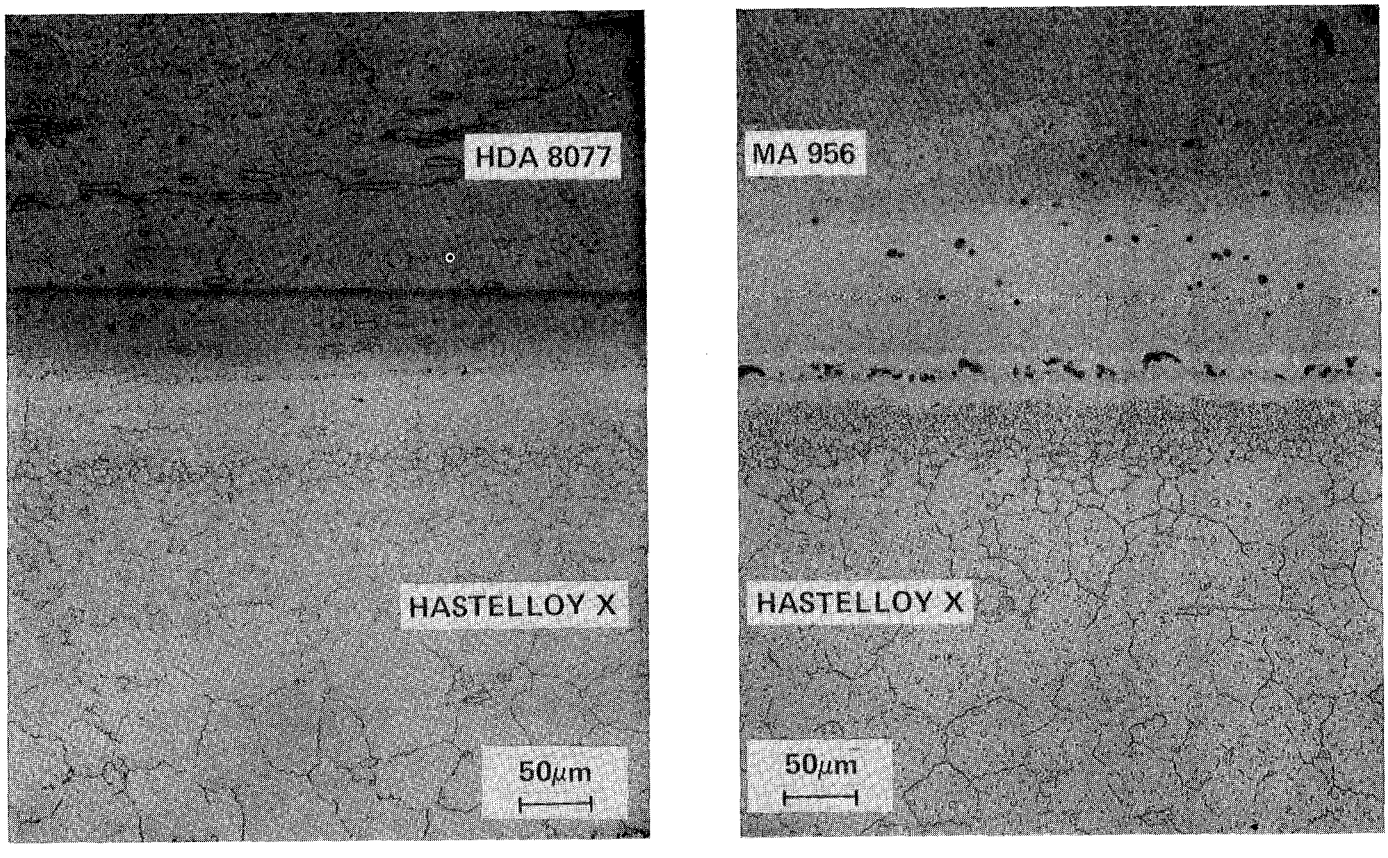

(A) (B)

Figure 5-51 Typical Brazed Joints Using METGLAS BNi1A

[R] Registered Trademark of Allied Chemical Corp.

Peel testing revealed an embrittling effect in MA 956 adjacent to the braze area as shown in Figure 5-52a. MA 956 - Hastelloy X peel tests showed braze material failure and braze affected zone failure adjacent to the MA 956. HDA 8077 - HDA 8077 joints failed through the braze material (Figure 5-52b), while HDA 8077 - Hastelloy X showed a strong, ductile, base metal failure mode of either HDA 8077 or Hastelloy X depending upon the loading during peel testing.

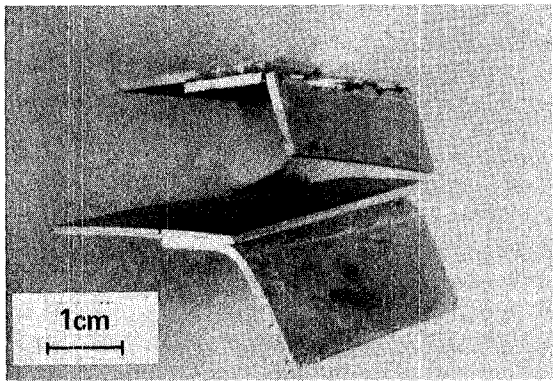

A) MA 956 — MA 956:
METGLAS® BNi1A BRAZE

B) HDA 8077 — HDA 8077:
METGLAS® BNi1A BRAZE

Figure 5-52 Peel Tests of Brazed Joints

Closer examination of these braze joints on the microprobe identified a Widmansttaten phase in the MA 956 BAZ (Braze Affected Zone) and limited porosity in the HDA 8077 side of HDA 8077/Hastelloy X joints. Examples of these two observation are shown in Figure 5-53. Energy Dispersive Spectra (EDS) investigation revealed the Widmansttaten-type phase in the MA 956 to be rich in iron and chromium. (The BNi IA braze composition is Ni-14Cr-4.5Fe-4.5Si- 3.1B-low C.) In addition, blocky phases in the braze zone were determined to be rich in nickel and aluminum (Figure 5-53A). The yttrium introduced in both ODS alloys in the form of Y_2O_3 is very stable during the brazing and diffusion cycles. There was no evidence of yttrium enrichment of braze alloy grain boundaries in either the ODS/ODS or ODS/Hastelloy X brazed combinations. However, discrete particles of an yttrium-rich phase were observed in the braze region as well as in the matrix. Improvements to the braze processes are discussed in the next section.

5.2.3 Braze Development and Evaluation

Identification of entrapped oxides in MA 956 joints, noted in the last section, indicated the need for an improved pre-braze cleaning procedure. Initially, pre-braze surfaces were given an alkaline rinse and vapor degrease

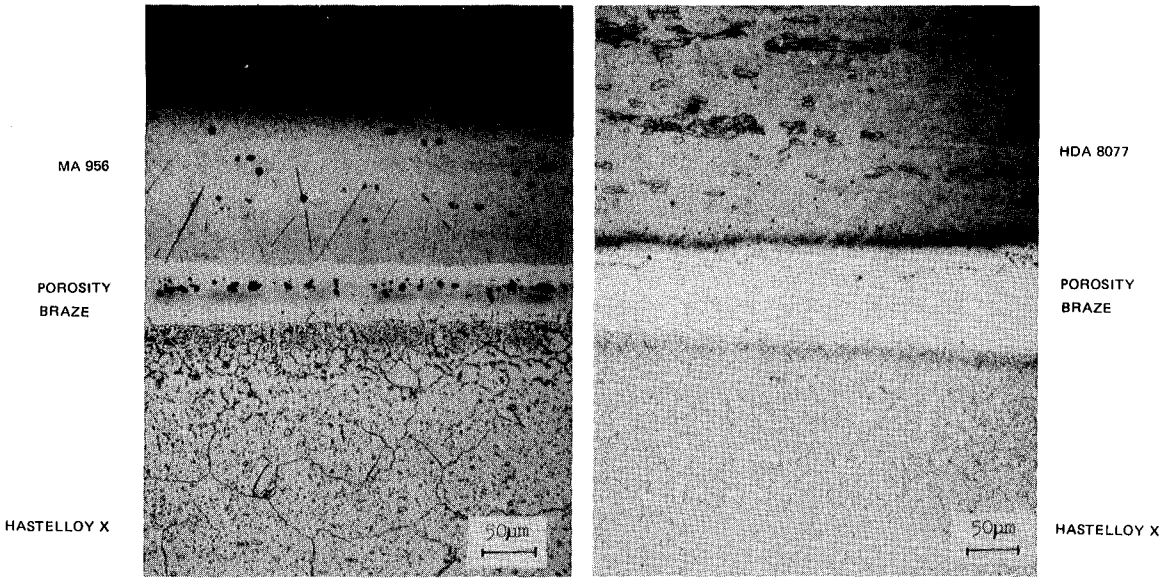

Figure 5-53 BNi1A Braze Microstructures

in perchlorethylene; this procedure resulted in incomplete wetting of the braze alloy and in the entrapment of surface oxides in the braze zone during the brazing operation. Surface preparation was improved by employing an alkaline rinse followed by: vapor blasting with -325 mesh Novaculite^{R} to remove surface oxides, water rinsing, and vapor degreasing in perchlorethylene. This technique resulted in improved wetting and a reduction in the amount of entrapped oxides in the braze zone. However, optimum braze wettability was achieved with the application of a nickel flash to the cleaned surfaces.

Using these cleaning and pre-plating procedures, additional braze trails were conducted to assess alternate process conditions and braze compositions. As indicated in Table 5-XV, these trials included evaluation of a post-braze diffusion treatment and of an alternate nickel-chrome-silicon braze alloy (BNi5) for MA 956 joints. As seen in Figure 5-54a, diffusion treatment did not eliminate the Widmansttaten precipitate in MA 956/Hastelloy X joints. The BNi5 alloy produced a better quality joint between these two materials, with no evidence of precipitation (Figure 5-54b). The Process C joints (see Table 5-XV) exhibited good reproducibility with those discussed in the earlier section. Process D joints were not distinguishable microstructurally from those produced by Process C.

TABLE 5-XV

BRAZE REPRODUCIBILITY TRIALS

Material Combinations	Process Designation	Braze Material	Braze Cycle	Diffusion Cycles
MA 956/MA 956 MA 956/HAST X	A	BNi1A®	1149°C (2100°F) 25 minutes	982°C (1800°F) 6 hours
MA 956/MA 956 MA 956/HAST X	B	BNi5®	1177°C (2150°F) 25 minutes	982°C (1800°F) 6 hours
HDA 8077/HDA 8077 HDA 8077/HAST X	C	BNi1A®	1149°C (2100°F) 25 minutes	None
HDA 8077/HDA 8077 HDA 8077/HAST X	D	BNi1A®	1149°C (2100°F) 25 minutes	982°C (1800°F) 6 hours

® Registered Trademarks of the Allied Chemical Corp.

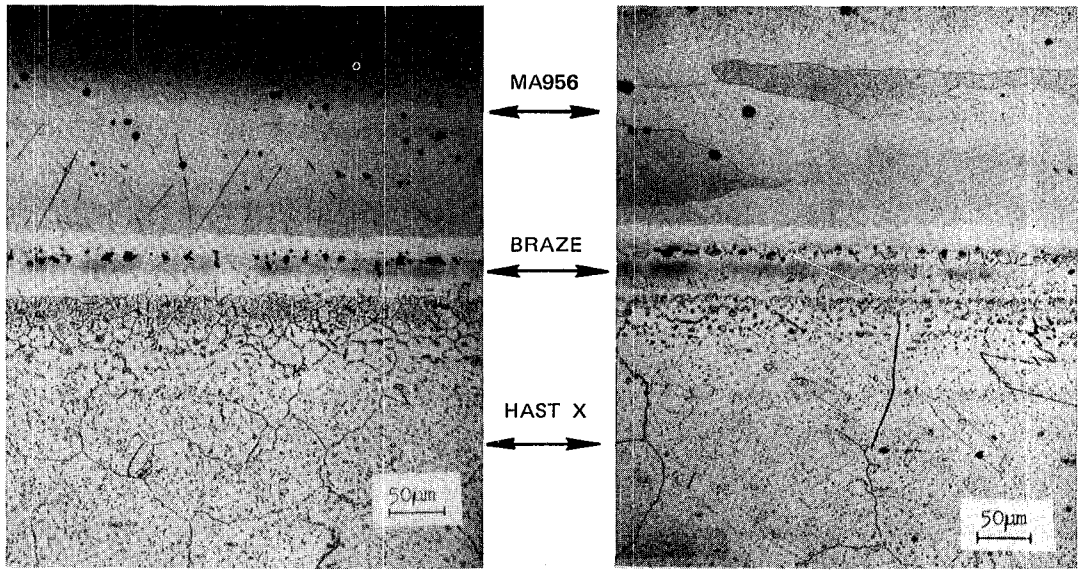

A) MA956/HASTELLOY X – BNi1A® BRAZE

B) MA956/HASTELLOY X – BNi5® BRAZE

Figure 5-54 MA 956/Hastelloy X Brazed and Diffusion Heat Treated Joints

The strength of brazed joints was evaluated at ambient temperature and at 982°C (1800°F) using the specimen shown in Figure 5-55. Results of tension tests conducted on specimens of this configuration are reported in Table 5-XVI. At both test temperatures, the ODS alloys brazed to Hastelloy X generally exhibited stronger and more consistent joint shear strengths compared to the ODS alloys brazed to themselves. Brazing Process B (for MA 956) and Process D (for HDA 8077) offered the better bond shear strengths at both test temperatures. At the 982°C (1800°F) test temperature and with the better brazing process (B for MA 956, D for HDA 8077), all of the ODS/Hastelloy X joints failed through the braze zone. Metallography of typical failed braze joints of ODS/Hastelloy X are shown in Figure 5-56. Based on these results, brazing Processes B and D are identified as the respective preferred methods for brazing of MA 956 and HDA 8077.

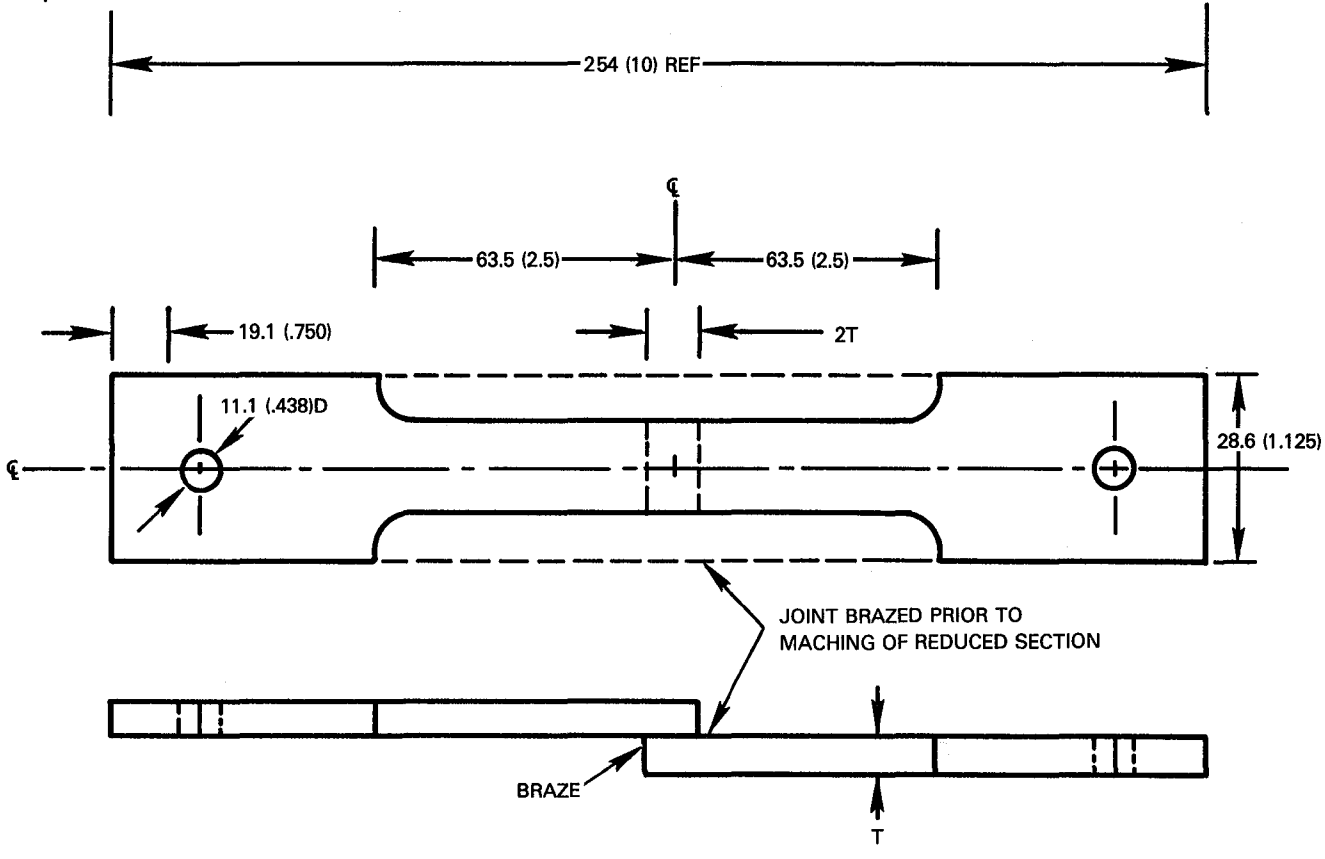

DIMENSIONS ARE mm (INCHES)

Figure 5-55 Geometry of Specimen Used to Evaluate Lap Braze Strength

TABLE 5-XVI

TENSILE PROPERTIES OF BRAZED LAP JOINTS

Material Combination	Braze[1] Alloy/Process	Test Temperature °C	Test Temperature (°F)	Ultimate Tensile Strength* Mn/M^2	Ultimate Tensile Strength* (ksi)	Failure Location
MA 956 - MA 956	A	18	(70)	133.9	(19.4)	MA 956 Parent Material
				91.7	(13.3)	MA 956 Parent Material
				132.0	(19.1)	MA 956 Parent Material
	B	18	(70)	158.4	(23.0)	Braze
				184.1	(26.7)	Braze
				121.0	(17.6)	Braze
	A	982	(1800)	36.7	(5.3)	MA 956 Diffusion Zone
				37.8	(5.5)	MA 956 Diffusion Zone
	B	982	(1800)	38.9	(5.6)	MA 956 Diffusion Zone
				35.9	(5.2)	MA 956 Diffusion Zone
				43.3	(6.3)	MA 956 Diffusion Zone
Hastelloy X - MA 956	A	18	(70)	110.0	(16.0)	MA 956 Parent Material
				111.9	(16.2)	MA 956 Parent Material
				111.9	(16.2)	MA 956 Parent Material
	B	18	(70)	165.0	(23.9)	Braze
				180.4	(26.2)	Braze
				163.2	(23.7)	Braze
	A	982	(1800)	40.3	(5.8)	MA 956 Diffusion Zone
				39.6	(5.7)	Braze
				48.0	(7.0)	MA 956 Parent Material
	B	982	(1800)	42.5	(6.2)	Braze
				44.0	(6.4)	Braze
				55.0	(8.0)	Braze
HDA 8077 - HDA 8077	C	18	(70)	209.0	(30.3)	Braze
				187.8	(27.2)	Braze
				194.4	(28.2)	Braze
	D	18	(70)	273.0	(39.6)	Braze
				238.4	(34.6)	Braze
				249.4	(36.2)	HDA 8077 Parent Material
	C	982	(1800)	34.1	(4.9)	Braze
				48.8	(7.1)	HDA 8077 Parent Material
				48.4	(7.0)	Braze
	D	982	(1800)	40.0	(5.8)	HDA 8077 Diffusion Zone
				38.5	(5.6)	Braze
				41.4	(6.0)	Braze
Hastelloy X - HDA 8077	C	18	(70)	253.1	(36.7)	Braze
				233.6	(33.9)	Braze
				194.3	(28.2)	HDA 8077 Parent Material
	D	18	(70)	238.4	(34.6)	Braze
				233.6	(33.9)	Braze
				229.2	(33.2)	HDA 8077 Parent Material
	C	982	(1800)	39.2	(5.7)	Braze
				44.7	(6.5)	Braze
				45.5	(6.6)	Braze
	D	982	(1800)	50.2	(7.3)	Braze
				51.3	(7.4)	Braze
				40.0	(5.8)	Braze

[1] See Table 5-XV

*"2T" lap joints whose area assumed to be 12.13mm^2 (1.88 x 10^{-2} in^2); cross head speed = 0.76 mm/min (3 x 10^{-2} in min)

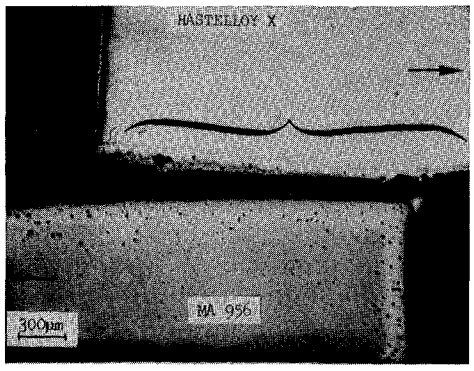

HASTELLOY X - MA 956

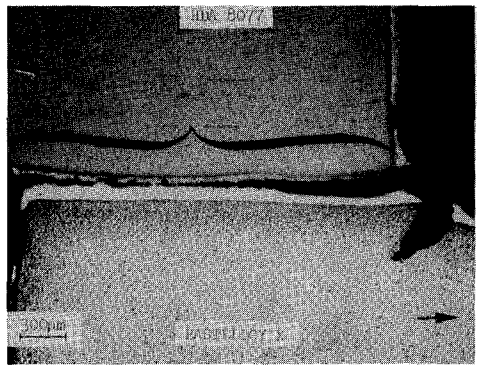

HASTELLOY X - HDA 8077

Figure 5-56 Photomicrographs of Sections Through MA 956 (Braze Process B) and HDA 8077 (Braze Process D) Lap Joints Showing Typical R.T. Fractures (Brackets). Arrows indicate loading direction.

5.2.4 Evaluation of Mechanical Attachment

Based on Task I selection of mechanical attachment as the primary means of joining ODS segments to a conventional alloy frame, the capabilities of rivets made from MA 956 and from Hastelloy X were evaluated. HDA 8077 was not evaluated because material was not available in a form suitable for rivet fabrication.

Two approaches were evaluated for fabrication of MA 956 rivets. One approach involved cold heading of MA 956 wire; the other involved machining to shape from MA 956 bar stock. Examples of each are shown in Figure 5-57. The wire clearly has a much finer grain structure, leading to concern about the creep strength of rivets made from this material. Also of concern was the potential for recrystallization of the severely cold worked material created during forming (Figure 5-58A).

To investigate the possibility for recrystallization, cold headed rivets were exposed in air for four hours at temperature increments of 56°C (100°F) in the range between 760 and 1260°C (1400-2300°F). Figure 5-59 shows the variation of hardness and microstructure found in these rivets as a function of exposure temperature. The decrease in initial hardness at 760°C (1400°F) and 816°C (1500°F) resulted from recovery of some of the residual cold work. The microstructures show a better defined, but elongated, grain structure.

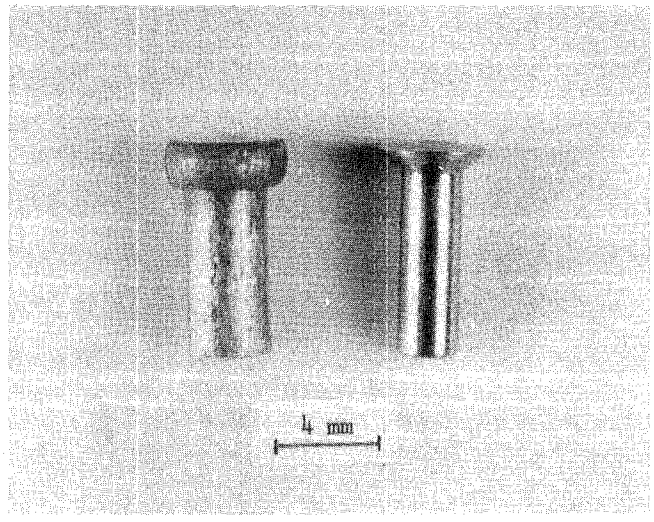

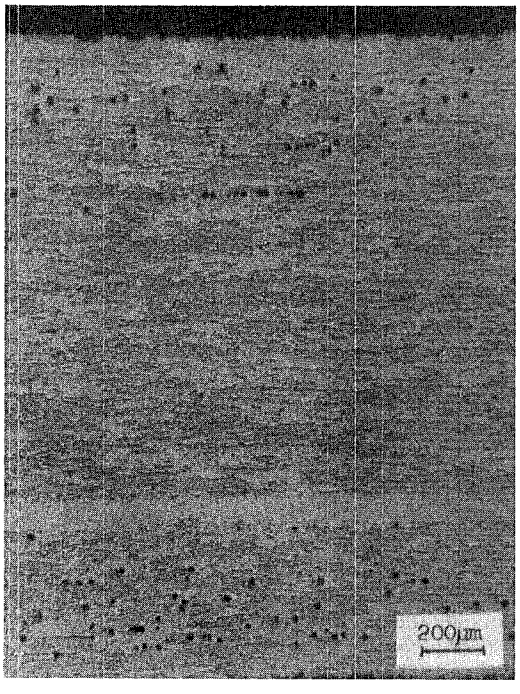

MA 956 WIRE – HEAT ZBXA

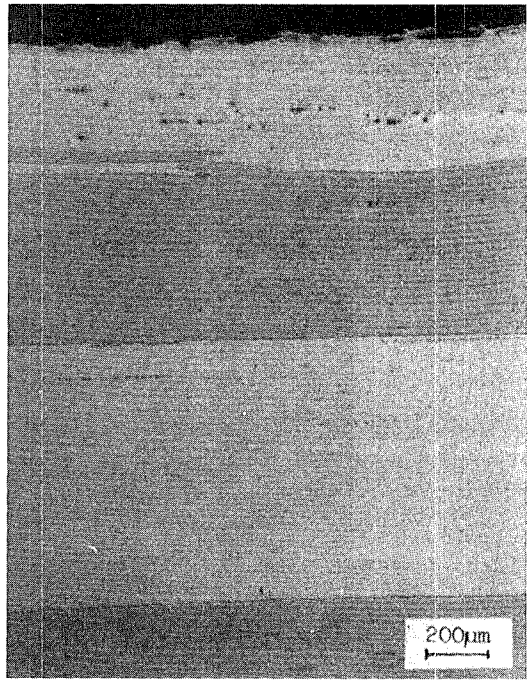

MA 956 BARSTOCK – HEAT ZDBC

Figure 5-57 MA 956 Rivets and Associated Pre-forming Microstructures

A) AS FORMED 500μm

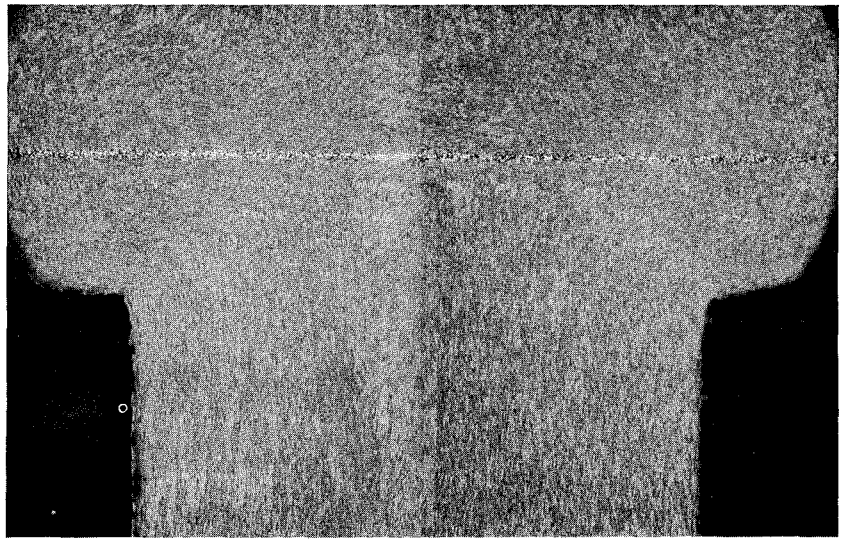

B) EXPOSED 4 HOURS AT 1093C (2000F) 500μm

Figure 5-58 Microstructures Found in As-formed and Thermally Exposed MA 956 Rivets Fabricated by Cold Heading of Wire

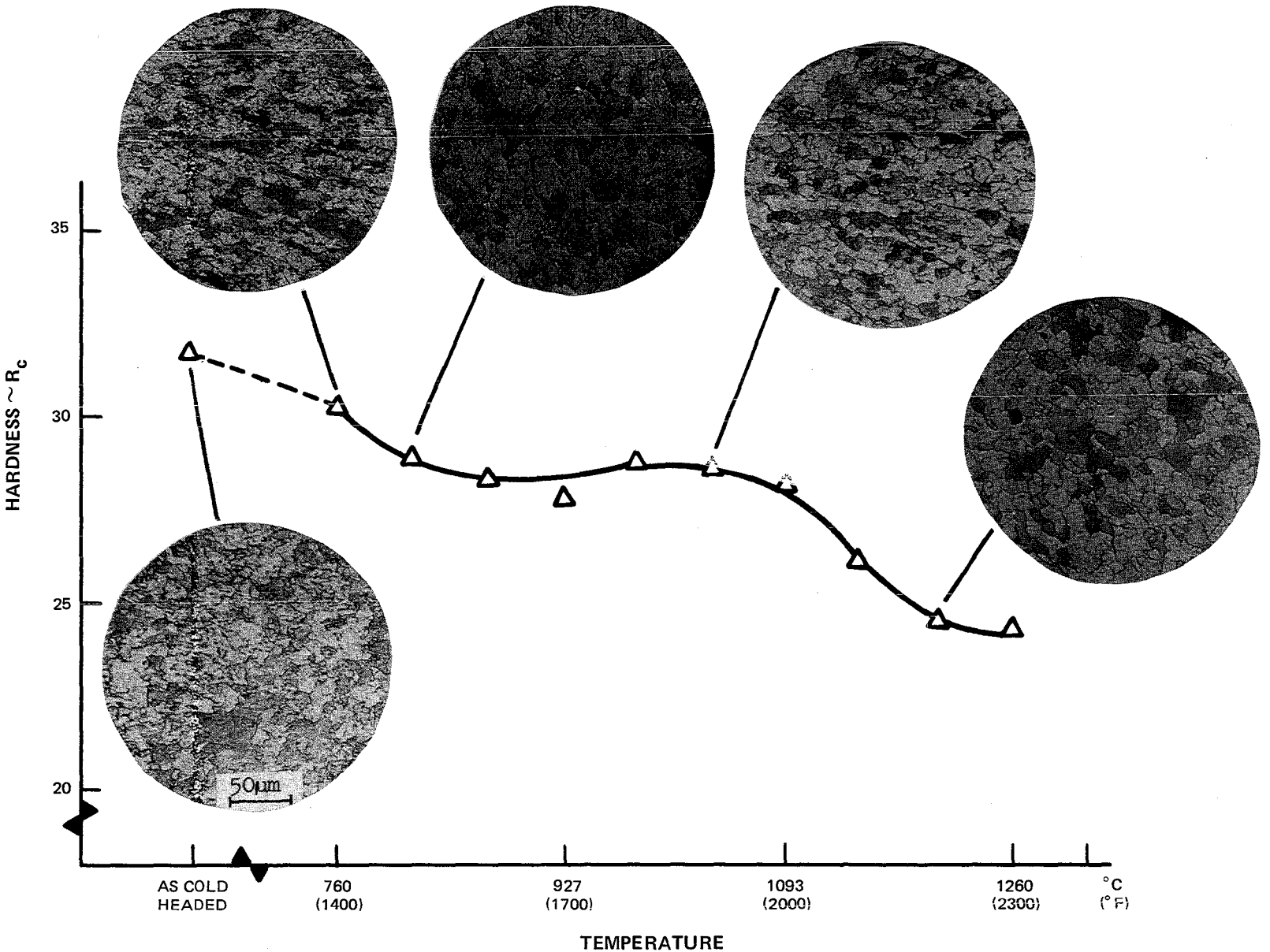

Figure 5-59 Recrystallization Stability of Lot ZBXA Cold Headed Wire Rivets - 4 Hours at Temperature

Recrystallization and grain growth occurred above 1093°C (2000°F), giving a further reduction in hardness. The microstructure of a rivet exposed at 1093°C (2000°F) is shown in Figure 5-58B. Because of this recrystallization at relatively short times, a decision was made to proceed only with rivets machined from bar stock.

To measure rivet strengths, bi-metal (ODS/Hastelloy X) lap specimens joined with either MA 956 or Hastelloy rivets (Figure 5-60) were tensile tested to failure at room and elevated temperature. Creep shear tests also were performed on joints between MA 956 and Hastelloy X formed with both rivet materials.

Results of tensile shear tests are reported in Table 5-XVII. All failures occurred by shear fracture of the rivet. Comparison of Hastelloy X and MA 956 rivet materials at room temperature and 982°C (1800°F) showed the average ultimate shear strength of joints fabricated with Hastelloy X rivets to have approximately a 15% and 35% advantage, respectively, compared to joints fabricated with MA 956 rivets.

The results of creep-shear testing of Hastelloy X/MA 956 riveted lap joints at 982°C (1800°F) are listed in Table 5-XVIII. The rupture life of joints fabricated with MA 956 rivets showed a 1.5 - 8.0X life improvement over those fabricated with Hastelloy X rivets. Visual examination revealed that the Hastelloy X rivets failed in shear through the rivet shaft, whereas, the MA 956 rivets failed by fracturing through the rivet head. Bending of the Hastelloy X sheet material was evident in the MA 956 riveted specimens. Metallography of failed Hastelloy X rivets revealed circumferential intergranular cracking in the shaft of the rivet which apparently reduced the cross-sectional area and resulted in a shear failure (Figure 5-61). Failed MA 956 rivets showed circumferential transgranular cracking in the rivet shaft which propagated (sheared) longitudinally through the machined rivet head along grain boundaries (Figure 5-61). Bending of the Hastelloy X sheet material during testing may have contributed to the failure. After test, Hastelloy X rivets exhibited substantially more surface oxidation than MA 956 rivets exposed for longer times.

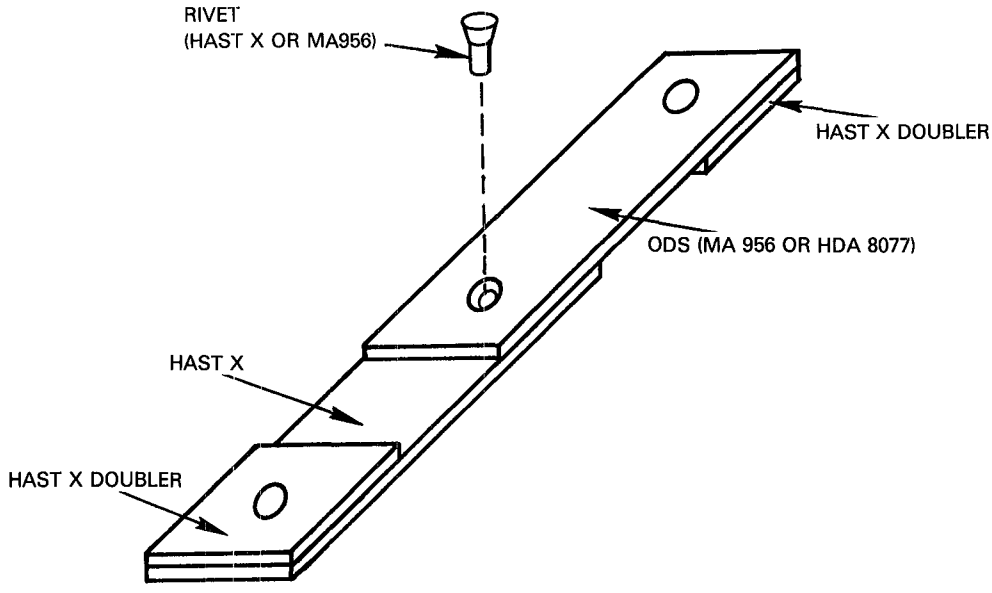

a) PERSPECTIVE VIEW

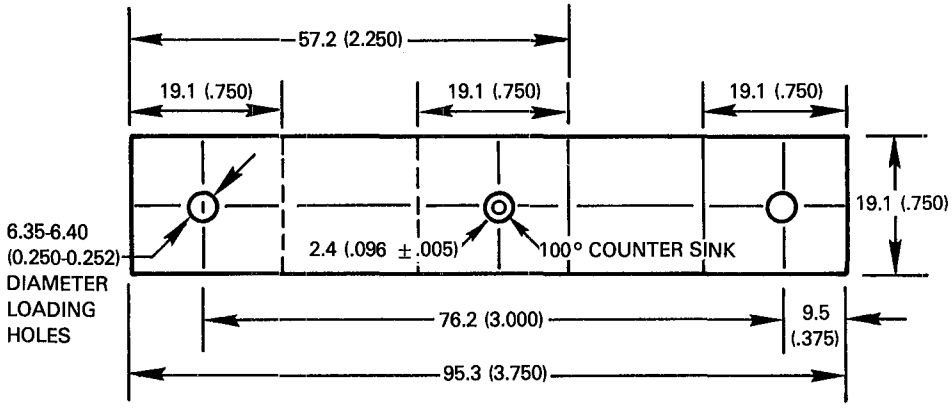

b) TOP VIEW — DIMENSIONS ARE mm (INCHES)

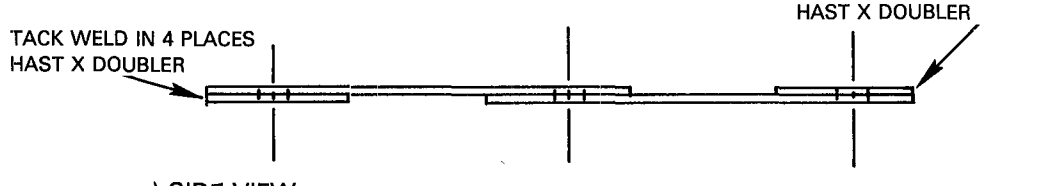

c) SIDE VIEW

Figure 5-60 Tensile and Creep Rupture Test Specimen Design for Shear Testing Hastelloy X and ODS Rivets

TABLE 5-XVII

SHEAR STRENGTH OF RIVETED LAP JOINTS

	Temperature °C	Temperature (°F)	Rivet Material	Joint Materials	Ultimate Shear Stress* MPa	Ultimate Shear Stress* (ksi)
A.	18	(64)	Hastelloy X	Hastelloy X/MA 956	622.6	(90.3)
					612.9	(88.9)
					633.0	(91.8)
			Hastelloy X	Hastelloy X/HDA 8077	632.0	(91.7)
					665.6	(96.5)
			MA 956	Hastelloy X/MA 956	565.0	(81.9)
					531.5	(77.1)
					535.3	(77.6)
			MA 956	Hastelloy X/HDA 8077	521.9	(75.7)
					521.9	(75.7)
B.	659	(1200)	Hastelloy X	Hastelloy X/MA 956	464.5	(67.4)
					469.2	(68.1)
			Hastelloy X	Hastelloy X/HDA 8077	464.5	(67.4)
					445.3	(64.6)
C.	982	(1800)	Hastelloy X	Hastelloy X/MA 956	86.2	(12.5)
					105.3	(15.3)
					99.6	(14.4)
			Hastelloy X	Hastelloy X/HDA 8077	100.6	(14.6)
					105.3	(15.3)
			MA 956	Hastelloy X/MA 956	76.6	(11.1)
					76.6	(11.1)
					72.8	(10.6)
			MA 956	Hastelloy HDA 8077	67.0	(9.7)
					71.8	(10.4)

---

* Based on ultimate load and assumed area of rivet = 4.7mm^2 (7.2 x 10^{-3}in^2)

All rivets failed in shear.

Crosshead speed = 5 x 10^{-3} min^{-1}

TABLE 5-XVIII

CREEP-SHEAR OF RIVETED LAP JOINTS

TEST CONDITIONS: 982°C (1800°F)/44.75 Mn/M^2 (6.94 KSI)*

Rivet Material	Joint Materials	Life (Hrs.)	Failure Character
Hastelloy X	Hastelloy X-MA 956	2.3 1.8	Shear of Rivet.
MA 956	Hastelloy X-MA 956	4.0 14.4	Machined head pull out failure; bending of Hastelloy X half of specimen.

* Based on a load of 110 KG (50 lb.) and an initial area of 4.7mm^2 (7.2 x 10^{-3}in^2)

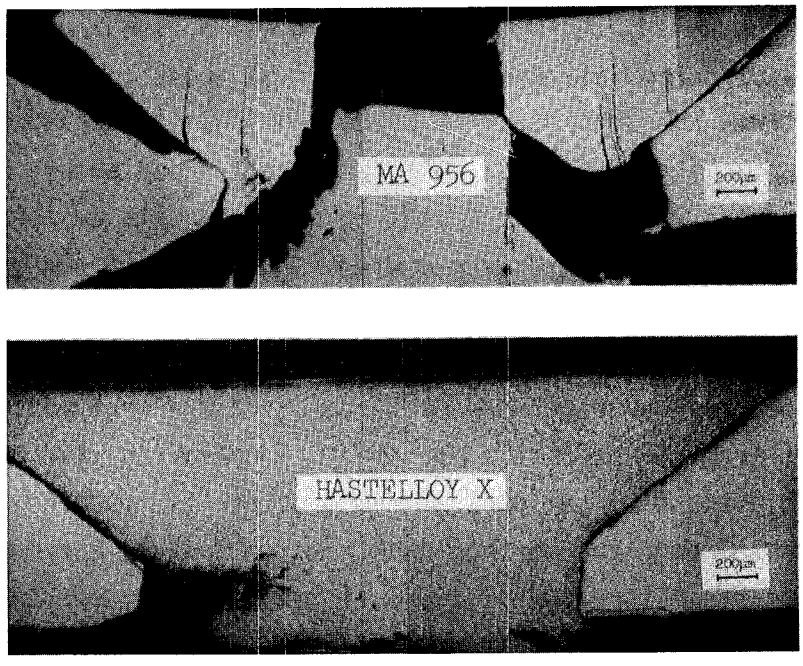

Figure 5-61 982°C (1800°F) Creep Shear Fracture Microstructures of Riveted Joints

5.3 TASK III COMBUSTOR RIG TEST METHODS DEVELOPMENT

5.3.1 Introduction and Summary

The objective of this sub-task was to develop methods for subscale laboratory thermal fatigue testing of the film cooled mechanically attached segmented louver and the transpiration cooled twin wall combustor designs identified in Task I (Section 3). While limited preliminary evaluations were conducted with HDA 8077 alloy, most of this work was done with MA 956 and Hastelloy X because of the reproducibility difficulties with HDA 8077 (Section 4).

The subcomponent test article developed to evaluate the film cooled mechanically attached segmented design is illustrated in Figure 5-62. The outer supporting shell of this article is Hastelloy X; mechanically attached segments were fabricated of Hastelloy X or MA 956 as appropriate to the evaluation being conducted. The initial test method involved cyclic induction heating and still or forced air cooling. Results of these initial experiments indicated that it was not possible to produce a uniform temperature on all twenty-four segments. The "test section" therefore was defined as the center set of eight segments. While the "up" and "downstream" sets of segments were necessarily heated and cooled with the center set, no effort was made to control the temperatures in these two sets of segments. After evaluation of numerous induction and cooling coil configurations on the eight segment test section, it was determined that the required temperature control could not be achieved on multi-segment assemblies with induction heating. Two major problems were achievement of the desired temperature distribution in the eight segments and unwanted coupling of the induction field with, and consequent overheating of the Hastelloy X outer shell. Two approaches were taken to overcome these problems. First, a heating coil configuration was developed which provided the desired temperature distribution in a single segment without undue shell heating. The second approach involved alternate radiant gas burner heating and forced air cooling of the eight segment ring. Both of these methods were used in Task V for comparative testing of MA 956 and Hastelloy X segments (see Section 7).

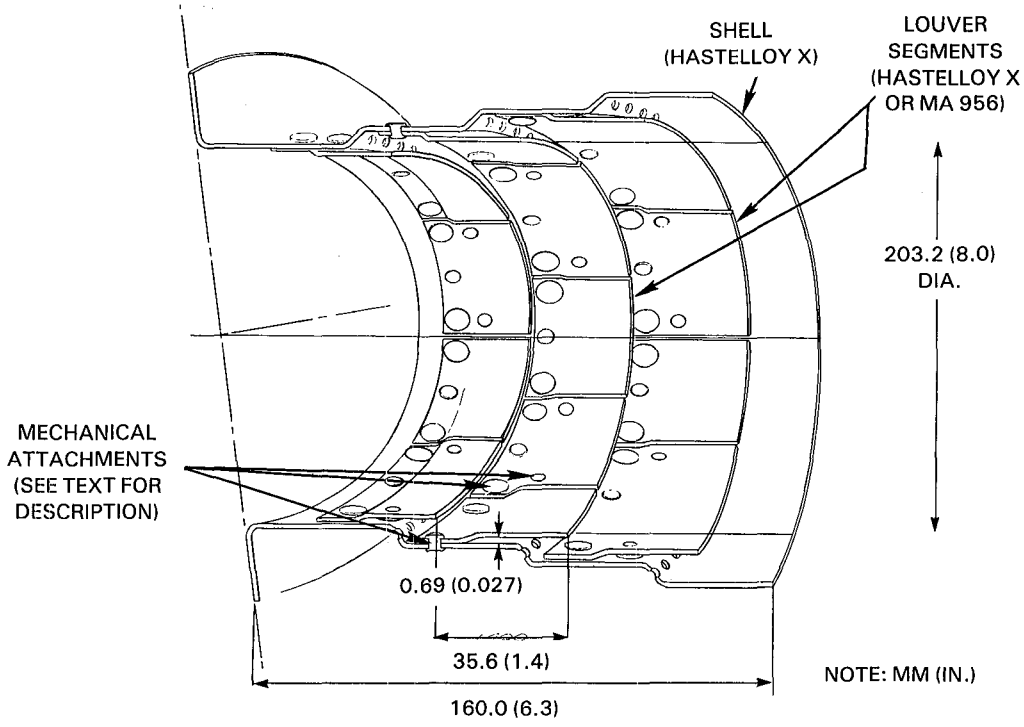

Figure 5-62 Film Cooled Mechanically Attached Louver Thermal Fatigue Test Component Design

The subcomponent test article initially developed to evaluate the transpiration cooled twin wall design is illustrated in Figure 5-63. As with the louvered design, initial attempts to induction heat the transpiration cooled panel did not achieve the desired temperature distribution. A method for radiant gas burner heating, which involved the application of three separate heaters on the center and two sides of a single panel, therefore was developed to produce satisfactory temperatures. At this point in the program, a determination was made in the parallel Task I activity that the strain range in the hook attachment region of this design would exceed the thermal fatigue capabilities of oxide dispersion strengthens alloys (Section 3.5.2). The alternate prestressed transpiration cooled twin wall subcomponent test article shown in Figure 5-64, therefore was developed to simulate the revised design described in Section 3.6. Radiant gas burner heating was used for cyclic thermal testing of this design. Using this method, comparative testing of Hastelloy X and MA 956 transpiration cooled panels was conducted in Task V (Section 7). Details of the test methods development activities are described in the following sections.

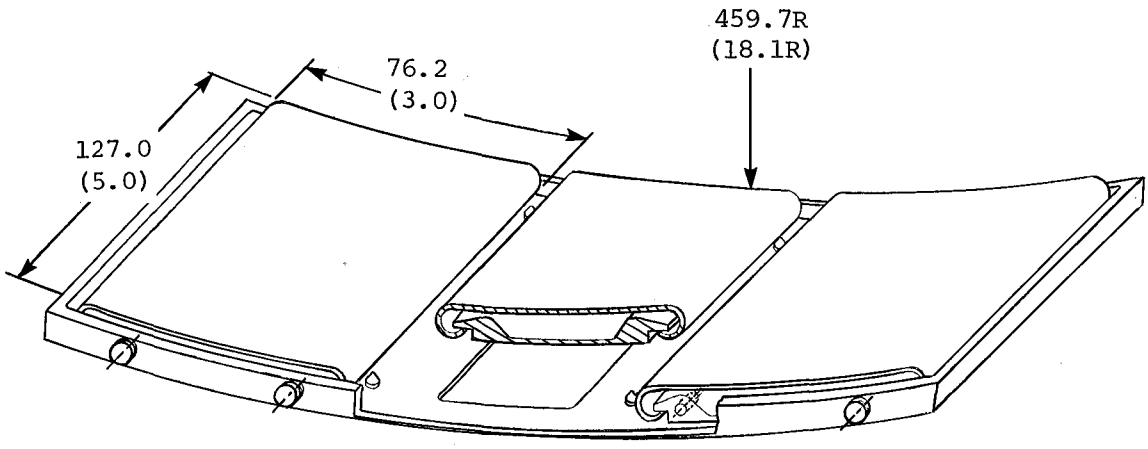

Figure 5-63 Initial Hooked Transpiration Cooled Thermal Fatigue Test Component Design. (Note impingement and transpiration cooling holes omitted for clarity).

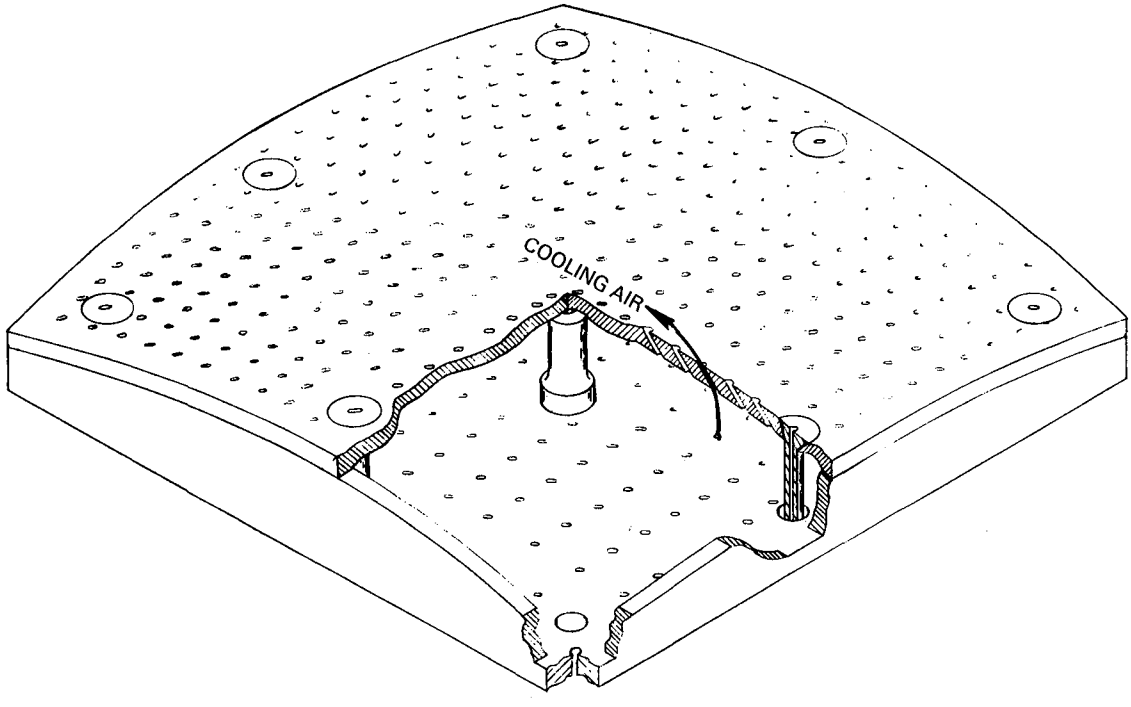

Figure 5-64 Pre-Stressed Transpiration Cooled Twin Wall Thermal Fatigue Test Specimen

5.3.2 Film Cooled Mechanically Attached Segmented Louver Specimen Configuration and Fabrication

The objective of this effort was to develop a test method to evaluate the thermal fatigue capability of the segmented louver design concept identified in Task I (Figure 3-12). The configuration shown previously in Figure 5-62 was developed to accomplish this objective. This assembly consists of a Hastelloy X shell with mechanically attached louver segments of either Hastelloy X or MA 956. The test methods development effort described in this section was conducted primarily with Hastelloy X segments. Comparative testing of the two alloys is described in Section 7.

Several configurations were identified for mechanical attachment of segments to the Hastelloy X shell. These configurations are illustrated in Figure 5-65. The rivet configuration shown in Figure 5-65A was designed to firmly anchor the center of the upstream ("cold") end of the segment where in-plane relative motion of the two clamped panels is not required to relieve thermal strain in ODS alloy sheet (See Section 3.3.2 for discussion of attachment requirements). Because this fully clenched rivet was intended to operate at temperatures no higher then 760°C (1400°F), Hastelloy X was considered to be a suitable rivet material.

For "cold" locations where relative sheet motion is anticipated (upstream segment corners), the Hastelloy X pin and washer configuration shown in Figure 5-65A was used.

Two alternative attachment approaches were developed for attachment of the downstream (hot) end of the segments. As shown in Figure 5-65C and 5-65D, both of these approaches are designed to allow relative in-plane motion between the attached sheets.

The hot attachment configuration illustrated in Figure 5-65D incorporates a stud brazed to the back side of the segment. Because this stud is located on the cold side of the segment, Hastelloy X was judged suitable for this application. Photomicrographs of a Hastelloy X stud brazed to an MA 956 panel are shown in Figure 5-66.

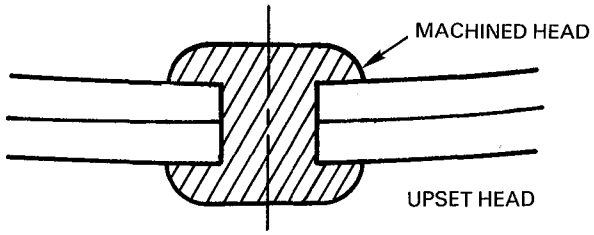

A) "COLD" RIVET (HASTELLOY X)

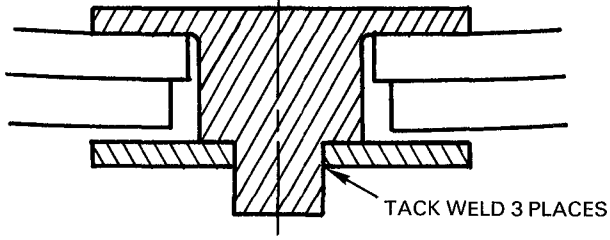

B) PIN AND WASHER (HASTELLOY X)

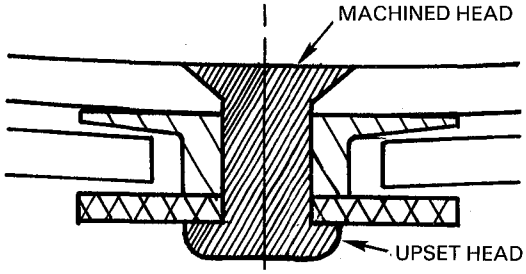

C) "HOT" RIVET AND SPACER — (SPACER AND WASHER HASTELLOY X; RIVET HASTELLOY X OR MA 956)

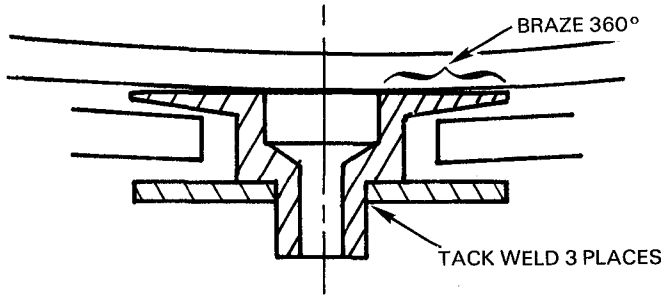

D) BRAZED SPACER AND WASHER (HASTELLOY X)

Figure 5-65 Geometry of Mechanical Attachments Evaluated on Segmented Louver Test Component (All configurations shown gas stream side up).

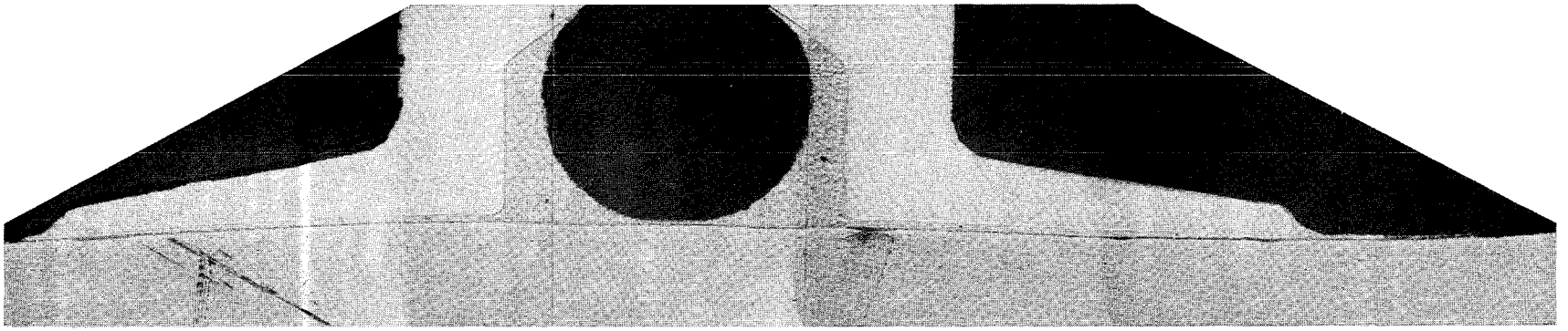

A) COMPOSITE PHOTOMICROGRAPH 30X

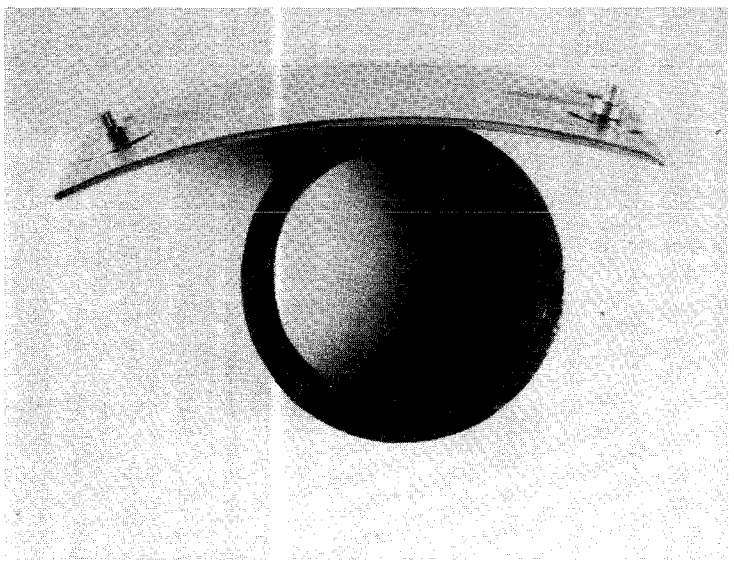

B) PHOTOGRAPH OF STUDS BRAZED TO SEGMENT

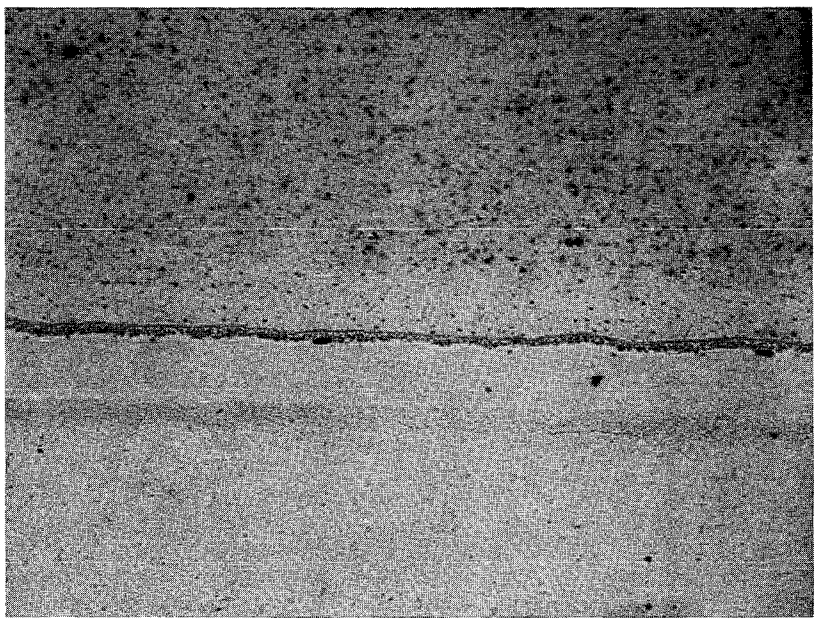

C) BRAZE MICROSTRUCTURE 200X

Figure 5-66 Hastelloy X Stud Brazed to MA 956 Panel Using Procedure "B" (Table 5.2-IV)

The hot attachment configuration illustrated in Figure 5-65C incorporates a rivet headed against a washer and spacer assembly. As discussed in a later section, both Hastelloy X and MA 956 rivets were used, depending on the segment material. MA 956 rivets were machined from Lot ZDBC bar stock as described in Section 5.2.4. The microstructure observed in a headed MA 956 bar-stock rivet is shown in Figure 5-67. Because the headed end of this rivet is located on the cold side of the assembly, recrystallization of the cold worked structure, such as described in Section 5.2.4, was not a concern.

Figure 5-67 Microstructure Observed in Headed End of MA 956 Rivet Fabricated From Lot ZDBC Bar Stock

Fabrication of the test article sheet metal components was accomplished using routine shop practices except for forming of the ODS segments. Because segment fabrication trials were conducted prior to elimination of HDA 8077 from the program, both ODS alloys were involved.

MA 956 segments used in the riveted louver design were fabricated by welding strip into a ring and spin forming an 0.64-0.76 mm (0.025-0.030 in.) offset joggle into the ring. The joggled rings were stress relieved at 1177°C (2150°F) for 1/2 hour after spinning and prior to being sectioned into segments. A spun ring of MA 956 is shown in Figure 5-68. The more limited formability of HDA 8077 dictated a tool and die technique to joggle individual segments to this same geometry. An 1177°C (2150°F) stress relief anneal was

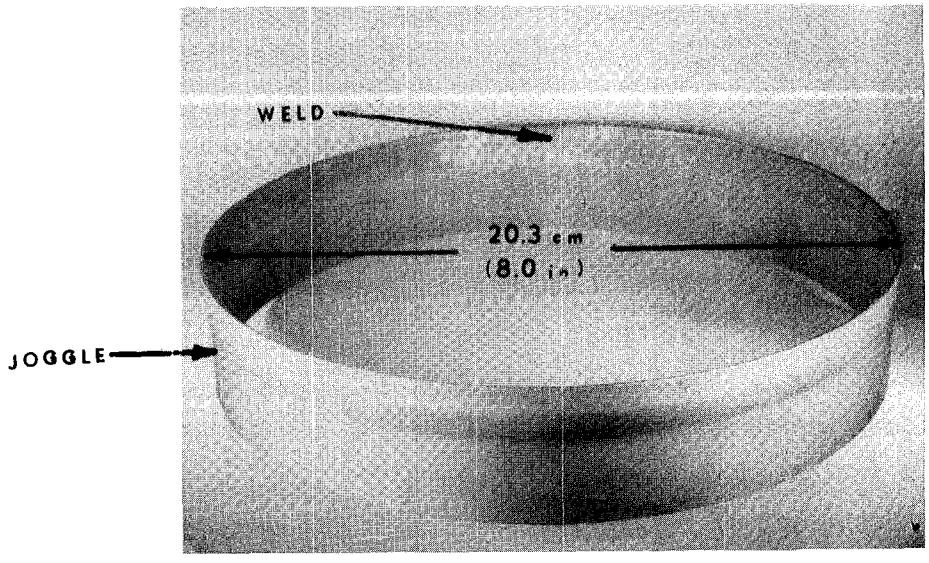

Figure 5-68 MA 956 Spun Joggle

used after forming HDA 8077. Visual, fluorescent penetrant, and metallographic examination of as-formed details showed no evidence of cracking (Figure 5-69). Metallographic examination of annealed joggles showed 10 μm (3.9×10^{-4} in.) of surface recrystallization throughout the MA 956, attributed to grit blasting of lot ZDEW during sheet manufacture. This surface recrystallization was not observed in later segments formed from lot XBB-004, which did not have the surface worked layer. The HDA 8077 exhibited 20 μm (7.8×10^{-4} in.) of surface recrystallization in the joggle area.

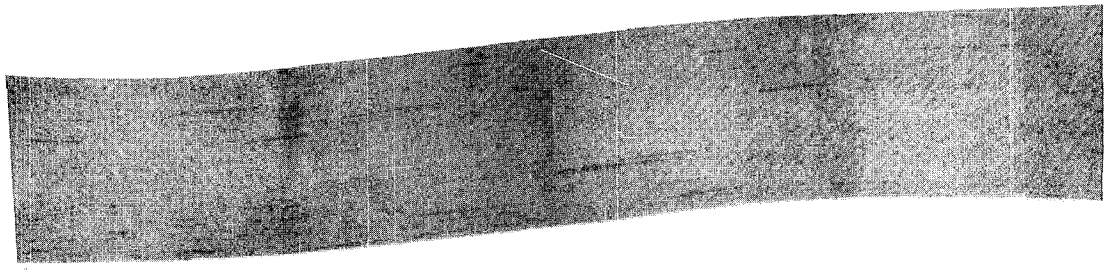

AS-FORMED HDA 8077 (MS-154)

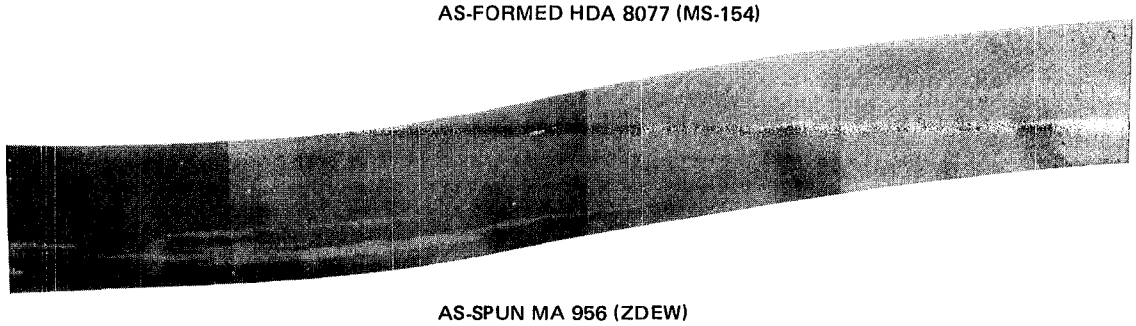

AS-SPUN MA 956 (ZDEW)

Figure 5-69 Joggled Sheet with 0.6mm (0.025") Offset

5.3.3 Louvered Specimen Induction Heating Trials

As noted previously, the initial approach evaluated for thermal cycle testing of the film cooled louver design involved induction heating of all twenty-four segments on the test specimen illustrated in Figure 5-62. Prior to the fabrication of segmented specimens, initial induction heating trials were conducted on an instrumented "dummy" specimen incorporating slotted Hastelloy X louvers welded to a Hastelloy X shell (Figure 5-70A). Preliminary induction heating trials indicated that all twenty-four segments could not be heated uniformly. A second set of trials involving only the center set of eight segments thus was initiated. These tests were conducted using a Lepel High Frequency Induction Heating Generator capable of either manual or programmed controlled output from zero to 100 KW at 350 KHz. Due to the relatively small specimen size, a load coil transformer was required to match the impedance of the small heating coils to the induction unit to optimize power transfer to the specimen. These trials were conducted on the downstream (largest diameter) louver of the dummy specimen as shown in Figure 5-70B. Using a close coupled single turn induction coil made of rectangular copper tubing near the louver lip and a stainless steel air cooling coil in the knuckle region, the temperature distribution shown in Figure 5-71 was attained on the downstream louver. This temperature distribution was judged to be acceptably close to the desired distribution also shown in Figure 5-71. As noted in Figure 5-70B, some local heating of the Hastelloy X shell was observed near the louver slots. The level of this heating was judged acceptable in this trail.

Following successful achievement of the desired louver temperature distribution on the "dummy" specimen containing a single slotted hoop, efforts were made to reproduce this distribution on the middle set of segments in the specimen shown in Figure 5-72. This specimen was constructed entirely of Hastelloy X and was assembled entirely with mechanical fasteners (no brazed studs). As summarized in Table 5-XIX, this effort included six successive trials in which the problem of achieving the desired temperature distribution without overheating the Hastelloy X shell was never overcome. In the first of these six trials, (Table 5-XIX, Trial I), temperature distributions approximating the desired distribution were achieved in individual segments,

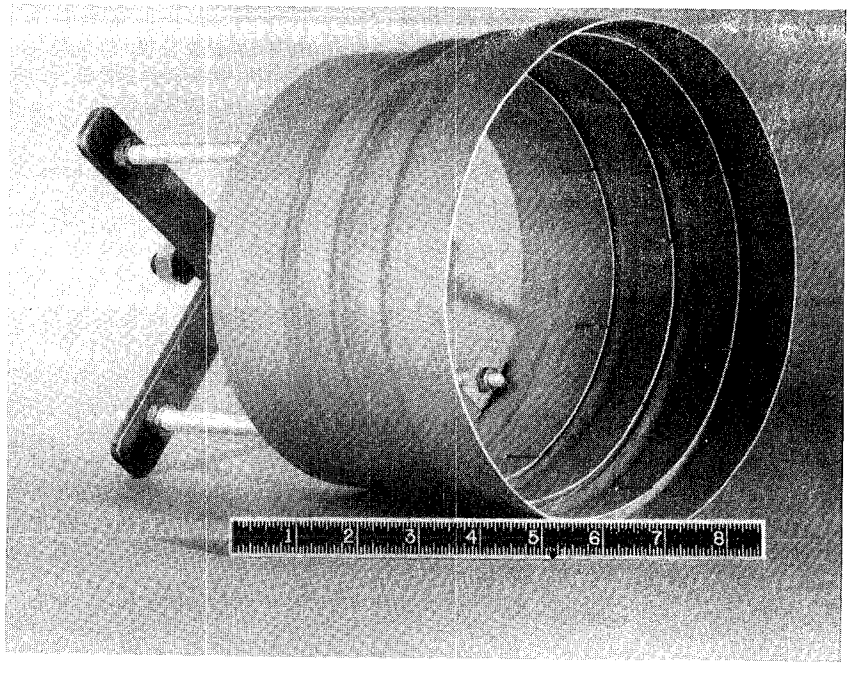

A) ''DUMMY'' TEST SPECIMEN

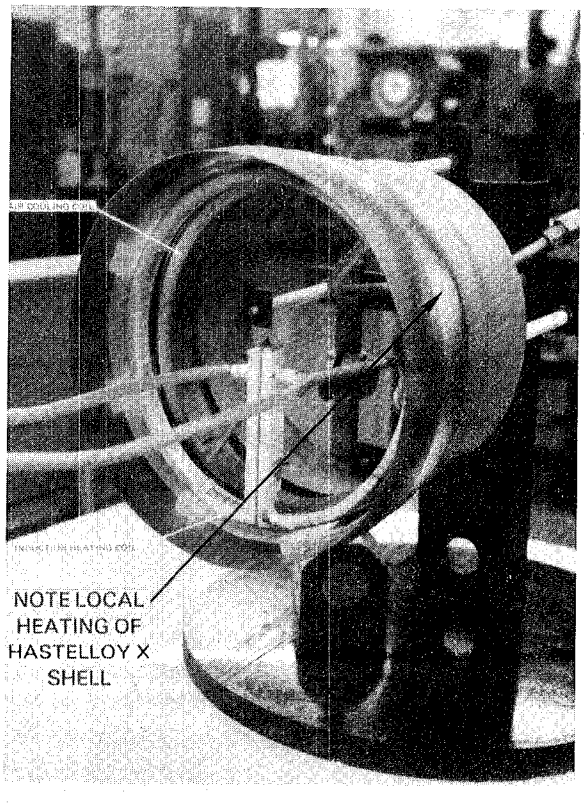

B) PLACEMENT OF INDUCTION HEATING AND COOLING COILS

Figure 5-70 Test Setup of "Dummy" Louver Specimen

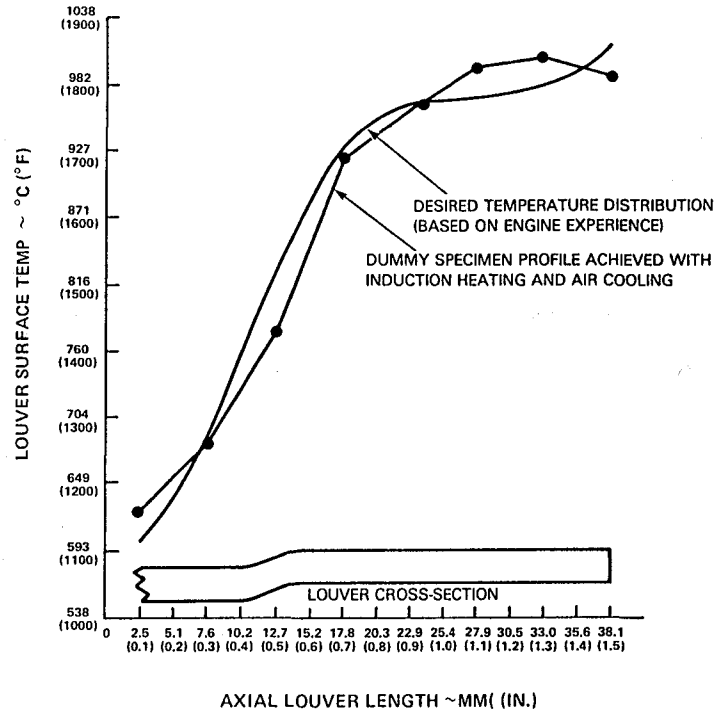

Figure 5-71 Temperature Distribution in "Dummy" Louver Specimen

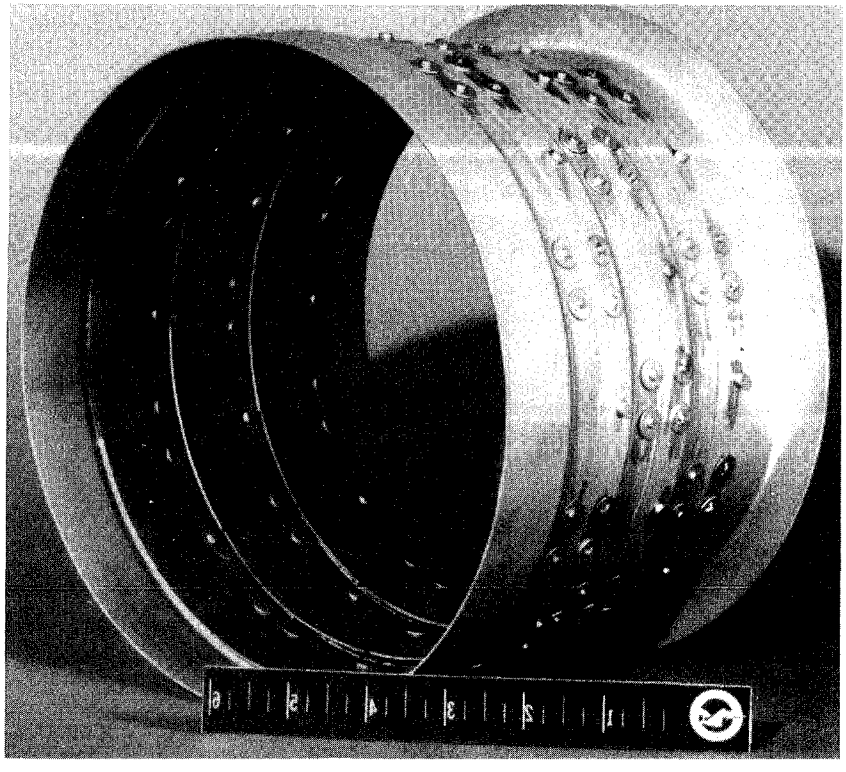

Figure 5-72 Hastelloy X Riveted Louver Thermal Fatigue Test Specimen

TABLE 5-XIX

SEQUENCE OF INDUCTION HEATED SEGMENTED LOUVER RIG MODIFICATIONS

Trial Number	Experimental Configuration	Results
I.	Specimen Test of Horizontal Axis Specimen Employing: ° 1/2" wide x 7 1/2" diameter induction heating coil. ° I.D. stainless steel air cooling coil. ° Cooling air applied selectively to the "cold" end of the rivets.	An approximate profile was achieved. However, cold wall over heating resulted in cracking at a rivet hole in the cold wall. The specimen was discontinued after 537 cycles for weld repair and installation of 8 new louver segments.
II.	Shakedown Trails of Horizontal Axis Specimen Employing: ° 3/4" wide x 7 3/4" diameter induction heating coil. ° Water cooled I.D. stainless steel air cooling coil. ° O.D. cooling manifold to cool the cold wall uniformly.	Cold wall overheating occurred neither the desired temperature profile nor the desired Tmax was achieved. The cold wall was slotted behind the louver segments being heated to break up the inductive eddy current heating of the cold wall.
III.	Shakedown Trails of Horizontal Axis Specimen Employing: ° Slotted cold wall. ° Combination of 3/4" wide x 7 3/4" diameter and 1/2" wide x 7 1/2" diameter induction heating coils. ° No O.D. cooling manifold.	Cold wall overheating occurred and a localized melt through occurred in the cold wall at the end of a slot which necessitated a weld repair. Neither the desired Tmax were achieved.
IV.	Shakedown Trails of Horizontal Axis Specimen Employing: ° Slotted cold wall. ° Both heating coils (as in IV) and a 2-turn copper tube coil. ° I.D. Hastelloy X air cooling coil (water cooled). ° Cooling air applied selectively to the ends of the slots.	Cooling coil overheating as well as cold wall overheating occurred. Neither the desired temperature distribution nor the desired Tmax were achieved. Total rig modification required to reduce excessive cold wall heating and flux losses. Employment of a power shunt to improve transfer to specimen. Reorient specimen vertically.
V.	Shakedown Trails of Vertical Axis Specimen Employing: ° Slotted cold wall with one slot all the way through the cold wall. ° Both heating coils (as in IV) and a 2-turn copper tube coil. ° Power shunt ° I.D. copper air cooling coil (water cooled).	Cold wall overheating continued to occur. Totally slotted specimen had a lot of movement between heating and cooling and is now out of of round. Flux losses continue to prevent achievement of Tmax. Secondary heating coil leads were shortened by placing transformer under specimen.
VI.	Shakedown Trails of Vertical Axis Specimen Employing: ° Slotted cold wall with one slot all the way through the cold wall. ° Both heating coils (as in IV). ° Power shunt. ° I.D. copper air cooling coil (water cooled).	Tmax achieved, however overheating of hot and cold wall rivets leading to localized melting. Cold wall overheating continued to be a problem.

but these distributions were not the same in all eight louvers (Figure 5-73). In addition, severe overheating of the Hastelloy X shell was observed (Figure 5-74). To gain test experience, thermal cycle testing was attempted with this setup. A test cycle consisting of 45 seconds heat to a Tmax of 1010°C (1850°F), a two minute hold, and a 30 second cool to a Tmin of 427°C (800°F) was applied to simulate anticipated combustor thermal strains. This testing resulted in cracking and localized melting of the shell after 537 thermal cycles.

A study of the Trial I observations suggested that a wider induction coil might couple more closely with the segments and thus provide a better temperature profile. This modification was incorporated in the Trial II configuration, together with the addition of water cooling to the inner air cooling coil to provide more effective internal cooling of the upstream end of the segment. To reduce heating of the shell, a large outer air cooling coil was added. Trials employing this increased cooling failed to prevent overheating of the cold wall and prevented achievement of the desired segment temperature even at full induction power.

As indicated in Table 5-XIX, four subsequent groups of trials were conducted. These trials included further successive modifications to the heating and cooling configuration, slotting of the cold wall, and re-orientation of the specimen from a horizontal to a vertical position. None of these modifications resolved the basic problem of achieving the desired temperature distribution without overheating the cold wall. This effort therefore was discontinued in favor of alternative testing approaches described below.

The induction heating approach which was employed to successfully achieve the desired segment temperature distribution without cold wall overheating involved testing of a single segment as illustrated in Figure 5-75A. A double return pie-wound induction heating coil was used together with an external air cooling manifold to achieve the temperature profile shown in Figure 5-75B on a single louver segment of Hastelloy X. No overheating of the cold support shell was experienced. The use of this test method for thermal fatigue evaluation of individual Hastelloy X and MA 956 louver segments is described in Section 7. The development of gas burner heating for evaluation of multi-segment assemblies is described in the following section.

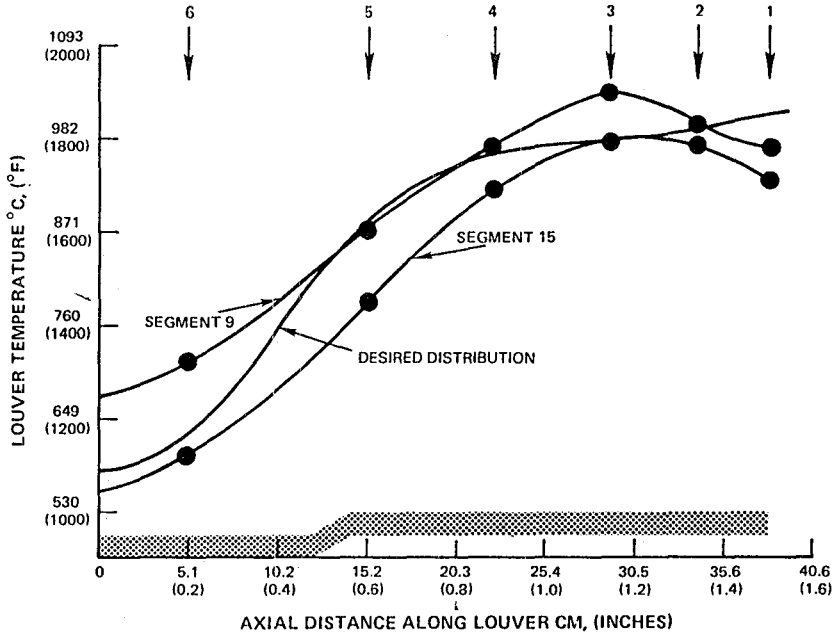

Figure 5-73 Typical Temperature Profiles Achieved in the Hastelloy X Riveted Louver Specimen (Arrows indicate thermocouple locations).

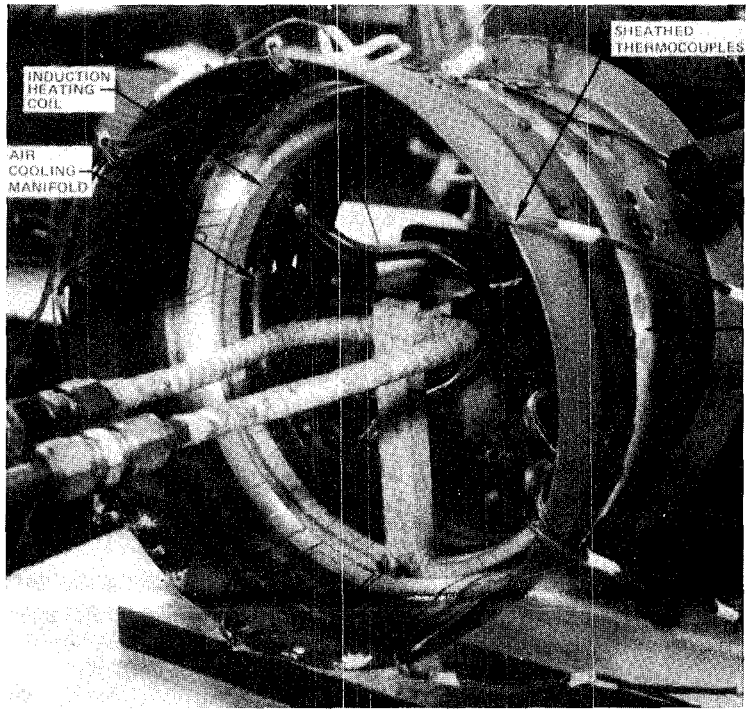

Figure 5-74 Test Setup for Induction Heating of the Hastelloy X, Riveted Louver Specimen

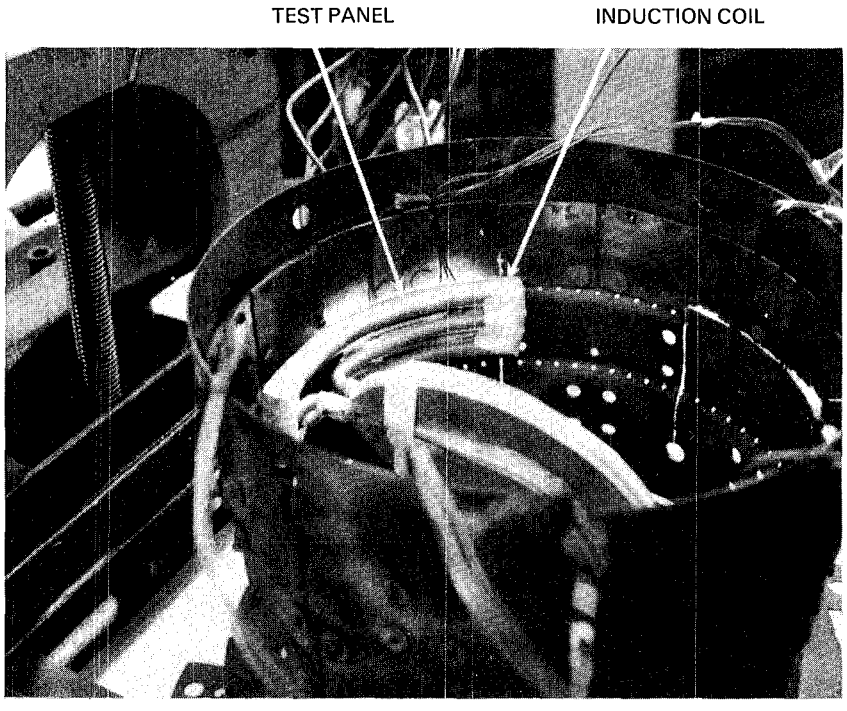

A) TEST SETUP

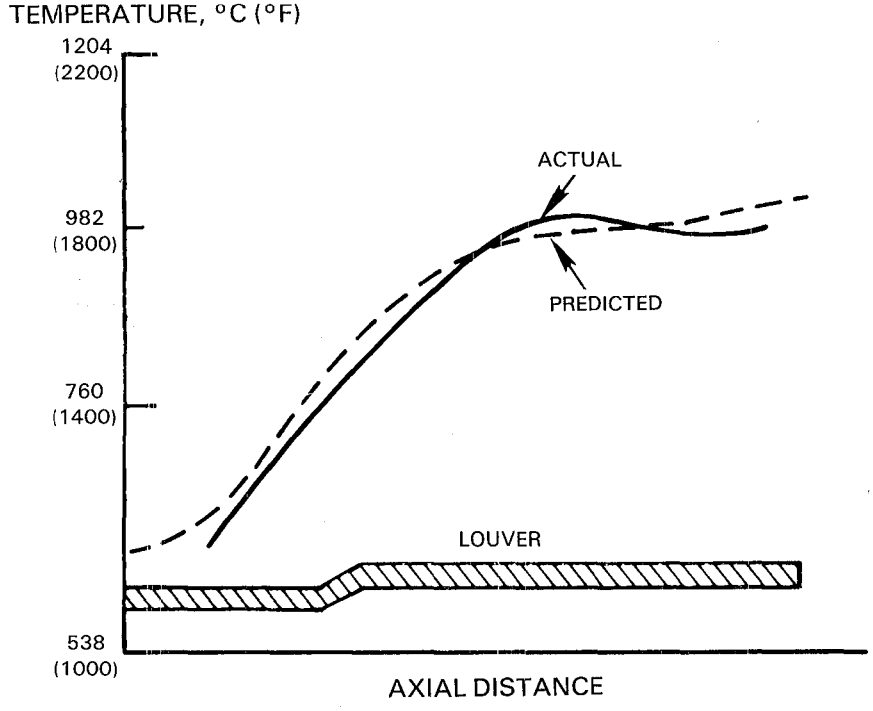

B) TEMPERATURE DISTRIBUTION

Figure 5-75 Test Configuration and Temperature Distribution Achieved with Induction Heating of a Single Segment

5.3.4 Radiant Gas Burner Test Development

The approach which was used to successfully thermal cycle the eight segment louvered sub-component configuration involved alternate gas burner heating an forced air cooling applied to the center ring of the test article shown in Figure 5-72. Photographs of this article installed on the test apparatus are shown in Figures 5-76 and 5-77. The burner assembly contains six individual heaters which rotate about the axis of the cylinderical subcomponent to provide circumferentially uniform heating of the louver lips. Achievement of the axial thermal gradient shown in Figure 5-78 involved careful axial positioning of the burner assembly to heat the segment lip more than the joggle area. While the actual temperatures achieved were not quite as high as desired, this test was judged an adequate simulation of the projected combustor segment operating environment. The use of this test method for comparative testing of Hastelloy X and MA 956 segments is described in Sectio 7.

5.3.5 Transpiration Cooled Specimen Configuration and Fabrication

The objective of this effort was to develop a test method to evaluate the thermal fatigue capability of the transpiration cooled design concept identified in Task I. Initial work involved simulation of the hooked attachment design shown in Figure 3-18, using the specimen design concept illustrated in Figure 5-63. Subsequent effort was directed toward development of a thermal fatigue test for the prestressed design concept shown in Figure 3-21 after it was determined in Task I that attachment strains in the hooked configuration exceeded the fatigue capabilities of oxide dispersion strengthened alloys. The test article developed to simulate the prestressed design consists of a single transpiration cooled panel and frame assembly as illustrated in Figure 5-64.

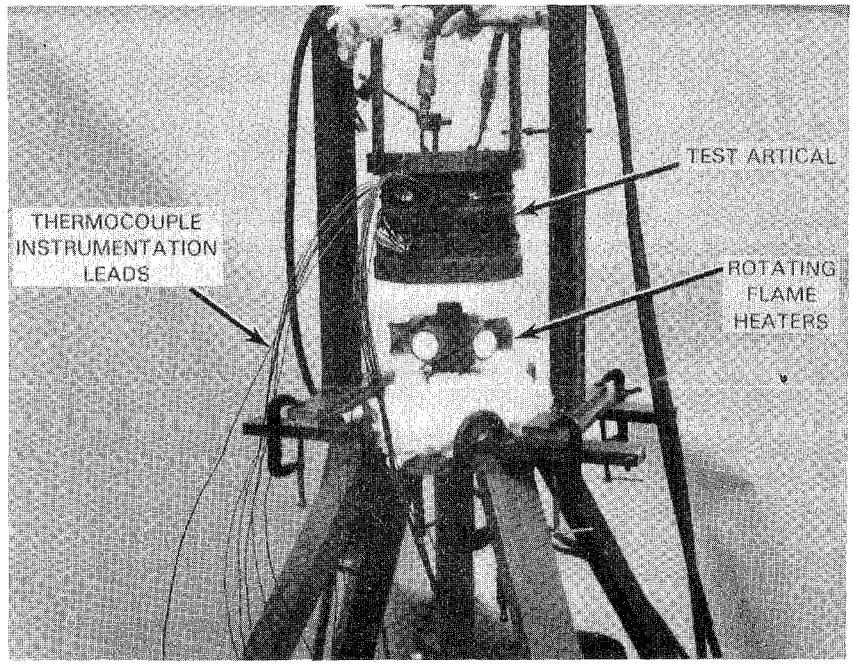

a) COOLING POSITION

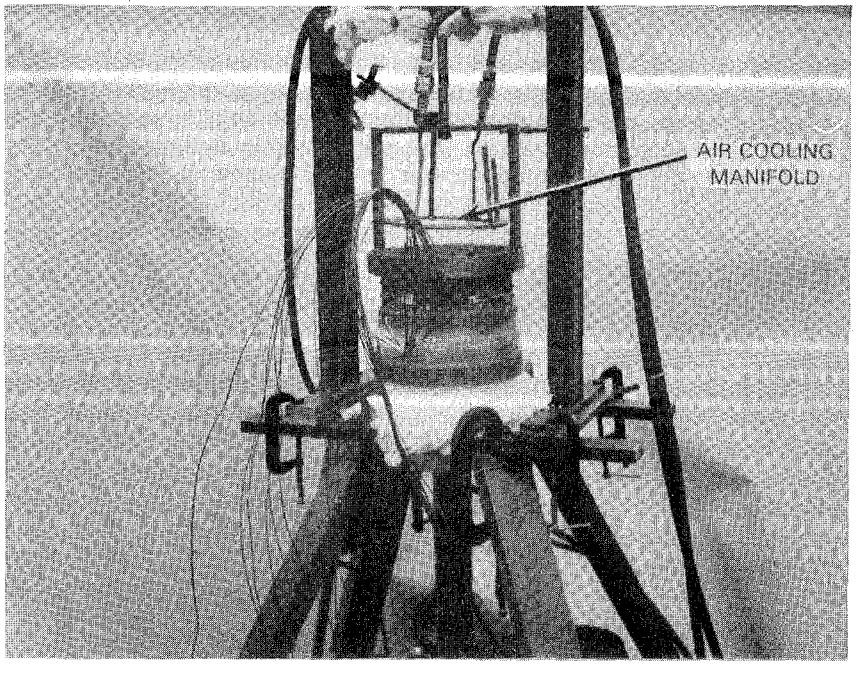

b) HEATING POSITION

Figure 5-76 Louver Thermal Cycle Subcomponent Test Article Installed in Test Apparatus

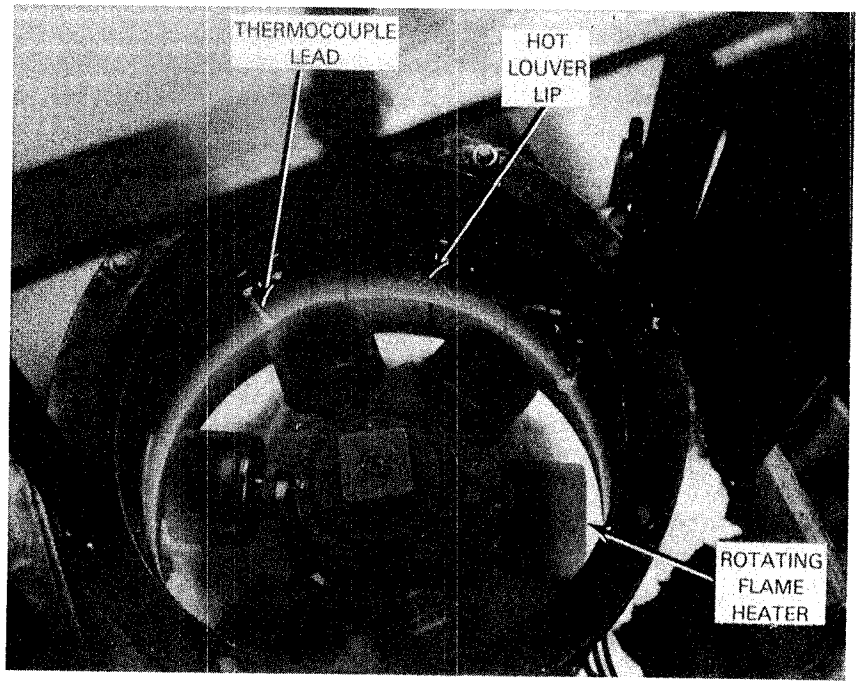

Figure 5-77 Riveted Louver Thermal Cycle Subcomponent Test Article Under Test. (Note that burner rotation has been stopped temporarily to clearly show the burner assembly).

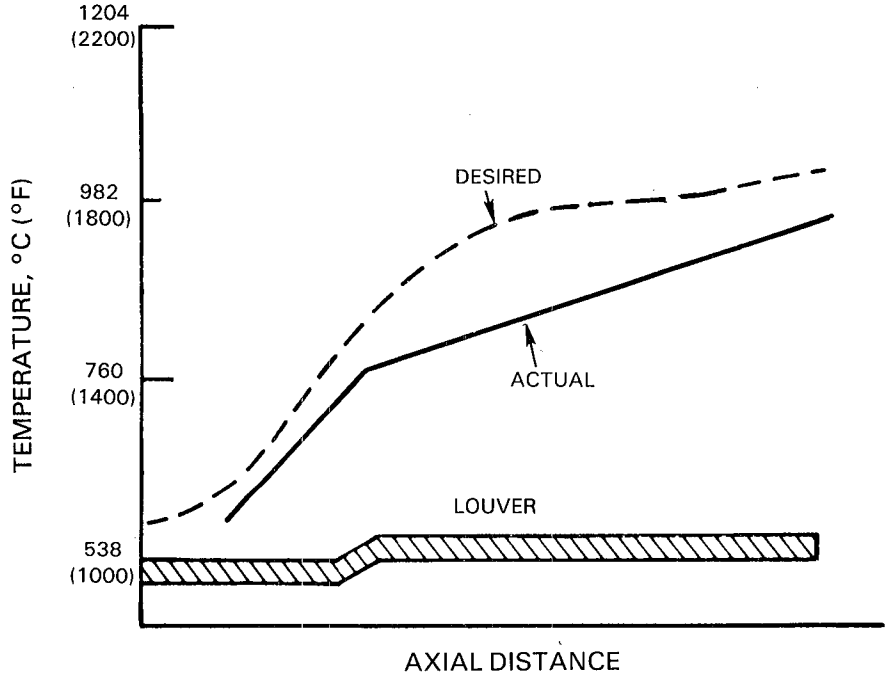

Figure 5-78 Segment Thermal Gradient Produced by Radiant Gas Burner Test Apparatus Shown in Figures 5-76 and 5-77

Both of the thermal fatigue test components illustrated in Figures 5-63 and 5-64 are full size replicas of segments anticipated for use in a full scale combustor. The attachment concepts incorporated in each specimen also replicate the approach envisioned for full scale application. In the case of the hooked panel, the attachment consists of a relatively simple mechanical interlock between the hook and frame. Difficulty anticipated in sealing this attachment was one of the concerns which led to its elimination in the detailed Task I analysis. The attachment scheme used for the prestressed twin wall specimen also is relatively straight forward, as illustrated in Figure 5-79. Eight countersunk, threaded, air cooled studs clamp the square transpiration cooled panel against a post and frame having geometries which force the panel to the indicated spherical radius. This radius is calculated to be the thermally distorted shape which the panel naturally will assume at maximum combustor operating conditions. Photographs of the prestressed specimen before and after assembly are shown in Figure 5-80.

Cooling air is supplied to the prestressed test panel through 441 metering holes, 0.762 mm (0.030 inch) in diameter, EDM drilled perpendicular to the Hastelloy X support frame base in a square array with 4.65 mm (0.183 inch) spacing. The test panel contains 1,326 holes, 0.508 mm (0.020 inch) in diameter, in a 2.72 mm (0.107 inch) square array oriented at 45 to the panel sides. The cooling hole axis is oriented 30° from the plane of the sheet and lies in a plane defined by a sheet edge and the sheet normal.

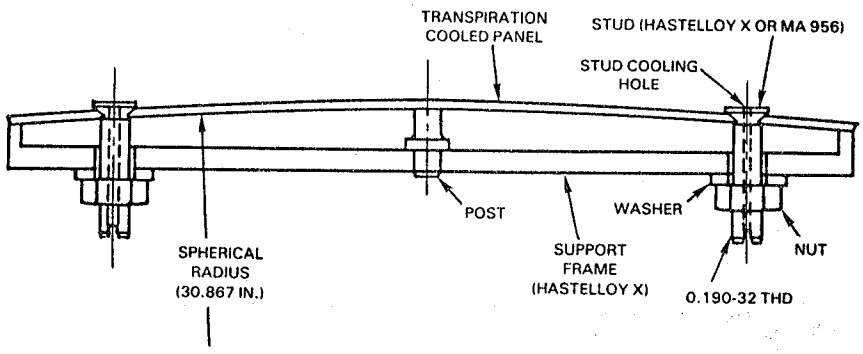

Figure 5-79 Attachment Geometry for Pre-Stressed Transpiration Cooled Twin Wall Specimen. (Note transpiration cooling holes omitted for clarity)

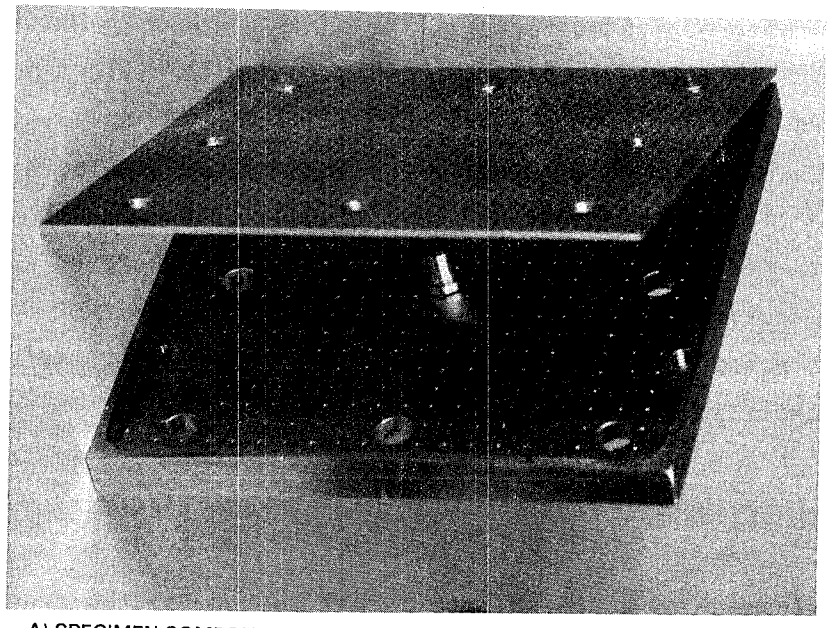

A) SPECIMEN COMPONENTS (NOTE STUDS INSERTED IN REAR THREE HOLES)

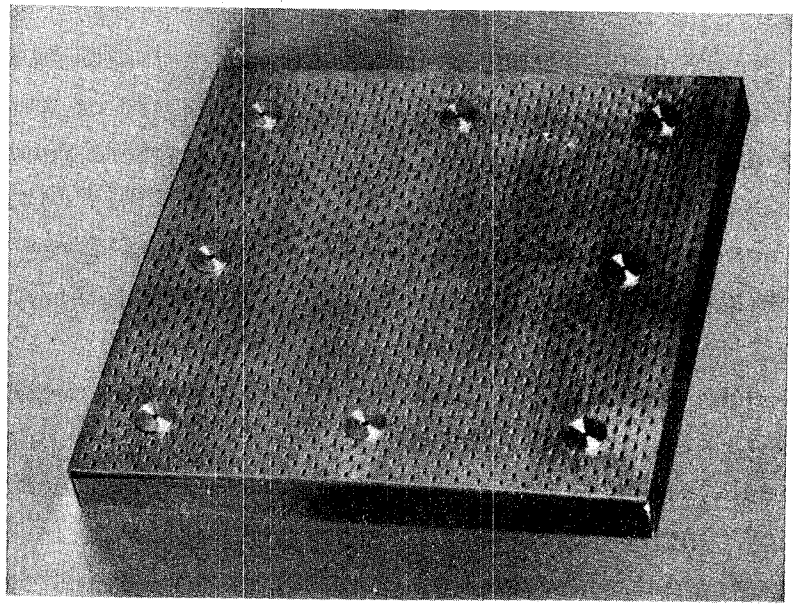

B) ASSEMBLED TEST SPECIMEN

Figure 5-80 Pre-Stressed Transpiration Cooled Twin Wall Thermal Fatigue Test Specimen

Three methods were evaluated for drilling cooling holes in MA 956 alloy. They were laser, EDM (Electro-Discharge Machining), and ECM (Electrochemical Machining). As shown in Figure 5-81, both laser and EDM holes contain recast and cracking, while ECM holes are free of both of these defects. Because of the significantly reduced process time and cost, laser drilling was selected for initial thermal fatigue test trials, despite the observed cracking. As described in Section 7, thermal fatigue cracking was observed to initiate from laser drilled holes during thermal cycle testing and ECM therefore was used for most of the Task V tests.

5.3.6 Preliminary Hooked Transpiration Cooled Panel Testing

Prior to development of a thermal cycle test method for the prestressed twin-wall specimen, preliminary thermal tests were conducted with the hooked panel specimen illustrated in Figure 5-63. These preliminary tests were conducted on a single panel rather than the three panel assembly. Initial induction heating trials indicated that this method would be unable to produce the temperature distribution and through thickness gradient required to properly simulate service in this design. Subsequent trials conducted with radiant gas burner heating led to development of the configuration shown in Figure 5-82A. This set-up involves the use of oscillating vertical burners directed at the flat portion of the panel and horizontally oriented burners directed at the hook regions. The temperature distribution measured with this set-up is shown in Figure 5-82B. Thermal stress analysis performed with this distribution predicts a 0.32 percent maximum strain in the hook area. The application of 501 thermal cycles of 48 seconds duration to an HDA 8077 hooked panel led to development of several fluorescent penetrant indications in the hook region. This observation is consistent with the conclusion made in Task I that thermal strains on the hook region exceed the thermal fatigue capability of ODS alloys.

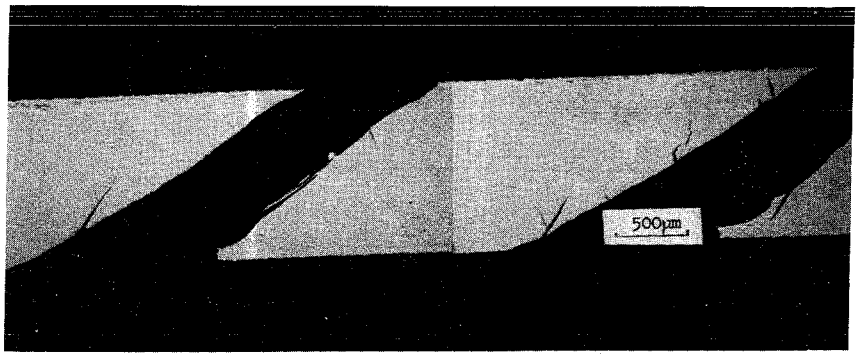

A) LASER DRILLED

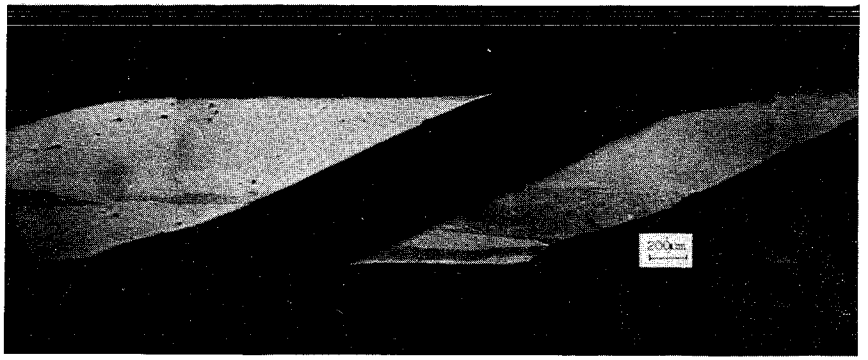

B) ECM DRILLED

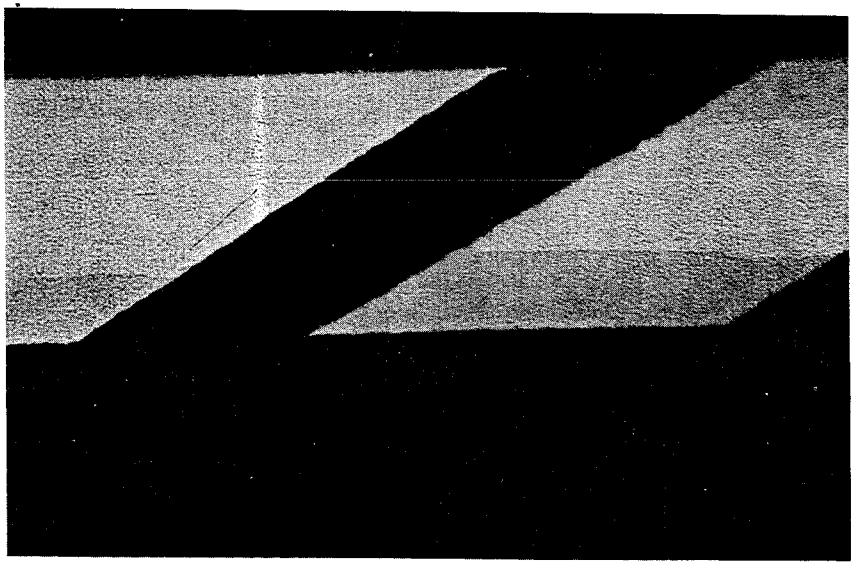

C) EDM DRILLED 30X

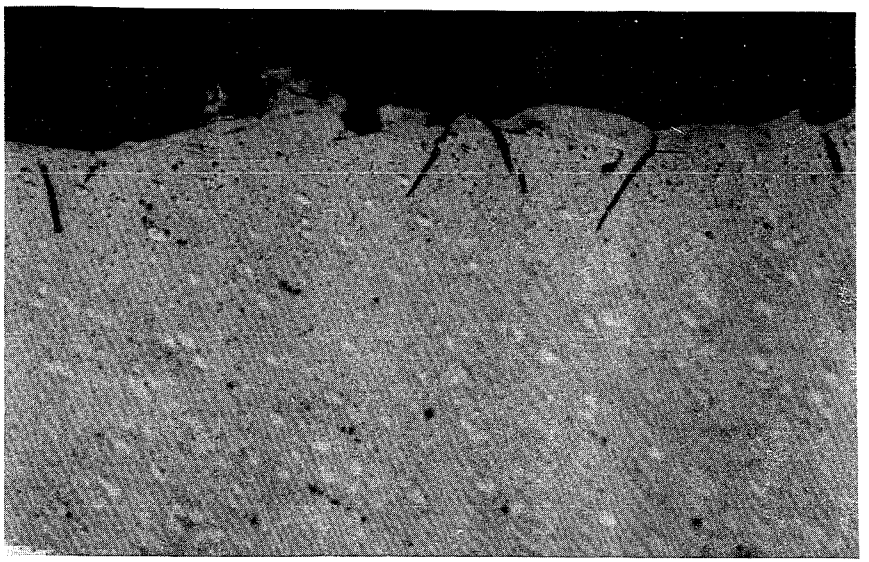

D) CRACKS IN EDM HOLE BARREL 500X

Figure 5-81 Transpiration Cooling Holes in MA 956 Twin Wall Panel

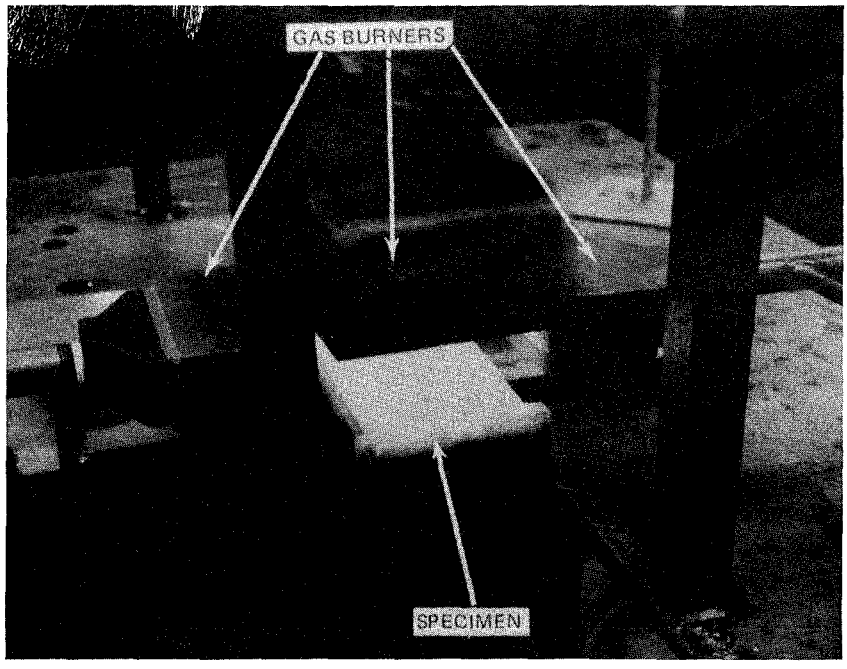

A) TEST SET-UP

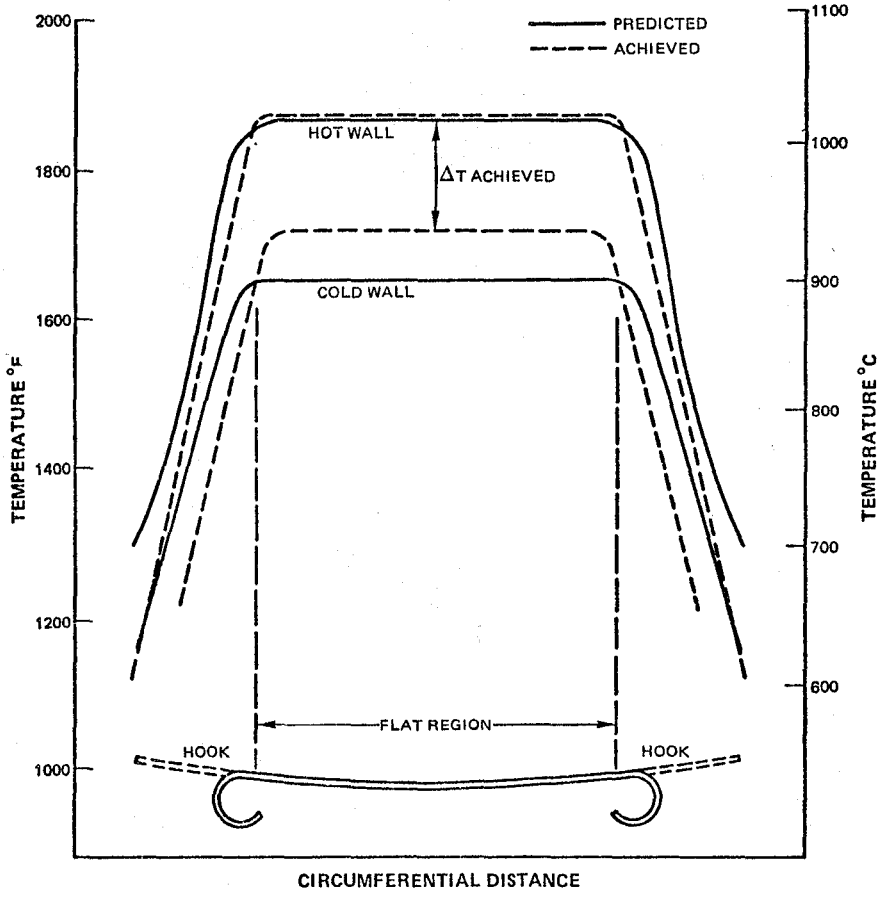

B) TEMPERATURE DISTRIBUTION MEASURED IN HOOKED PANEL

Figure 5-82 Test Rig for Hooked Transpiration Cooled Twin Wall Panel

5.3.7 Pre-Stressed Transpiration Cooled Panel Evaluation

Structural analysis of an MA 956 prestressed twin wall panel indicated that in the as-prestressed condition at room temperature, high tensile strain would occur at the center and the edge centers of the panel and that high compressive strains would occur at the corners. This initial strain distribution was verified by prestressing a solid panel (no transpiration holes) with a surface application of Stresscoat^{R} lacquer and with strain gage measurements on the outer surface. Figure 5-83A shows the cracked coated panel (0.08% strain to cracking of the lacquer) in the prestressed position indicating the high tensile strain areas in the center over the positioning post and in the edge centers. After unloading of the panel, the Stresscoat^{R} cracked in the corners indicating high compressive strain in those regions. The results of strain gage measurements in the prestressed condition (Figure 5-83B) are in excellent agreement with both the structural analysis and the visual appearance of the Stresscoat^{R}. Structural analysis shows that, during heat-up, stress redistribution occurs throughout the panel and the maximum strain (critical location) is located at the center of each edge. In the prestressed condition and during heat-up all stresses are in the elastic field so that no plastic damage occurs.

Building on the experience gained with the hooked panel, development of a thermal cycle test heat method for evaluation of the prestressed twin wall specimen illustrated in Figure 5-64 involved the use of a radiant gas burner for heating the test panel (Figure 5-84). A laser drilled MA 956 panel was used for the initial set-up of this test, which involved adjustments to the relative position of gas burner and to the volume of cooling air. The distribution of hot and cold side temperatures achieved on this panel with the best combination of test parameters which could be identified is shown in Figure 5-85. While this distribution is not entirely uniform and does not quite meet the desired through thickness gradient of 100°C (180°F), it was judged adequate for thermal cycle evaluation of transpiration cooled panels in Task V. Results of this evaluation, described in Section 7, suggested that the actual through thickness gradient in this test specimen was lower than indicated by these initial measurements.

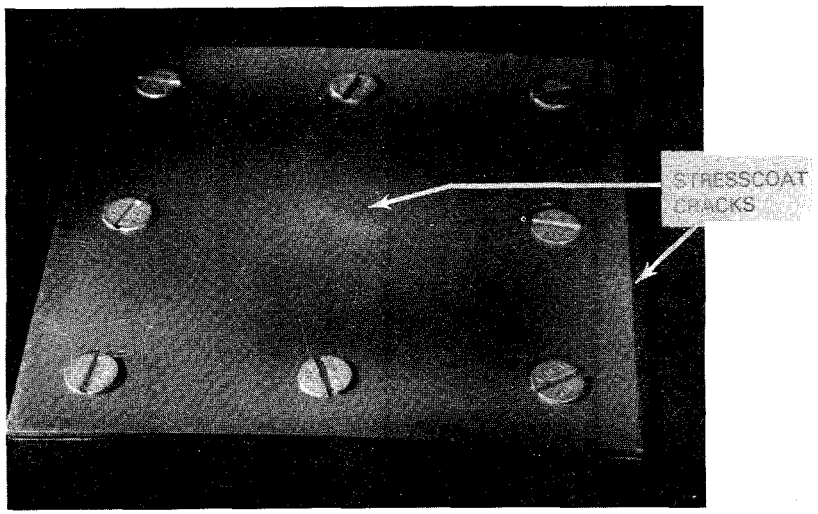

A) STRESSCOAT® LACQUER COATED
NOTE: CORNERS CRACK DURING UNLOADING

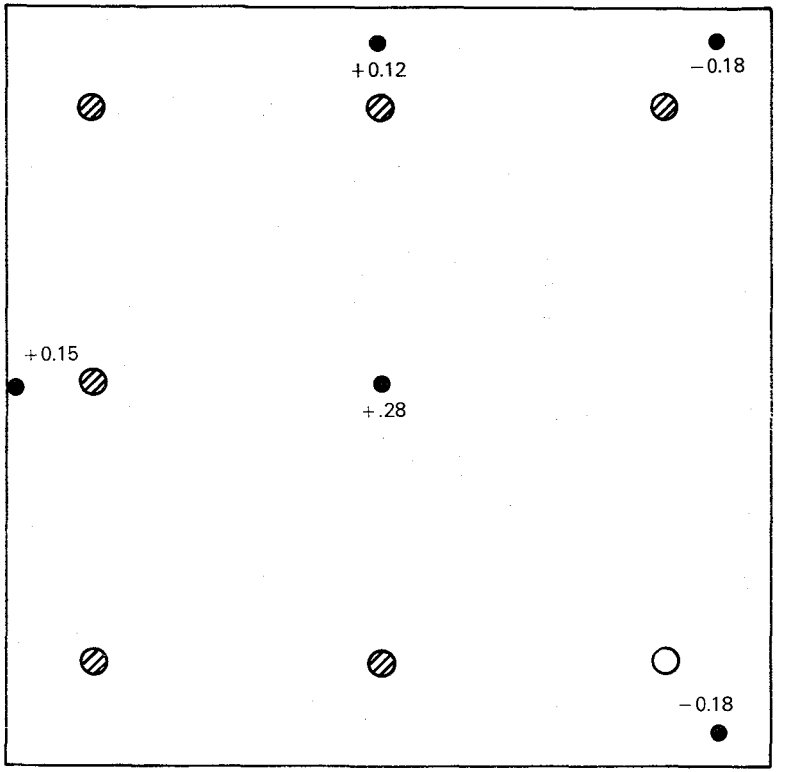

STRAIN GAGED PANEL

B) AVERAGE STRAIN (%) FOR THREE
MECHANICAL LOADING TRIALS

Figure 5-83 Twin Wall Test Panel in Prestressed Condition Showing Tensile Strains in Center and Edge Centers and Compressive Strain in Corners

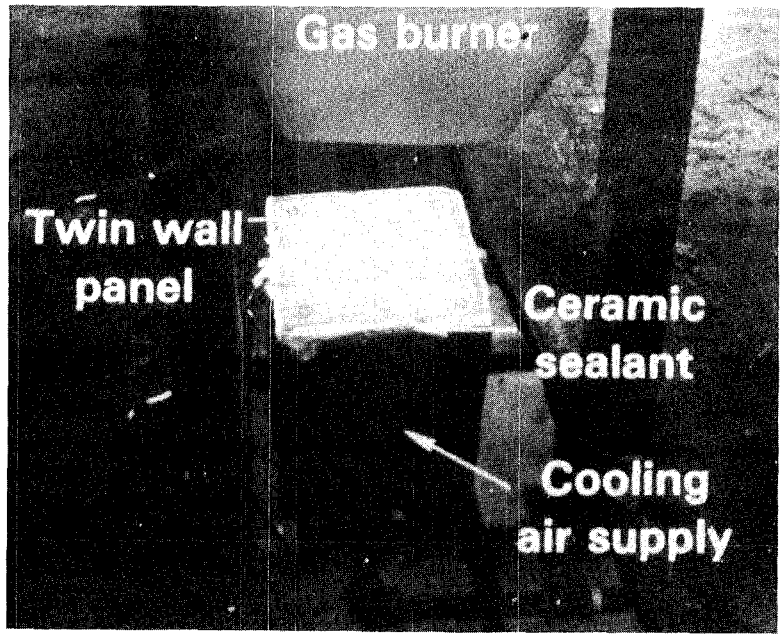

Figure 5-84 Prestressed Transpiration Cooled Twin Wall Specimen Installed in Test Apparatus. Thermal cycling is accomplished by moving the specimen toward and away from the burner.

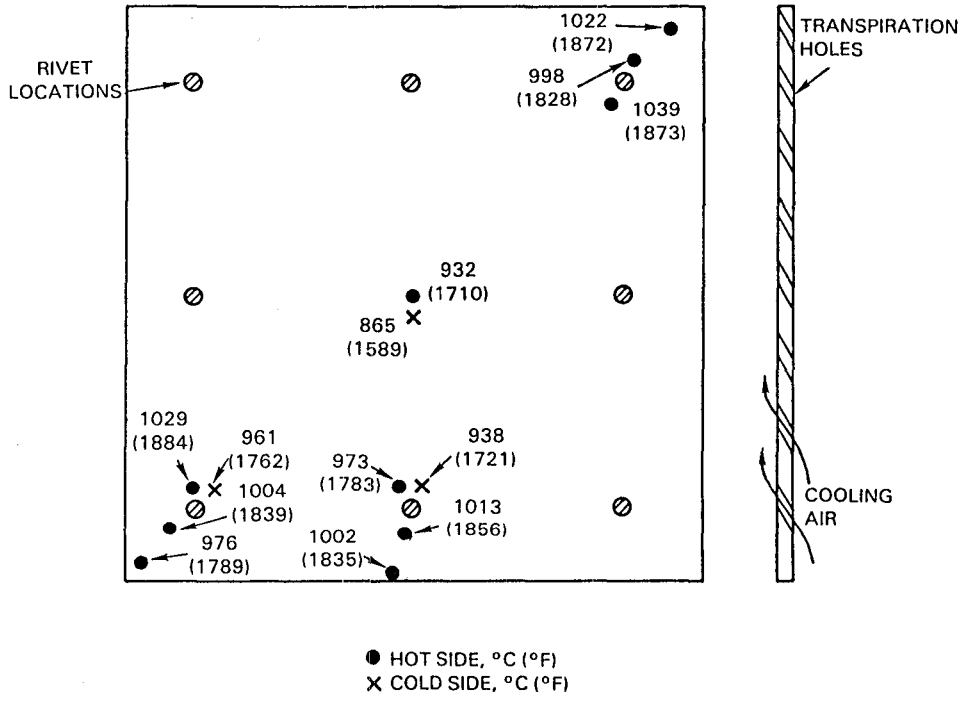

Figure 5-85 Optimized Temperature Distribution Measured on Laser Drilled MA 956 Prestressed Transpiration Cooled Twin Wall Panel

6.0 TASK IV - DETAILED MATERIAL EVALUATION

6.1 INTRODUCTION AND SUMMARY

The objective of this task was to perform additional property measurements on the material selected for engine demonstration of ODS combustor components. Because of the manufacturer's inability to reproducably fabricate HDA 8077 sheet (discussed Section 4), MA 956 was selected for this demonstration.

The material tested was MA956 lot XBB-004. Chemistry, microstructure, and results of "acceptance tests" conducted in this lot are reported in Section 4. These results indicate this material to have acceptable chemistry, microstructure, tensile, and creep resistance and to exhibit good formability with no trace of the surface hardened layer found on lot ZDEW.

Properties evaluated in this task include elevated temperature tensile and creep, isothermal low cycle fatigue life and crack propogation rate, thermal fatigue (hot spot blister), cyclic oxidation, and alloy stability.

Results of tests conducted on this task confirmed the good properties of XBB-004 and provided data for use in design of the combustor test article in Task VI.

6.2 TENSILE AND CREEP TESTS

Tensile and creep tests were conducted as described in Section 5.1.3. Tension test results are reported in Table 6-I; longitudinal results are plotted as a function of temperature in Figure 6-1. These results are approximately comparable to those reported for lot ZDEW in Section 5-1 (Table 5-II), except for somewhat less evidence of anisotropy in elevated temperature ductility. It is not known whether the high ductility value reported at 649°C (1200°F) is real or represents experimental error. Failed specimens from all test temperatures and both orientations revealed a transgranular failure mode with substantial localized deformation for all conditions except the 1093°C (2000°F) transverse test which displayed a combination of inter- and transgranular failure mode with secondary cracks adjacent to the fracture (Figure 6-2).

TABLE 6 - I

TENSILE PROPERTIES OF INCOLOY MA 956 LOT XBB-004

Temperature °C (°F)	Orientation[1]	0.2% YS Mn/M^2 (ksi)	UTS Mn/M^2 (ksi)	Elongation %
24 (75)	L	537.1 (77.9)	665.4 (96.5)	14.5
24 (75)	L	529.5 (76.8)	637.8 (92.5)	13.9
427 (800)	L	426.8 (61.9)	524.0 (76.0)	9.6
427 (800)	L	411.6 (59.7)	518.5 (75.2)	11.2
649 (1200)	L	204.8 (29.7)	226.8 (32.9)	26.7
871 (1600)	L	114.5 (16.6)	126.9 (18.4)	9.6
871 (1600)	L	113.8 (16.5)	127.6 (18.5)	10.6
871 (1600)	T	111.7 (16.2)	124.1 (18.0)	10.3
871 (1600)	T	120.0 (17.4)	126.9 (18.4)	12.6
982 (1800)	L	102.7 (14.9)	108.3 (15.7)	8.5
982 (1800)	L	103.4 (15.0)	109.6 (15.9)	6.6
1093 (2000)	L	90.3 (13.1)	94.5 (13.7)	5.0
1093 (2000)	L	82.1 (11.9)	95.2 (13.8)	4.0
1093 (2000)	T	86.9 (12.6)	89.6 (13.0)	2.8
1093 (2000)	T	88.3 (12.8)	92.4 (13.4)	5.4

1 L - Stress axis parallel to rolling direction
T - Stress axis transverse to rolling direction
Crosshead Rate = 0.005 min^{-1}

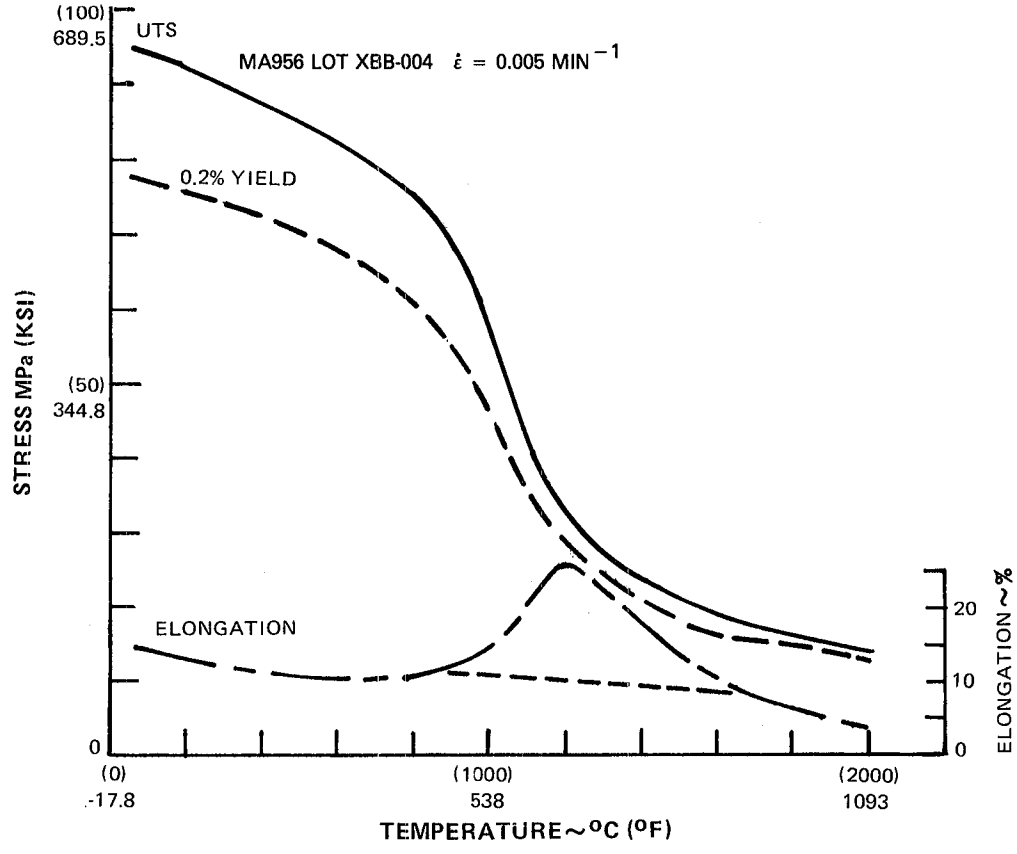

Figure 6-1 Longitudinal Tensile Properties of Incoloy MA 956 Lot XBB-004

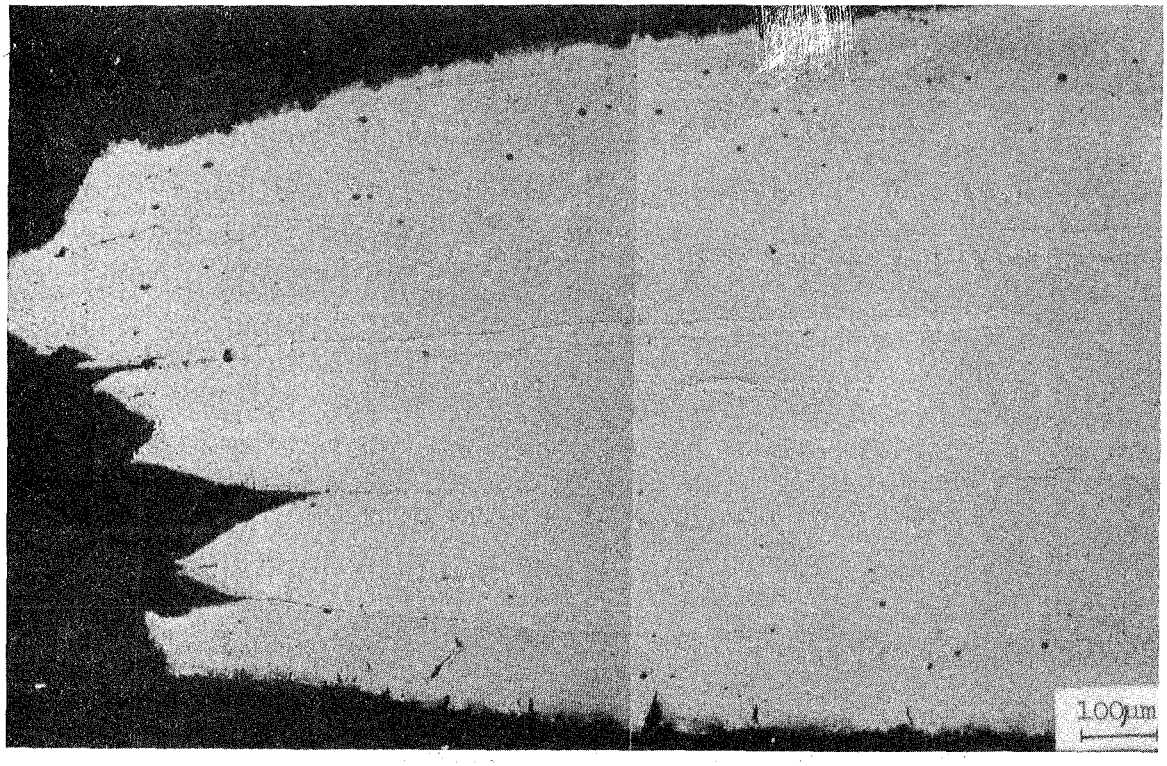

LONGITUDINAL

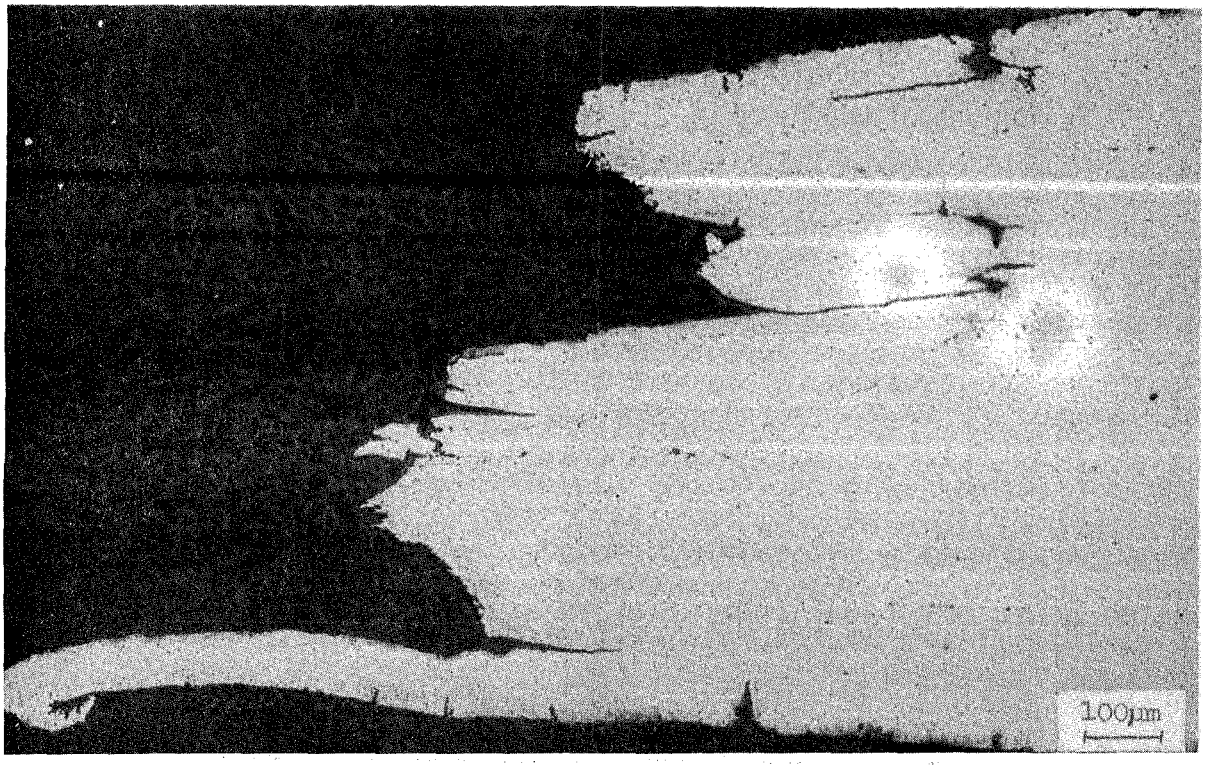

TRANSVERSE

Figure 6-2 Tensile Fracture Microstructures of Incoloy MA 956 Lot XBB-004 tested at 1093C (2000F) and Strain Rate of 0.005 min^{-1}

Creep rupture test results are reported in Table 6-II; a Larson-Miller plot of the longitudinal data is presented in Figure 6-3. Except for one somewhat low data point at 82.7 MN/m^2 (12KSI), these results are similar to those measured on lot ZDEW in Task III (Table 5-IV). The transverse test results on Heat XBB-004 are considerably lower in life and ductility than the longitudinal data but in good agreement with lot ZDEW transverse test results generated in Task III.

TABLE 6 - II

CREEP RUPTURE PROPERTIES OF MA956 LOT XBB-004

Temperature °C (°F)	Stress Mn/M^2 (ksi)	Orientation	Time to Rupture (hrs)	Prior Creep (%)	RT Elong. (%)
871 (1600)	89.6 (13.0)	Longitudinal	>2371.0*	--	>0.25*
	103.5 (15.0)	Longitudinal	291.3	NA	NM
	103.5 (15.0)	Longitudinal	117.1	--	NM
982 (1800)	82.7 (12.0)	Longitudinal	200.6	0.21	4.9
	82.7 (12.0)	Longitudinal	28.7	--	3.2
	82.7 (12.0)	Transverse	7.2	0.10	NM
	82.7 (12.0)	Transverse	4.1	--	2.9
	75.9 (11.0)	Longitudinal	1608.1	0.75	3.4
1093 (2000)	72.5 (10.5)	Longitudinal	96.4	0.33	5.2
	72.5 (10.5)	Longitudinal	1.5	--	2.5
	72.5 (10.5)	Transverse	0.7	--	2.9
	72.5 (10.5)	Transverse	0.5	--	4.0
	62.1 (9.0)	Longitudinal	1271.0	0.26	NM

* Test Discontinued, No Failure

NM Not Measured
NA Not Available

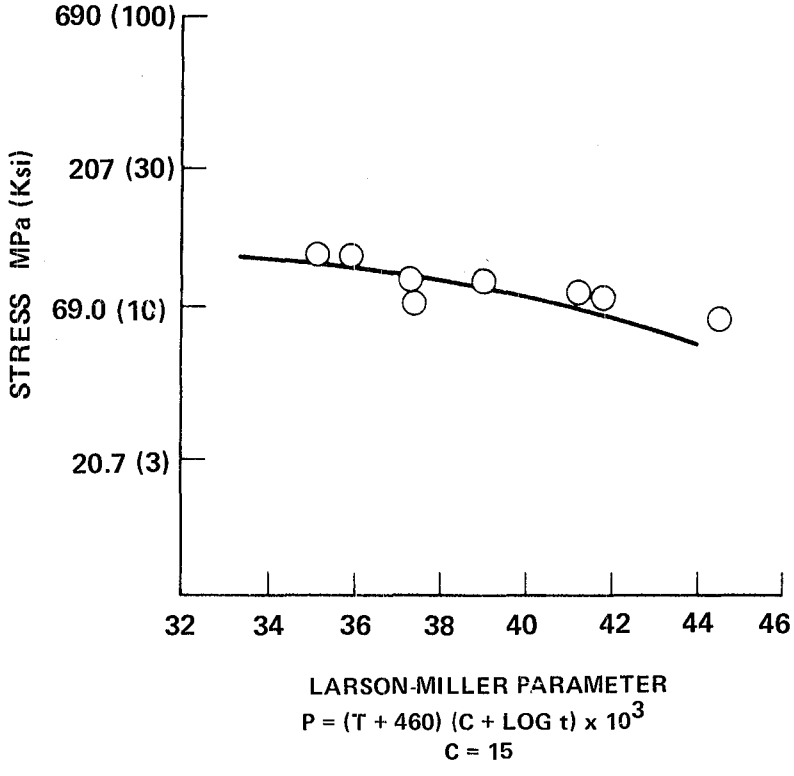

Figure 6-3 Longitudinal Creep-Rupture Life of MA 956 Lot XBB-004

Photomicrographs presented in Figures 6-4 and 6-5 shown respective longitudinal and transverse creep fracture morphologies similar to those seen in lot ZDEW (Figures 5-8 and 5-9). Longitudinal fracture occurs predominantly by a transgranular mode, with evidence of void coalescence and/or dimpling at transgranular secondary cracks perpendicular to the stress axis (Figure 6-4B). The transverse fractures show evidence of integranular failure at selected transverse grain boundaries, with flat, transgranular cracking similar to the longitudinal morphology in intervening grains.

6.3 ISOTHERMAL LOW CYCLE FATIGUE

Low Cycle fatigue tests were conducted using the low frequency test method describe in Section 5.1.4. Tests were conducted at three temperatures (760, 871, and 982°C; 1400, 1600, and 1800°F) and two frequencies (0.67 and 0.067 Hz) and with the principal stress axis oriented parallel and transverse to the rolling direction. All tests were conducted with a total strain range of 0.005 mm/mm.

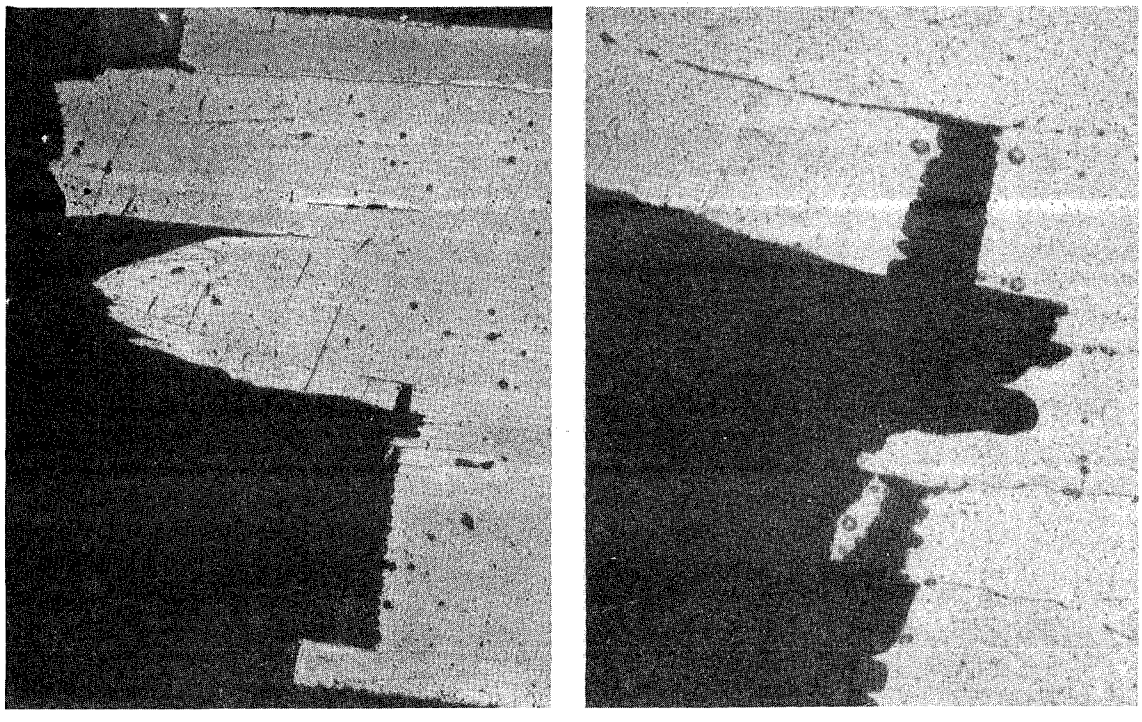

A) 80X B) 500X

Figure 6-4 Fracture Observed in Longitudinal MA 956 Lot XBB-004 Creep Specimen Tested to Failure in 200.6 Hours at 982C (1800F)/82.7 MN/m^2 (12 ksi). Extension immediately prior to failure 0.21%; elongation after failure 4.9%.

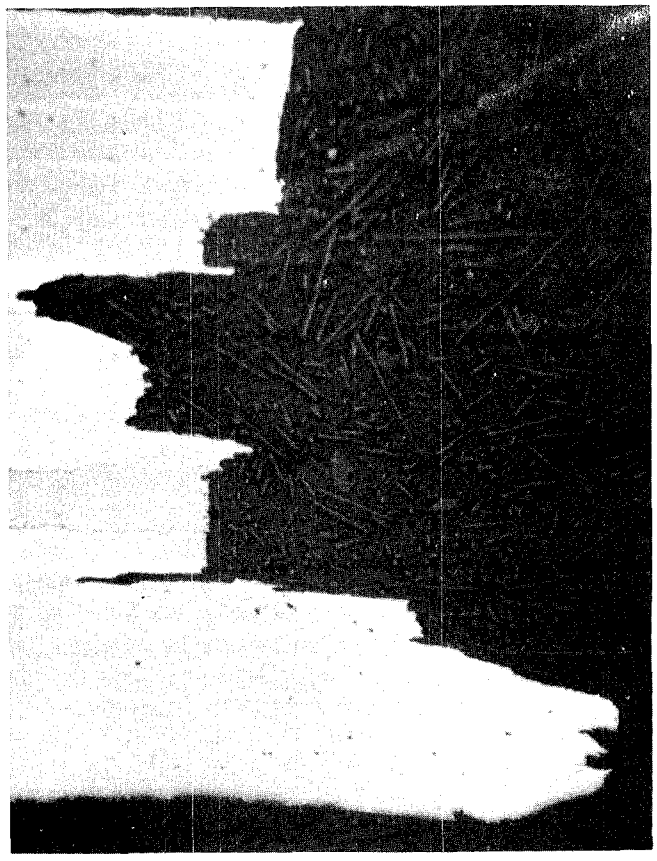

85X

Figure 6-5 Fracture Observed in Longitudinal MA 956 Lot XBB-004 Creep Specimen Tested to Failure in 7.2 Hours at 982C (1800F)/82.7 MN/m^2 (12 ksi). Extension immediately prior to failure 0.10%; elongation after failure not measured.

Results of these tests are presented in Table 6-III. Compared to the lot ZDEW data in Task III (Table 5-V), the lot XBB-004 lives are similar at the lower test temperatures but somewhat lower at 982°C (1800°F).

The influence of temperature, orientation, and test frequency on LCF life are shown in bar chart form in Figures 6-6 and 6-7; representative fracture photomicrographs are presented in Figures 6-8 and 6-9. Comparison of the two orientations (Figure 6-6) indicates similar fatigue lives at 760°C (1400°F) and slightly lower lives for the transverse orientation at 982°C (1800°F). As seen in Figure 6-7, reduction of strain rate by an order of magnitude causes 50 to 65% reduction of fatigue life, with the debit being larger at the higher test temperature. Visual and metallographic examination of failed longitudinal specimens showed less secondary surface cracking and less grain boundary delamination at the lower test frequency (Figure 6-8). Metallography of the

TABLE 6-III

LOW CYCLE FATIGUE PROPERTIES OF INCOLOY MA 956, LOT XBB-004
(Fully Reversed Bending, 0.005 mm/mm Total Strain Range)

Temperature	Specimen Orientation	LIFE, CYCLES ~ = 0.67 hz.	LIFE, CYCLES ~ = 0.067 hz.
760°C (1400°F)	Longitudinal	4581	-
		5785	-
		4880	-
	Transverse	4915	-
		3962	-
		5816	-
871°C (1600°F)	Longitudinal	6360	2783
		4256	2521
		6719	3418
982°C (1800°F)	Longitudinal	3601	1128
		3335	1030
		1967	-
	Transverse	2562	-
		2409	-
		2018	-

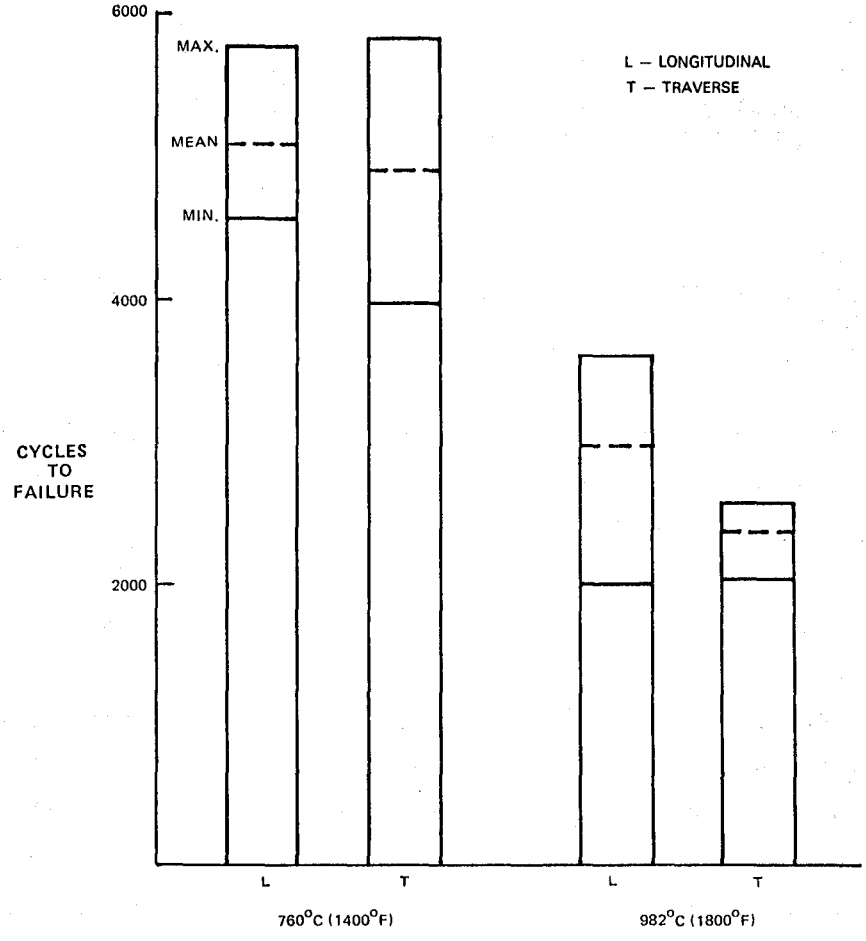

Figure 6-6 Influence of Temperature and Specimen Orientation on the Low Cycle Fatigue Life of MA 956 Lot XBB-004 Sheet; Total Strain Range 0.005 mm/mm.

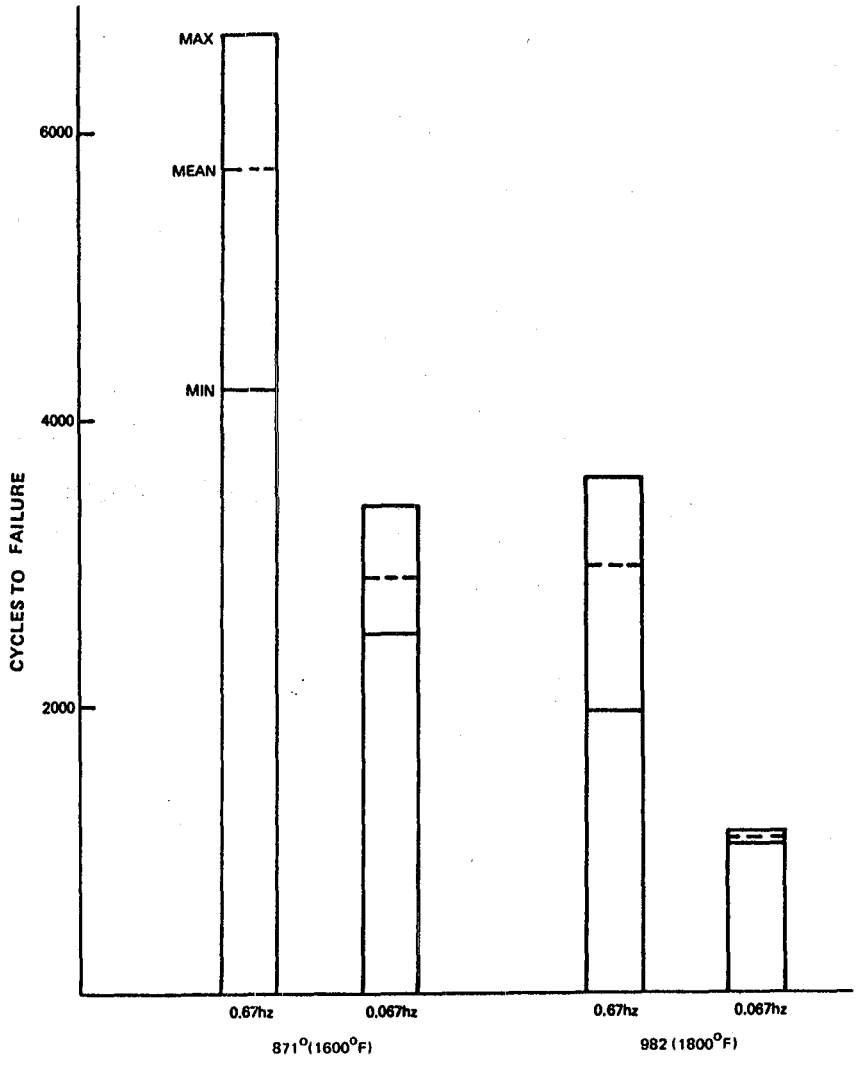

Figure 6-7 Influence of Temperature and Frequency on the Low Cycle Fatigue Life of MA 956 Lot XBB-004 Sheet. Longitudinal orientation, total strain range 0.005 mm/mm.

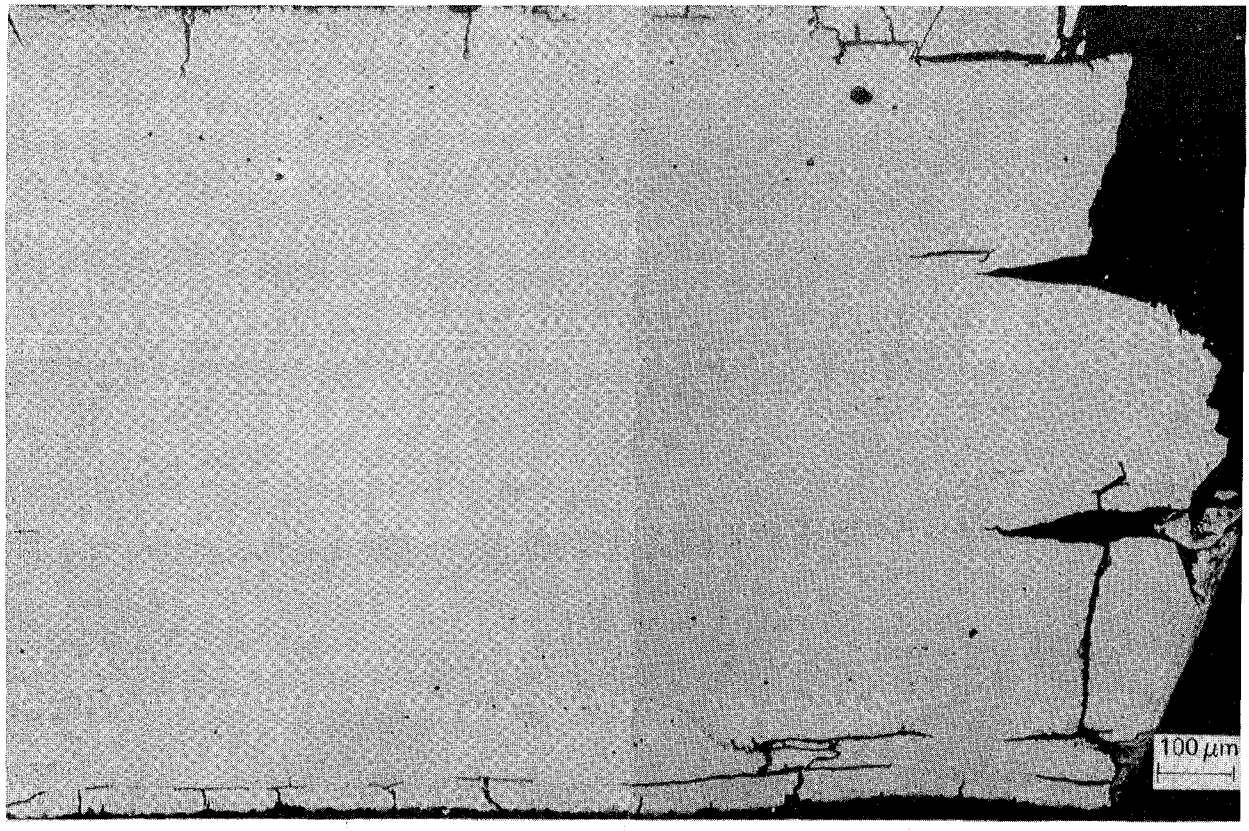

0.67 HZ 3335 CYCLES

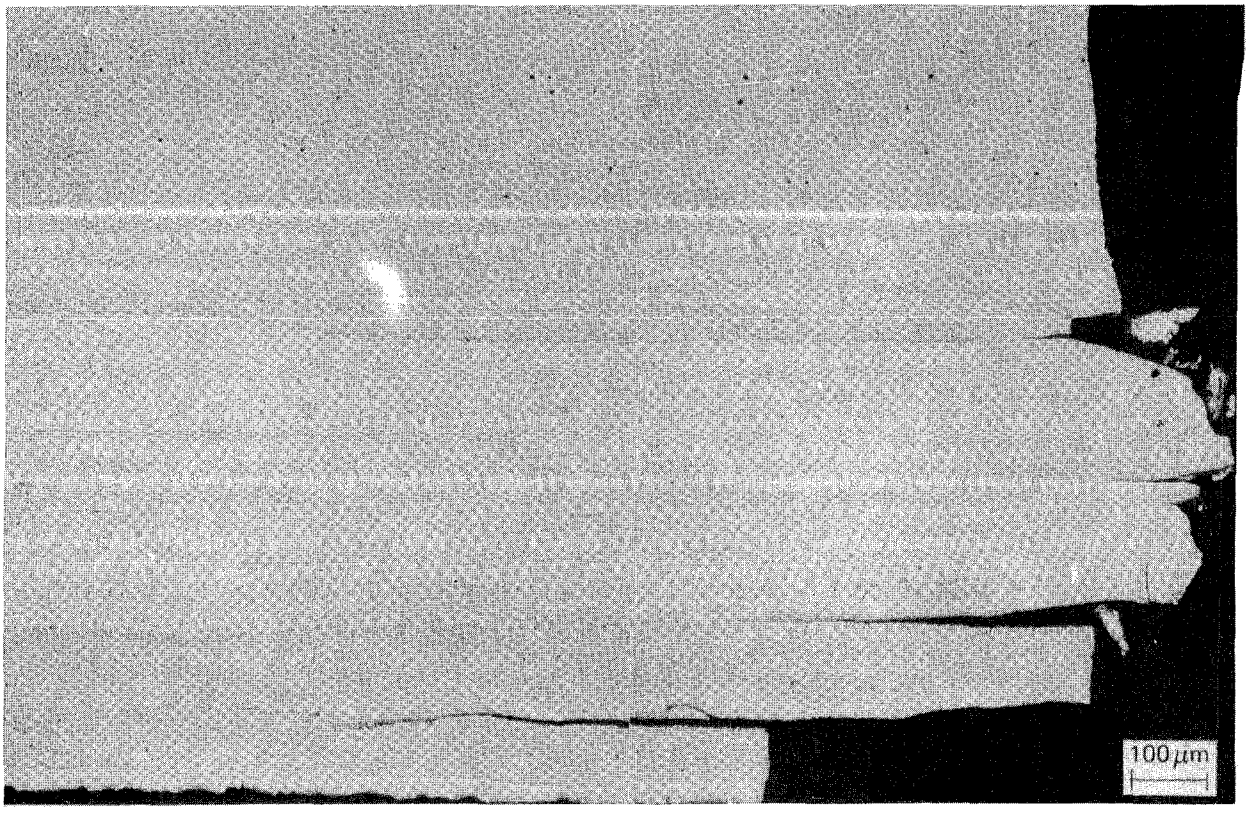

0.067 HZ 1128 CYCLES

Figure 6-8 Photomicrographs of MA 956, Lot XBB-004, Failed Low Cycle Fatigue Specimens Tested at 982C (1800F) with Longitudinal Orientation. Note abundance of surface cracking and grain boundary delamination in 0.67 hz specimen.

failed transverse oriented specimens (Figure 6-9) indicated that crack initiation and growth in the surface grains occurred at 90° to the specimen surface at 760°C (1400°F) and at 45° to the surface at 982°C (1800°F). Crack propagation through subsurface grains was perpendicular to the specimen surface. It was noted that substantially less grain boundary delamination occurred in the transversely oriented specimens compared to the longitudinally oriented specimens (Compare Figures 6-8 and 6-9). The nature of cracking (45° versus 90°) and the increased amount of grain boundary delamination may account for the slightly higher failure lives for the longitudinally oriented specimens.

6.4 ISOTHERMAL FATIGUE CRACK PROPAGATION

Fatigue crack propagation rate tests were conducted at 871 and 982°C (1600 and 1800°F) on specimens with the principal stress axis oriented parallel and 45° to the rolling direction. Tests were conducted in uniaxial tensile loading at a frequency of 0.17hz and an R ratio of zero (cycled from zero to maximum tensile stress) on the center notched specimen illustrated in Figure 6-10. Fatigue cracks at each end of the slot were initiated by high frequency cycling at room temperature prior to the initiation of elevated temperature crack propagation rate measurements. Crack growth was measured with a traveling telescope; stress intensity ranges were calculated from measured crack length and load range values using standard formula for this specimen geometry.

Crack propagation test results (Table 6-IV and Figure 6-11) indicate exponents (n) above 10 in the crack propagation equation

$$da/dn = A\,(\Delta K)^n$$

for the range of da/dn values above 2.5×10^{-4} mm/cycle (10^{-6} inches/cycle) where engineering values of crack propagation rate commonly are measured. These very high n values made it difficult to select appropriate loads because of the extreme sensitivity of propagation rates to small load changes. Thus, for example, specimen MACP-4 propagated rapidly to failure in 85 cycles at the 55.1 MN/m^2 (8 KSI) stress level which provided substantial

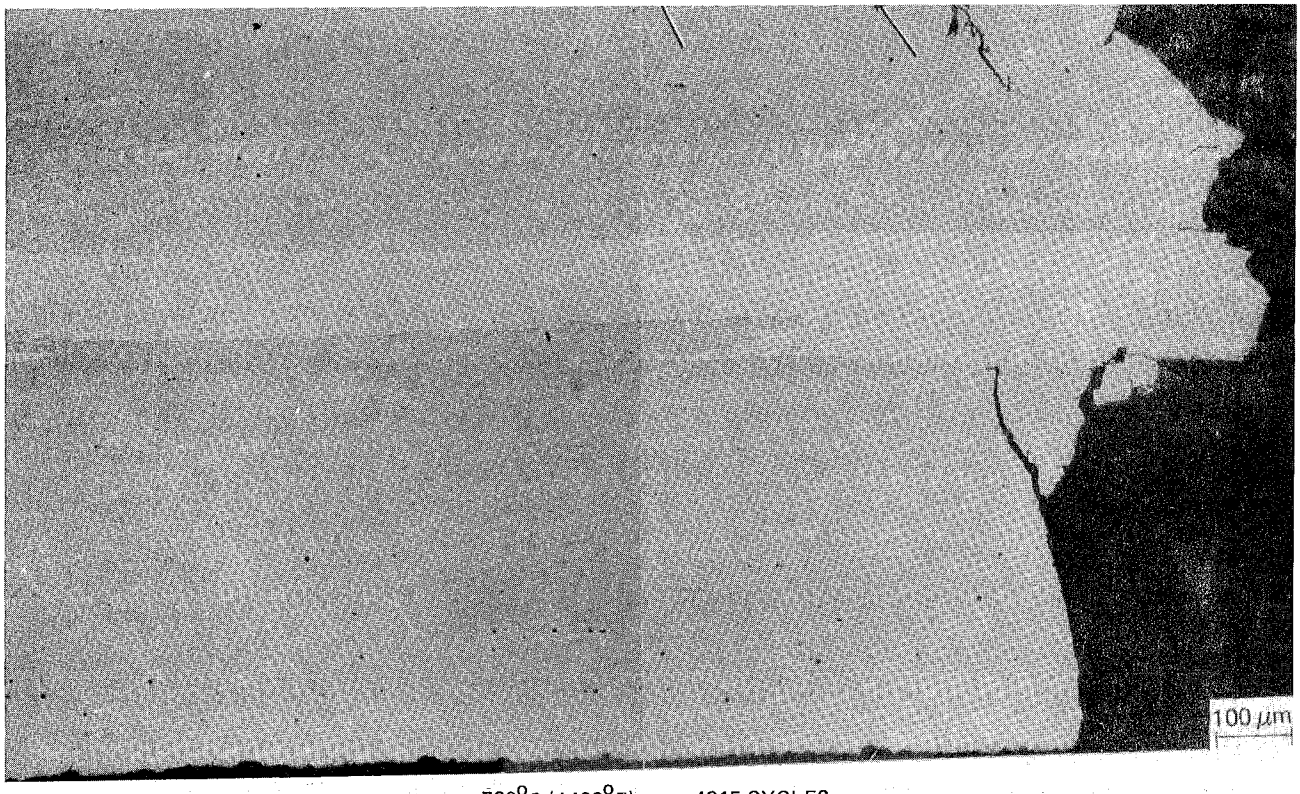

760°C (1400°F) 4915 CYCLES

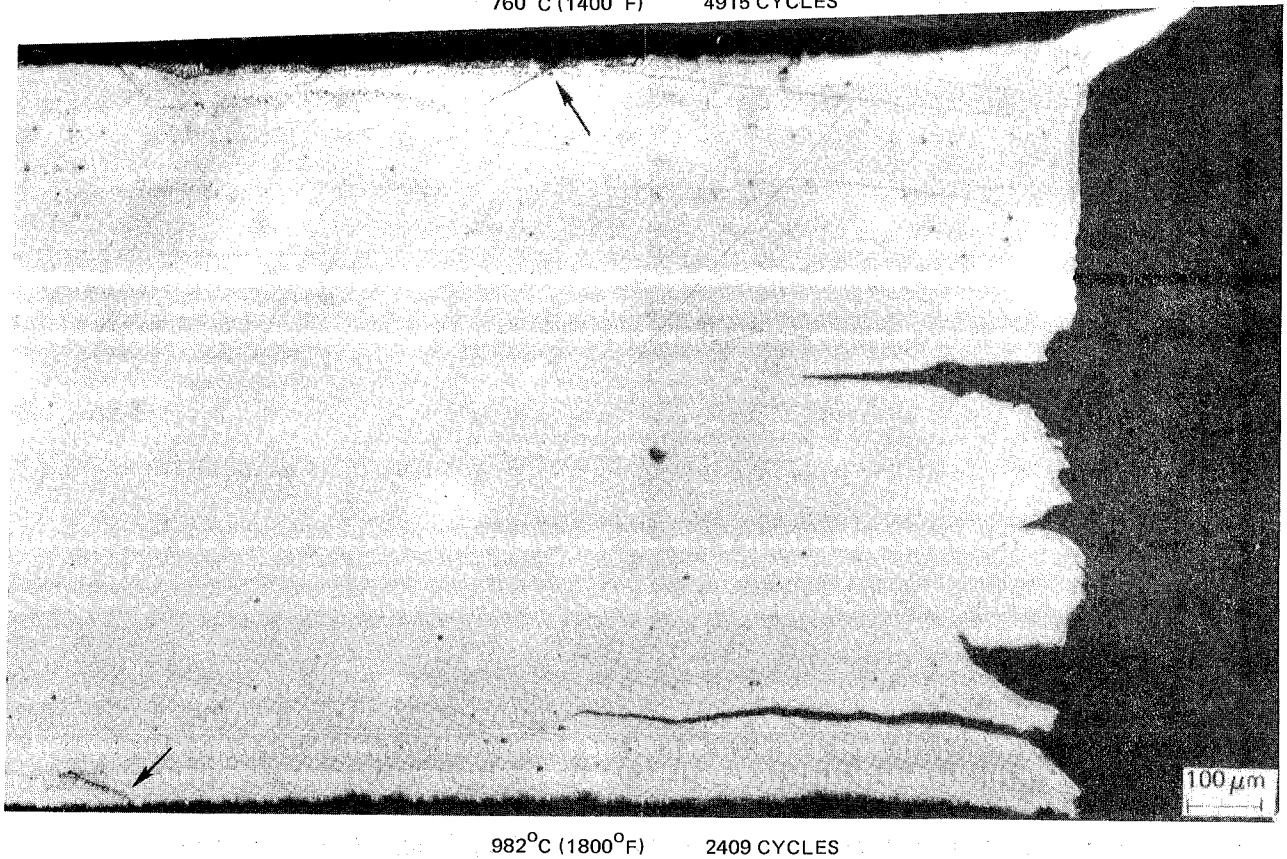

982°C (1800°F) 2409 CYCLES

Figure 6-9 Photomicrographs of MA 956, Lot XBB-004, Failed Transverse Low Cycle Fatigue Specimens Tested at 0.67 hz. Note perpendicular surface cracking at 760C (1400F) and 45° surface cracking at 982C (1800F) (arrows).

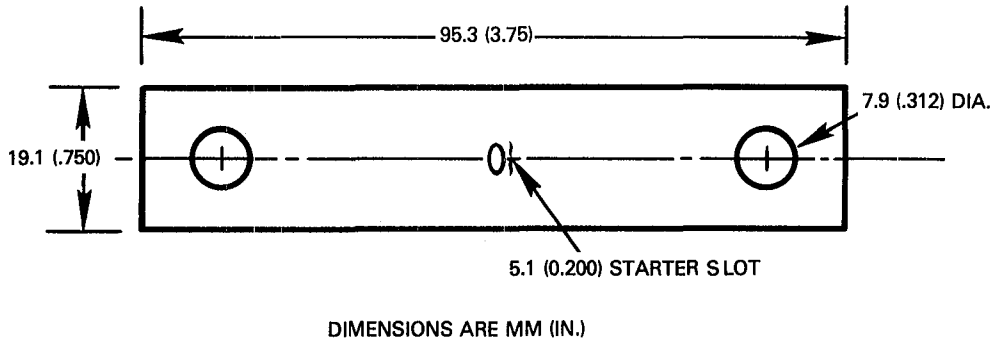

Figure 6-10 Center Notched Specimen Used to Measure Fatigue Crack Propagation Rate

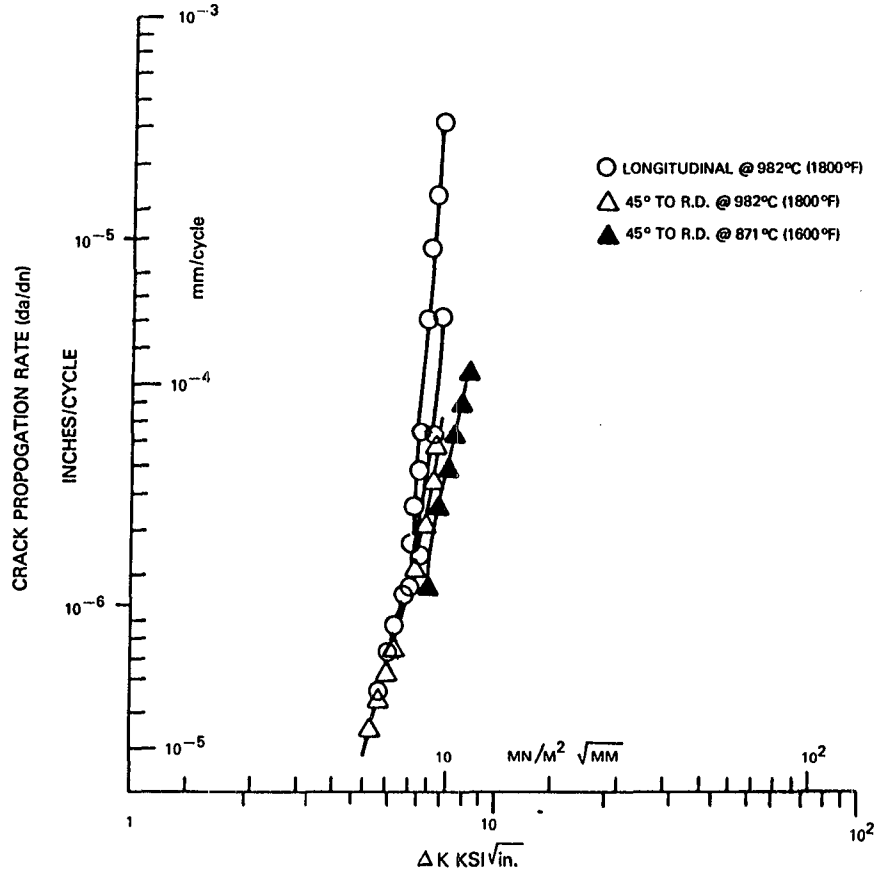

Figure 6-11 Crack Propagation Data Obtained on MA 956 Lot XBB-004

TABLE 6-IV

SUMMARY OF CRACK PROPAGATION TESTS ON MA956 LOT XBB-004

Specimen Number	(1) Orientation	Test Temp °C	Test Temp °F	Loading Sequence Number	Applied Stress[2] MN/M^2	Applied Stress[2] KSI	Cycles Applied
MACP-1	45	982	1800	1	48.2	7.0	123,370
MACP-2	45	871	1600	1	55.1	8.0	33,720
				2	68.9	10.0	58,010
MACP-3	L	982	1800	1	55.1	8.0	FOL[3]
				2	34.5	5.0	1,460[4]
MACP-4	L	982	1800	1	55.1	8.0	85
MACP-5	L	982	1800	1	41.3	6.0	FOL[5]
MACP-6		982	1800	1	41.3	6.0	9,770
				2	48.2	7.0	86,260
MACP-7	L	982	1800	1	51.7	7.5	50,500
				2	55.1	8.0	67,110
MACP-8	L	871	1600	1	55.1	8.0	12,980
				2	68.9	10.0	41,210[6]

1 L = Stress axis parallel to rolling direction; 45 indicates stress axis 45° to rolling direction

2 0.17Hz, R = 0 (cycled in pulsating tension from zero to indicated maximum stress)

3 Attachment pinhole failed on loading; weld repaired for second test

4 Failed at weld repair

5 Failed on loading as a result of equipment malfunction

6 Crack bifurcation in plane of sheet - propagation not perpendicular to stress axis

data on specimen MACP-7. Useful crack growth data obtained on four of the eight specimens tested are plotted in Figure 6-11. Inspection of this data shows relatively little variation among the temperatures and orientations tested, indicating essentially no temperature or orientation effects based on this limited data.

Results of the metallographic examination on failed specimens indicated that a transgranular mode of primary crack propagation occurred at all test conditions evaluated. However, as illustrated in Figure 6-12, some lateral secondary cracking occurred in grain boundaries perpendicular to the stress axis, with a tendency for out-of-plane propagation in selected grains. An extreme example of this latter effect is illustrated in Figure 6-13, where out-of-plane propagation having the appearance of a stage I facet is observed on a surface grain. The out-of-plane angle of this facet was sufficiently large as to preclude the acquisition of meaningful propagation data on this specimen (Table 6-IV).

6.5 CYCLIC OXIDATION AND THERMAL FATIGUE

Cyclic Oxidation and Hot Spot Blister thermal fatigue tests were conducted as described respectively in Section 5.1.6 and 5.1.5.

Results of cyclic oxidation tests conducted concurrently on MA956 lot XBB-004 and on Hastelloy X at 982°C (1800°F) (Figure 6-14) indicate attack on both alloys which was slightly greater than observed in Task III tests (Figure 5-26). This difference is attributed to variability of the burner test rig. Variability notwithstanding, these results continue to demonstrate the outstanding oxidation resistance of the MA956 alloy.

As indicated in Table 6-V, hot spot blister thermal fatigue tests were conducted on MA956 lot XBB004 and on Hastelloy X with minimum (background) temperatures of 427 and 538°C (800 and 1000°F) and maximum temperatures of 982 and 1093°C (1800 and 2000°F). Whereas hot spot temperature was measured using a thermocouple spot welded to the cold side of the specimen in Task III, tests in this task were conducted with an optical pyrometer focused in the hot side of the specimen. Because there is a through thickness gradient of about 22°C (40°F), the maximum temperature for tests in this task were approximately 22°C (40°F) lower than those stated for the Task III tests.

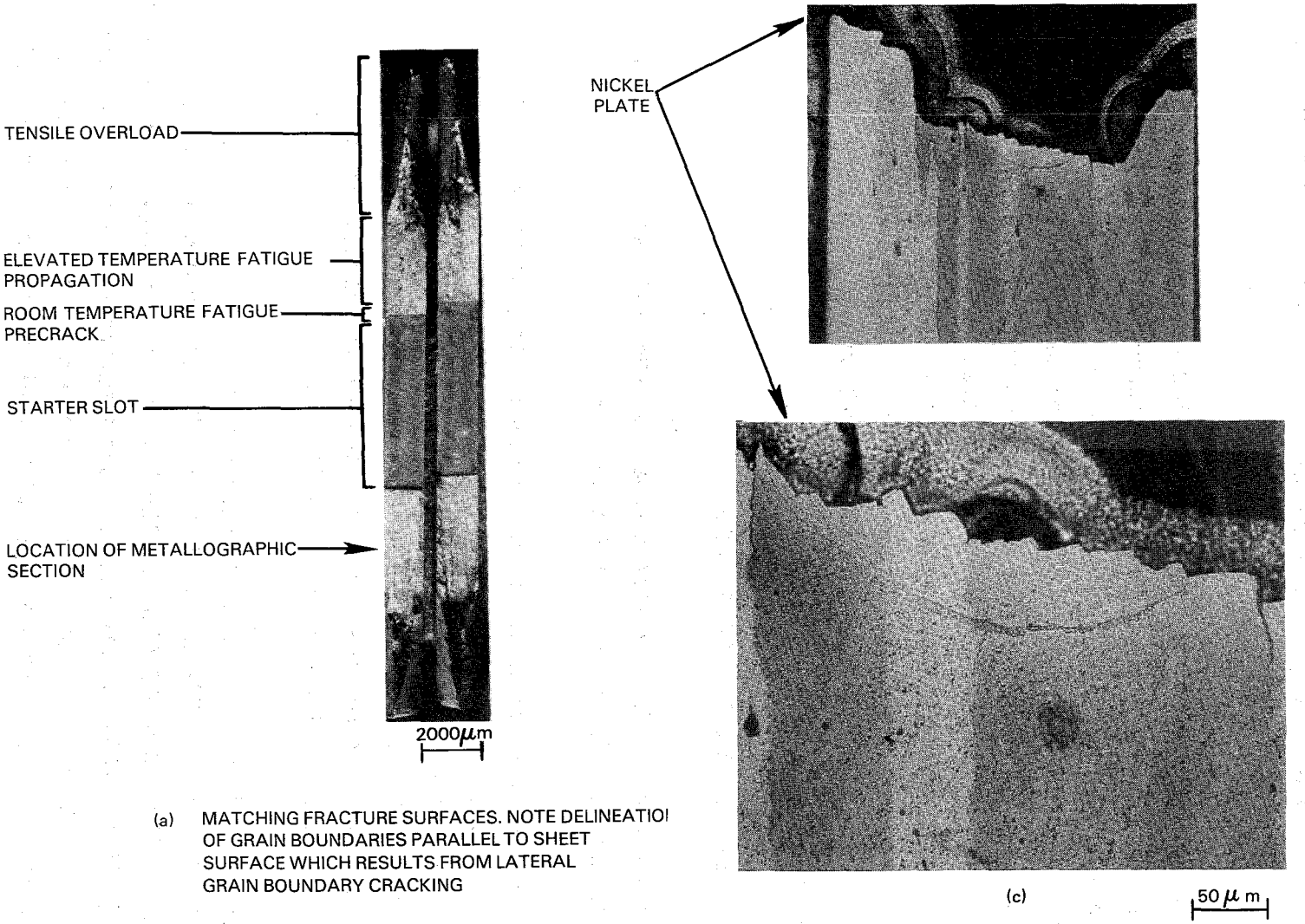

Figure 6-12 Fracture Surface and Metallographic Cross-Sections of Specimen MACP-1 Tested at 982C(1800F) with the Stress Axis at 45° to the Rolling Direction. Cross-sections b and c are on a plane parallel to the stress axis and perpendicular to the surface of the sheet. Note sceondary of cracking grain boundaries perpendicular to the stress axis in sections b and c. This observation is typical of all specimens tested in fatigue crack propagation.

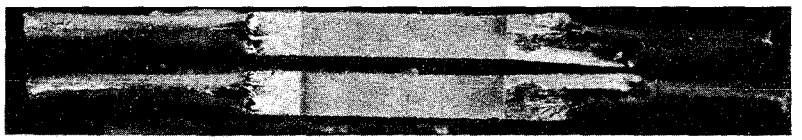

(a) MATCHING FRACTURE SURFACES VIEWED PARALLEL TO STRESS AXIS

OUT-OF-PLANE FACET

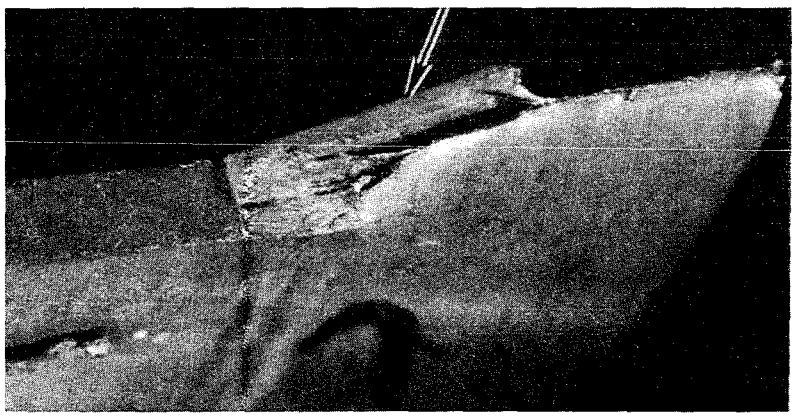

(b) OBLIQUE VIEW OF FRACTURE SHOWING OUT-OF-PLANE PROPAGATION IN SURFACE GRAIN

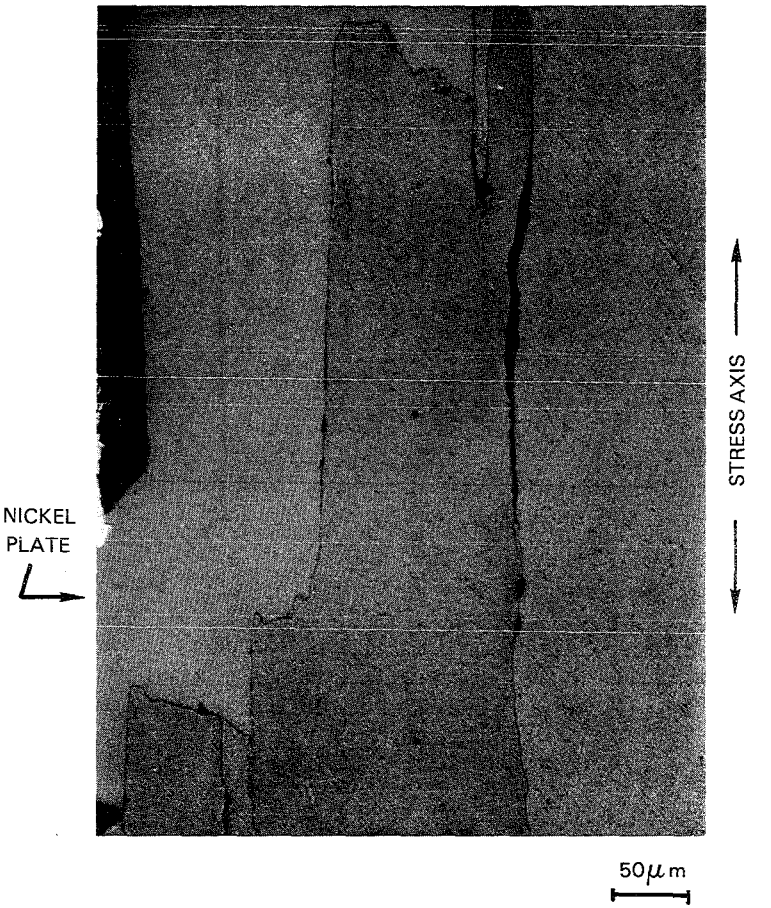

(c) METALLOGRAPHIC CROSS-SECTION OF FRACTURE IN VIEW (b) SHOWING GRAIN BOUNDARY CRACKING AND LARGE VERTICAL STEP AT GRAIN BOUNDARY. PLANE OF PHOTOGRAPPH NORMAL TO SPECIMEN SURFACE

Figure 6-13 Views of Lateral Grain Boundary Cracking and Out-of-Plane Propagation in Specimen MACP-8

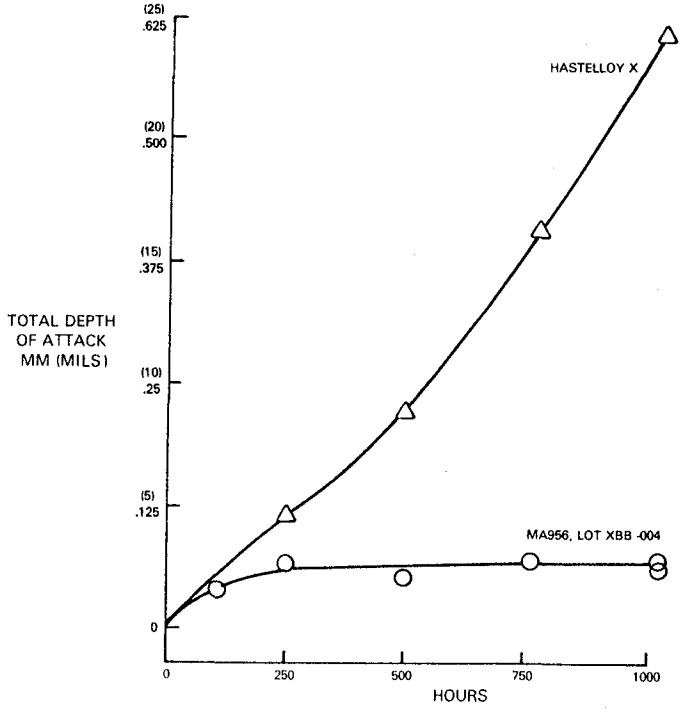

Figure 6-14 Cyclic Oxidation Testing at 982C (1800F) - 6 Minute Cycle

TABLE 6-V

SUMMARY OF RESULTS OF TASK IV HOT SPOT BLISTER THERMAL FATIGUE TESTS ON MA956 LOT XBB-004

Test Temperature						Average Deflection at 500 Cycles				Range of Maximum Cold Side Crack Penetration at 500 Cycles			
Minimum		Maximum		Range		Milimeters		Inches x 10^{-3}		Milimeters		Inches x 10^{-3}	
C	F	C	F	C	F	HAST X	MA 956	HAST X	MA 956	HAST X	MA 956	HAST X	MA 956
538	1000	982	1800	444	800	0.83	0.53	33	21	.013-.038	.038-.090	0.5-1.5	1.5-3.6
427	800	982	1800	556	1000	0.95	0.45	38	19	.050	.23-.33	2	9-13
427	800	1093	2000	667	1200	1.63	0.70	65	28	.25-.30	.68-.75	10-12	27-30

As discussed in Section 5.1.5, results of these tests are analyzed in terms of the ability of the test material to resist progressive distortion (bulging) at the point of heat application and cracking as a result of strain cycling. The strain-temperature phase relationship on the cold surface of the disk, opposite the point of heat application, closely simulates that experienced in a combustor application, with tensile strain occurring during the low temperature and compressive strain during the high temperature portion of the cycle. The strain temperature phase relationship on the opposite ("Hot") side tends to be the opposite of this (tension hot, compression cold), with a substantially lower calculated strain range.

Results of the hot spot blister tests conducted on this task are summarized in Table 6-V and Figures 6-15 through 6-17. Results of progressive deflection measurements (Figure 6-15) clearly demonstrate the superior thermal distortion resistance provided by the higher creep strength MA 956 alloy. These results also indicate that the majority of distortion occurs during the initial part of the test and that, except for Hastelloy X tested at a maximum temperature of 1093°C (2000°F), the level of distortion tends to stabilize beyond 100 cycles. Comparison of average distortion measured at 500 cycles (Table 6-V) indicates that distortion is controlled primarily by the peak exposure temperature, which controls the rate at which stress relaxation (creep) occurs, as opposed to temperature range, which controls the range of strain through which the material is cycled.

The capability of both materials to resist thermal fatigue cracking was evaluated through metallographic measurements of maximum depth of crack penetration on each tested specimen. Results of cold side measurements, Table 6-V and Figures 6-16 and 6-17 indicate less thermal fatigue crack resistance for MA 956 than for Hastelloy X, as expected. Also as expected, the extent of cracking tends to increase with increasing temperature range (and hence strain range). Metallographic observations of cold side crack morphology (Figures 6-18 and 6-19) indicate transgranular crack initiation in both alloys, with transgranular propagation in Hasteloy X. In MA 956, crack propagation occurs in a mixed mode with substantial cracking and delamination occurring along longitudinal grain boundaries intersected by propagating transgranular cracks.

In contrast to observations made on hot spot blister tests conducted in Task III, no hot wall cracking was observed at the 982°C (1800°F) peak temperature. This observation is assumed to result from the previously noted change in the test procedure from cold side tack welded thermocouple temperature measurement on the Task III tests to hot side optical temperature measurement on the Task IV tests, which means that the Task III tests actually were 22°C (40°F) hotter for the same nominal temperature. Thus the two sets of tests cannot be compared directly.

At the 1093°C (2000°F) peak temperature, some transgranular hot wall cracking was observed in the Task IV tests on MA 956, while intergranular hot wall cracking was the dominant failure mode in Hastelloy X (Figure 6-19a). The

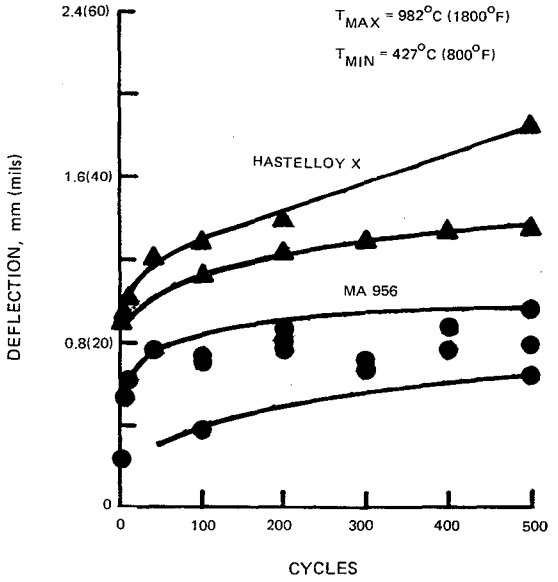

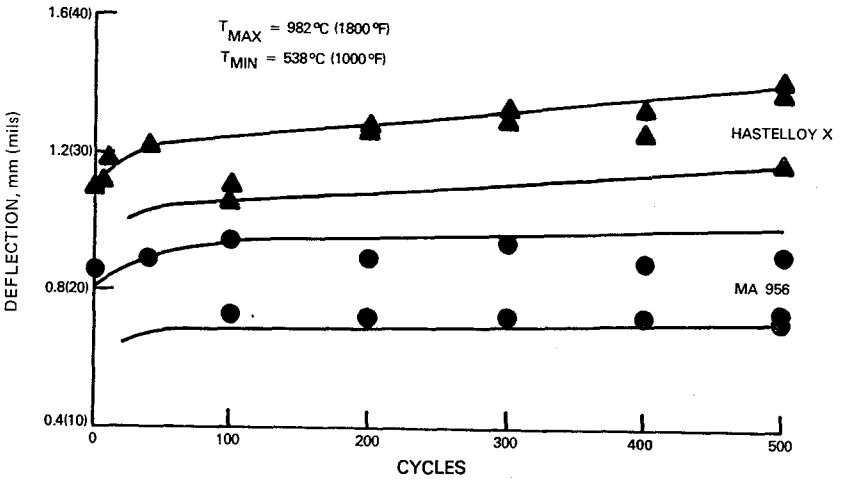

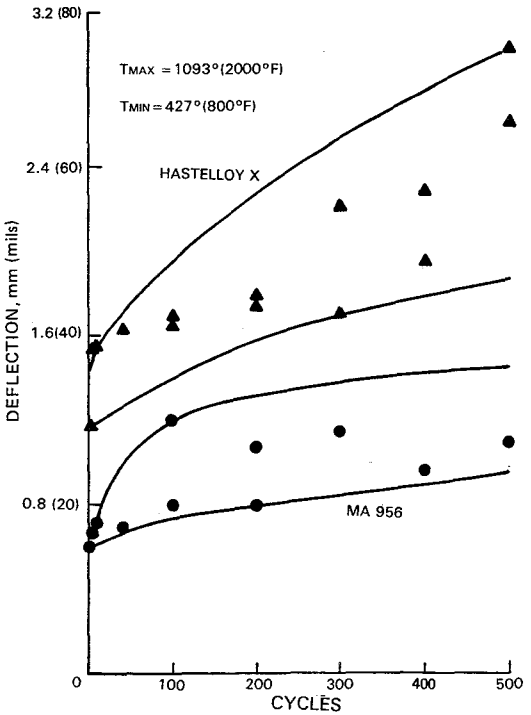

Figure 6-15 Hot Spot Blister Thermal Fatigue Deflection

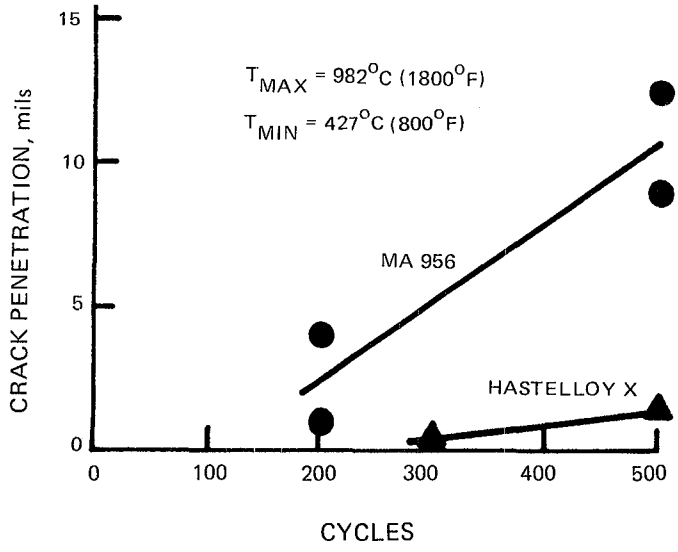

Figure 6-16 Hot Spot Blister Thermal Fatigue Cracking (Cold Side)

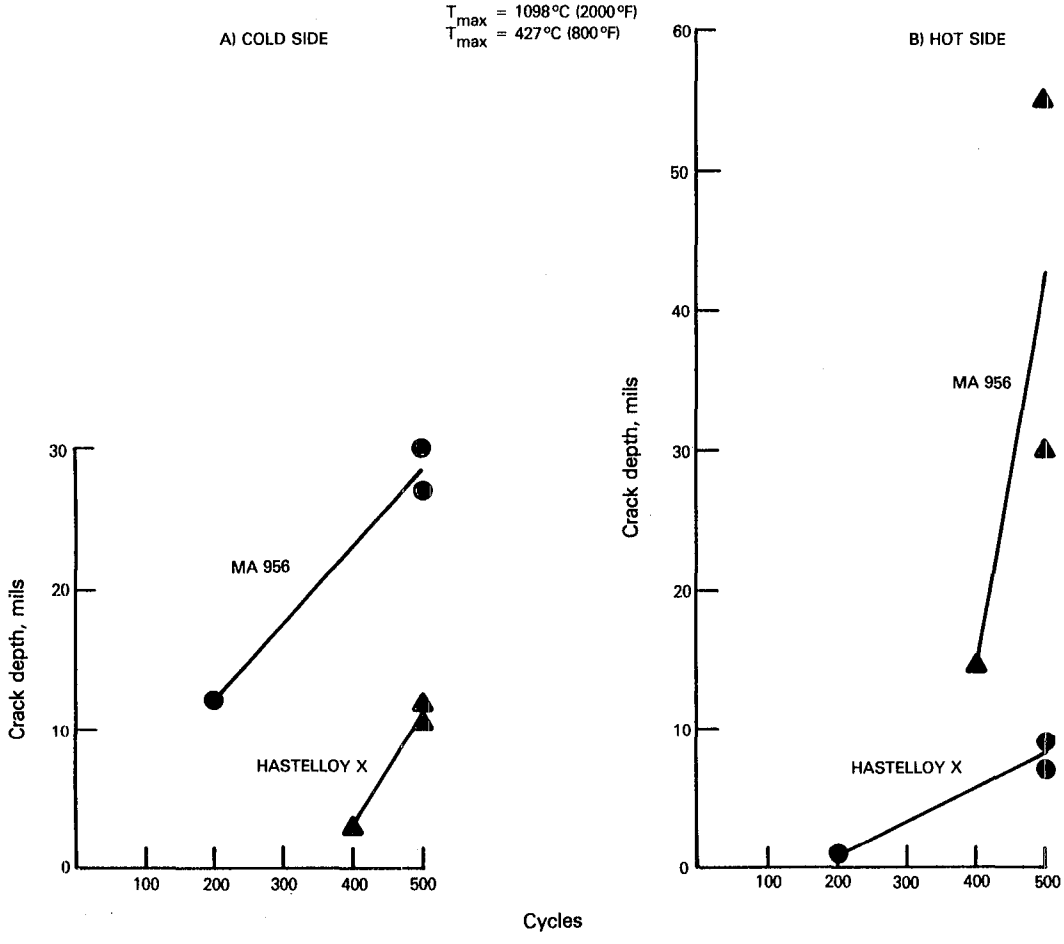

Figure 6-17 Hot Spot Blister Thermal Fatigue Cracking

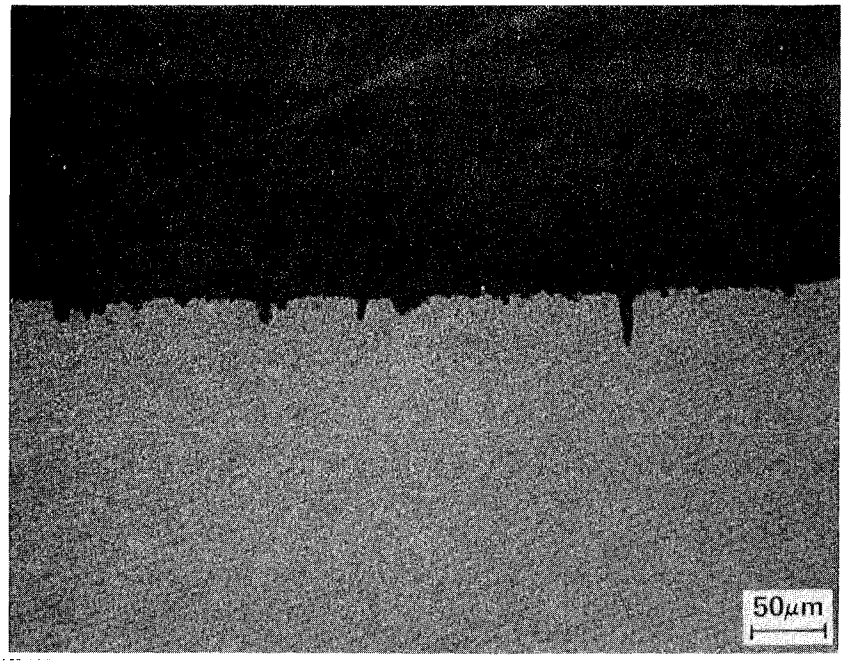

A) Hastelloy X

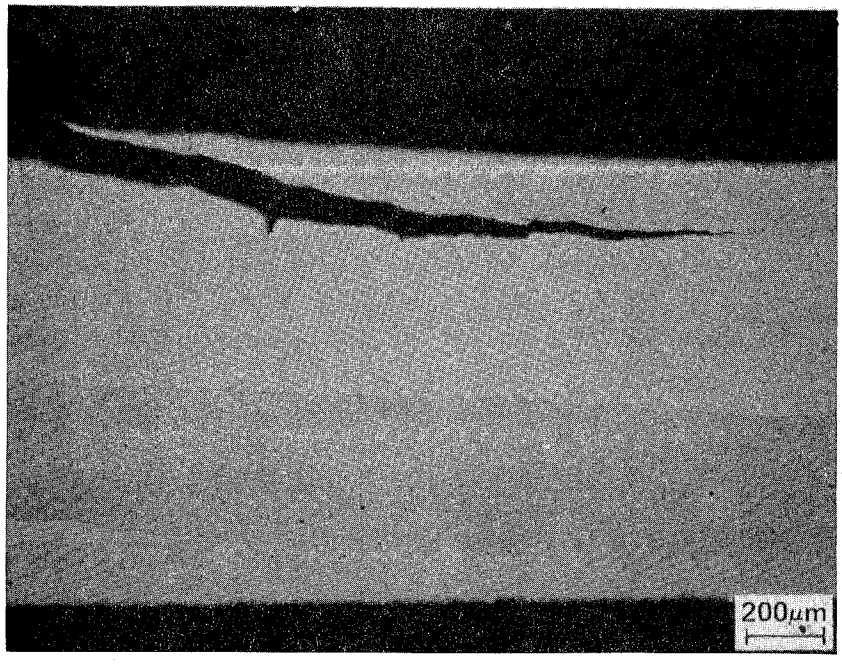

B) MA 956

Figure 6-18 Typical Cold Wall Cracking in Hot Spot Blister Specimen After 500 Cycles: T_{min} = 427C (800F), T_{max} = 982C (1800F)

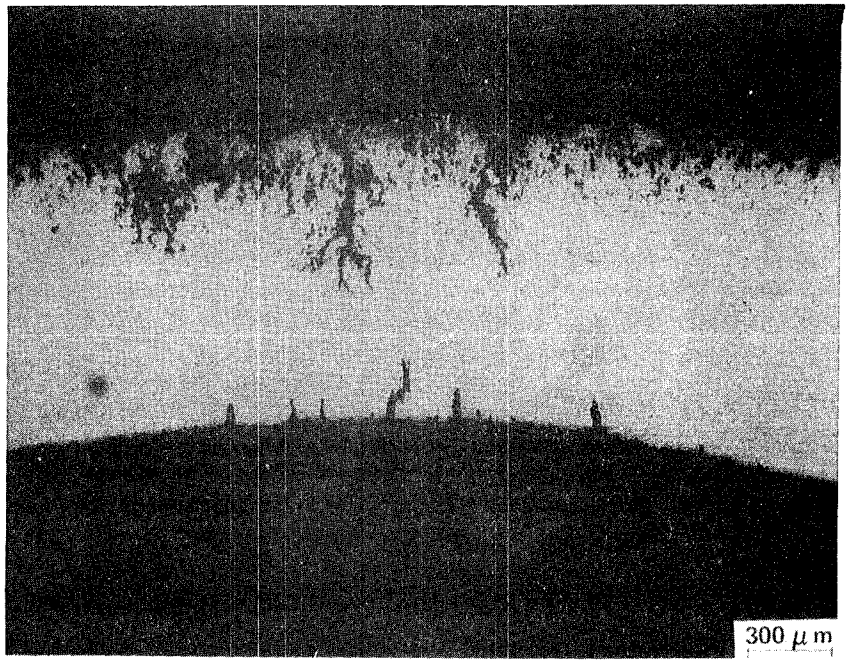

(a) Hastelloy X

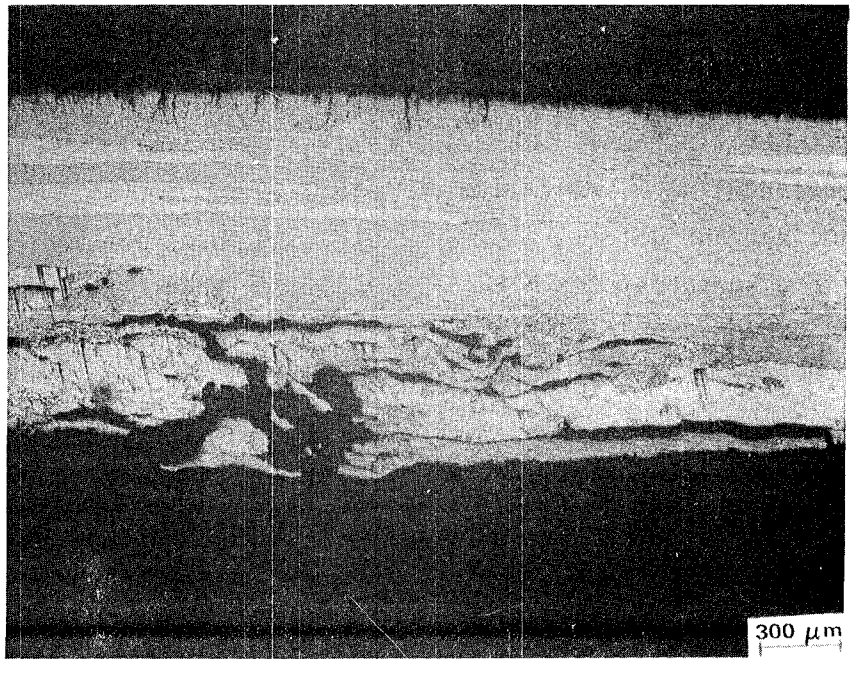

(b) MA 956

Figure 6-19 Hot and Cold Wall Cracking in Hot Spot Blister Specimen after 500 Cycles: T_{min} = 427C (800F), T_{max} = 1093C (2000F)

observed reversal of thermal fatigue cracking resistance observed on the hot side at 2000°F (Figure 6-19) reflects the poorer creep resistance of Hastelloy X exposed to a strain-temperature cycle where tensile strain peaks at the hot end of the cycle. The much poorer oxidation resistance of Hastelloy X also may have contributed to its lower hot side crack resistance at 1093°C (2000°F).

6.6 ALLOY STABILITY

Alloy stability studies on MA956 lot XBB-004 paralleled those conducted in Task III (Section 5.1.7). Hardness and metallographic evaluation were performed on furnace exposed coupons of as received material and on material cold worked 20% to simulate combuster forming strains. In addition, room temperature tensile and Erichson cup tests were performed to determine the susceptibility of XBB-004 to the previously discussed post exposure embrittlement phenomenon.

Results of hardness tests on furnace exposed coupons of as-received and cold worked materials are summarized respectively in Figures 6-20 and 6-21. These results are similar to those obtained on MA956 lot ZDEW in Task III (Figures 5-27 and 5-37). Metallographic observations also were similar to those made in Task III; representative microstructures are shown in Figures 6-22 and 6-23. In both as-received and cold worked material, void formation is observed to nucleate near the surfaces of the sheet, with voids being larger and concentrated near the center of the sheet as exposure time increases.

Results of post exposure room temperature tensile ductility and Erichson cup tests are summarized respectively in Table 6-VI and Figure 6-24. The tensile ductility data indicate that lot XBB-004 is not susceptible to the embrittlement found in lot ZDEW. However, results of the Erichson cup test, which appears to be more sensitive to embrittlement, indicate that XBB-004 can be embrittled by 1093°C (2000°F) exposure. Comparison with prior data on ZDEW (Figure 6-24) indicates that, whereas XBB-004 embrittles more slowly than ZDEW, the reduction of ductility is larger. As discussed in Section 5.1.7.4, this embrittlement phenomenon is not considered to be a significant limitation on the potential of MA956 for segmented combustor applications.

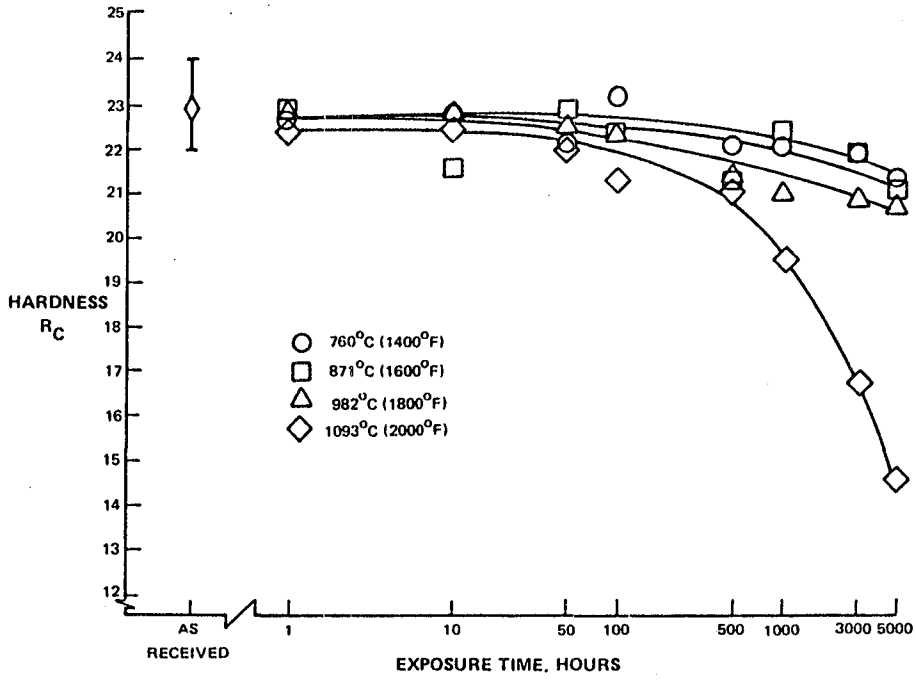

Figure 6-20 Alloy Stability of Incoloy MA 956 Lot XBB-004

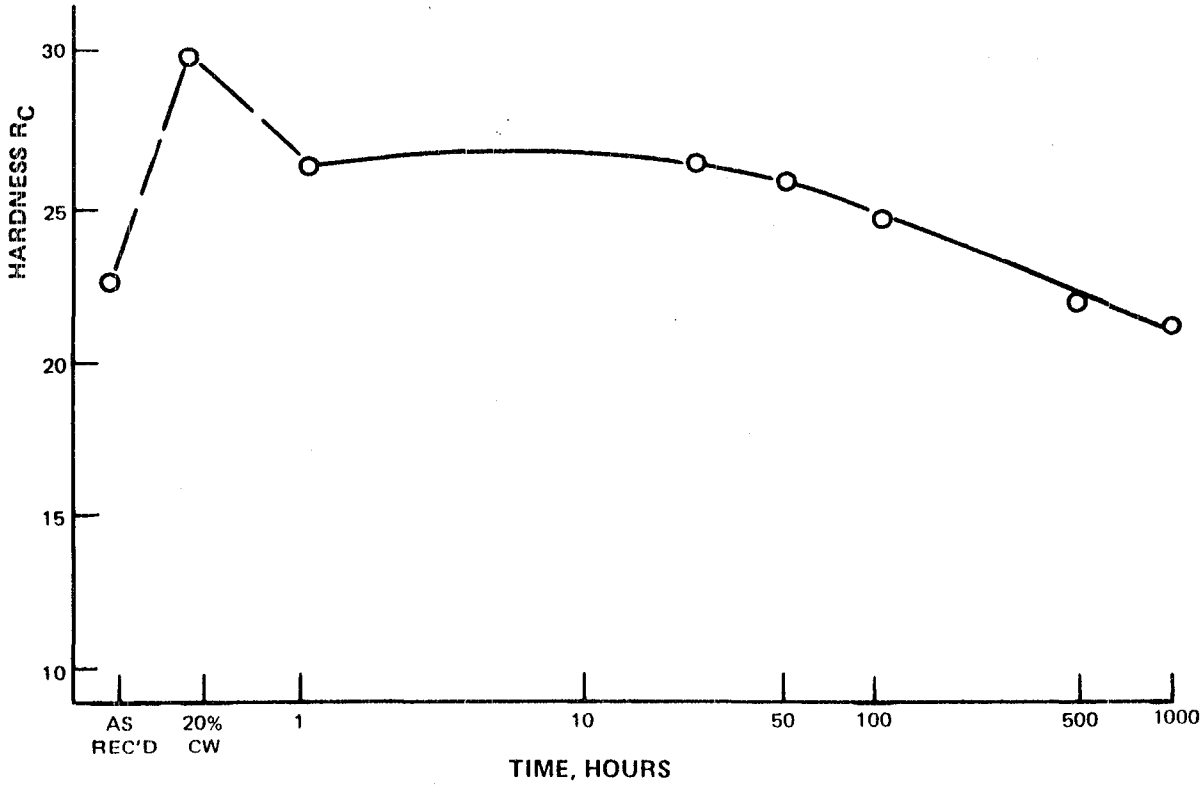

Figure 6-21 Hardness of 20% Cold-Rolled MA 956 Lot XBB-004 as a Function of Exposure Time at 1093C (2000F)

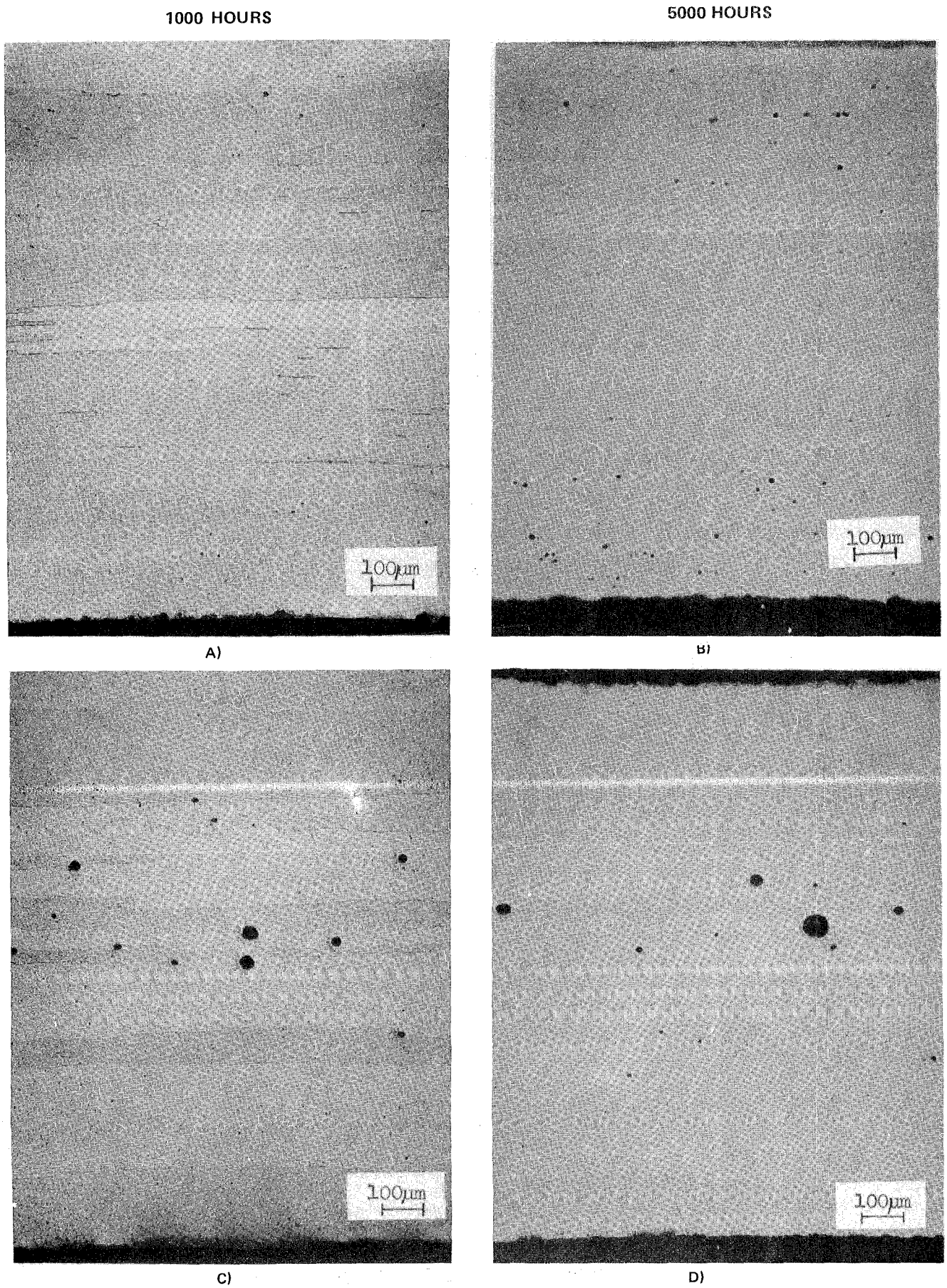

Figure 6-22 Typical Alloy Stability Microstructures of MA 956 Lot XBB-004

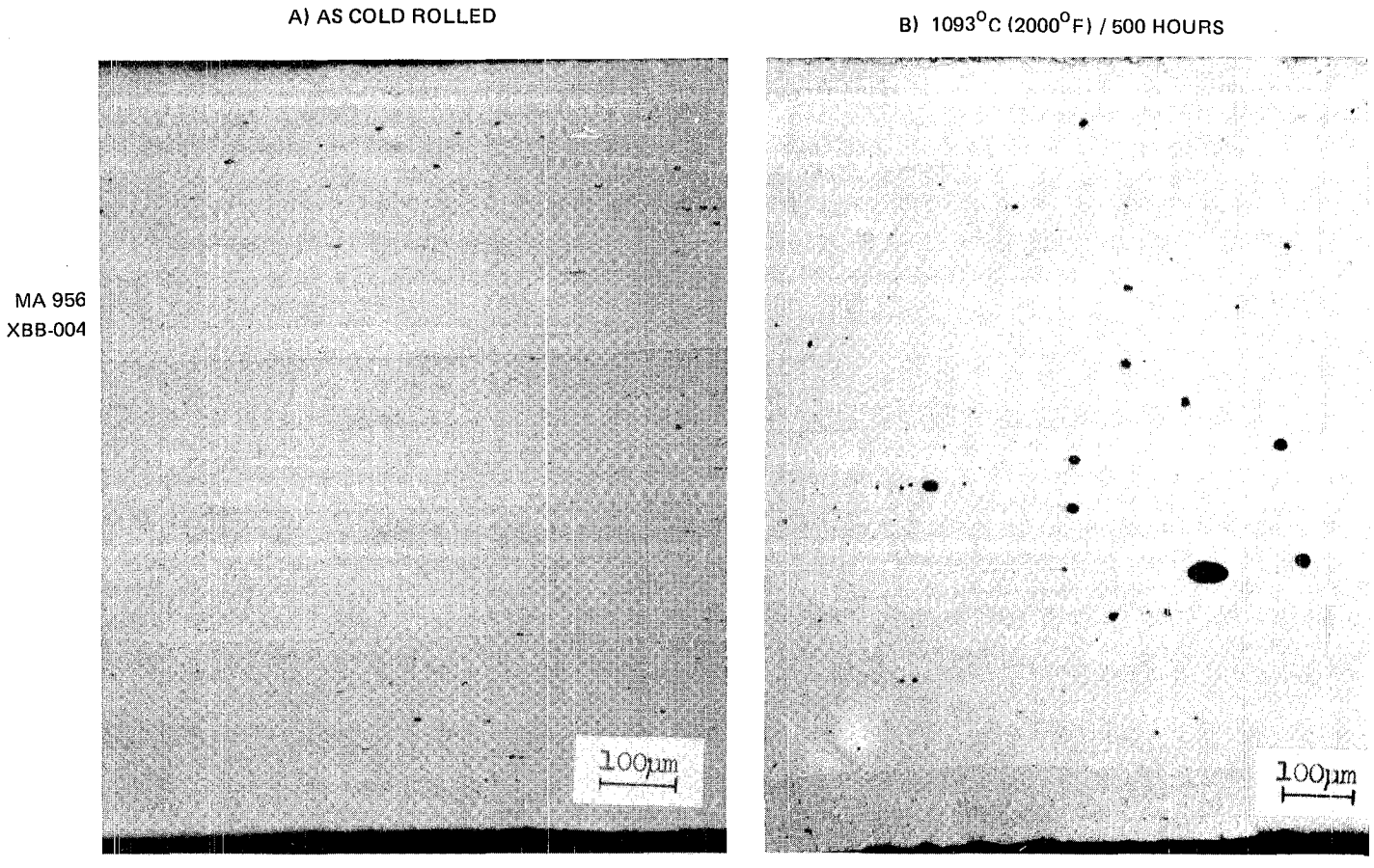

Figure 6-23 Typical 20% Cold-Rolled Alloy Stability Microstructures of MA 956 Lot XBB-004

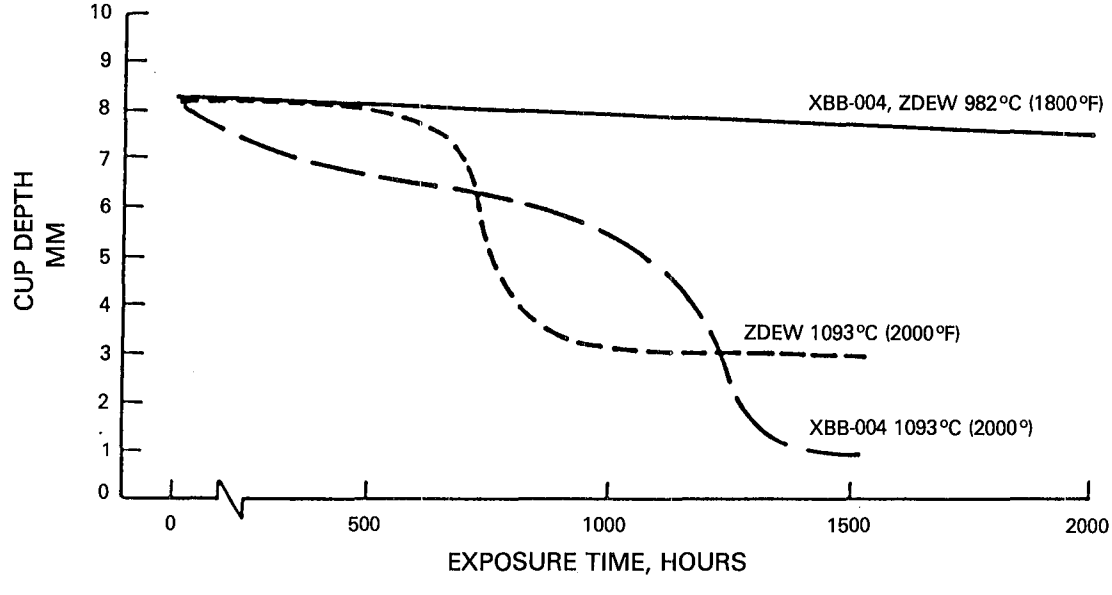

Figure 6-24 Erichsen Cup Depth of MA 956 after 982C and 1093C (1800F and 2000F) Exposures

TABLE 6-VI

RESULTS OF POST EXPOSURE TENSILE DUCTILITY
TESTS PERFORMED AT INCO ON MA956 LOT XBB-004

Pre-Exposure Condition(1)	Exposure Temperature °C (of)	Room Temperature Tensile Elongation (%) for Indicated Exposure Time		
		500 hr.	1000 hr	2000 hr
AR	982 (1800)	11, 11	12, 15	12, 14
AR & HA	982 (1800)	11, 12	11, 14	12, 13
AR	1093 (2000)	11, 12	15, 16	11, 12
AR & HA	1093 (2000)	10, 15	13, 14	13, 13

(1) As Received

HA - Hydrogen Annealed 1177°C (2150°F) 1/2 hour

7.0 TASK V - SUBCOMPONENT THERMAL FATIGUE TESTS

7.1 INTRODUCTION AND SUMMARY

The objective of this task was to experimentally evaluate the relative capability of the two previously identified segmented combustor design concepts to accommodate the limited thermal fatigue resistance of oxide dispersion strengthened alloys. The approach involved thermal fatigue testing of louvered and transpiration cooled subcomponent test specimens using thermal cycle test methods developed in Task III C (Section 5.3). Comparative tests were conducted on the ODS alloy MA 956 and Hastelloy X.

Three types of thermal cycle tests were conducted; two on the mechanically attached louver and one on the prestressed transpiration cooled design. As described in Section 5.3, evaluation of the louvered design involved thermal cycle testing of individual segments using induction heating, and of an eight-segment simulated combustor subassembly using radiant gas burner heating. Tests of the transpiration cooled design were conducted on single full size transpiration cooled panels attached to a support frame having a geometry which provided the desired pre-stress at ambient temperature.

Results of this testing clearly demonstrated the enhanced thermal fatigue resistance of both designs, with no thermal fatigue cracking being observed in properly fabricated specimens of either alloy in tests extending as many as 15,000 thermal cycles. Neither of the two design concepts demonstrated a clear advantage over the other. The large creep and oxidation benefits of the ODS alloy were clearly demonstrated, with the MA 956 exhibiting substantially less thermal distortion and oxidation as compared to Hastelloy X. These results are discussed in detail in the following sections.

7.2 INDUCTION HEATED SINGLE LOUVER TESTS

These tests involved cyclic induction heating and forced air cooling of single louver segments. Test specimen geometry and test methods are described in

detail in Section 5.3.3. As shown in Table 7-I, ten tests were conducted, five on Hastelloy X and five on MA 956 segments fabricated from lot XBB-044. Eight of these tests were conducted with a "baseline" thermal cycle, designated "A", and two with a shorter cycle, designated cycle "B". Both of these cycles involved induction heating the segment to a louver lip temperature of 1010°C (1850°F) and forced air cooling to a lip temperature of 538°C (1000°F). Cycle "A" included a two minute hold at the maximum temperature, while cycle "B" was continuous. The axial temperature distribution observed on the segment at the maximum temperature point in the cycle was shown previously in Figure 5-75.

Results of these tests, summarized in Table 7-I, clearly demonstrate the thermal fatigue resistance of the segmented louver design. Fluorescent penetrant and selective metallographic examinations showed no evidence of thermal fatigue cracking in any of the ten tested segments.

TABLE 7-I

RIVETED LOUVER SEGMENT INDUCTION HEATED THERMAL FATIGUE TEST RESULTS

Alloy	Specimen Number	Thermal Cycle (1)	Test Duration Cycles	Post-Test Distortion mm (inches)	Post-Test Distortion cycles/mm (cycles/mil)	Fluorescent Penetrant Inspection	Surface[3] Oxidation
Hastelloy X	1	A	1500[5]	1.5 (0.059)	1.0×10^3 (25.4)	No Indications	General = 13μm Intergranular = 75μm
Hastelloy X	5	A	1451	1.5 (0.059)[2]	-	No Indications	Not Measured
Hastelloy X	7	A	242[5]	2.9 (0.115)	8.3×10^1 (2.1)	No Indications	Not Measured
Hastelloy X	8	A	66[5]	2.4 (0.095)	2.75×10^1 (0.7)	No Indications	Not Measured
Hastelloy X	3[4]	B	1066[5]	3.9 (0.154)	2.7×10^2 (6.9)	No Indications	Not Measured
MA 956	9	A	844	Not Measurable[2]	-	No Indications	Not Measured
MA 956	10	A	5000	0.25 (0.010)	2.0×10^4 (500.0)	No Indications	Not Measured
MA 956	2	A	4000	1.0 (0.039)	4.0×10^3 (102.5)	No Indications	General = 10μm
MA 956	6	A	5004	0.4 (0.015)	1.25×10^4 (33.6)	No Indications	Not Measured
MA 956	4	B	5000	0.6 (0.024)	8.3×10^3 (208.3)	No Indications at 3000. Linear Edge Indications at 5000	General = 4μm

(1) Cycle A - 45 sec. Heating to Tmax; 2 min. Hold at Tmax;/ 30 sec. Cooling to Tmin
Cycle B - 45 sec. Heating to Tmax; 30 sec. cooling to Tmin.

(2) Overheat on last cycle; Bow Prior to Overheating is Unknown.

(3) Measured Metallographically

(4) Metallographic examination showed these indications were related to an unusual oxidation pattern, not to cracking - See test.

(5) Test terminated; temperature control not maintainable because of specimen distortion.

Except for specimen number 9, which overheated early in testing because of an equipment malfunction, all of the MA 956 segments were exposed at least to 4000 and most to 5000 thermal cycles. Testing of the Hastelloy X specimens was terminated at smaller numbers of cycles because excessive distortion of the segments changes the coupling with the induction coil so that temperature control could not be maintained. A photograph comparing the pre- and post-test shape of a typical Hastelloy X panel is shown in Figure 7-1. Distortion values based on measurements of panel dimensions before and after testing are listed in Table 7-I and summarized in Figure 7-2a. These measurements exhibit substantial variability from specimen-to-specimen, which is not fully understood. Variability notwithstanding, these results clearly show the benefit of the higher creep strength ODS alloy. A photograph comparing the post-test appearance of typical Hastelloy X and MA 956 segments is shown in Figure 7-2b.

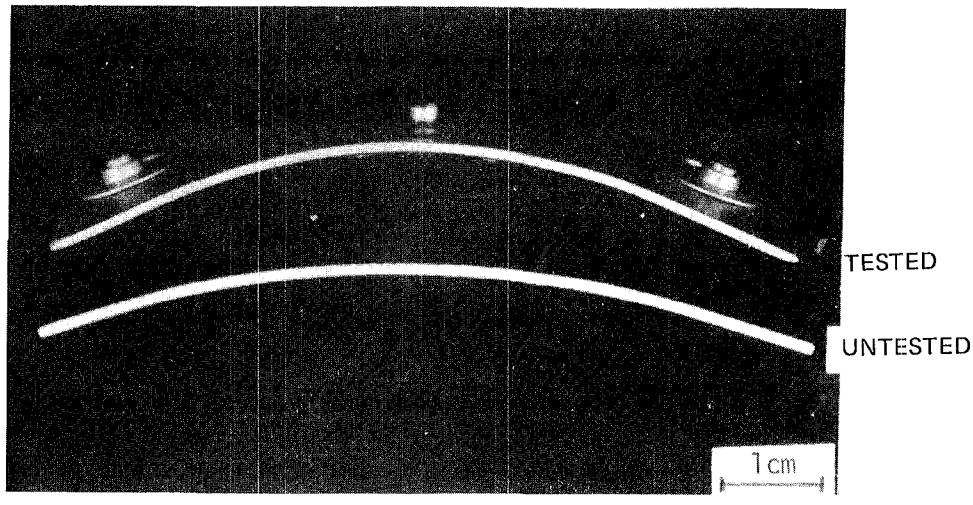

Figure 7-1 Hastelloy X Riveted Louver Segment, S/N3, Showing Distortion After 1066 Cycles (Cycle B)

Metallographic examination of selected specimens showed a clear difference in the amount and nature of oxidation on the two alloys, as noted in Table 7-I. Photomicrographs made in the hot zone of Hastelloy X specimen number 1 (Figure 7-3) show general surface oxidation about 13 μm (0.0005 inches) thick together with intergranular oxidation penetrating to a depth of several grain diameters ($\approx 75\,\mu$m; 0.003 inches). Hot zone photomicrographs of MA 956 specimen number 2 (Figure 7-4) show a 10 μm (0.0004) oxide layer with no intergranular oxidation or cracking. Void formation similar to that observed during alloy stability testing (Section 5.1.7 and 6.6) was found in the hot zone. No evidence of surface recrystallization, such as that seen on lot ZDEW specimens (Section 5.3.2), was seen in the thermal fatigue tested lot XBB-004 segments.

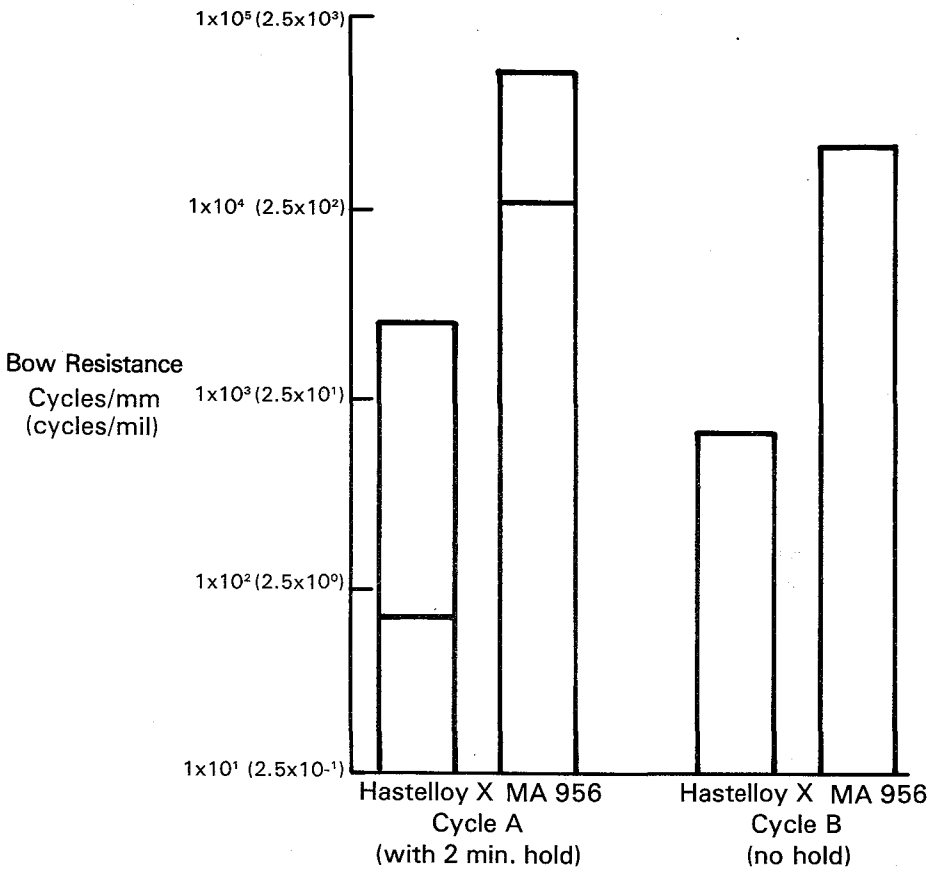

A) SUMMARY OF DISTORTION MEASUREMENTS

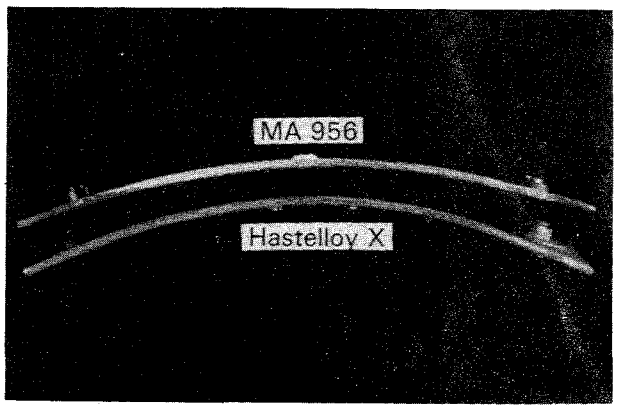

B) POST TEST PHOTOGRAPHS OF TYPICAL SEGMENTS

Figure 7-2 Comparison of Post Test Distortions Observed in Hastelloy X and MA 956 Segments

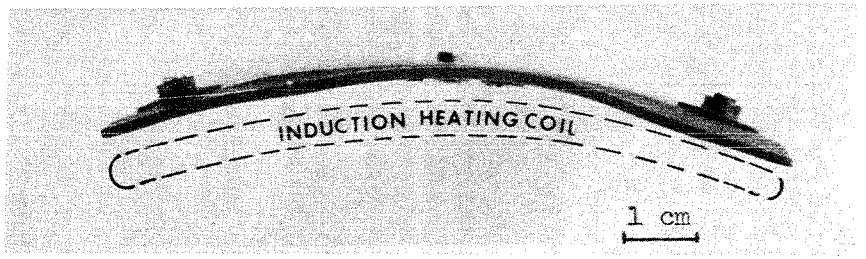

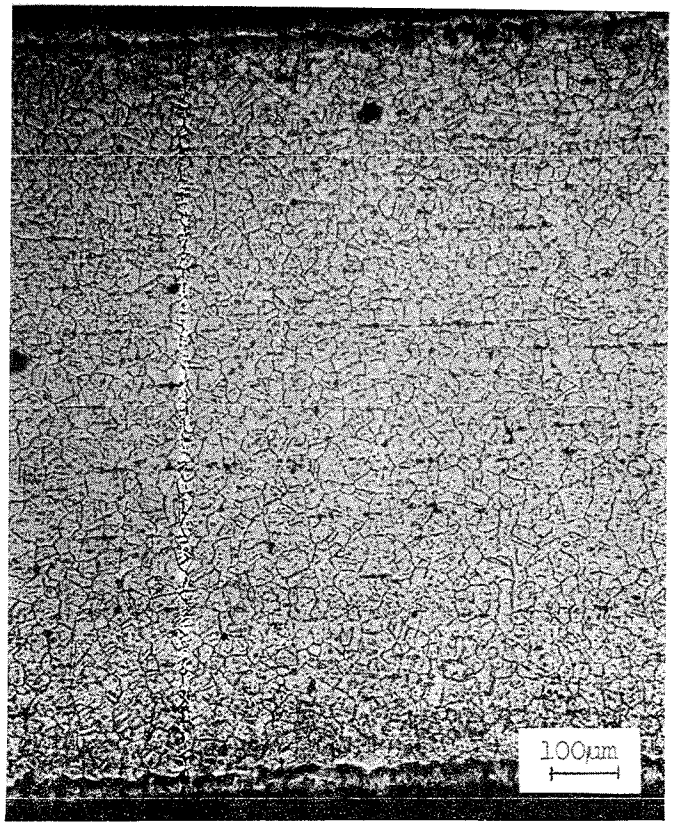

HOT ZONE

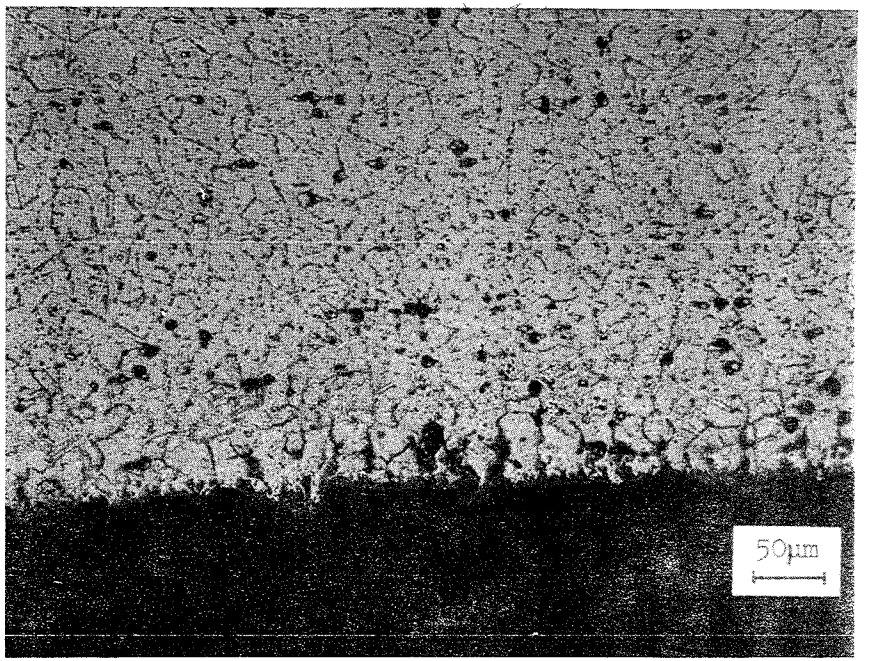

Figure 7-3 Hastelloy X Induct Heated Louver Segment after 1500 Thermal Fatigue Cycles

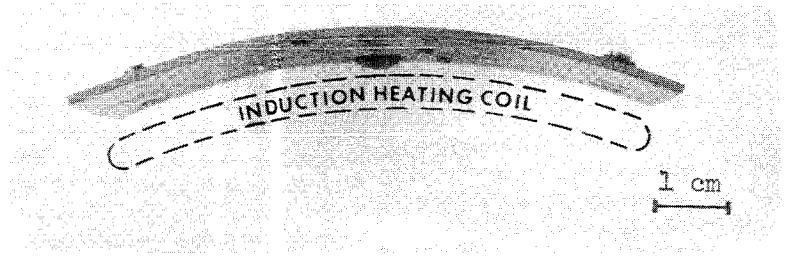

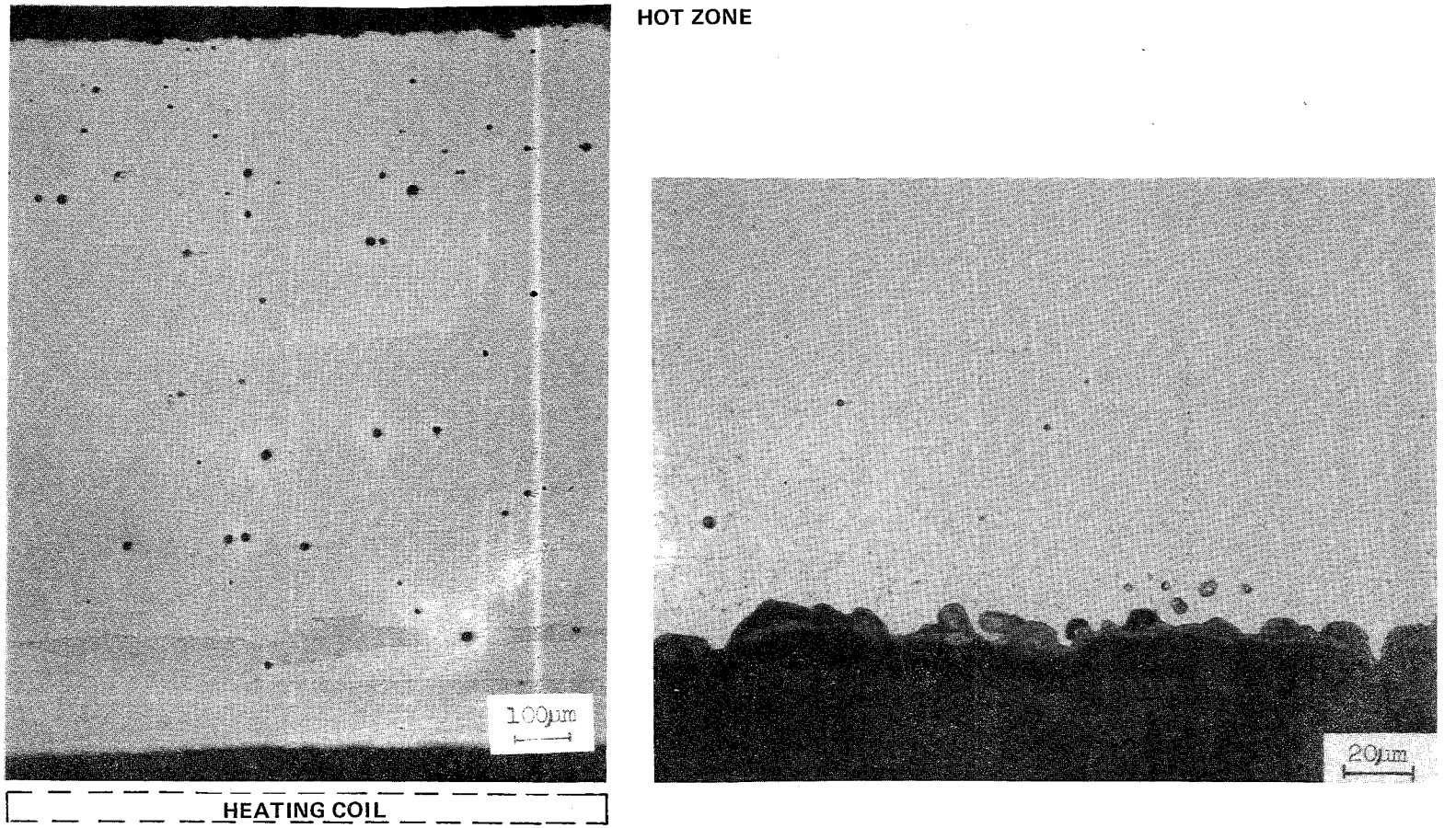

Figure 7-4 MA 956 Lot XBB-004 Induction Heated Louver Segment after 4000 Thermal Fatigue Cycles

As indicated in Table 7-I, fluorescent penetrant examination of MA 956 specimen number 4, tested with the "B" cycle, produced unusual linear indications on the hot edge of the louver lip after 5000 thermal cycles. Metallographic examination in the area of these indications, which originally were thought to be thermal fatigue cracks, showed an unusual pattern of oxidation associated with the grain boundaries (Figure 7-5). Scanning electron microscopy of the intersection of the oxidized and polished surfaces (Figure 7-6) indicates that the linear suface indications "line-up" with the grain boundaries. X-ray energy spectroscopy across the polished edge shows no chemistry variation at the grain boundaries which might be responsible for this preferential oxidation. However, investigation of the oxidized surface reveals the presence of aluminum rich oxides in the vicinity of the grain boundaries. The cause of this oxidation phenomenon occurring in specimen number 4 and not in any of the other MA 956 specimens is not understood.

7.3 CYCLIC BURNER RIG TESTING OF MULTI-SEGMENT SUBCOMPONENTS

The objective of this effort was to substantiate the very favorable single segment results described in the last section, with emphasis on a more thorough investigation of the mechanical attachment behavior and durability. The test methods used for this evaluation are described in Section 5.3.4, with the multi-segment test specimen being described in Section 5.3.2 and shown in Figure 5-72. Two specimens were tested, each containing eight test louvers, four each of MA 956 lot XBB-004 and Hastelloy X in an alternating arrangement. Attachments were as described in Section 5.3.2, with the hot rivet material being the same as the segment material (i.e., MA 956 hot rivets on the MA 956 segments and Hastelloy X hot rivets on the Hastelloy X segments). In the first test, various constraints were applied to artifically increase the strain in the attachment area. In the second test, selective attachments were removed to demonstrate the redundancy of the attachment system.

Testing involved the application of a 60 second cycle during which the louver lip was heated to 954°C (1750°F) and cooled to 593°C (1100°F). The axial gradient observed in the segment at the maximum cycle temperature was shown previously in Figure 5-78. As described below, various portions of the first test were conducted with and without external cooling on the Hastelloy X shell. Without cooling, the shell reached a maximum temperature of 760°C (1400°F); the application of external cooling reduced the maximum shell temperature to 538°C (1000°F).

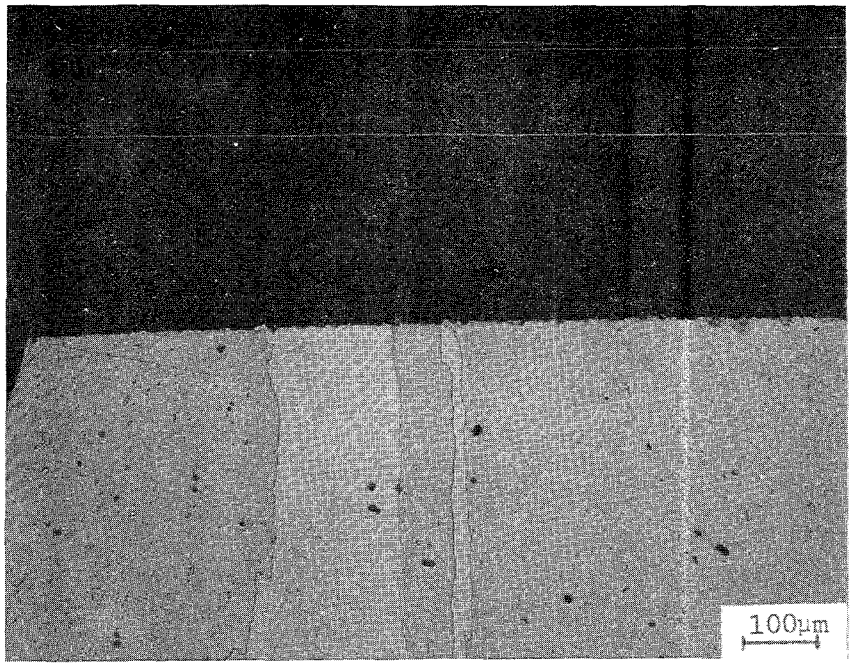

Figure 7-5 Cross-section of MA 956 Riveted Louver Segment S/N 4 after 5000 Cycles (Cycle B) Showing Increased Grain Boundary Oxidation (Brackets)

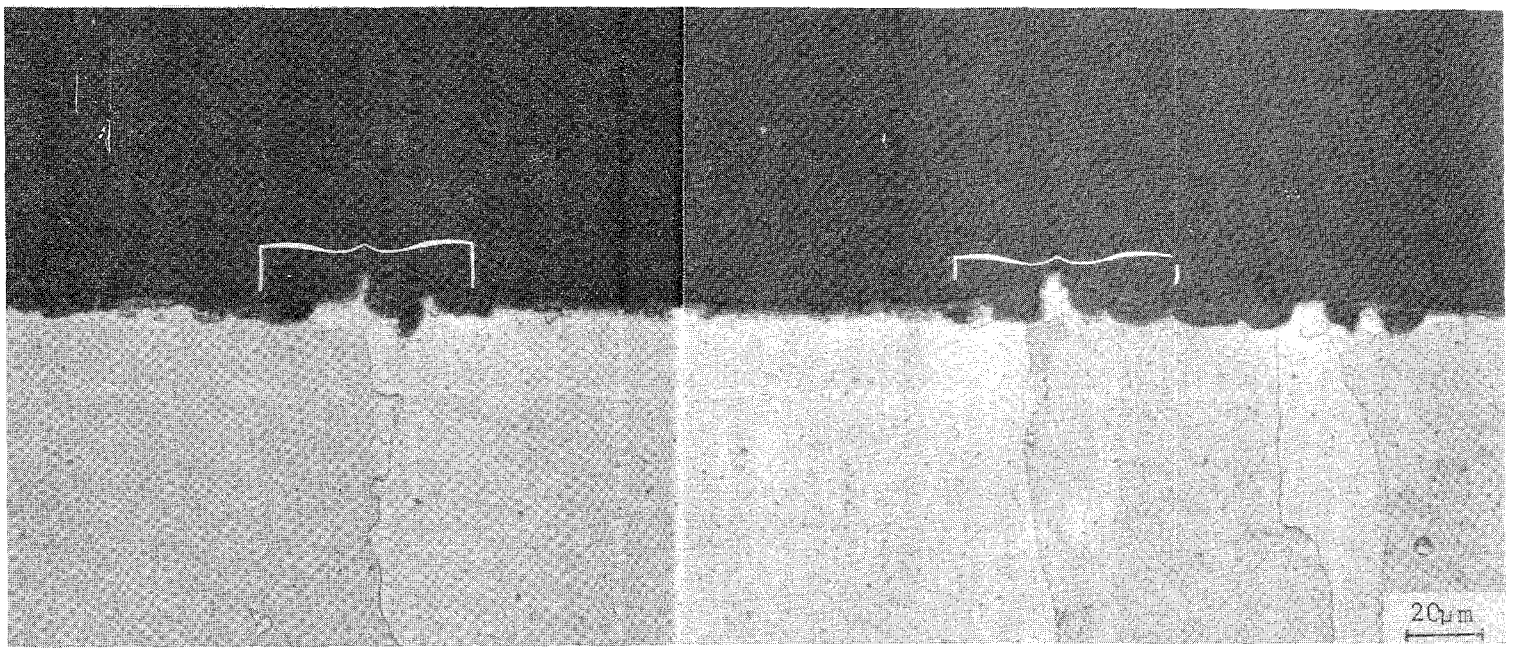

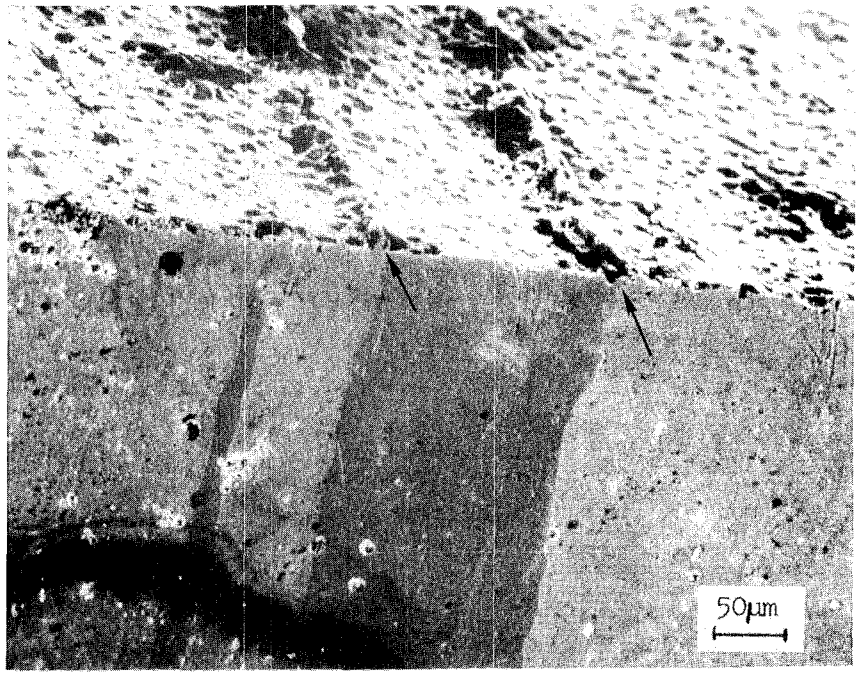

Figure 7-6 Scanning Electron Micrograph of Polished Edge of MA 956 Riveted Louver S/N4 Showing Oxidized Areas (arrows) In-line with Grain Boundaries at the Intersection of the Polished Surface and the Edge of the Panels

Results obtained on the first of the two gas burner heated louver specimens are summarized in Table 7-II. This specimen was tested in three separate campaigns, with a total of 15,000 thermal cycles being applied. Fluorescent penetrant inspection revealed no cracks or other defect indications in any of the segments after the accumulation of 15,000 thermal cycles. Visual and binocular examination indicated the attachments to be in good condition also. As shown in Table 7-II, the first four thousand thermal cycles were applied to the "Bill-of-Material" specimen configuration with no external shell cooling and no indication of distress. To artificially increase in-plane constraint (and hence strain) in the hot attachment area, an additional 6000 cycles were applied with one half of the hot rivets welded to the cold shell; again with no indication of distress. In the final 5000 cycle campaign, external cooling was applied to the Hastelloy X shell to provide additional thermal constraint within the test component, with no distress being observed after testing. These results clearly demonstrate the high thermal fatigue tolerance of the segmented louver design and attachment concept.

Table 7-II Initial Radiant Gas Burner Heated Thermal Fatigue Component Test Results

Shell Temperature °C (°F)	Specimen Configuration	Applied Cycles	Fluorescent Penetrant Inspection Results
760 (1400)	As Fabricated	4000	No Distress
760 (1400)	50% Hot Rivets Welded	6000	No Distress
593 (1100)	50% Hot Rivets Welded	5000	No Distress
		15000 Total	

- Tests conducted on Film Cooled Riveted Louver Specimen Containing four MA956 segments and four Hastelloy X segments.
- Sixty Second Test Cycle:
  Maximum Lower Lip Temperature: 954°C (1750°F)
  Minimum Lower Lip Temperature: 593°C (1100°F)

The second of the two gas burner heated louver specimens was tested with selected attachments removed to demonstrate the redundancy of the mechanical attachment system. The use of brazed studs also was evaluated in this test. As described in Section 5.3.2 and summarized in Figure 7-7, the attachment scheme for each panel consists of a tightly headed "structural" Hastelloy X rivet (labeled "S" in FIgure 7-7) located in the center of the upstream (cold) edge of each 3.8 cm (1-1/2 inch) by 7.6 cm (3 inch) panel, two "loose" Hastelloy X rivets (labeled "C" in Figure 7-7) located at each of the upstream (cold) corners, and two "snug" rivets of the panel material (labeled "H" in Figure 7-7) located along the axial edges of the panel about half way between the upstream and downstream edges. Primary attachment loads are carried by the tight structural rivet, with the other four being present primarily to resist twisting and out-of-plane distortion of the panel.

Modifications of the second burner rig test article to substantiate attachment redundancy included pre-test removal of the structural rivet, (S), from one pair of panels (one each of Hastelloy X and MA 956), and removal of the two "hot" (downstream) rivets, (H), from a second pair of panels, together with the spacer which maintains panel separation of the hot louver from the cold

wall at this location (see Figure 5-65C). An alternate attachment scheme involving replacement of the hot rivets, (H), with brazed studs was evaluated on a third pair of panels (see Figure 5-65D), while the fourth pair was tested with the baseline attachment configuration.

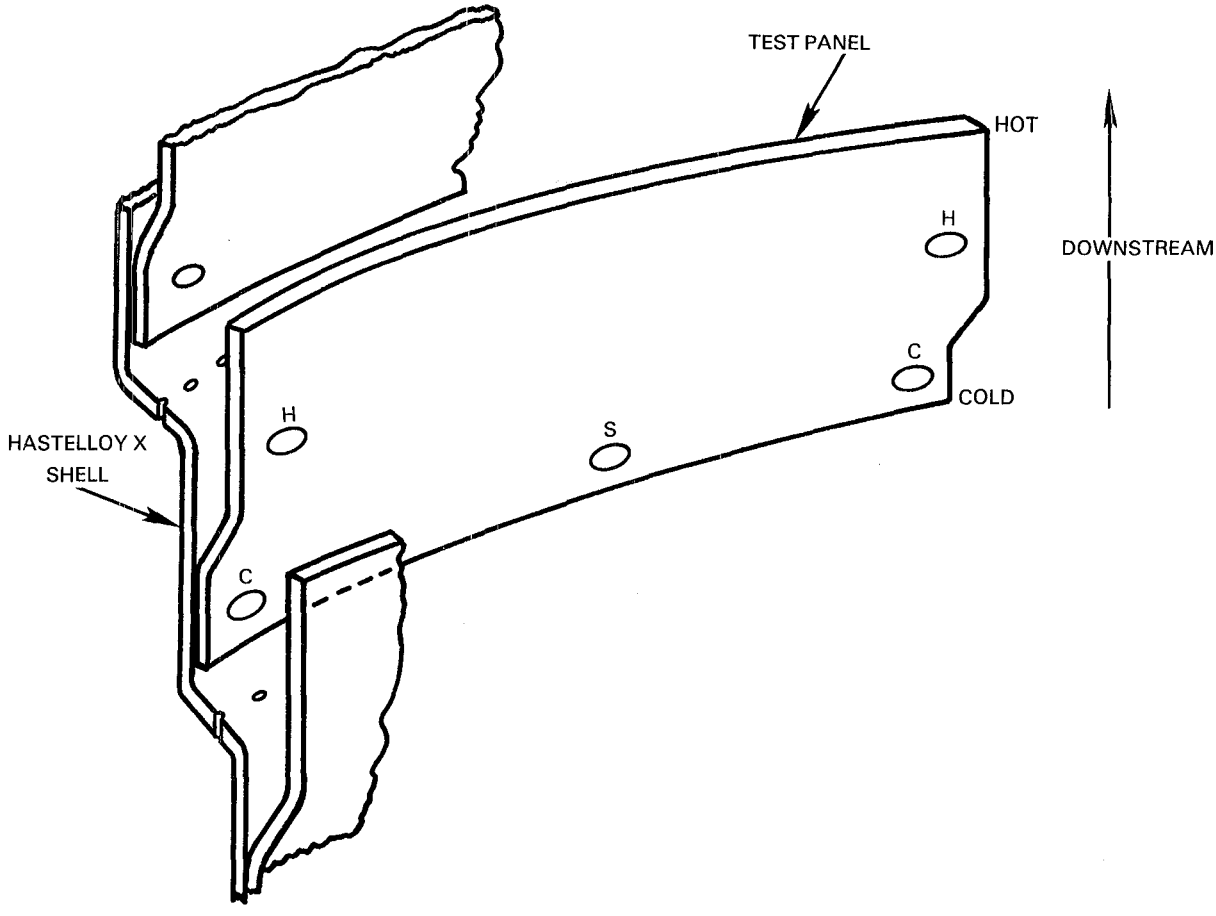

Figure 7-7 Arrangement of Rivets Attaching Panels to Shell of Thermal Cycle Test Article (See text for rivet designations.)

Exposure of this article for 10,000 thermal cycles from 593 to 954°C (1100 to 1750°F) louver lip temperature and 760°C (1400°F) shell temperature was completed with no cracking of either the panels or attachments apparent by visual (30X) or zyglo penetrant inspection. This result convincingly demonstrates the capability and redundancy of the mechanical attachment design, and indicates that the brazed stud is an acceptable alternative to the hot rivet.

To evaluate the dimensional stability of segments with reduced out-of-plane constraint, progressive panel distortion measurements were obtained after test as shown in Figure 7-8. Results of these measurements are reported in Table 7-III and summarized in Figure 7-9. These results clearly show the superior dimensional stability of MA 956 as compared to the current state-of-the-art Hastelloy X burner material. The data in Figure 7-9 also indicate that the primary mode of panel distortion is curling of the corners of the panel toward the hot gas stream, coupled with some tendency of the center of the panel to move toward the cold wall. This latter tendency is analogous to the louver lip collapse mode of failure sometimes observed in conventional full hoop burners. While not apparent from the data shown in Figure 7-9, by far the greatest distortion occurred in the Hastelloy X panel from which the hot rivets were removed. As shown in Figure 7-10, this is the only panel in which distortion was clearly apparent to the naked eye. While the measurements presented in Figure 7-9 would suggest that the louver lip corners of this Hastelloy X panel initially curled toward the cold wall, followed by a return to the original geometry, the visual examination suggests a much more complex pattern of distortion. As illustrated in Figure 7-11, this distortion appears to take the form in inward (toward the hot gas stream) bulging of the panel in the vicinity of the missing hot rivet, coupled with distinct outward kinks seen on the louver lip. These kinks represent the form of geometrical distortion which is responsible for louver lip collapse in conventional full hoop Hastelloy X burner liner.

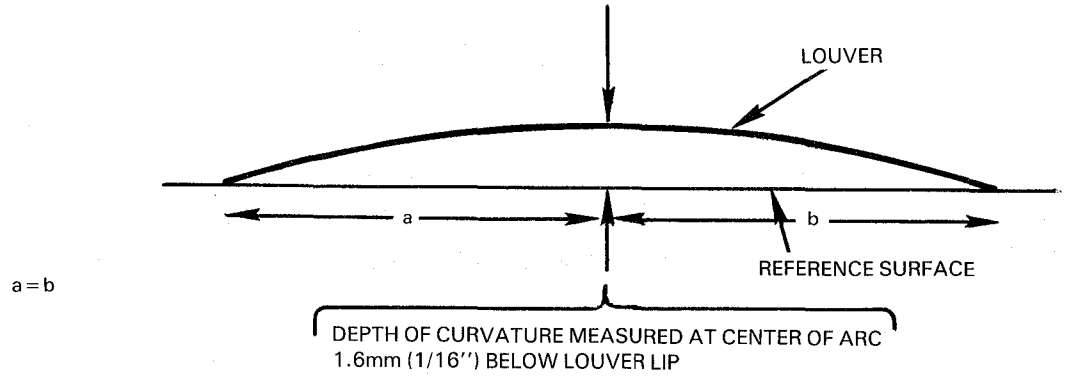

Figure 7-8 Location of Louver Lip Distortion Measurement

Table 7-III

LOUVER CURVATURE MEASUREMENTS ON THERMAL CYCLED SUBCOMPONENTS, mm (in.)

Panel Number	Material	Attachment Modification	Applied Thermal Cycles 0	2680	6040	8719	10,000
1	MA 956	Baseline	6.96 (0.274)	6.99 (0.275)	6.96 (0.274)	7.01 (0.276)	7.01 (0.276)
2	HAST X	Brazed Hot Attachment	6.91 (0.272)	-(1)-	7.52 (0.296)	7.52 (0.296)	7.54 (0.297)
3	MA 956	Hot Rivets Removed	6.73 (0.265)	6.76 (0.266)	6.63 (0.261)	6.81 (0.268)	6.78 (0.267)
4	HAST X	Hot Rivets Removed	8.08 (0.318)	-(1)-	7.62 (0.300)	8.03 (0.316)	8.03 (0.316)
5	MA 956	Structural Rivet Removed	6.88 (0.271)	6.86 (0.270)	6.91 (0.272)	6.86 (0.270)	6.78 (0.267)
6	HAST X	Structural Rivet Removed	7.57 (0.298)	-(1)-	8.00 (0.315)	8.08 (0.318)	8.05 (0.317)
7	MA 956	Brazed Hot Attachment	6.99 (0.275)	-(1)-	7.01 (0.276)	7.09 (0.279)	7.09 (0.279)
8	HAST X	Baseline	6.99 (0.275)	7.44 (0.293)	7.34 (0.289)	7.47 (0.294)	7.44 (0.293)

(1) Physical interference between the thermocouples and the measuring device precluded accurate measurement.

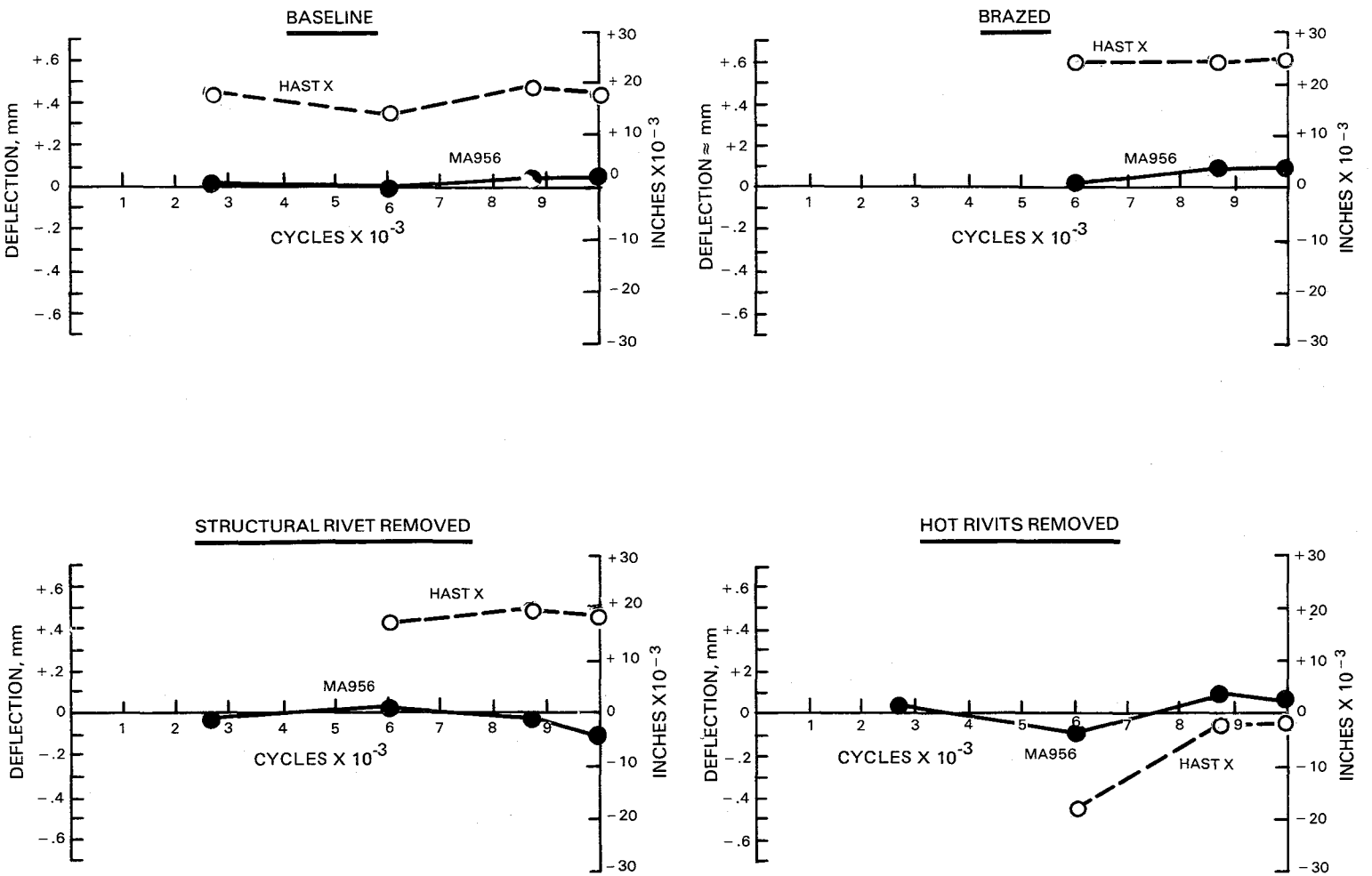

Figure 7-9 Distortion of Louver Segments Measured on 10,000 Cycle Subcomponent Thermal Cycle Test Article

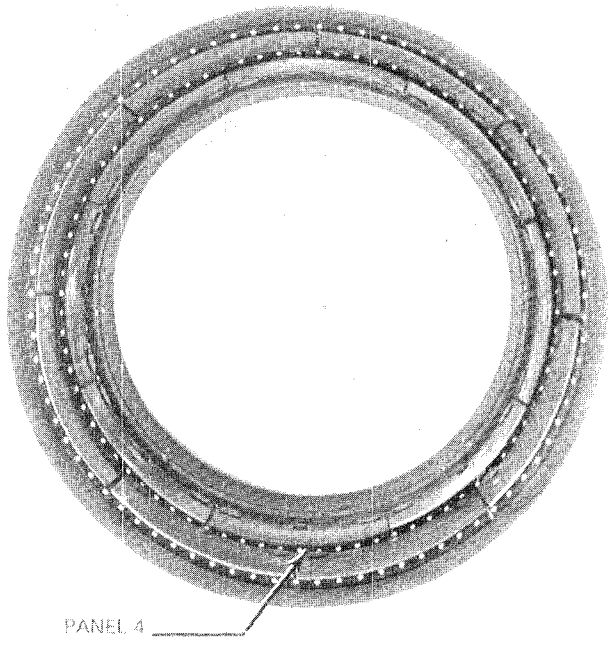

a) THERMAL CYCLE SUBCOMPONENT TEST ARTICLE EXPOSED TO 10,000 CYCLES FROM 593 TO 594C(1100 to 1750F)

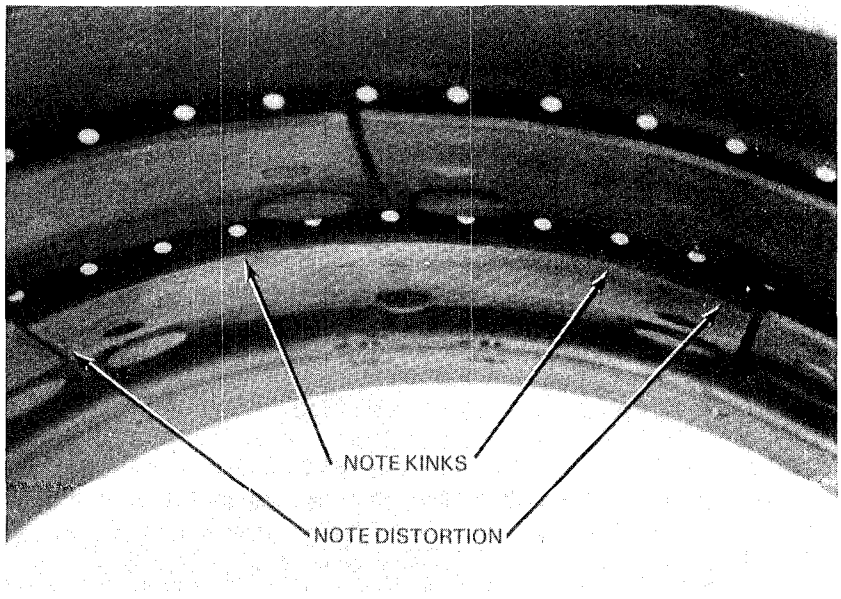

b) CLOSE-UP VIEW OF DISTORTION OBSERVED ON HASTELLOY X PANEL NO.4

Figure 7-10 Photographs of 10,000 Cycle Subcomponent Test Article

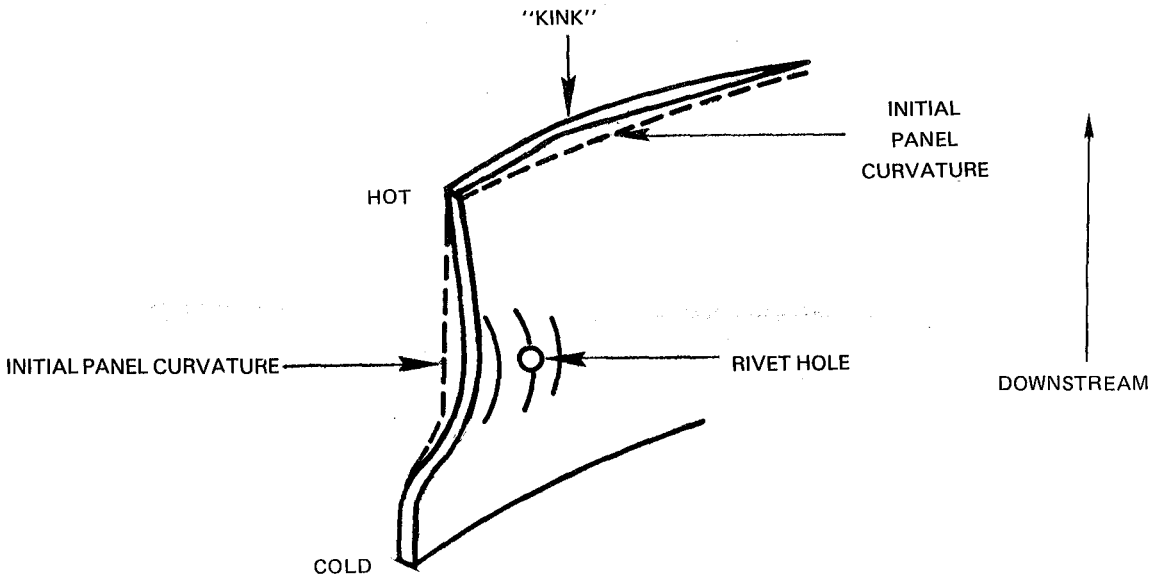

Figure 7-11 Distortion Observed on Hastelloy X Panel From Which Hot Rivets Were Removed

7.4 PRESTRESSED TRANSPIRATION COOLED TWIN WALL THERMAL CYCLE TESTS

The objectives of this effort were to experimentally evaluate the capability of the prestressed, transpiration cooled, twin wall design concept to accommodate the limited thermal fatigue capability of the oxide dispersion strengthened alloy MA956, and to compare the performance of MA956 and Hastelloy X in this design.

A total of five transpiration cooled subcomponent thermal cycle tests were conducted. Details of the specimen design and test method are discussed respectively in Sections 5.3.5 and 5.3.7. A thirty second test cycle was employed with 22 seconds heating to a maximum temperature of 927°C (1700°F) and 8 seconds cooling to minimum temperatures in the range of 593 to 649°C (1100 to 1200°F).

Results of these five tests are summarized in Table 7-IV. With the exception of the initial test on a panel containing pre-cracked laser drilled cooling holes, no cracking of the transpiration cooled panels was observed after 10,000 thermal cycles. These results clearly demonstrate the thermal fatigue capability of the prestressed transpiration cooled design. Details of these tests are discussed in the following paragraphs.

Table 7-IV

PRESTRESSED TRANSPIRATION COOLED TWIN WALL COMPONENT THERMAL CYCLE TESTS

Hole Fabrication Method	Test Conditions	Configuration	Applied Cycles	Inspection Results
Laser	Tmax=927°F (1700°F) Tmin=593°C (1100°F) Tgradient=55°C (100°F) (Apparent)	Prestressed MA 956	2,000	Cracks Propagating from Laser Pierced Holes
ECM	Tmax=927°C (1700°F) Tmin=649°C (1200°F) Tgradient=22°C (40°F)	Prestressed MA 956	10,000	No Cracks
		Prestressed Hastelloy X	10,000	No Cracks
		Not prestressed[1] MA 956	10,000	No Cracks
		Not prestressed[1] Hastelloy X	10,000	No Cracks

[1] See text for explanation of "Not Prestressed" configuration

The initial transpiration cooled segment thermal cycle test was conducted on the laser drilled MA956 panel used for temperature calibration in Task III (Section 5.3.7). The cooling holes in this panel contained cracks as deep as 1.3 mm (0.050 inches), as shown previously in Figure 5-81A. During thermal cycling, these pre-cracks propagated from acute cooling hole corners parallel to the cooling hole axes in the high stress upstream edge-center area of the panel. As shown in Figure 7-12, crack link-up between adjacent cooling holes occurred after 2000 thermal cycles. Crack link up was defined as the criterion for failure of the transpiration cooled panel in the Task I design phase; this laser drilled panel thus is considered to have failed in thermal fatigue.

As indicated in Table 7-IV, four additional panels with electro-chemically machined (ECM) cooling holes were subjected to 10,000 thermal cycles with no evidence of thermal fatigue cracking. As discussed previously in Section 5.3.5, ECM produced holes did not contain pre-cracks (Figure 5-81B). It thus is concluded that the intrinsic thermal fatigue capability of the prestressed twin wall design is good, but that care must be exercised in panel fabrication to assure good quality (uncracked) cooling holes for this intrinsic capability to be realized in practice.

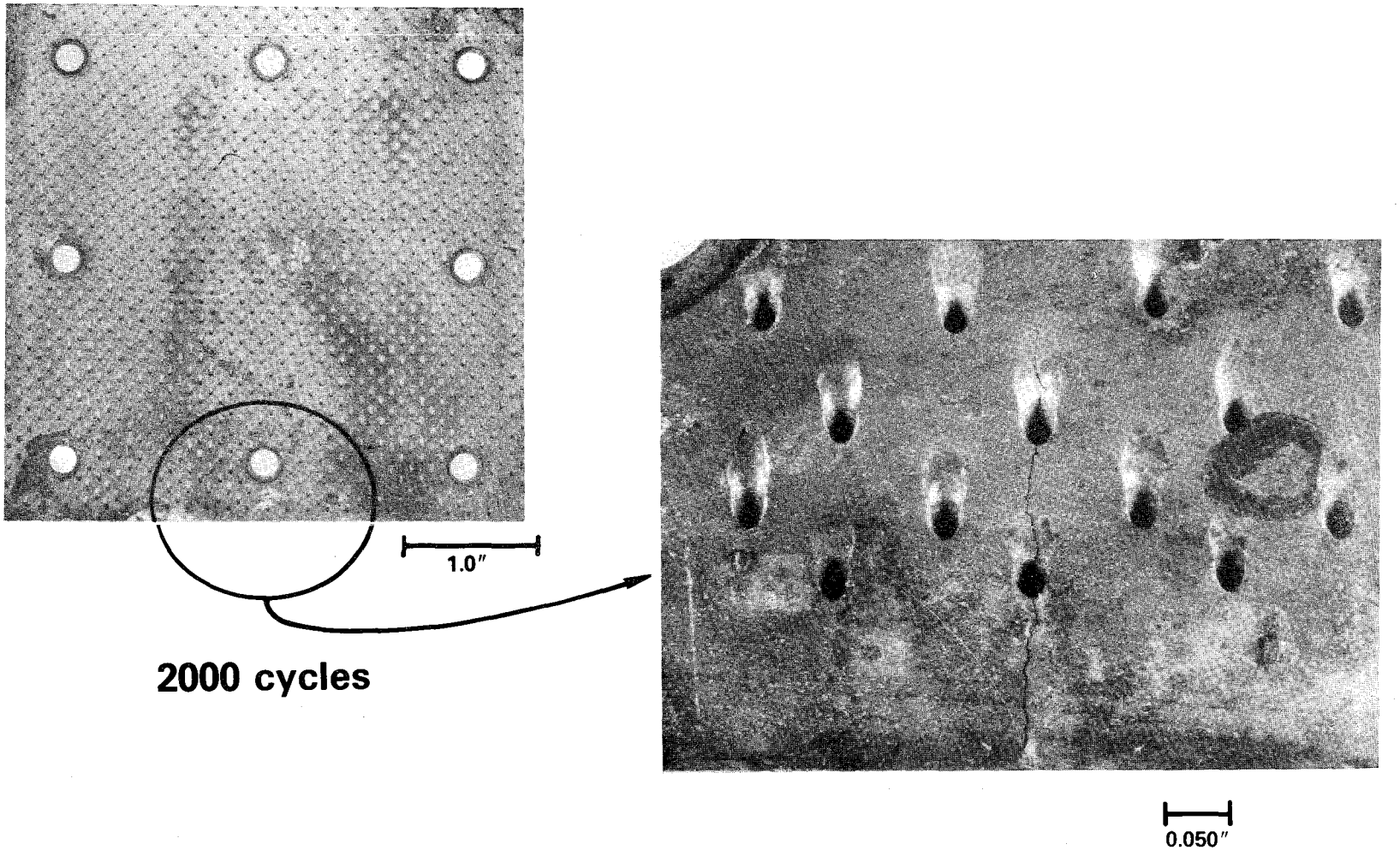

Figure 7-12 Prestressed Twin Wall Panel Tested for 2000 Thermal Cycles, Showing Link-up of Cracks Extending from Pre-cracked Laser Drilled Cooling Holes

Test conditions noted in Table 7-IV indicate that the thru-thickness gradient of 55°C (100°F), which apparently was achieved in the laser drilled panel (See Figure 5-85), was not achieved in any of the four subsequent tests on ECM drilled panels, despite numerous efforts to "re-optimize" the heating and cooling parameters. Results of post-test panel distortion measurements, which are discussed below, show virtually no difference in distortion between corresponding laser and ECM drilled panels. This observation suggests that the apparent gradient difference between the two sets of tests is not real. Based on the reproducibility of the 22°C (40°F) gradient measured in two separate tests, it is assumed that the original measurement of 55°C (100°F) was in error.

The panel configurations listed in Table 7-IV indicate that two different configurations were tested. Two tests were conducted on panels which were bent to the spherical radius indicated in Figure 5-79. For the other two tests, the side rails on the support frame were machined flat to eliminate the ambient temperature pre-stress. This was done in an effort to determine the effect of pre-stressing on thermal distortion, as discussed below.

Measurement of post test distortion was accomplished by measuring the elevation of the hot surface above a reference plane established by placing the tested specimens cold side down on a flat reference plate. Results of these measurements, which were made at the intersections of a 12.7 mm (0.5 inch) square grid marked on the hot side surface, are shown in Figure 7-13. A plot of the averages of four measurements at corresponding locations along each diagonal and along each plate centerline (Figure 7-14) clearly shows the better dimensional stability of MA956 as compared to Hastelloy X, particularly in the constrained (not prestressed) condition. These measurements also show excellent reproducibility between results obtained on the two prestressed MA 956 panels drilled by different techniques. This reproducibility indicates that essentially all of the observed distortion occurs in the first 2000 cycles of testing. As discussed earlier, it also suggests that the apparent difference of gradient between these two tests is not real. Comparison of the prestressed and not-prestressed results indicates that prestressing did not fully accomplish its objective, which was to pre-configure the panel to its elevated temperature shape so that essentially no stress would be experienced at the peak temperature where stress relaxation occurs. This may have been a result of failure to achieve the through-thickness gradient of 100°C (180°F) on which the calculated prestress configuration was based.

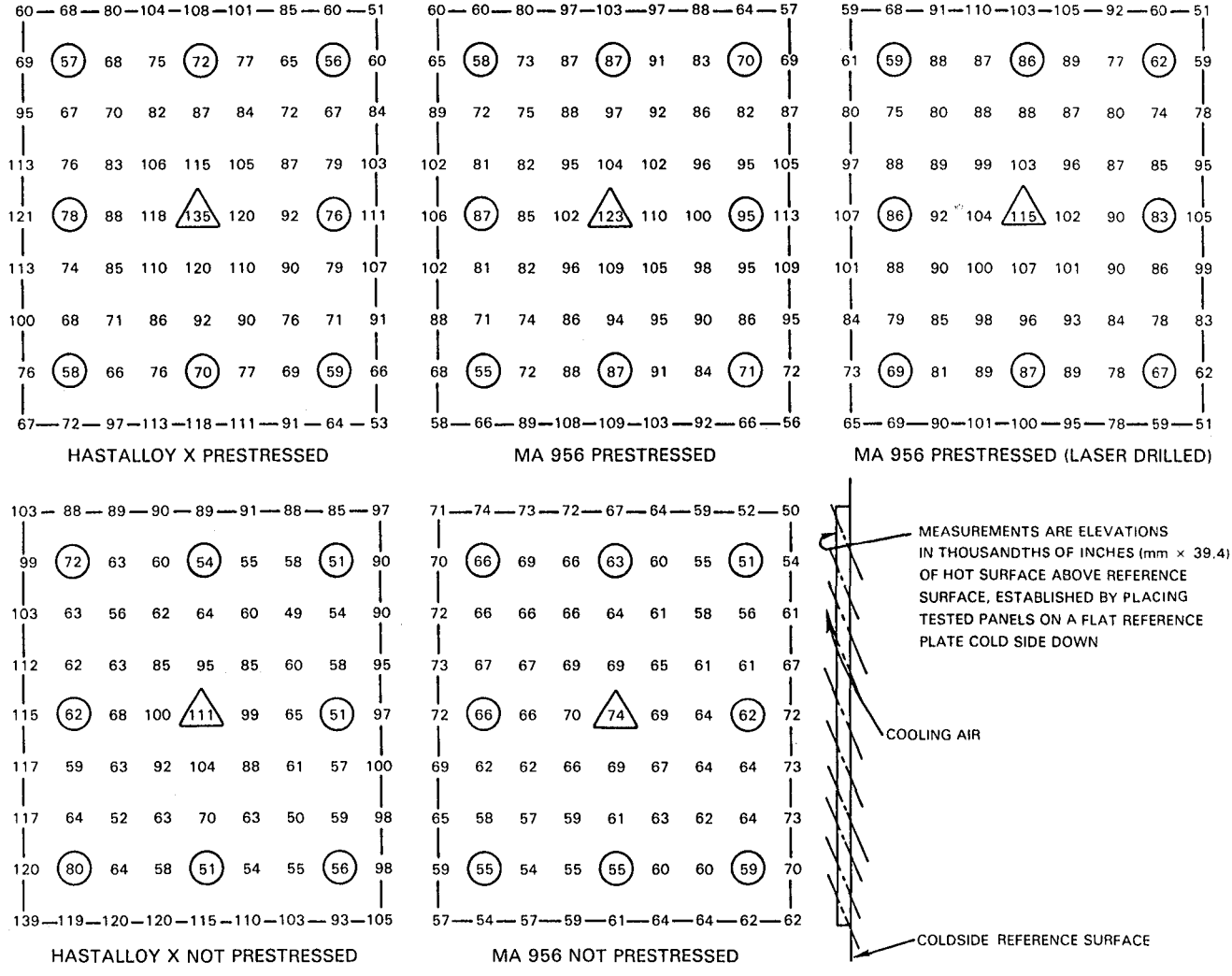

Figure 7-13 Distortion Measurements on Thermal Cycled Transpiration Cooled Subcomponent Plates. Circled numbers represent locations of retaining rivets; triangle indicates location of cold side center post.

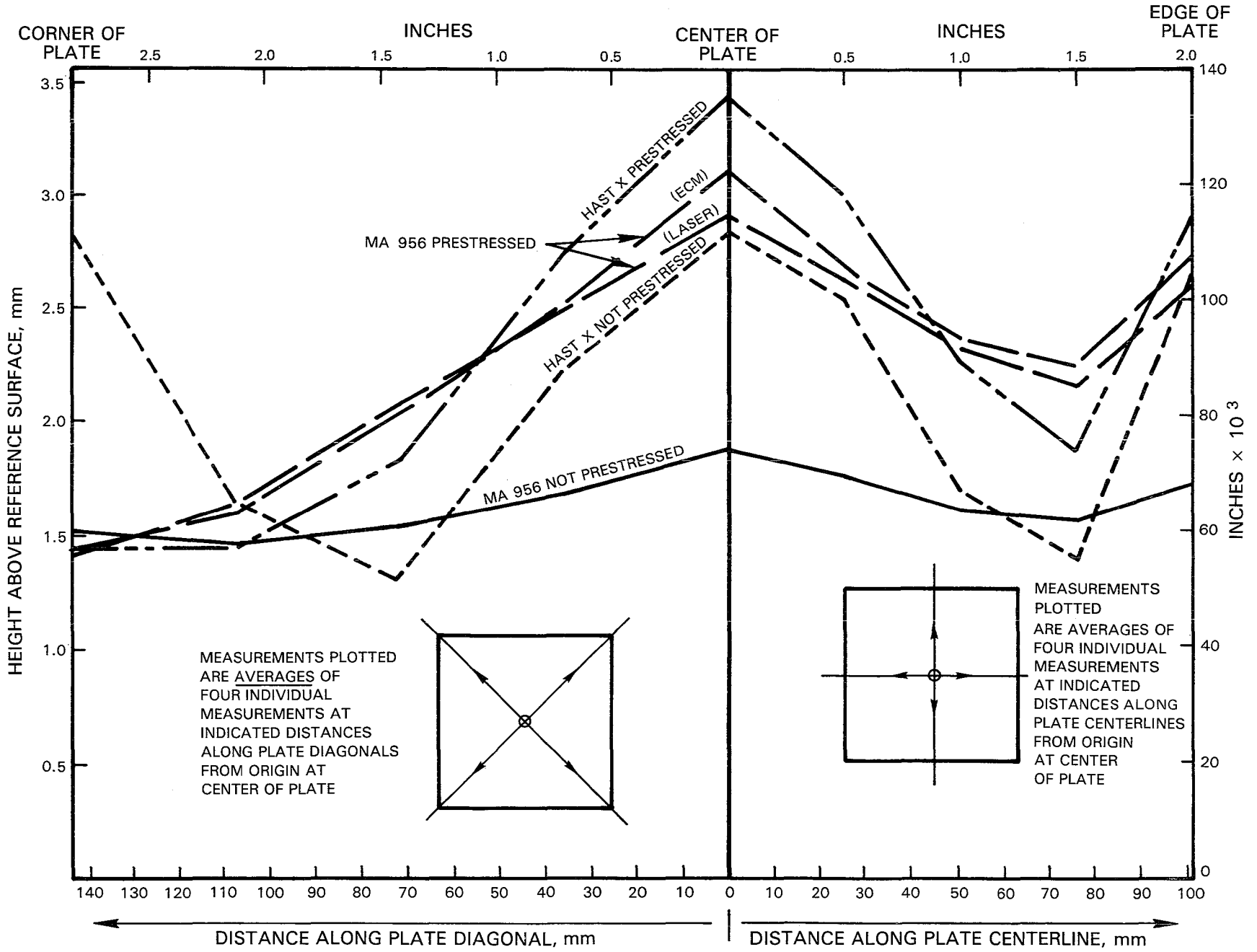

Figure 7-14 Average Distortions Along Centerline and Diagonal of Tested Transpiration Cooled Subcomponent Plates

8.0 TASK VI ENGINE TEST COMBUSTOR LINER

8.1 TASK VIA COMBUSTOR COMPONENT DESIGN

The objectives of this subtask were to select one of the two design concepts evaluated in Task V, and to design and analyze a full scale MA 956 combustor test article for Task VII engine evaluation.

8.1.1 Design Selection

As discussed in prior sections, the two low strain design concepts which were identified as candidates for engine evaluation of oxide dispersion strengthened combustor components were the mechanically attached, film cooled, segmented louver and the transpiration cooled segmented louver. Both of these candidate designs meet the 10,000 cycle thermal fatigue goal as determined by life prediction analyses performed in Task I (Section 3). Neither design exhibited a clear superiority in the component rig tests described in the last section. Selection of the design approach to be used for experimental engine evaluation thus was based on an assessment of the risk associated with each approach. Based on this assessment, the film cooled design was selected because it represented a lower risk in the engine test. This configuration is only a small departure from the conventional combustor design which has accumulated millions of cycles of flight operation and the component test of this design was a good test simulation of predicted operating conditions. These two factors provided a high confidence level for an experimental cyclic endurance engine test of the film cooled design.

8.1.2 Component Configuration

The test vehicle selected for demonstration of MA 956 combustor components is the inner combustor liner of the advanced technology PW2037 engine. A cutaway illustration of this engine, showing the location of the inner liner, is presented in Figure 8-1. Also included in Figure 8-1 is a schematic cross-sectional view of the after (downstream) portion of the inner liner,

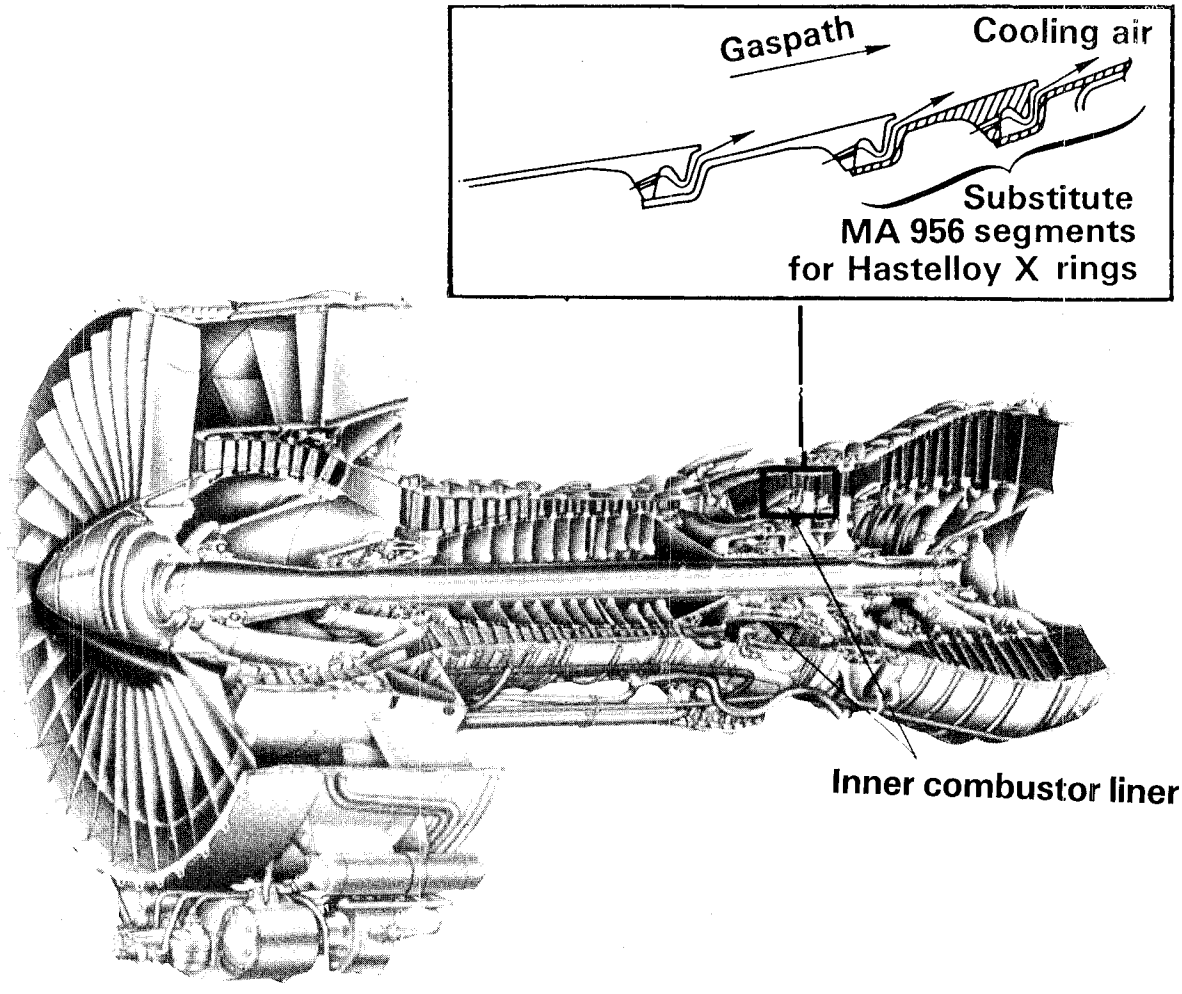

Figure 8-1 Cutaway View of PW2037 Engine Showing Location of Inner Combustor Liner and Schematic Illustration of Aft (downstream) End of Current Inner Liner Design Including Hastelloy X Components for Which MA 956 Segments will be Subsituted.

showing in cross-hatch the current Hastelloy X rings for which MA 956 segments will be substituted. Based on a review of several candidate configurations, the segmented MA 956 louver geometry illustrated in Figure 8-2 was developed to replace the last two Hastelloy X louvers with a single hoop consisting of MA 956 segments attached to a Hastelloy X shell. The configuration of an individual MA 956 segment is illustrated in Figure 8-3. There are twenty-four (24) segments around the circumference of the combustor, with each segment covering an arc of 15° and having a circumferential length of approximately 8-1/4 cm (3 1/4 inches). These segments are attached to the upstream end of the shell by brazing of a mechanically interlocked tab and in downstream locations by MA 956 rivets which are designed to permit in-plane motion of the ODS panel. The interlocked upstream braze attachment, which operates in a relatively cool location, is designed to retain the panel even in the event of complete failure of all downstream rivets.

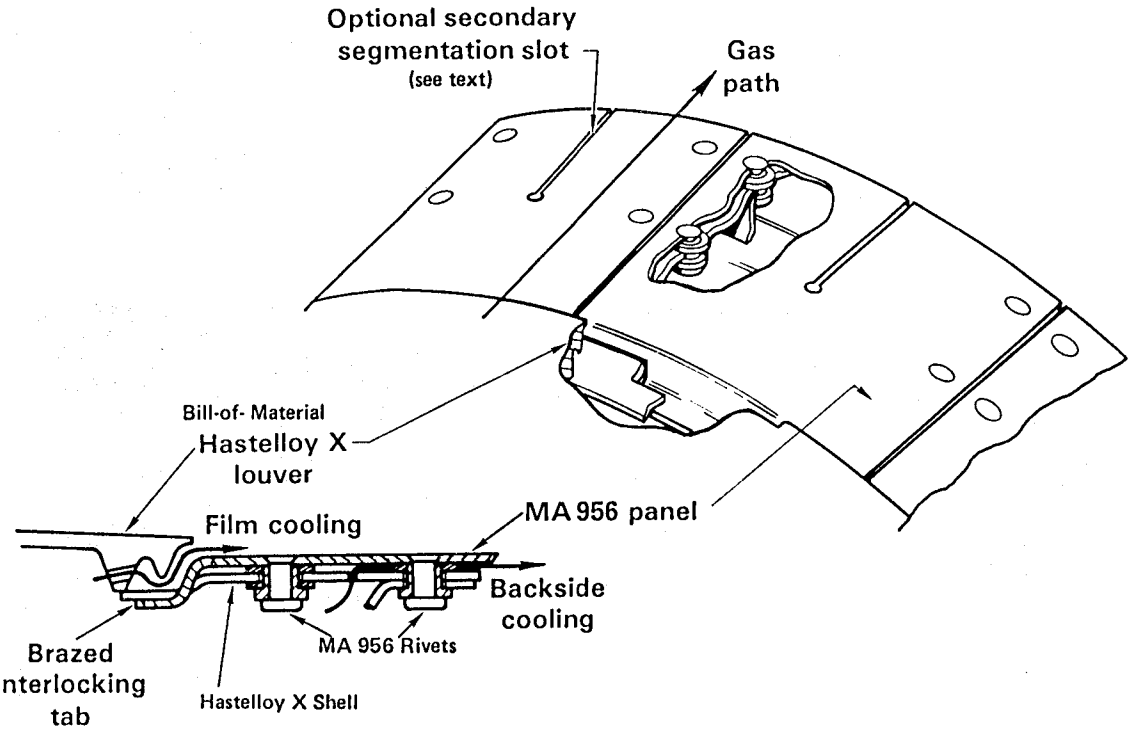

Figure 8-2 Schematic Illustration of Segmented MA 956 Louver Design Configuration Which will Replace the Last two Continuous Hastelloy X Louvers in the PW2037 Inner Combustor Liner

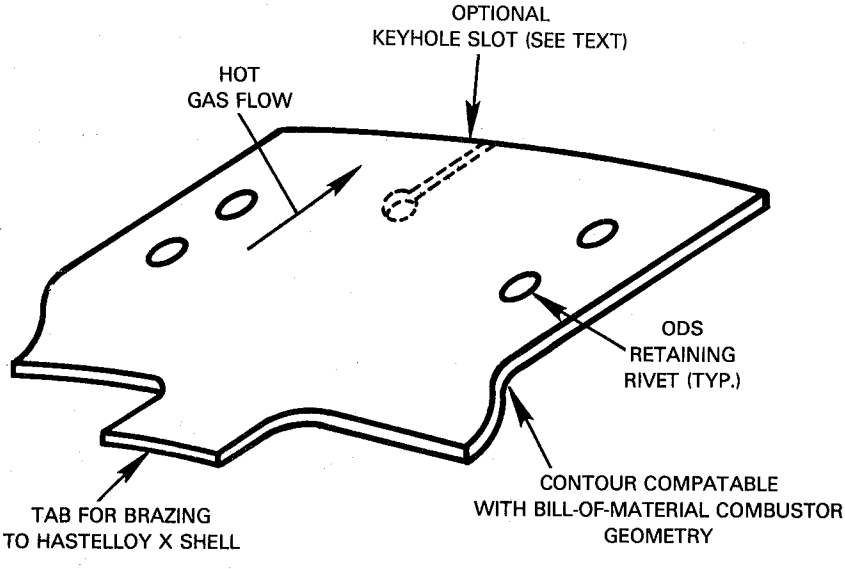

Figure 8-3 Schematic Illustration of MA 956 Combustor Segment Configuration

8.1.3 Thermal Analysis and Cooling Configuration

The design illustrated in Figures 8-2 and 8-3 provides an MA 956 panel of about 3.8 cm (1-1/2 inches) axial length, which is similar to the panel size evaluated in the Task V structural LCF tests. A primary concern with this design was the feasibility of replacing the last two Hastelloy X louvers shown in Figure 8-1 with a single longer panel and still maintaining adequate film cooling at the segment lip. Preliminary calculations indicated that unacceptably high lip temperatures would develop in the absence of backside cooling. Effort thus was directed toward development of an optimized backside cooling configuration to maintain acceptable louver lip temperature, particularly in hot streak locations. Based on thermal analysis of several candidate backside cooling schemes, the configuration shown in Figure 8-4 was selected as providing the maximum cooling effectiveness with the available cooling air. Thermal analysis of this configuration (Figure 8-5) indicates an average lip temperature of 921°C (1690°F), which is well within the capability of the MA 956 alloy. The maximum hot streak temperature, on the order of 1066°C (1950°F), also is considered to be within the capability of MA 956, providing stress levels are maintained below the point at which significant creep deformation would occur. Analyses of panel stresses are addressed in a later section.

8.1.4 Stress Analysis of Braze Attachment

Prior to completion of the thermal analysis described above, a preliminary finite element stress analysis was conducted to address a concern regarding the potential for development of large thermal stresses in the sharply bent joggle and brazed attachment tab areas at the cold (upstream) end of the panel. As this effort was performed prior to development of the optimized cooling geometry, these stresses were investigated by conducting a preliminary three-dimensional finite element analysis using an extremely severe set of hypothetical operating conditions involving a realistic 899°C (1650°F) average panel temperature with an extremely hot 1121°C (2050°F) hypothetical hot streak imposed on the center of the panel as shown in Figure 8-6.

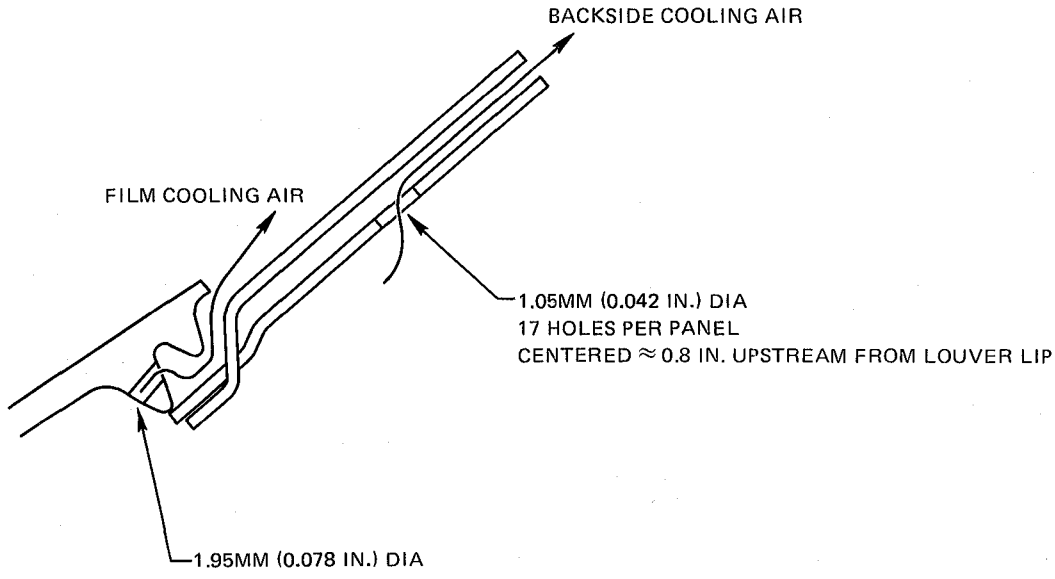

Figure 8-4 Cooling Configuration Selected for MA 956 Combustor Panel.(Note: rivets omitted for clarity)

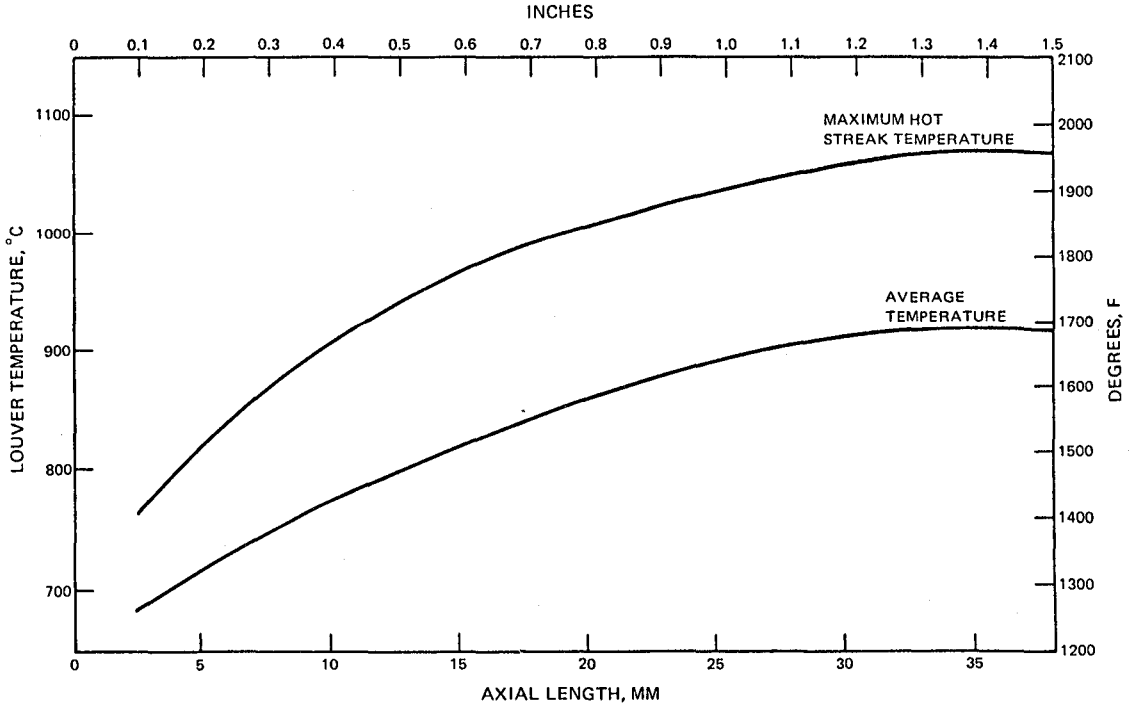

Figure 8-5 Calculated Temperature Distribution Along the Length of MA 956 Segment Operating in PW2037 Combustor (Gaspath side - see text for through thickness gradients).

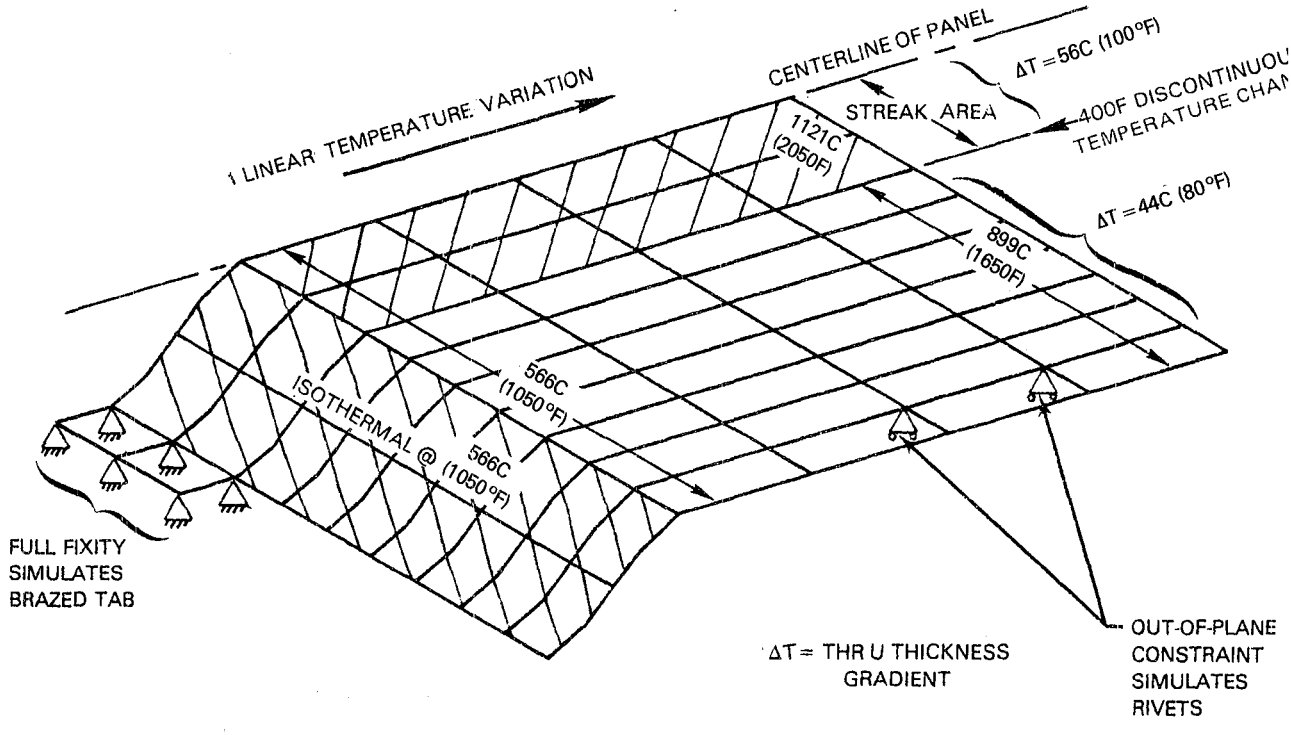

Figure 8-6 Finite Element Model used to Perform Preliminary Thermal Distortion and Stress Distribution Analysis in MA 956 Combustor Segment. Note only half of the panel is analyzed.

For this preliminary analysis, a linear axial temperature gradient was assumed. The circumferential gradient was assumed to be a step function at the junction between the hot streak and the nominal temperature area. To simulate the maximum potential for thermal distortion, the upstream end of the panel was held isothermally at 566°C (1050°F) and through thickness gradients ranging from 17°C to 56°C (30 to 100°F) were imposed on the panel. The panel was fully constrained at the brazed tab location and was constrained out-of-plane only at four arbitrarily selected hot rivet locations.

Results of this analysis show relatively little thermal distortion, on the order of 0.05 - 0.075 mm (2-3 mils), in the hot section of the panel, coupled with an upward (toward the gas stream) defection on the order of 0.25-0.275 mm (10-11 mils) at the outboard edge of the cold joggle (Figure 8-7). The elastic stress distribution resulting from this thermal distortion (Figure 8-8) indicates relatively low stresses, on the order of 41 to 58 MPa (6000 to 8400 psi) in the cold joggle region except for the sharp corner where the attachment tab meets the panel, where a relatively high concentrated stress above 100 MPa (15,000 psi) was found. As no effort was made to minimize stress

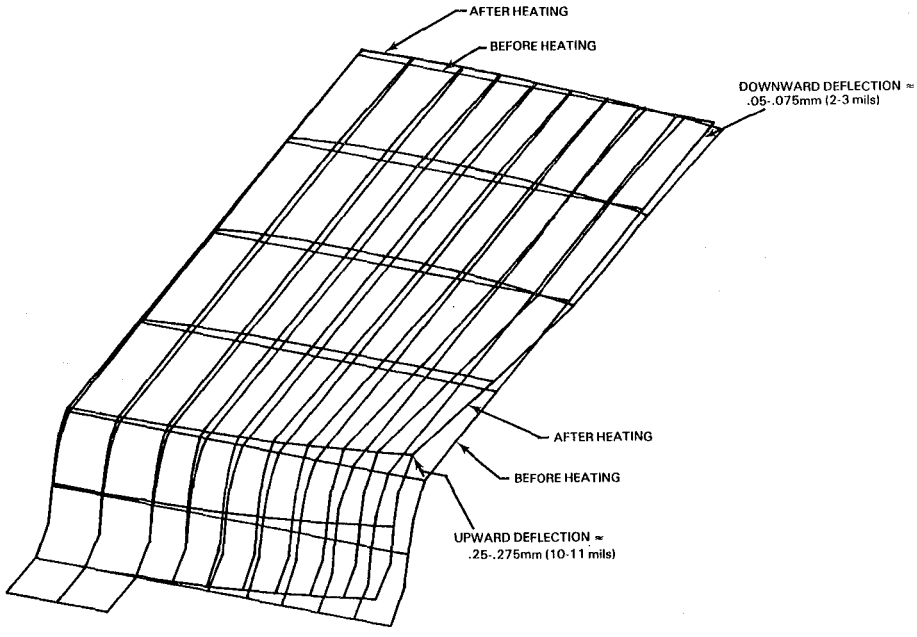

Figure 8-7 Thermal Distortion Calculated for Figure 8-6 Boundary Conditions Applied to MA 956 Segment. Note that distortions are exaggerated for clarity.

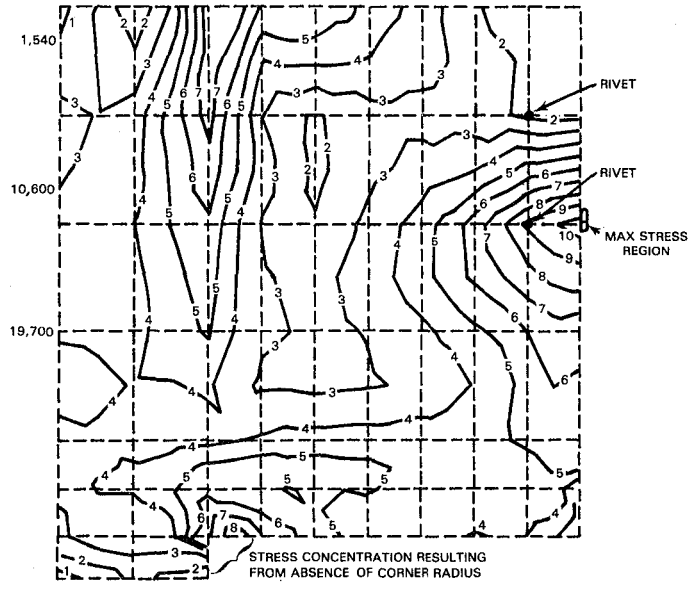

CALCULATED STRESS LEVELS

	MPA	PSI
1	-0-	-0-
2	10.8	1540
3	26.3	3810
4	41.9	6080
5	57.5	8340
6	73.0	10,600
7	88.9	12,900
8	104.0	15,100
9	119.9	17,400
10	135.7	19,700

Figure 8-8 Mises (effective) Stress Distribution Calculated for Figure 8-6 Boundary Conditions Applied to MA 956 Segment.

concentrations in this initial analyses, this stress concentration was not considered to be of concern because the actual part would be radiused at this location. Even in the absence of a radius, this stress is less than one half the yield strength of MA 956 in the 566C (1050°F) temperature range. Based on the above analysis, the brazed tab upstream attachment method was judged acceptable for attachment of MA 956 panels in the PW2037 combustor.

8.1.5 Rivet Placement and Stress Analysis

Based on the preliminary analysis described above, which confirmed the viability of the brazed upstream attachment concept, additional analyses were performed to optimize the location of rivets and to determine loads for rivets placed at the optimum locations. The initial step in this analysis was to repeat the centerline hot streak analysis using boundary conditions such as those shown in Figure 8-6, but with the rivet constraints eliminated. The objective of the "free panel" analysis was to identify locations of minimum out-of-plane deflections, where minimum out-of-plane loads would be imposed on rivets whose primary function is to constrain out-of-plane deflections. Based on preliminary information developed in the previously described thermal optimization study, which was performed concurrently with this analysis, a non-linear axial temperature gradient similar to that shown in Figure 8-5 was used for this analysis. To provide conservative results, this analysis was conducted with the 899°C (1650°F) nominal and 1121°C (2050°F) maximum streak temperatures used for the brazed tab analysis described previously.

Results of this analysis, Figure 8-9, indicate that the unconstrained panel deflects radially inward (away from the hot gas path) in most locations. This result suggests that out-of-plane loads carried by the rivet-spacer attachment configuration illustrated in Figure 8-2 will be compressive in most locations, thus alleviating concern regarding the ability of the rivets themselves to sustain tensile loading. Based on these results, it was elected to place one rivet just on the compressive side of the point on plane 4 where no deflection was calculated, with the other rivet being located in plane 2 in axial alignment with the first rivet, as shown in Figure 8-9.

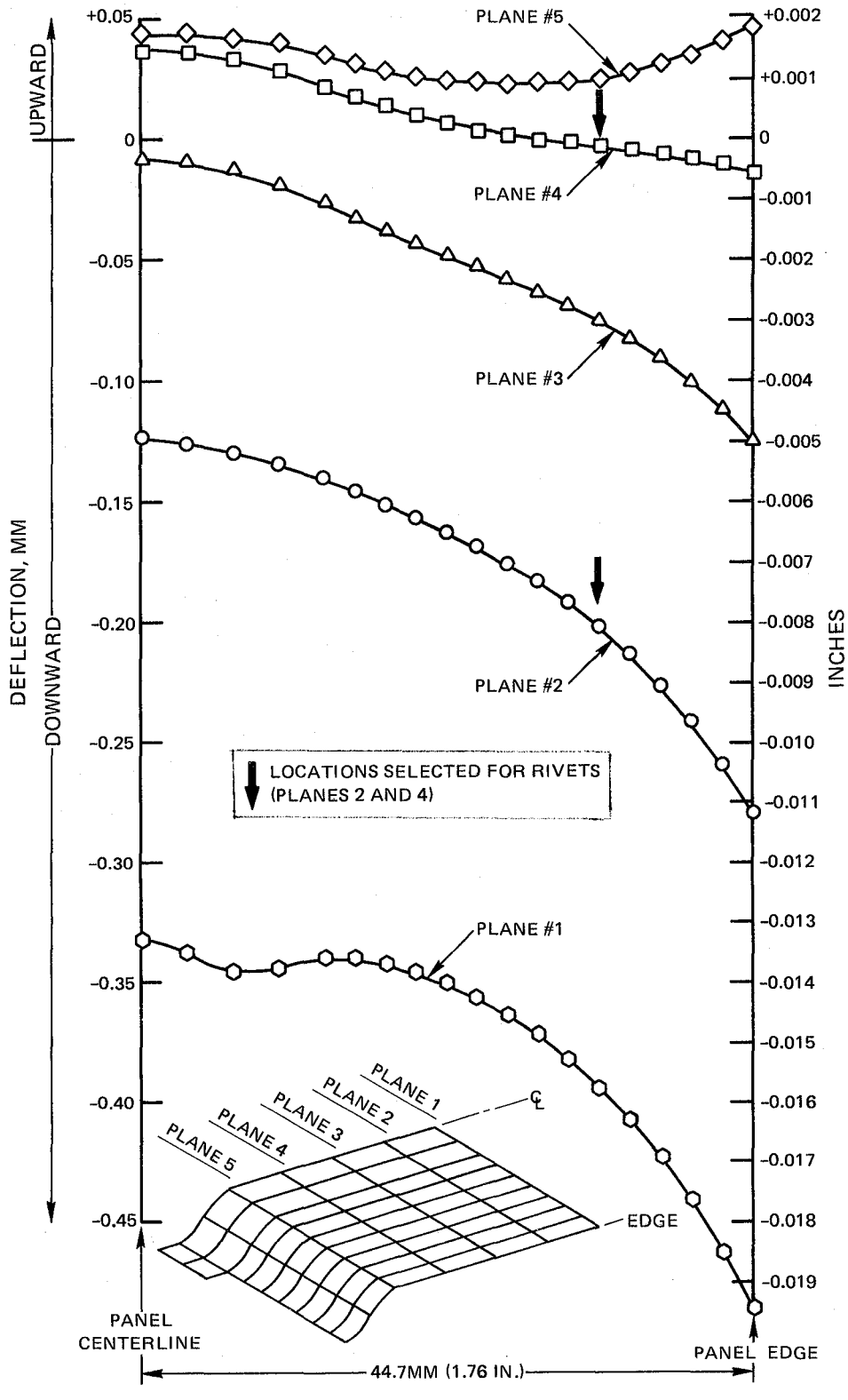

Figure 8-9 Out-of-Plane Free Panel Deflections with Centerline Hot Streak

Using the specific rivet locations described above, two additional analyses were performed to determine deflections and rivet stress levels in a panel constrained out-of-plane at the optimized rivet locations. The first of these analyses was identical to the free panel analysis described above except for the addition of the rivet constraints. The second analysis was conducted to evaluate panel deflections and rivet stresses for the case of a hot streak located at the edge instead of at the center of the panel. Deflections calculated from these two analyses, Figures 8-10 and 8-11, indicate a substantial reduction of panel deflections for the centerline hot streak case, as compared to the free panel case. Deflections for the edge streak case are similar to the centerline streak case both in character and magnitude. These extremely small deflections are highly desirable to minimize perturbation of cooling air flows which are established based on the un-deflected geometry.

Rivet loads calculated for the two cases (Table 8-I) are on the order of 5 kg (11 pounds) or less. Using the standard rivet configuration shown in Figure 8-12, a 5 kg (11 lb) out-of-plane load results in a negligibly small shear stress on the order of 1.9 MPa (275 psi). This result clearly substantiates the viability of the selected attachment configuration.

8.1.6 MA 956 Segment Stress Analysis

Stress distribution in the MA 956 segment was analyzed for the optimum rivet placement using the optimized cooling configuration illustrated in Figure 8-4 and the resulting temperature distribution shown in Figure 8-5. A preliminary review of segment stresses associated with the overtemperature streak panel deflections calculated for the rivet analysis (Figures 8-10 and 8-11) suggested that louver lip stresses might exceed the capability of MA 956 alloy. Because of this concern, two segment configurations were analyzed, one with and the other without the optional 2.5cm (1 inch) secondary segmentation slot illustrated in Figures 8-2 and 8-3.

Boundary conditions used for the detailed three-dimensional finite element stress analysis are shown in Figure 8-13. These boundary conditions are based on the predicted temperature distribution shown in Figures 8-5 for a centerline hot streak. Because of the similarity of centerline and edge streak

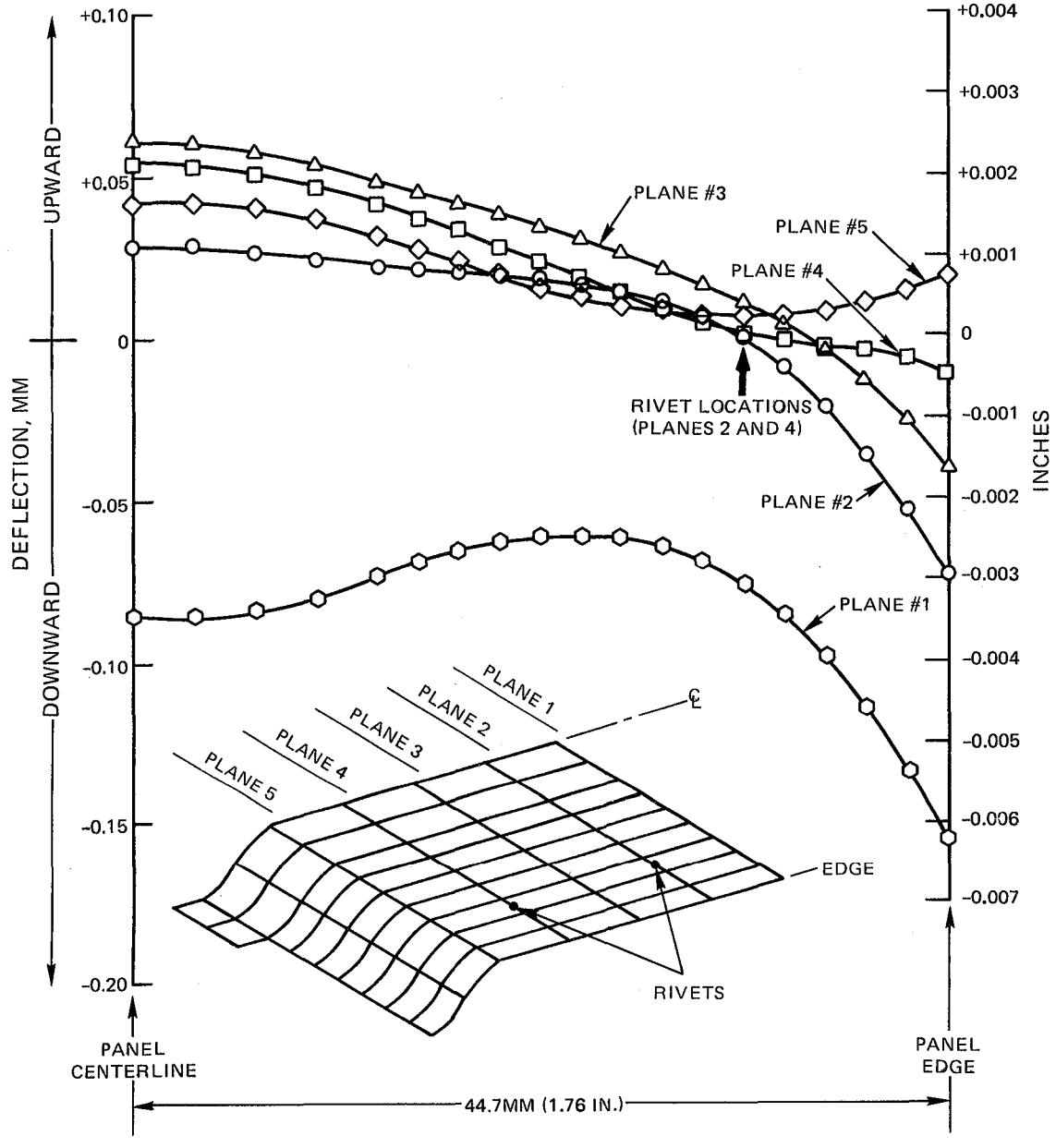

Figure 8-10 Out-of-Plane Panel Deflections with Optimized Rivet Locations-Centerline Hot Streak

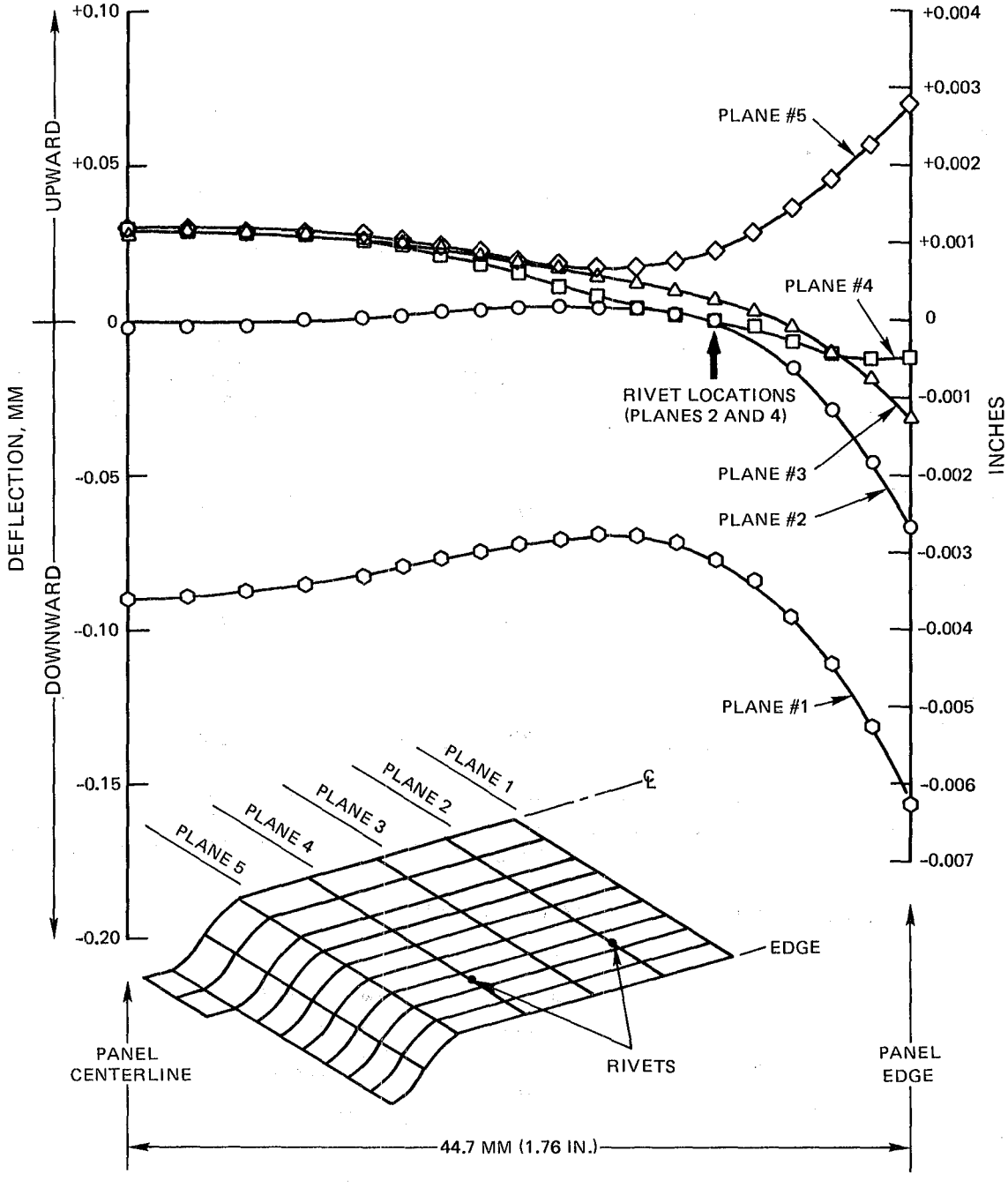

Figure 8-11 Out-of-Plane Deflections with Optimized Rivet Locations - Edge Hot Streak

TABLE 8-I

OUT-OF-PLANE RIVET LOADS FOR MA 956 COMBUSTOR SEGMENT

Hot Streak Location	Rivet Location			
	Upstream		Downstream	
	Kg	Pounds	Kg	Pounds
Panel centerline	3.8	8.4	-1.8	-3.9
Panel edge	4.9	10.9	-2.1	-4.7

TABLE 8-II

FATIGUE CRACK INITIATION LIFE ESTIMATES

Configuration	Strain Range, Percent	(2) Local Wall Temperature °C (°F)	Predicted Crack Initiation Life (Cycles)
(1) Hypothetical Hastelloy X Ring	0.4%	1066 (1950)	350
Unslotted MA 956 Segment	0.252%	1066 (1950)	700
Slotted MA 956 Segment	0.141%	1032 (1890)	10,000

---

(1) Hypothetical ring having the same axial length as the MA 956 segment. Note that this does not represent the Bill-of-Material PW 2037 configuration

(2)Temperature at location of maximum strain.

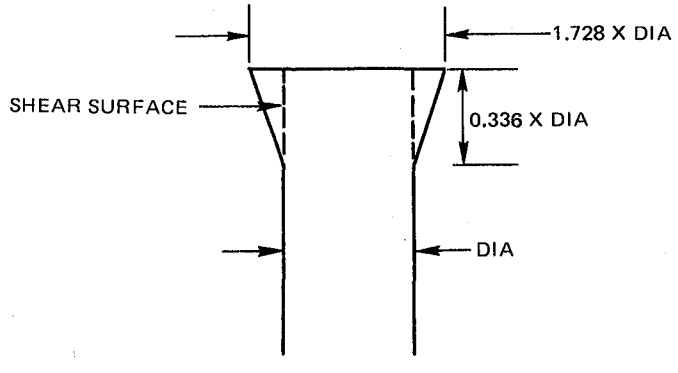

Figure 8-12 Standard Rivet Configuration used to Calculate Rivet Shear Stress

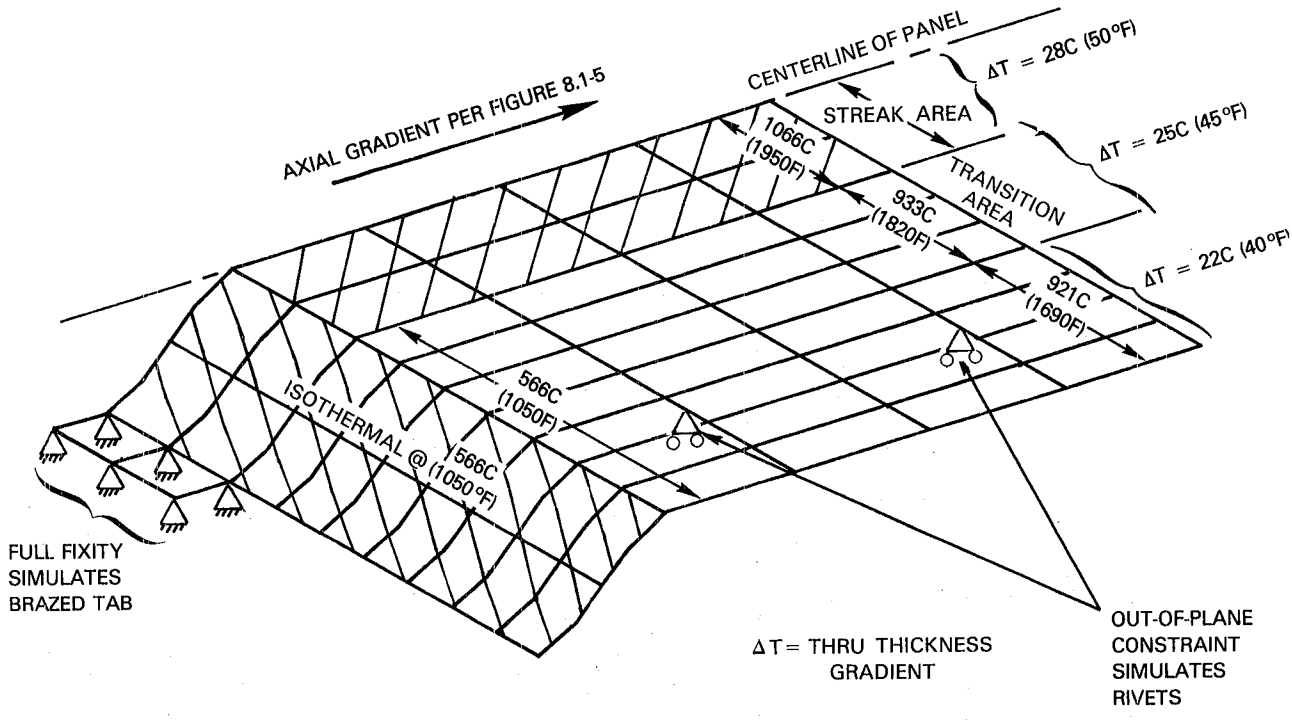

Figure 8-13 Finite Element Model used for Detailed MA 956 Segment Stress Analysis (Note: Only half of panel analyzed).

results in the previously discussed preliminary analysis, only the centerline streak was analyzed in detail. To more realistically simulate circumferential gradients associated with the centerline streak, a transition area was added between the streaked and unstreaked portion of the panel.

Results of these analyses are shown in Figures 8-14 through 8-19. These results are for the cold side of the panel where the highest stresses and strains were calculated. The highest stresses and strains observed in the unslotted panel were circumferentially oriented as shown in Figures 8-14 and 8-15. While the maximum stress of 127 Ma (18.4 ksi) is well within the capability of MA 956 at the 566°C (1050°F) operating temperature where this stress occurs, the lower stress levels on the order of 100 MPa (14.7 ksi) calculated at the hotter panel lip are of concern when compared to the creep strength of MA 956 at the lip temperature. Strains calculated for this location also are of concern. It should be noted, however, that these stress and strain levels are the result of a worst case analysis with the maximum anticipated streak concentrated in the center of the panel, and that more typical operating conditions would be expected to result in much lower stresses and strains.

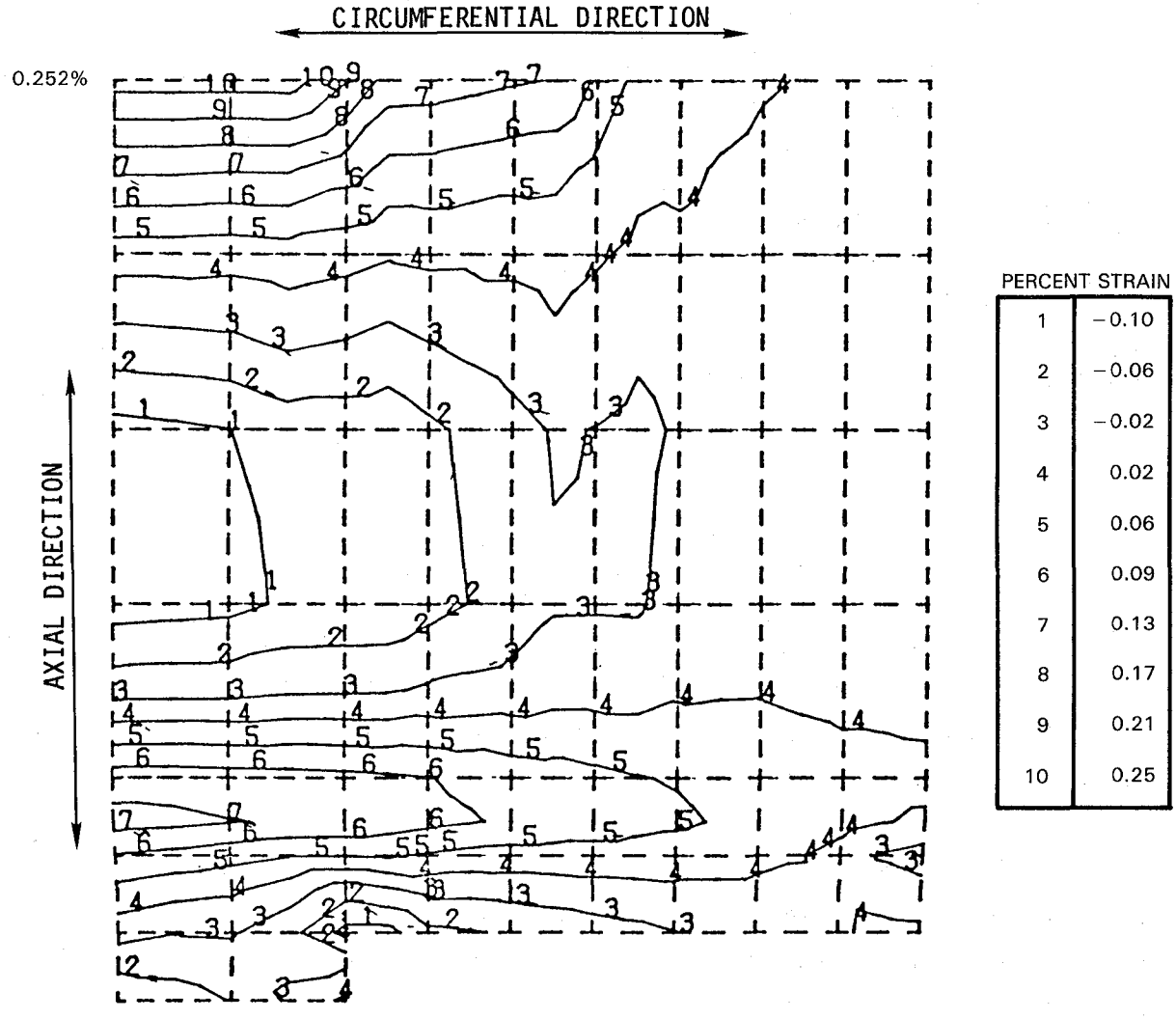

Figure 8-14 PW2037 MA 956 Combustor Segment Cold Side Circumferential Strain Distribution - Unslotted Panel

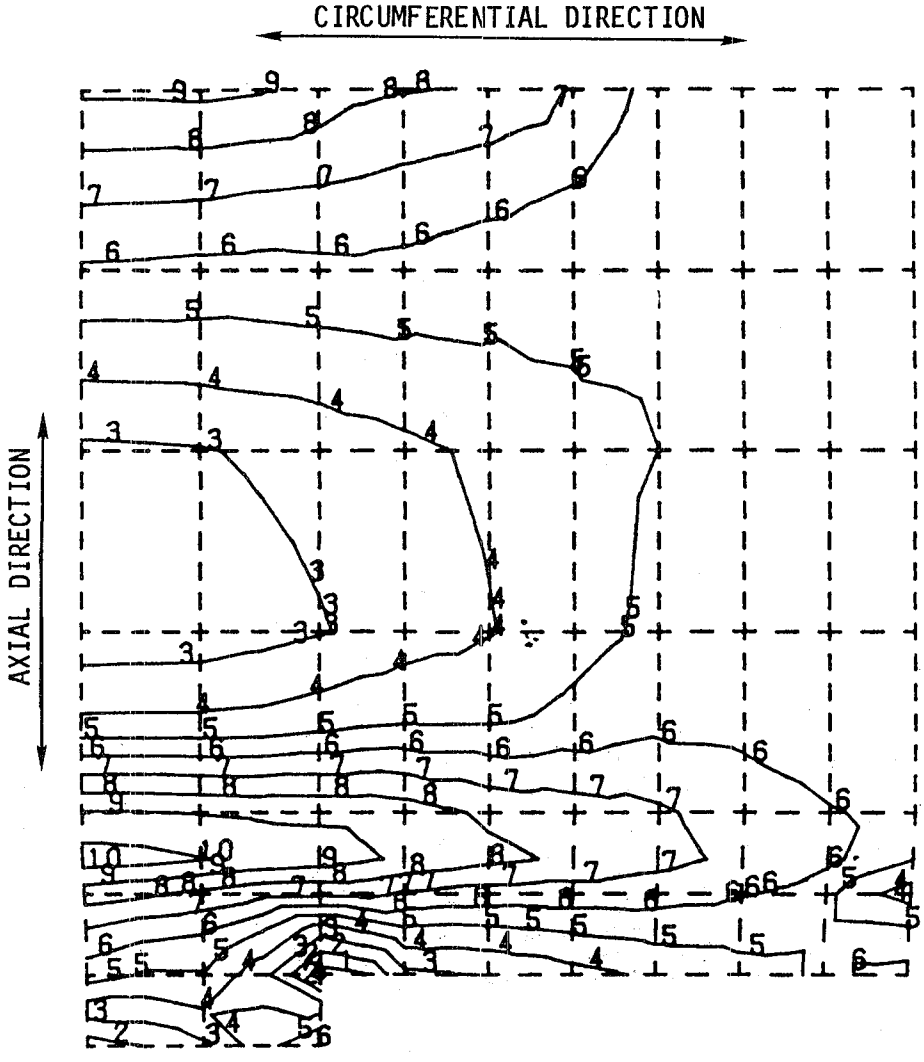

CALCULATED STRESS

	MPA	KSI
1	−107	−15.6
2	−81	−11.8
3	−55	−8.0
4	−29	−4.2
5	−3	−0.5
6	23	3.3
7	49	7.1
8	75	10.9
9	101	14.7
10	127	18.4

Figure 8-15 PW2037 MA 956 Combustor Segment Cold Side Circumferential Stress Distribution - Unslotted Panel

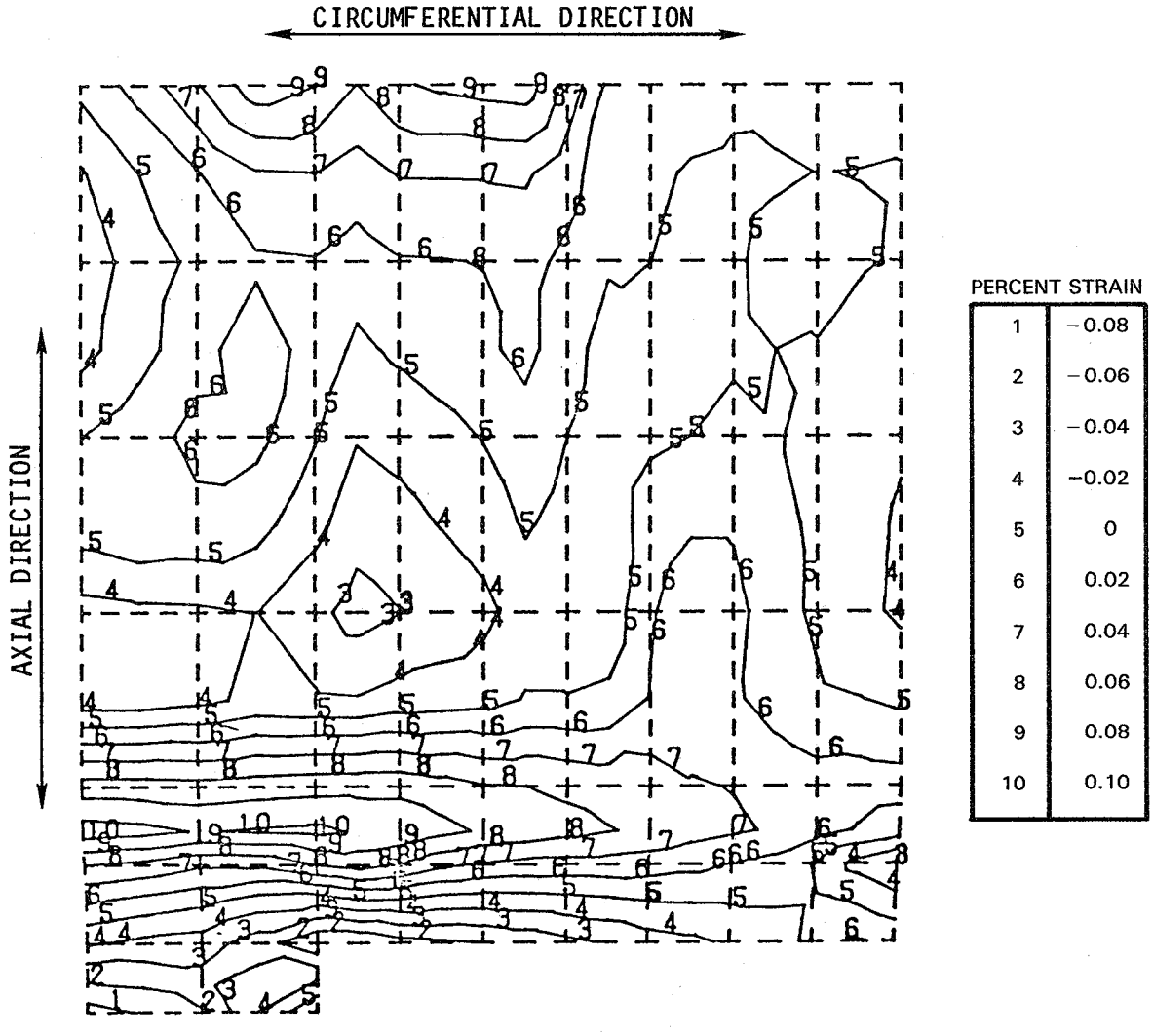

Figure 8-16 PW2037 MA 956 Combustor Segment Cold Side Circumferential Strain Distribution for Panel Having Secondary Segmentation Slot

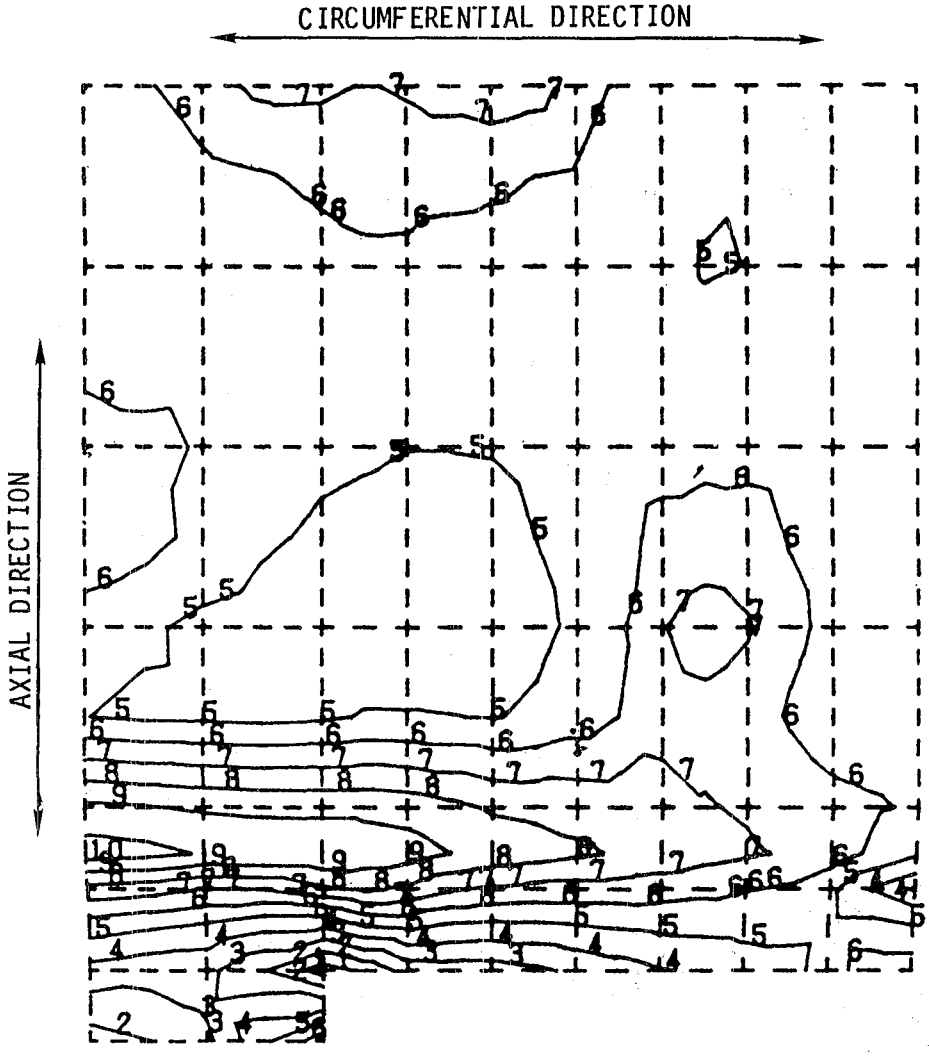

CALCULATED STRESS

	MPA	KSI
1	−82	−11.9
2	−63	−9.1
3	−43	−6.3
4	−24	−3.5
5	−4	−0.6
6	15	2.2
7	35	5.1
8	54	7.9
9	74	10.7
10	94	13.6

Figure 8-17 PW2037 MA 956 Combustor Segment Cold Side Circumferential Stress Distribution for Panel Having Secondary Segmentation Slot

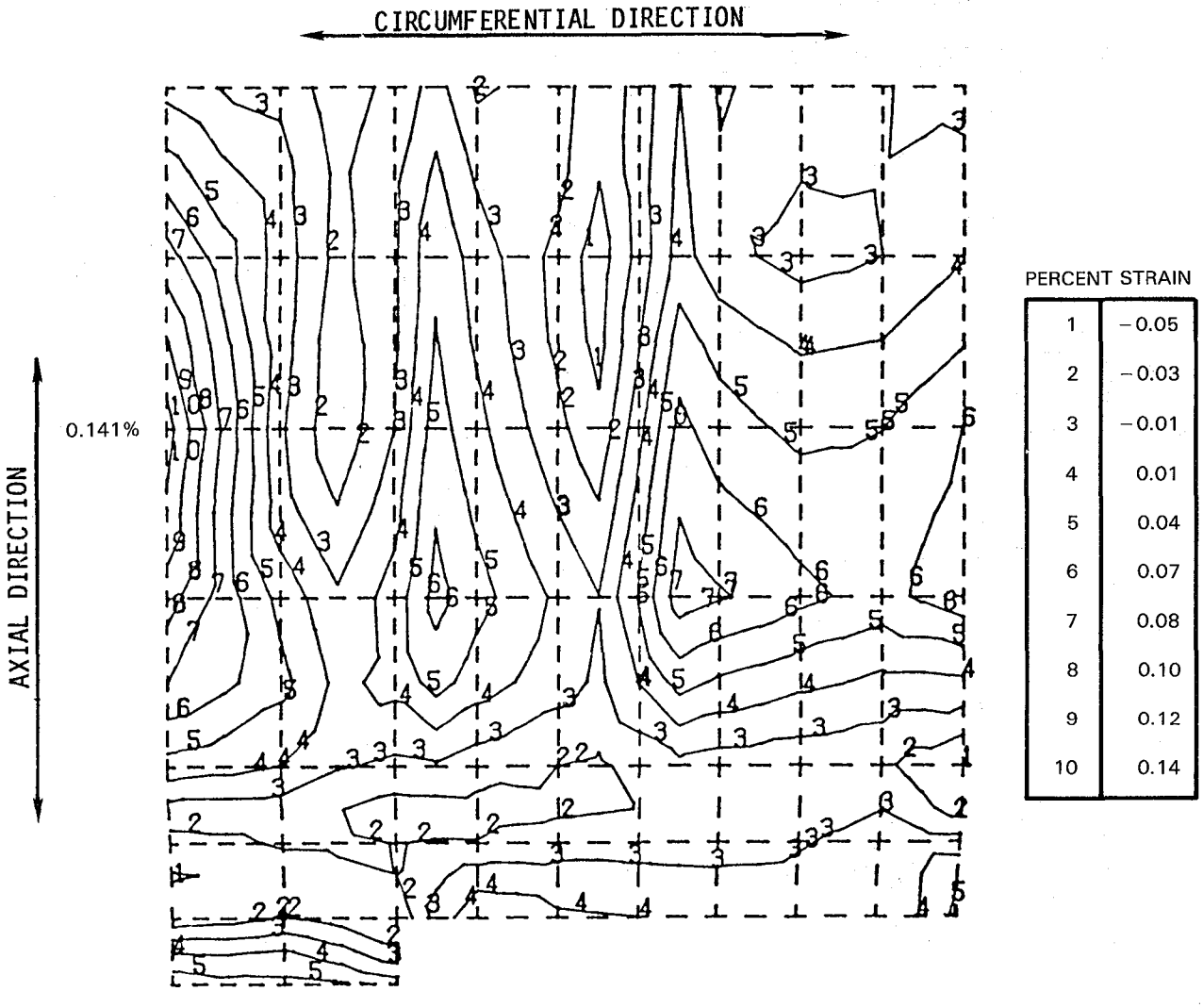

Figure 8-18 PW2037 MA 956 Combustor Segment Cold Side Axial Strain Distribution for Panel Having Secondary Segmentation Slot

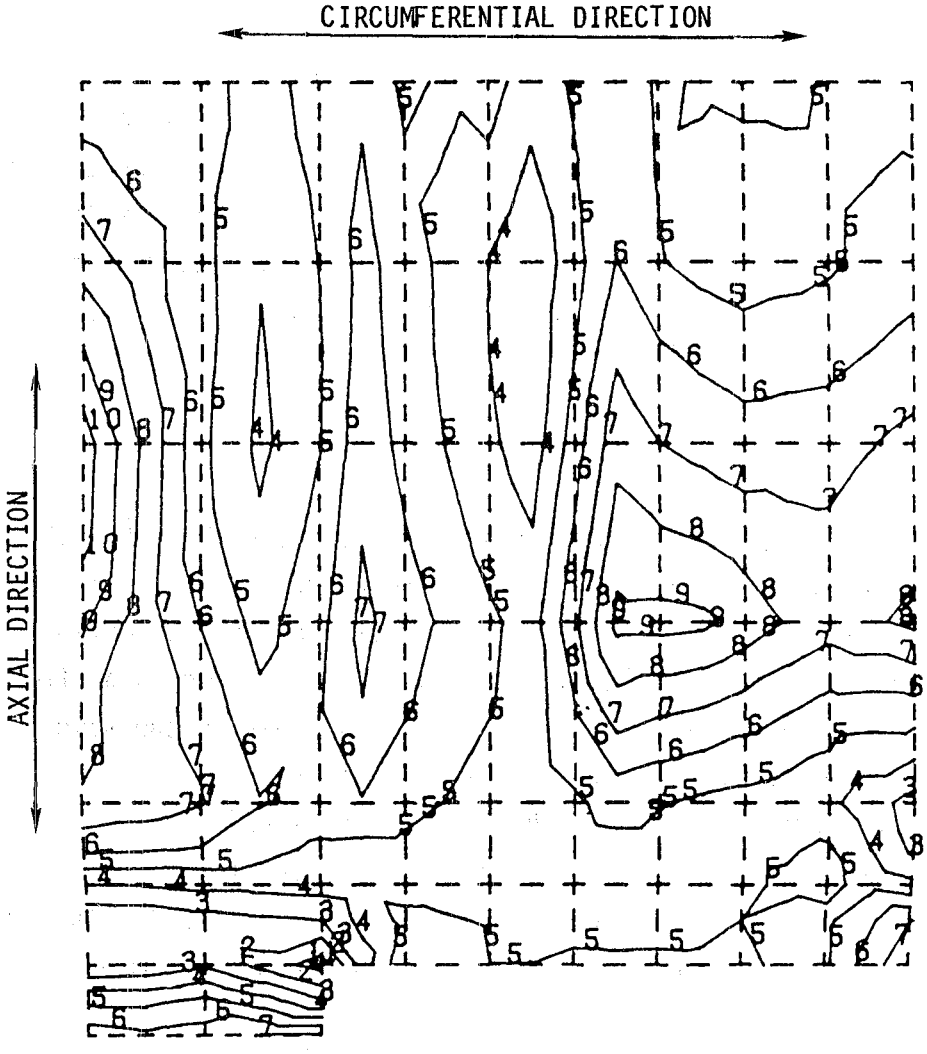

CALCULATED STRESS

	MPA	KSI
1	−63	−9.2
2	−48	−6.9
3	−32	−4.7
4	−17	−2.4
5	−1	−0.2
6	14	2.1
7	30	4.4
8	45	6.6
9	61	8.9
10	76	11.1

Figure 8-19 PW2037 MA 956 Combustor Segment Cold Side Axial Stress Distribution for Panel Having Secondary Segmentation Slot

Circumferential strains and stresses calculated for the panel with the added secondary segmentation slot are shown in Figures 8-16 and 8-17. Both the maximum and the lip stresses for this configuration are much lower than for the panel which does not have the secondary segmentation slot, and are well within the capability of MA 956 alloy. As opposed to the unslotted panel where axial stresses were relatively low, the double segmented panel exhibits relatively high but acceptable levels of axial strain and stress adjacent to the root of the secondary segmentation slot (Figures 8-18 and 8-19). No effort was made in the analysis to simulate relief of concentrated strain at this location. As the detailed design of this segmentation slot will incorporate a radius at the root, the strain and stress levels in this location are expected to be lower than calculated.

8.1.7 Predicated Material Performance

Using the strain distributions calculated above, together with the materials properties generated in Tasks III and IV, as input to the life prediction system described in Section 3, the fatigue crack initiation life estimates shown in Table 8-II were made. Included for purposes of comparison is a life prediction for a hypothetical Hastelloy X full hoop louver having the same axial length as the MA 956 segment. It must be emphasized that this hypothetical louver does not represent the Bill-of-Material PW2037 configuration, which is composed of two shorter louvers occupying the same axial space (See Figure 8-1). For reasons discussed below, comparative fatigue life analysis of a Hastelloy X segmented construction was not performed.

The results in Table 8-II indicate that the slotted MA 956 segment meets the program goal of 10,000 cycle life, even for the worst case streak analysis. The worst case life of the unslotted panel is considerably lower, but still above that of a hypothetical Hastelloy X ring. As explained below, fatigue life comparison with a Hastelloy X segment was not possible because the conventional alloy segment fails by creep distortion before fatigue life is exhausted.

Out-of-plane distortion is an important degradation mode for combustor liner components. Excessive distortion can alter cooling characteristics and exacerbate the effect of hot spots. With normal operating conditions, full hoop combustors are not "free" to deflect under thermal loading. This constraint leads to large strains and consequently failure by fatigue cracking. The segments, on the other hand, have free edges that can deflect and potentially cause cooling perturbations. Thus it is important to observe the predicted distortion of the MA 956 segments. As shown in Figure 8-20, the distortions predicted for the ODS component design are small and are judged acceptable with regard to flow distortion. Based on the low calculated stress levels (Figures 8-15, 8-17, and 8-19), these deflections are not expected to increase significantly as a result of creep during engine operation. While a similar analysis was not performed on Hastelloy X, stresses in this alloy would be expected to be of the same order as those in the ODS segments, based on the somewhat higher expansion coefficient and lower modulus. Using this assumption, the life of a Hastelloy X segment of design similar to the MA 956 segment would be expected to be significantly less than 100 cycles, with failure occurring by gross creep distortion and consequent restriction of cooling air.

Based on the life prediction results discussed above, the segmented MA 956 combustor design incorporating a secondary segmentation slot appears to be a satisfactory design for evaluation of MA 956 in the PW 2037 combustor. The capability of the un-slotted design appears to be marginal in a worst case streak condition, but may be adequate under most probable operating conditions. Based on the very conservative nature of the analysis, which was performed with a projected PW 2037 temperature distribution that was much more severe than nominal, a decision was made to evaluate a mixed hoop containing sixteen(16) slotted and eight(8) unslotted panels in the Task VII engine test. Construction of the engine test hardware is described in the next section.

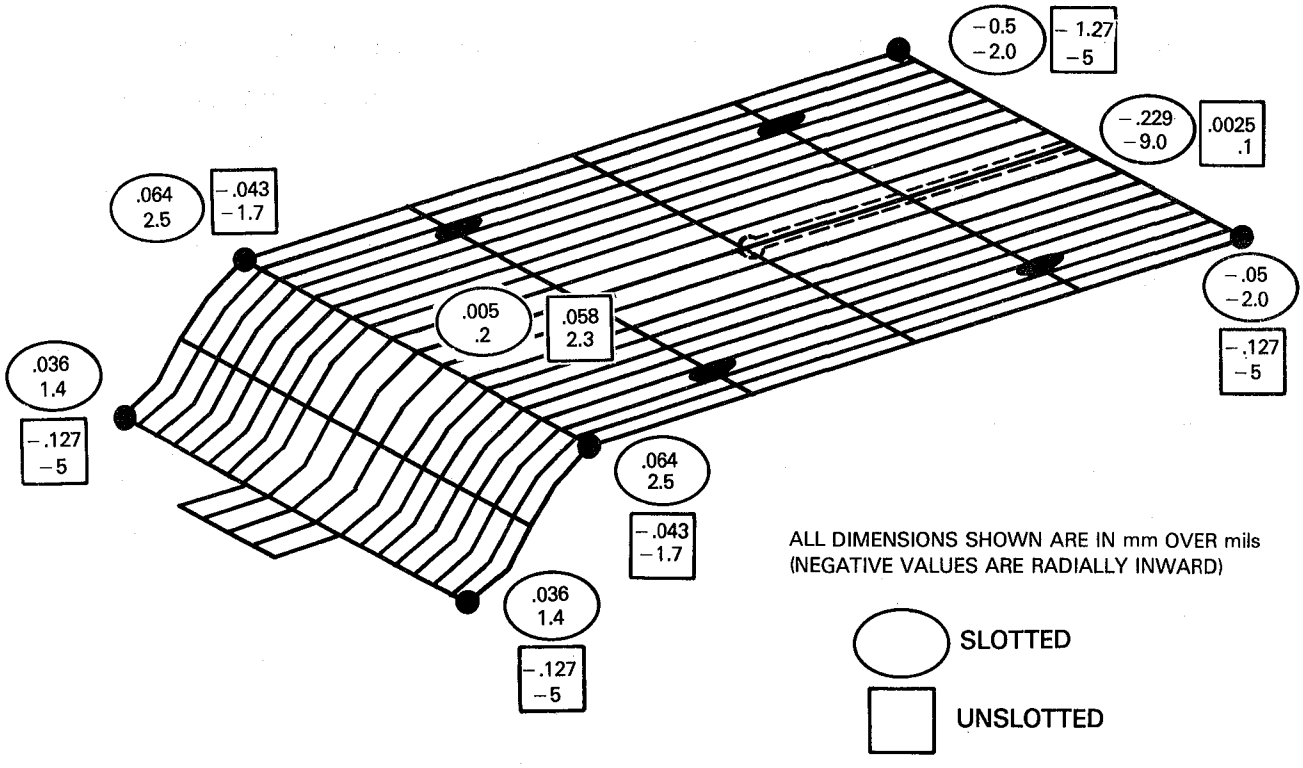

Figure 8-20 Radial Deflections at Full Power for Unslotted and Slotted Geometries

8.2 TASK VI B - COMBUSTOR COMPONENT FABRICATION

8.2.1 Introduction & Summary

The objective of this subtask was to fabricate the combustor test article described in the last section in preparation for engine evaluation in Task VII. Figure 8-21 shows the specific components in the test article subassembly. Item 1 in this sketch is the adjacent upstream bill of material louver. Item 3 is a Hastelloy X sheet metal ring which supports the MA956 segments. This ring is welded to the adjacent louver at the upstream end and is mechanically attached to adjacent engine structures at the downstream end.

Description of the test article construction will focus primarily on fabrication and assembly of the MA956 segments. Fabrication of other components was accomplished using standard shop methods, including fabrication of the MA956 rivets, which were machined from lot ZDBC barstock as discussed in Section 5.3

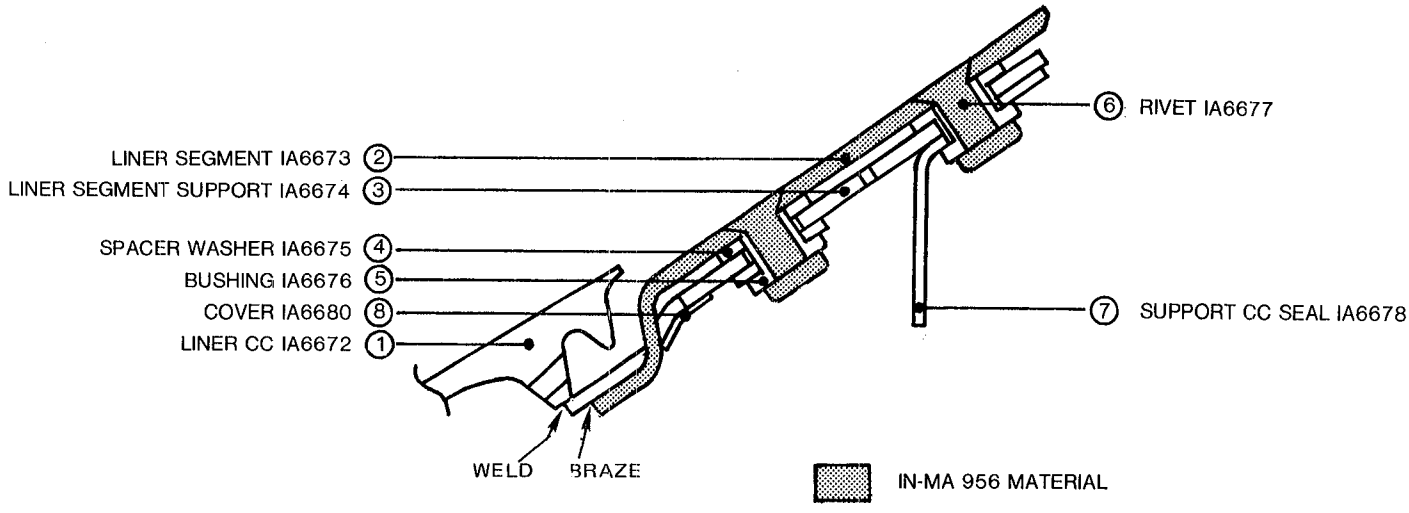

Figure 8-21 Assembly Sketch of MA 956 Combustor Component for PW2037 Task VII Engine Test

MA956 segments were formed with the sheet rolling direction oriented circumferentially. Two approaches were evaluated for MA956 segment fabrication. The first approach, which involved spin forming of MA956 lot XBB-004 sheet, was not successful. Despite earlier indications of good formability (Section 4.4), this material failed in cleavage at relatively small deformations during spinning. The second approach was stamping. Because all available lot XBB-004 material was consumed in the initial spinning trials, another commercially produced lot of MA956 sheet, designated ZCDY, was procurred and used for subsequent segment fabrication. As-received tests on this lot showed good formability, comparable to as-received lots ZDEW and XBB-004. Following initial stamping trials, in which the lot ZCDY sheet also failed in cleavage at relatively small deformations, a set of parameters was identified for stamping of MA956 panels without cracking (Figure 8-22).

Following resolution of panel forming problems, assembly of the combustor test article was completed with no further difficulties. Photographs of the finished MA956 sub-assembly, joined to the adjacent upstream Hastelloy X louver, are shown in Figure 8-23. Remaining to be completed prior to engine tests are joining of the subassembly to the balance of the inner liner and tip grinding of the MA956 louvers, which is performed during engine assembly. These activities presently are awaiting availability of a surplus inner liner and of a suitable PW2037 test engine.

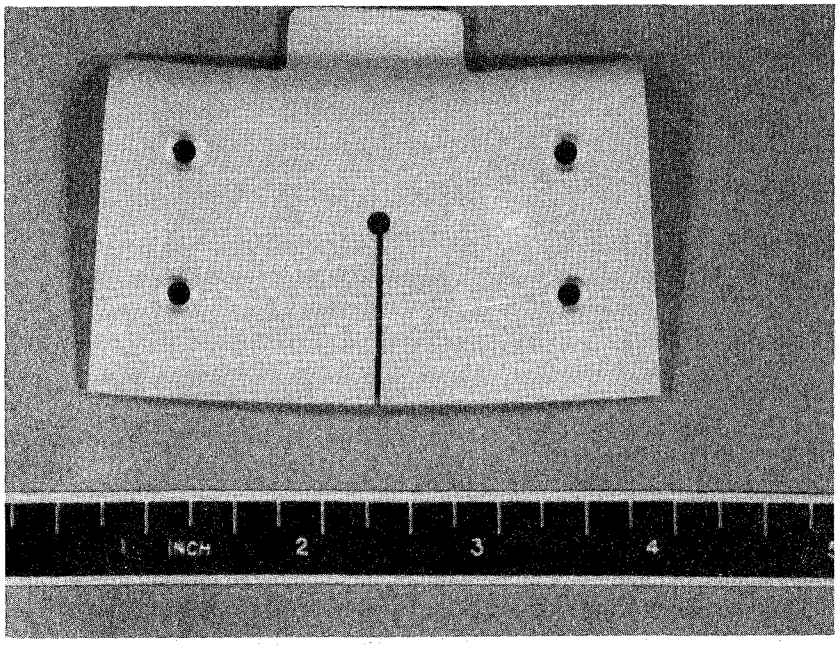

A) COMBUSTOR SEGMENT WITH OPTIONAL SECONDARY SEGMENTATION SLOT

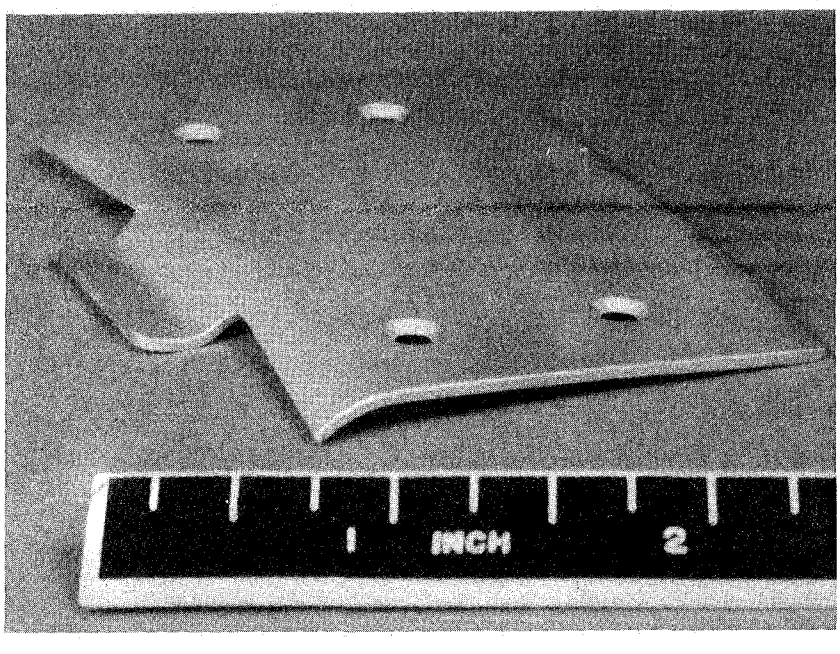

B) UNSLOTTED SEGMENT SHOWING DETAIL OF TAB GEOMETRY

Figure 8-22 Photographs of Finished MA 956 Combustor Segments

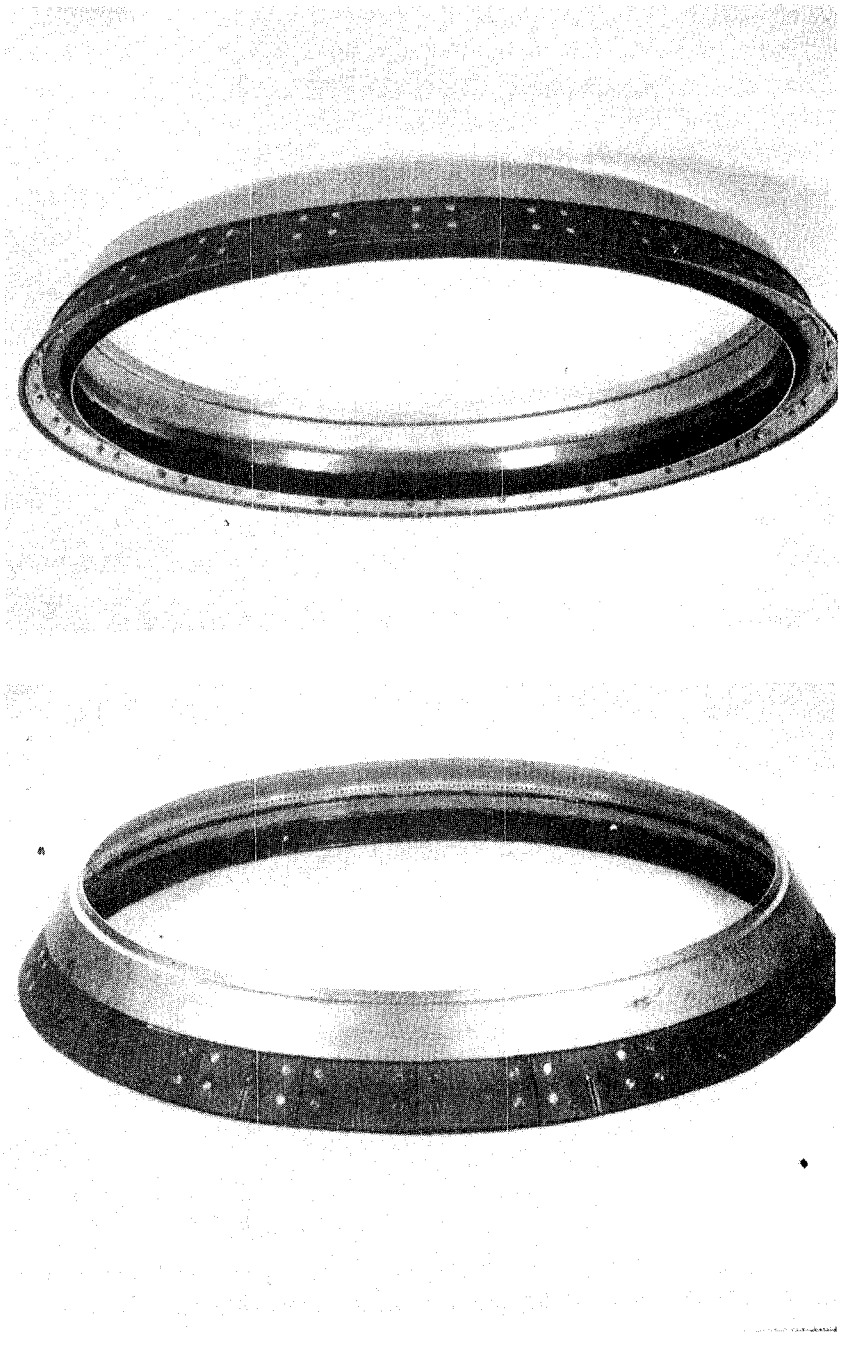

Figure 8-23 Two Views of Finished MA 956 Segmented Combustor Component Joined to Upstream Bill-of-Material Hastelloy X Louver

8.2.2 MA956 Segment Spin Forming Trials

The method which initially was evaluated for fabrication of MA956 segments was spin forming. This method was selected on the basis of the successful spin forming of MA956 rig test segments in Task III (see Figure 5-68). Spin forming trials were conducted on lot XBB-004 sheet described in Section 4.4 and 6. As illustrated in Figure 8-24, this approach involved the fabrication of electron beam welded and stress relieved[1] conical rings which were to be spin formed to the appropriate contour and machined to segments. While the cones were successfully formed and EB welded, the attempt to spin form was not successful. As shown in Figure 8-25, extensive cleavage cracking occurred at realtively small levels of deformation.

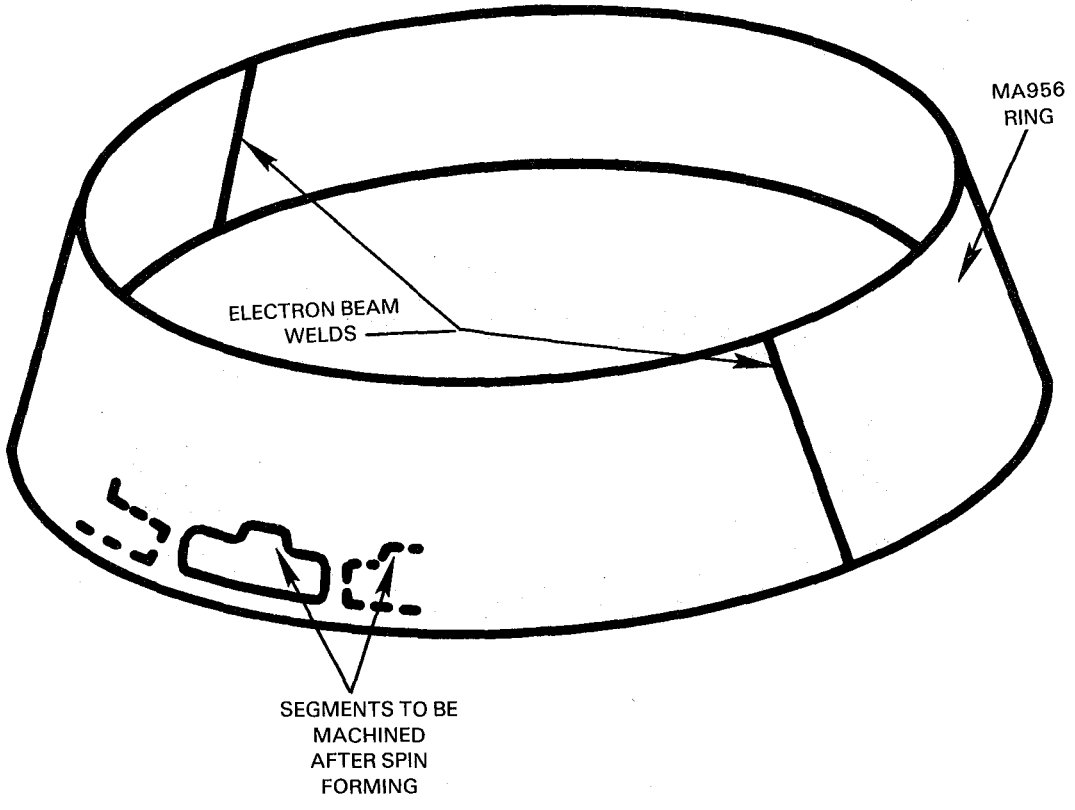

Figure 8-24 Schematic Illustration of the Approach to Spin Forming of MA 956 Segments

---

[1] 1177°C (2150°F) / 1/2 hour/hydrogen.

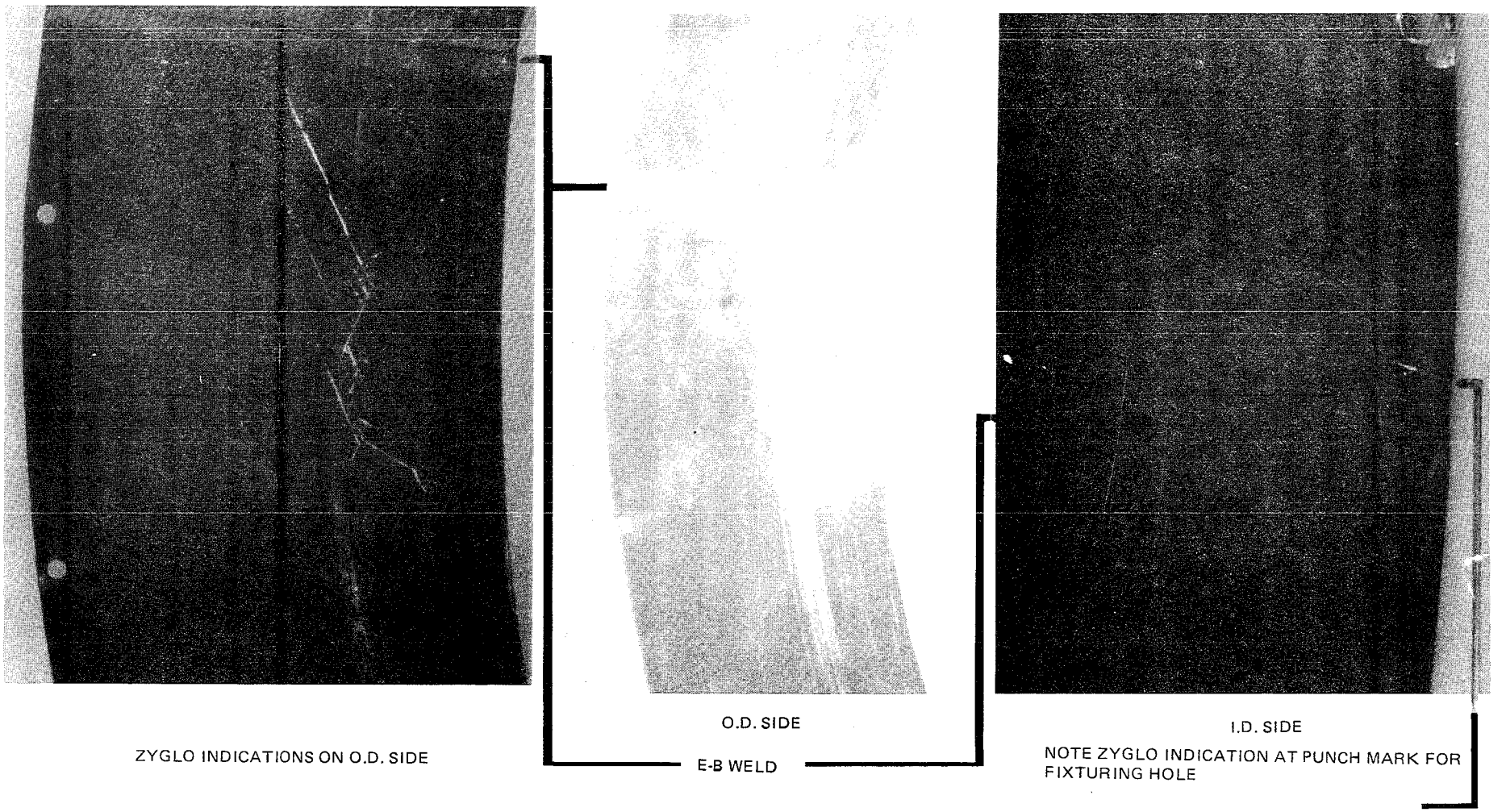

Figure 8-25 Cleavage Cracking Found in Partially Formed MA 956 Spun Ring

As indicated in Tables 8-III & IV, post forming evaluations were conducted by both P&W and INCO in an effort to diagnose the cause of the observed cleavage cracking. Tests at P&W included hardness measurements and Erichson cup formability on cone formed and stress relieved material. Bend and Erichson cup tests were performed at INCO on sections cut from the material which failed in spin forming trials.

TABLE 8-III

P&W MEASUREMENTS OF HARDNESS AND FORMABILITY
OF MA956 LOT XBB-004

	Hardness (Converted to R_C)		Erichson Cup Depth/mm
	Surface	Center	
As Received	21-24	21-24	8.4
Cone Formed and Stress Relieved[1]	29-30	26-28	3.1
Cone Formed, Stress Relieved[1] and polished	-	-	3.1

[1] 1177°C (2150°F)/ 1/2 hour /Hydrogen/Simulated Air Cool.

TABLE 8-IV

INCO MEASUREMENTS OF FORMABILITY ON MATERIAL
WHICH CRACKED DURING SPIN FORMING

	Test Temperature °C (°F)	2T Bend Angle at cracking °	Erichson Cup Depth (mm)
As Formed	20 (68)	51 56 131 148[1]	5.1 5.6
As Formed	100 (212)	150[1]	9.0 9.1
As Formed and Surface Ground	20 (68)	147[1] 150[1]	7.1 9.0

[1] Not cracked.

A review of these results provided no clear explanation for the poor spin formability. Formability clearly was reduced very significantly in the cone formed and stress relieved sheet as compared to as-received material (Table 8-III). While P&W polishing did not significantly alter this result, surface grinding at INCO provided essentially full recovery of formability (Table 8-IV), suggesting a form of oxide-scaled related embrittlement such as that caused by long time thermal exposure (Section 5.1.7.4). However, metallography at INCO indicated that a discontinuous Al_2O_3 scale formed together with some internal Al_2O_3 during the hydrogen stress relief treatment (Figure 8-26). Results reported in Section 5.1.7.4 indicate that exposure embrittlement usually is associated with a tightly adherent oxide scale.

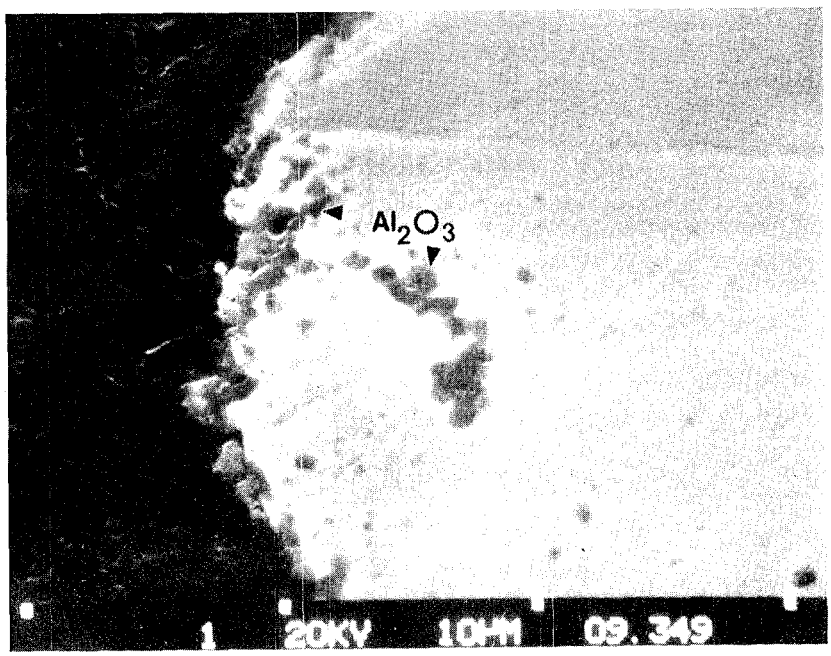

Figure 8-26 Example of Surface and Internal Alumina (Al_2O_3) Formation on MA 956 Lot XBB-0004 after Annealing in Hydrogen for 1/2 Hour at 1177C (2150F). (INCO photo)

A review of these and other results by INCO led to the conclusion that the inconsistent forming behavior of MA956 sheet was a temperature effect. While earlier results indicated that MA956 does exhibit a usable degree of formability at room temperature (Reference 8-1), recent work has shown the ductile-brittle transition temperature (DBTT) of this alloy to be in the vicinity of room temperature (Reference 8-2). As indicated in Table 8-IV, the cone formed and stress relieved material recovered full formability at 100°C

(212°F), with the failure mode in the cup test occurring by ductile shear instead of cleavage at the higher temperature (Figure 8-27). Because of the proximity of the DBTT to room temperature, INCO recently has recommended that all forming of MA956 be done at a minimum temperature of 100°C (212°F)

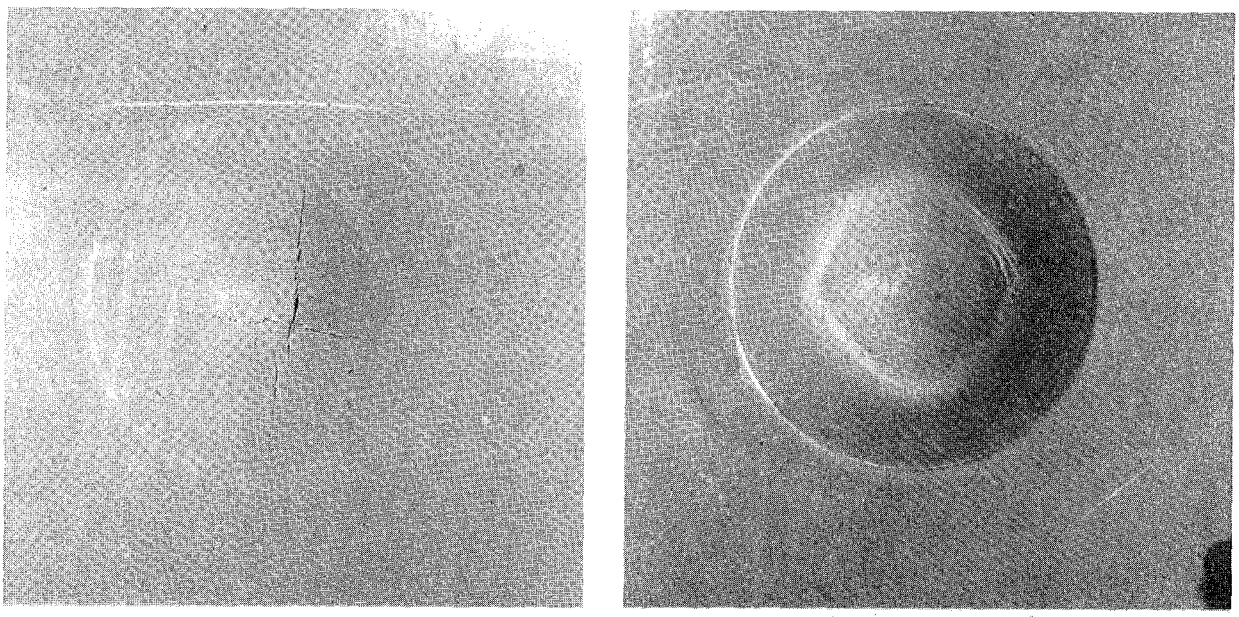

(a) (b)

Figure 8-27 Erichsen Cup Tested Specimens of MA 956 From Cone Formed and Stress Relieved Lot XBB004 Cup Tested at (a) Room Temperature and (b) 100C (212F). Note cleavage cracking and low ductility in (a), and ductile shear fracture and high ductility in (b). (INCO photo)

8.2.3 MA956 Segment Stamping

The second method which was evaluated for fabrication of MA956 segments was drop hammer die stamping. Because this work was done before the need to form MA956 at or above 100°C (212°F) was clearly recognized, all stamping was done at room temperature. Following initial trials in which the effect of blank size on "stampability" was established, this method was successfully used to form fifty-five of the segments shown previously in Figure 8-22. Because all available material from lot XBB-004 was consumed in the previously described spin forming trials, another lot of commercial sheet, designated ZCDY, was procured for this effort. This material was formed in the as-received condition.

A schematic illustration of the die configuration used for stamping is shown in Figure 8-28. The initial approach involved stamping of blanks which were 37% oversize. This standard shop practice reduces potential operational problems with allignment between die and workpiece. As shown in Figure 8-29, these attempts were unsuccessful, with severe cleavage cracking occurring in areas of large deformation. Successive trials with varied die stamp ram speeds in the range of 1.3 to 25mm (0.5 to 10 inches)/minute, did not significantly alter the cracking behavior. Results of Erichson cup tests performed on lot ZCDY before and after the initial die stamping trials (Table 8-V) are considered to be within the range of acceptable formability values for MA956, suggesting that the behavior seen in Figure 8-29 represents an intrinsic limit on the room temperature formability of this alloy. Based on the observations discussed in reference 8-2, it is probable that oversize panel stamping could have been conducted successfully at 100°C (212°F). (This observation also applies, at least in theory, to spin forming. However, the practicality of warm spin forming is open to question.)

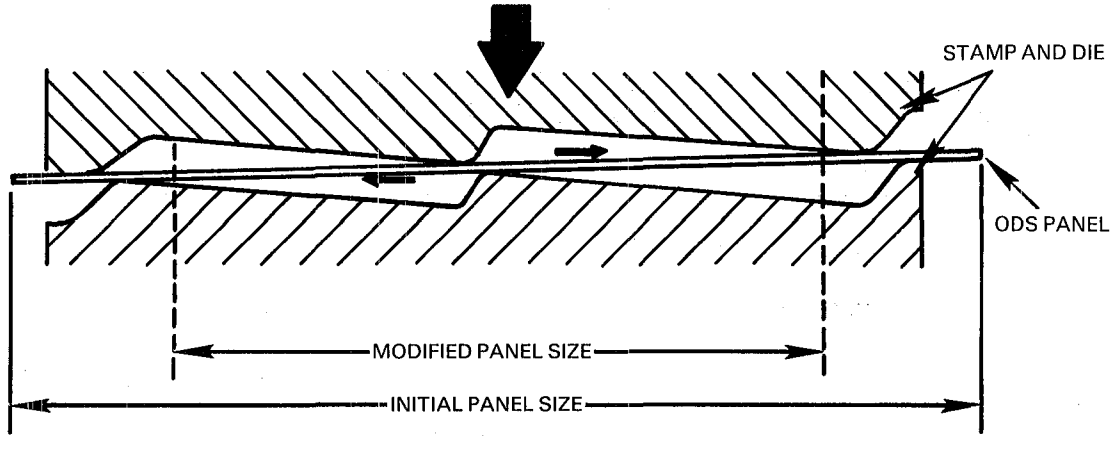

Figure 8-28 Die Configuration used for Drop Hammer Die Stamping of MA 956 Panels

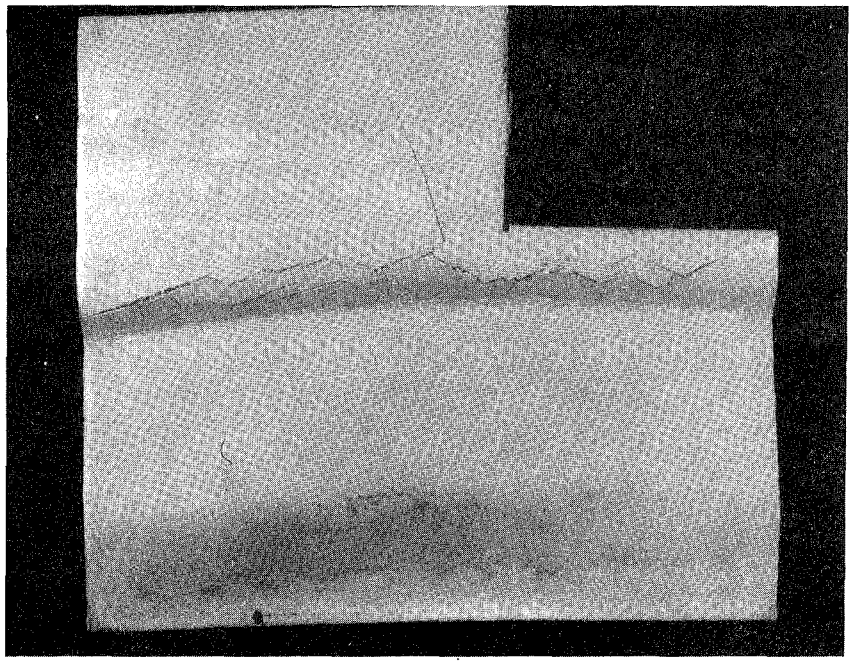

Figure 8-29 Result of Initial Drop Hammer Die Stamping Trials with 37% Overhang. (Note material cut from corner of panel for formability testing - see text).

TABLE 8-V

RESULTS OF ERICHSON CUP FORMABILITY TESTS CONDUCTED ON MA956 LOT ZCDY BEFORE AND AFTER OVERSIZE PANEL STAMPING TRAILS

Material Condition	Erichson Cup Depth, mm
As Received	6.7
Post-Stamp[1]	6.1 to 8.8

1 Post-stamp tests conducted on material cut from flat portion of stamped panel - see Figure 8-29.

The approach which was used to successfully stamp MA956 segments at room temperature involved reducing the blank size to the minimum possible value consistent with the finished part dimensions. This effectively reduced in-plane constraint and altered the distribution of stress to a more favorable state. As indicated by Davidson (reference 8-2), the influence of stress state on ductile-brittle transition behavior is complex and not fully understood;

however, it generally is recognized that the DBTT is higher for more complex states of stress. This observation is consistent with the influence of constraint on the ability to form the MA956 panels.

Rationalizations notwithstanding, the reduction of blank size effectively eliminated cracking and permitted the successful high rate (25mm, 10 inches/minute) stamping of fifty-five MA956 segments with no evidence of cracking in post-stamp Zyglo inspection. Photographs of two of these panels after finish machining are shown in Figure 8-22. A composite photomicrograph of a section through the joggle area of a panel is shown in Figure 8-30. Because of concern regarding the possible role of hydrogen stress relief in the previously noted spin forming difficulties, a single finished panel was stress relieved[1] and cup tested to determine if stress relieving was advisable. Based on a reduction of cup depth to 5.0 mm in this stress relieved panel, it was decided that post-stamp stress relieving of the rest of the panels was not advisable. Note that the panels are effectively "stress relieved" in vacuum during the subsequently described brazing operation.

8.2.4 Combustor Sub-Component Assembly

Construction of the combustor test article shown in Figure 8-23 involved straight forward application of standard shop assembly practices. Prior to initiation of assembly, the MA956 panels were pre-braze cleaned and nickel flashed using the procedures identified in Task III C (Section 5.3). The Hastelloy X support ring (Figure 8-21, Item 3) was pre-braze cleaned using standard shop practice for Hastelloy X. The MA956 segments, together with the Hastelloy X washer and bushings (Items 4 and 5), were hand fitted to the liner with 0.011 mm (2 mil) METGLAS^{R} BNi5 braze foil sandwiched between the MA956 and the Hastelloy X at the appropriate location on the braze tabs. The panels were temporarily bolted through the rivet holes using stainless steel bolts to hold the panels in place during brazing. Following panel assembly, the Hastelloy X support ring (Item 3) was welded to the adjacent upstream bill of material louver (Item 1) and the welded assembly was heated in vacuum (5 x 10^{-4} Torr) for 25 minutes at 1177°C (2150°F), followed by a 982°C

---

1 1177°C (2150°F)/ 1/2 hour / hydrogen.

R Registered Trademark of the Allied Chemical Corp.

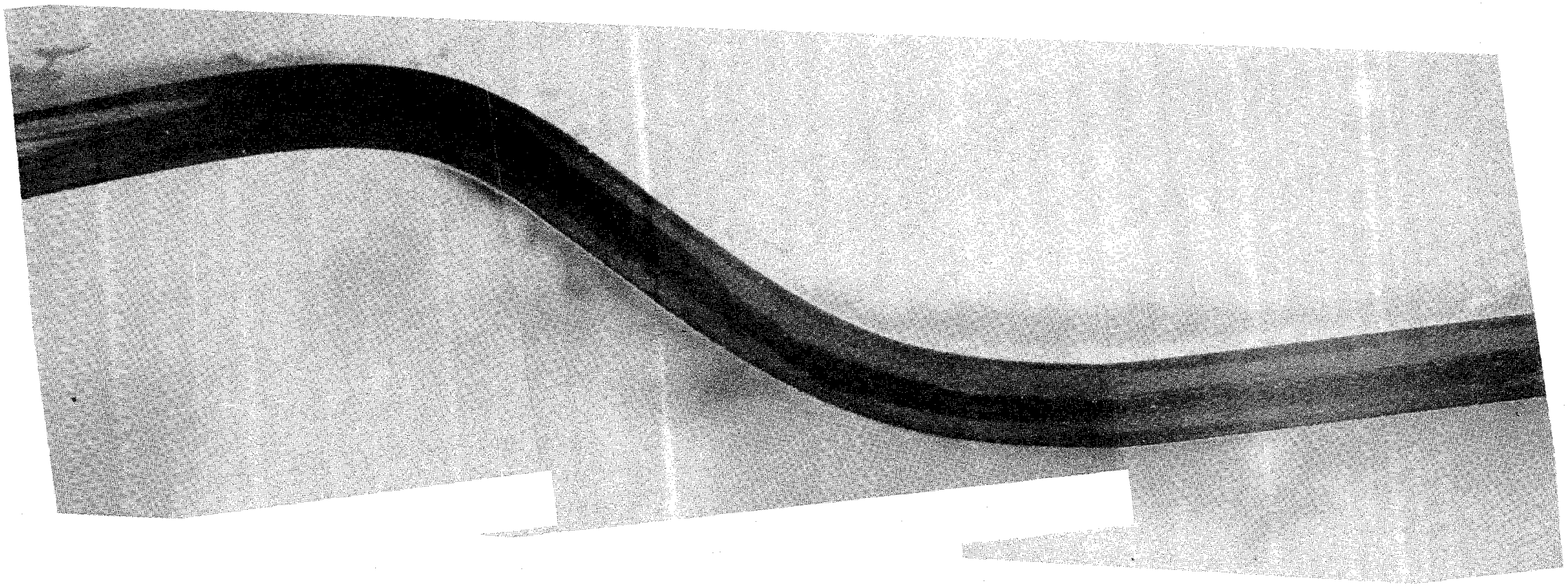

Figure 8-30 Microstructure Observed in Joggle Area of Stamped MA 956 Lot ZCDY Combustor Segment

(1800°F) diffusion treatment to complete brazing of the tabs (see Section 5.2 for discussion of braze conditions). After brazing, the temporary bolts were removed and MA956 rivets were hand set "snug" to eliminate free play between components with minimal clamping force to allow free in-plane motion of the panel during engine operation. Post-braze inspection indicated a very close fit between the panels and the Hastelloy X support ring. The covers shown as Item 8 in Figure 8-21 therefore were not needed to prevent cooling air leakage and were not installed on the completed subassembly.

The completed test article, shown in Figure 8-23, presently is awaiting availability of a suitable test engine and a surplus PW2037 burner prior to final inner burner liner assembly and 150 hour cyclic endurance testing. Remaining to be completed at final assembly are joining of the finished subassembly to the rest of the inner burner liner, finish grinding of the MA956 louver lips to fit the test engine, and installation of the finished combustor in the test engine.

9.0 CONCLUSIONS

- Laboratory performance evaluations were conducted on two wrought Oxide Dispersion Strengthened (ODS) sheet alloys:

  MA956 (FeCrAl - Y_2O_3)
  HDA8077 (NiCrAl - Y_2O_3)

  Properties evaluated include:

  Formability
  Tensile
  Creep
  Isothermal Fatigue
  Thermal Fatigue
  Oxidation
  Alloy Stability

  Results of these tests show both alloys to be viable candidates for gas turbine engine combustor applications, with neither material exhibiting a significant property advantage over the other. Comparison with a current combustor alloy (Hastelloy X) shows both alloys to have:

  +167°C (300°F) advantage in creep strength

  +167°C (300°F) advantage on cyclic oxidation resistance

  However, neither alloy shows any improvement of thermal fatigue capability over Hastelloy X.

- Sheet processing modifications directed toward improvement of ODS alloy thermal fatigue resistance through refinement of grain structure were not successful. MA956 alloy was shown to have better manufacturing reproducibility than HDA8077.

- Brazing and riveting were shown to be viable methods for attachment of ODS combustor components. Parameters were identified for brazing of both ODS alloys to themselves and to Hastelloy X.

- Segmentation was shown to be a promising combustor design approach to accommodate the limited thermal fatigue capability of ODS alloys. Two mechanically attached, segmented design configurations were identified:

  - Film cooled louver

  - Transpiration cooled panel

  The predicted life of both of these designs was $\geqslant$10,000 engine cycles for MA956 alloy. The high thermal fatigue resistance of both designs was confirmed in a series of combustor rig tests on subscale MA956 and Hastelloy X combustor components. No cracking was observed in over 10,000 thermal cycles applied to each of the two designs and materials. These tests also confirmed the superior oxidation and thermal distortion resistance of the ODS alloy.

- A hybrid PW2037 inner burner liner containing MA956 and Hastelloy X components was designed and constructed. The louvered configuration was selected for this component because of greater field experience with louvered construction and because of compatability with the bill-of-material PW2037 design. This component currently is awaiting availability of a suitable ground based experimental engine for 150 hour cyclic endurance testing.

REFERENCES

3-1 A. E. Gemma and J. S. Philips, "The Application of Fracture Mechanics to Life Predictions of Cooling Hole Configurations in Thermal- Mechanical Fatigue"; Engineering Fracture Mechanics, 1977, Vol. 9, Pergammon Press, Gr. Britain.

4-1 M. L. Robinson, "Incoloy Alloy MA956 Production Scale-Up-NASA MATE Project 3," Inco Project Report 4136.1, April 1980.

4-2 M. F. Rothman and H. M. Tawancy, "Effect of TMA Variables upon Structure and Properties in ODS Alloy HDA 8077 Sheet," Superalloys 1980, Proceedings of the Fourth International Symposium on Superalloys, Seven Springs, Pa., Sept. 1980, J. K. Tien, Ed., P. 179. Published by the American Society for Metals, Metals Park, Ohio.

5-1 W.H. Weigert and R.J. Henricks, "Tensile and Creep-Rupture Behavior of Two Advanced Oxide Dispersion Strengthened Sheet Alloys," Superalloys 1980, Proceedings of the Fourth International Symposium on Superalloys, Seven Spring, Pa., Sept. 1980, J.K. Tien, Ed. p 575ff. Published by the American Society For Metals, Metals Park, Ohio.

5-2 J.D. Whittenberger, "Elevated Temperature Mechanical Properties of the Iron Base Oxide Dispersion Strengthened Alloy MA 956 Bar," Met. Trans. A, 1981, Vol. 12A, pp. 845-851.

5-3 J.D. Whittenberger, "Effect of Prior Creep at 1365K on the Room Temperature Tensile Properties of Several Oxide Dispersion Strengthened Alloys," Met. Trans. A, 1977, Vol. 8A, pp. 1863-1870.

5-4 J.M. Davidson, C.M. Austin, and M.L. Robinson, "Oxide Scale Induced Cleavage in an ODS FeCrAl Alloy," Met. Trans. A, 1983, Vol. 14A, pp. 1516-1518.

5-5 Mitsubishi Technical Bulletin No. 122, "Changes in the Properties of Solid Solution Hardened and Dispersion Strengthened Nickel Base Superalloys by Long Term Heating", May 1977.

5-6 H.M. Tawancy, "Long Term Aging Characteristics of Hastelloy Alloy X," J. Mat. Sci., 1983, Vol. 18, pp. 2976-2986.

5-7 G.Y. Lai, "An Investigation of the Thermal Stability of a Commercial Ni-Cr-Fe-Mo Alloy (Hastelloy Alloy X)," Met. Trans. A, 1978, Vol. 9, pp. 827-833.

8-1 Robinson, M. L. and Astley, I., "Formability of INCOLOY Alloy MA 956: An Oxide Dispersion Strengthened Sheet Alloy," Formability of Metallic Materials-2000 A.D., ASTM STP 753, J. R. Newby and B. A. Niemeier, Eds., American Society for Testing and Materials, 1982, pp. 147-158.

8-2 Davidson, J. M., "Ductile-Brittle Transition Behavior of Incoloy MA956", proceedings of the Second International Conf. "Frontiers of High Temperature Materials II", May, 1983, London (to be published).

1. REPORT NO. NASA CR-174691	2. GOVERNMENT ACCESSION NO. NASA/Lewis	3. RECIPIENT'S CATALOG NO.
4. TITLE AND SUBTITLE Materials for Advanced Turbine Engines (MATE) Project 3 - Design, Fabrication, and Evaluation of an Oxide Dispersion Strengthened Sheet Alloy Combustor Liner		5. REPORT DATE February 1984 6. PERFORMING ORG. CODE
7. AUTHOR(S) Robert J. Henricks Keith D. Sheffler		8. PERFORMING ORG. REPT. NO. PWA 5574-175
9. PERFORMING ORG. NAME AND ADDRESS UNITED TECHNOLOGIES CORPORATION Pratt & Whitney Engineering Division East Hartford, Connecticut 06108		10. WORK UNIT NO. 11. CONTRACT OR GRANT NO. NAS3-20072
12. SPONSORING AGENCY NAME AND ADDRESS National Aeronautics and Space Administration Washington, D.C. 20456		13. TYPE OF REPT. AND PERIOD COVERED Contractor Report 14. SPONSORING AGENCY CODE

15. SUPPLEMENTARY NOTES
Final report. Project Manager, Robert Dreshfield, Materials Division, NASA Lewis Research Center, Cleveland, Ohio 44135.

16. ABSTRACT

The objective of this program was to evaluate the suitability of wrought Oxide Dispersion Strengthened (ODS) superalloy sheet for gas turbine engine combustor applications. Two yttria (Y_2O_3) dispersion strengthened alloys were evaluated; Incoloy MA 956 (FeCrAl base) and Haynes Developmental Alloy (HDA) 8077 (NiCrAl base). Preliminary tests, including formability, tensile, creep, isothermal and thermal fatigue, oxidation, and alloy stability, showed both alloys to be potentially viable combustor materials, with neither alloy exhibiting a significant advantage over the other. Both alloys demonstrated a +167C (300°F) advantage of creep and oxidation resistance with no improvement in thermal fatigue capability compared to a current generation combustor alloy (Hastelloy X). MA956 alloy was selected for further demonstration because it exhibited better manufacturing reproducibility than HDA8077. Additional property tests, including elevated temperature crack propagation, were conducted on MA956.

To accommodate the limited thermal fatigue capability of ODS alloys, two segmented, mechanically attached, low strain ODS combustor design concepts having predicted fatigue lives ≥10,000 engine cycles were identified. One of these was a relatively conventional louvered geometry, while the other involved a transpiration cooled configuration. A series of 10,000 cycle combustor rig tests on subscale MA956 and Hastelloy X combustor components showed no cracking, thereby confirming the beneficial effect of the segmented design on thermal fatigue capability. These tests also confirmed the superior oxidation and thermal distortion resistance of the ODS alloy. A hybrid PW2037 inner burner liner containing MA956 and Hastelloy X components was designed and constructed. The louvered configuration was selected for this component because of greater field experience with louvered construction and because of compatibility with the bill-of-material PW2037 combustor design. This component currently is awaiting the availability of a suitable ground based experimental engine for the 150-hour cyclic endurance testing.

17. KEY WORDS (SUGGESTED BY AUTHOR(S))	18. DISTRIBUTION STATEMENT
Oxide Dispersion Strengthened Alloys; ODS; Nickel Alloys; Iron Alloys; Gas Turbine Engines; Burners; Combustors; Creep; Oxidation; Thermal Fatigue	Unclassified - Unlimited STAR Category 26

19. SECURITY CLASS THIS (REPT)	20. SECURITY CLASS THIS (PAGE)	21. NO. PGS	22. PRICE *
Unclassified	Unclassified		

* For sale by the National Technical Information Service, Springfield, VA 22161

*USGPO: 1984-559-109-10414

End of Document